Group of nonlinear dynamics and synergetics - For historical purposes only. Current research here

Faculty of Electrical Engineering
University of Ljubljana, Slovenia

Main page
Research activities
Seminars
Colaboration

Faculty
University
Slovenia

The Group of Nonlinear Dynamics and Synergetics was established in December 1993 and is involved in the study of complex system and nonlinear dynamics, from both the theoretical and the experimental point of view.

Staff

Head:	Asst. Prof. Aneta Stefanovska
Research associate:	Maja Bračič Lotrič
Junior researcher:	Alan Bernjak
Visitor student:	Yuri Shiogai
Post-graduate students:	Janez Jamšek
	Robert Mavri
	Mojca Spazzapan

Address

Group of Nonlinear Dynamics and Synergetics
Faculty of Electrical Engineering
University of Ljubljana
Tržaška 25
SI-1000 Ljubljana, Slovenia

Phone: +386 (0)1 4768 246
Fax: +386 (0)1 4264 630

Last update: 17 Jun 2004

Group of nonlinear dynamics and synergetics

Faculty of Electrical Engineering
University of Ljubljana, Slovenia

Main page
Research activities
Some results
Projects
Theses
Seminars
Colaboration

Research activities

The cardiovascular system is a system of closed tubes - the blood vessels. Any oscillation in the system can be sensed at each point of it, with the intensity (amplitude) being different with respect to the place of recording and the nature of recorded signal.

It is our aim to reveal these dynamics from the measured signal and find the physiological nature of subsystems which contribute to the dynamics of the blood flow. Therefore, the frequency characteristics and the quantities that classify nonlinear systems in the phase space are estimated. Thus, not only the characteristic of the individual subsystem can be found, but also the nature of couplings between them. It is expected that various abnormalities due to different pathology will be reflected in changed phase and frequency couplings among the subsystems.

Last update: 28 May 2002

Group of nonlinear dynamics and synergetics

Faculty of Electrical Engineering
University of Ljubljana, Slovenia

[Main page](#)
[Research activities](#)
Seminars
[Colaboration](#)

Seminars

2002

12 June
[Synchronization and direction of coupling from time-series: an information-theoretic approach](#)
Milan Palus, Institute of Computer Science, Academy of Sciences of the Czech Republic, Prague, Czech Republic

30 May
[Introduction to classical and quantum chaos in Hamiltonian systems](#)
Marko Robnik, Center for Applied Mathematics and Theoretical Physics, University of Maribor, Maribor, Slovenia

29 May
[Modeling the cardiovascular and respiratory control systems](#)
Jerry Batzel, Karl-Franzens University of Graz, Graz, Austria

24 April
[The normal form method in the theory of ordinary differential equations](#)
Valery Romanovski, Center for Applied Mathematics and Theoretical Physics, University of Maribor, Maribor, Slovenia

17 January
[Large fluctuations, escape, and the control of chaos](#)
Peter V. E. McClintock, Low Temperature Laboratory/Nonlinear Laboratory, Department of Physics, Lancaster University, Lancaster, UK

2001

4 December
[Discrete Heisenber algebras and discrete Fourier transforms](#)
Andreas Ruffing, Department of Mathematics, Munich University of Technology, Munich, Germany

30 October
[Nonlinear dynamics of human bloodflow: computer analysis of cardiovascular data](#)
Peter V. E. McClintock, Low Temperature Laboratory/Nonlinear Laboratory, Department of Physics, Lancaster University, Lancaster, UK

24 October
[Information rates for signal analysis](#)
Milan Palus, Institute of Computer Science, AS CR, Prague, Czech Republic

15 October
[Synchronization in biological systems: An introduction](#)
Michael Rosemblum, Nonlinear Dynamics Group at the Institute of Physics, University of Potsdam, Potsdam, Germany

15 October

Stochastic phase resetting and phase synchronization: Application to neuroscience
Peter A. Tass, Institute of Medicine (MEG) Research Centre Jülich, Jülich, Germany

12 April
Optimal fluctuations and the control of chaos
Dmitrii G. Luchinsky, Department of Physics, Lancaster University, Lancaster, UK

Last update: 21 June 2002

Group of nonlinear dynamics and synergetics

Faculty of Electrical Engineering
University of Ljubljana, Slovenia

Main page
Research activities
Seminars
Colaboration

Colaboration

Institute for Theoretical Physics and Synergetics
Stuttgart University, Stuttgart, Germany

Department of Physics
Lancaster University, Lancaster, United Kingdom

Department of Anesthesia and the Institute for Experimental Medical Research
Ullevål Hospital, Oslo, Norway

Department of Nonlinear Dynamics
University of Florence, Florence, Italy

Institute of Pathophysiology
Medical Faculty, University of Ljubljana, Slovenia

Department of Internal Intesive Care and Department of Diabetes
University Clinical Centre, Ljubljana, Slovenia

Moor Instruments Limited
Axminster, England, U.K.

Depatment of Plastic and Reconstructive Surgery
Malmö University Hospital, Malmö, Sweden

Group for research in Angiology
Toulouse University Hospital, Toulouse, France

Department of Pulmonary Physiology
Latvian Medical Academy, Riga, Latvia

Department of Anaesthesia
Odense University Hospital, Odense, Denmark

Institute of Physics
Faculty of Natural Sciences and Mathematics
University Sv. Kiril i Metodij, Skopje, Macedonia

Department of Mechanical and Electrical Engineering
Universidad Iberoamericana, Mexico City, Mexico

Last update: 25 Aug 2003

Aneta Stefanovska

Assistant Professor
Head of the Group of Nonlinear Dynamics and Synergetics
Faculty of Electrical Engineering
University of Ljubljana, Slovenia

Main page
Recent publications
Meetings

Group page

I studied at the Faculty of Electrical and Computer Engineering, University of Ljubljana, Slovenia, where I received the M.Sc. degree in 1988 and the Ph.D. degree in 1992. Part of my Ph.D. I did at the Institute of Theoretical Physics and Synergetics, University of Stuttgart, Germany.

As a member of the Laboratory of Biocybenetics I was involved in various studies of therapeutic effects of electric currents in spasticity, rigidity, nerve regeneration, wound healing and modification of motor function. Searching for the mechanisms of therapetuic effects of electric currents brought me to measurments of peripheral blood flow and study of the blood flow dynamics in the cardiovascular system. Since December 1993 I have been leading the Group of Nonlinear Dynamics and Synergetics, dealing primarily with theoretical and experimental studies of the system of coupled oscillators that regulate the blood flow. My research interest is in developing and applying methods of nonlinear dynamics in studies of biological systems.

My research story in Slovene Download PDF.

Address

Aneta Stefanovska
Faculty of Electrical Engineering
Tržaška 25
SI-1000 Ljubljana, Slovenia

Phone	+386 (0)1 4768 246
Fax	+386 (0)1 4768 426
E-mail	aneta@osc.fe.uni-lj.si
	aneta@lancaster.ac.uk

Last update: 21 Mar 2001

Maja Bracic Lotric

Group of Nonlinear Dynamics and Synergetics
Faculty of Electrical Engineering
University of Ljubljana, Slovenia

Main page
Research area
Publications

Group page

I was born in 1968. After finishing the high school in Kranj, I started my studies at the Faculty of Electrical Engineering on the University of Ljubljana. In 1993 I received my B. Sc. Degree in electrical engineering for my work on the Lyapunov exponents of blood flow. In 1995 I joined the Group of Nonlinear Dynamics and Synergetics as a junior researcher. Within this group I have prepared Ph.D. thesis titled Couplings among subsystems that regulate blood flow in 1999.

My addresses

Faculty:

Maja Bracic Lotric
Faculty of Electrical Engineering
Trzaska 25
SI-1000 Ljubljana, Slovenia

Phone: +386 1 47 68 246
Fax: +386 1 42 64 630
E-mail: maja@osc.fe.uni-lj.si

Office:

Maja Bracic Lotric
Iskra Impuls
Gregorciceva 8,
SI-4000 Kranj, Slovenia

Phone: +386 4 20 23 696
Mobile: +386 31 653 413
Fax: +386 4 20 23 695
E-mail: maja@iskraimpuls.si

Home:

Maja Bracic Lotric
Ulica bratov Praprotnik 5
SI-4202 Naklo, Slovenia

Phone: +386 4 25 71 669
Mobile: +386 31 653 413
E-mail: maja@iskraimpuls.si

Last update: 21 Mar 2001

Alan Bernjak

Junior researcher

Faculty of Electrical Engineering
University of Ljubljana, Slovenia

Main page

Group page

I have finished the elementary school in Lendava. After finishing the secondary school at Gimnazija Murska Sobota in 1997, I have continued my studies at the Faculty of Electrical Engineering in Ljubljana. While working on my diploma thesis in April 2003, I have joined the Group of Nonlinear Dynamics and Synergetics. I graduated in July 2003 when I received my B.Sc. Degree in electrical engineering. From October 2004 I work with the group as a junior researcher.

Addresses

Faculty:
Faculty of Electrical Engineering
Tržaška 25
SI-1000 Ljubljana, Slovenia

Phone: +386(0)1 4768 249
Fax: +386(0)1 4264 630
E-mail: alan@osc.fe.uni-lj.si

Home:
Gornja ulica 9
Gaberje
9220 Lendava

Phone: +386(0)1 576 1482
Mobile: +386(0)31 332 971
E-mail: alanbernjak@hotmail.com

Last update: 09 Jun 2004

Group of nonlinear dynamics and synergetics

Faculty of Electrical Engineering
University of Ljubljana, Slovenia

[Main page](#)
[Research activities](#)
Some results
[Projects](#)
[Theses](#)
[Seminars](#)
[Colaboration](#)

Research Activities - Some Results

A mathematical model of coupled oscillators which regulate the blood flow was proposed. To reveal the nature of each subsystem (i.e. oscillator) and their mutual couplings, seven physiological signals are recorded simultaneously, namely the blood flow on four different sites, the electric activity of the heart (ECG), the blood pressure and the excursions of thorax due to the respiration activity. An additional signal of the heart rate variability (HRV) is derived from the ECG. Those time series have been recorded in healthy subjects, sportsmen and individuals with various cardiovascular diseases - the Raynaud's phenomenon, diabetes and miocardiac infarction and subjects with spinal cord injuries. The effect of denervation is also studied in animal experiments.

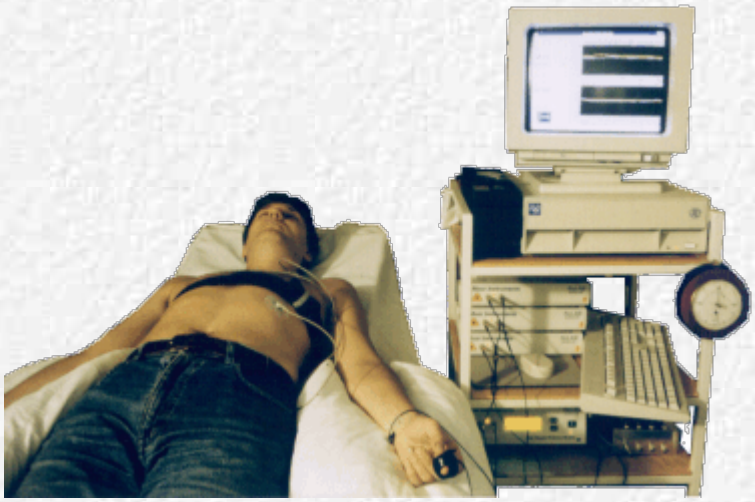

Algorithms for linear and nonlinear time series analysis have been developed and applied to measured signals. In terms of linear system theory, the estimations of time-varying frequency spectra by windowed Fourier transform, autoregressive modelling and wavelet based methods are used. Linear methods are supplemented by methods from nonlinear system theory such as calculation of correlation dimension, Lyapunov exponents and analysis of system determinism.

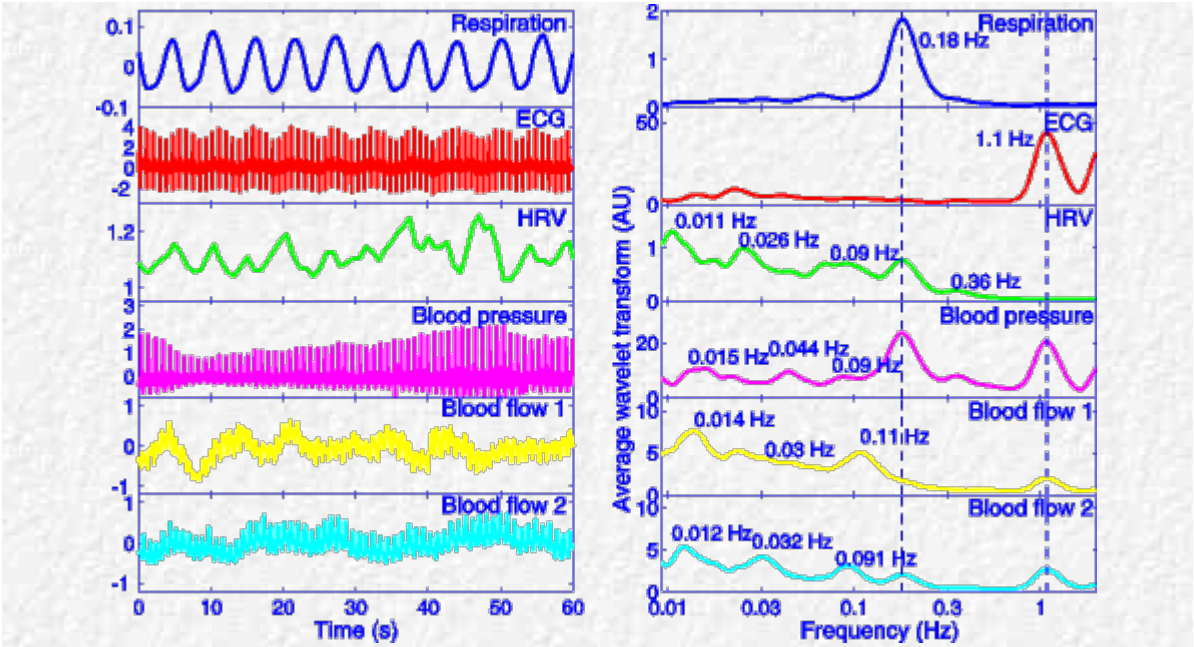

On the time scale of minutes 5 characteristic frequencies were found in measured cardiovascular signals, namely ~ 0.01 Hz, ~ 0.04 Hz, ~ 0.1 Hz, ~ 0.2 Hz and ~ 1 Hz. The physiological origin of the last two is known, ~ 0.2 Hz is synchronised with the respiration and ~ 1 Hz with heart rate. The physiological meaning of the slower oscillations is still to be revealed. There are some evidences in the literature that ~ 0.1 Hz corresponds to vessels oscillations resulting from a local miogenic regulation of their diameter. We hypothesise that ~ 0.05 Hz represents the neurogenic and ~ 0.01 Hz the metabolic regulation of flow of blood through the system of closed tubes.

Any disorder in cardiovascular system is reflected in the energy contribution of each characteristic frequency and the amplitude and frequency couplings between subsystems.

Last update: 28 May 2002

Group of nonlinear dynamics and synergetics

Faculty of Electrical Engineering
University of Ljubljana, Slovenia

Main page
Research activities
Some results
Projects
Theses
Seminars
Colaboration

Research Activities - Projects

2002 – 2006
STOCHASTIC DYNAMICS: FUNDAMENTALS AND APPLICATIONS
ESF Programme STOCHDYN

2001 – 2004
SYNCHRONIZATION OF BIOLOGICAL OSCILLATORS: EXPERIMENTS, ANALYSIS AND MODELLING
(network grant) INTAS 01-2061

2001 – 2003
FLUCTUATIONS, CHAOS, AND COMPLEXITY IN MULTISTABLE SYSTEMS
(network grant) INTAS

2001 – 2002
NONLINEAR DYNAMICS OF HUMAN BLOODFLOW
Bilateral Slovenian-British Scientific and Technological Cooperation Partnerships in Science

2001 – 2005
STUDYING THE REGULATION OF WAVES AND OSCILLATIONS IN VASCULAR SYSTEM
The Slovenian Ministry of Education, Science and Sport, Ljubljana, Slovenia, project #

1999 – 2001
ANALYSIS AND REGULATION OF BIOLOGICAL SYSTEMS
Bilateral Slovenian-Italian Scientific and Technological Cooperation

1998 – 2001
RECONSTRUCTING THE PHYSIOLOGICAL AND BIOCHEMICAL BASIS OF CARDIOVASCULAR OSCILLATIONS
Bilateral Slovenian-Norwegian Scientific and Technological Cooperation

1998 – 2001
STUDYING THE REGULATION OF WAVES AND OSCILLATIONS IN VASCULAR SYSTEM
The Slovenian Ministry of Science and Technology, Ljubljana, Slovenia, project # J2-0721-1538

1998 – 2000
RECONSTRUCTING CARDIOVASCULAR DYNAMICS
Bilateral Slovenian-German Scientific and Technological Cooperation

1997 – 1999
COMPUTER SYSTEMS IN MONITORING
The Slovenian Ministry of Science and Technology, Ljubljana, Slovenia, Bilateral SLO-I Scientific and Technological Collaboration Project

1997 – 1999
BLOOD FLOW DYNAMICS: OSCILLATORS COUPLINGS
The Slovenian Ministry of Science and Technology, Ljubljana, Slovenia, Bilateral SLO-Macedonian Scientific and Technological Collaboration Project

1995 – 1998
TOWARDS REVEALING COUPLINGS AMONG THE OSCILLATORS THAT REGULATE BLOOD FLOW

The Slovenian Ministry of Science and Technology, Ljubljana, Slovenia, project # J2-7156-0781-95

1994 – 1996

TOWARDS REVEALING PHASE AND FREQUENCY COUPLINGS AMONG THE OSCILLATORS THAT REGULATE BLOOD FLOW– IN NORMAL AND PATHOLOGICAL CASES

The European Concerted Action BIOMED II: Laser Doppler flowmetry for microcirculation monitoring, Brussels, Belgium, project # PL93-1041

Last update: 25 Aug 2003

Group of nonlinear dynamics and synergetics

Faculty of Electrical Engineering
University of Ljubljana, Slovenia

Main page
Research activities
Some results
Projects
Theses
Seminars
Colaboration

Research Activities - Theses

Ph.D. Theses

Model of transected peripheral nerve regeneration in a guidance channel with electromagnitc field
Martin Tomšiè, 2001.

Couplings among subsystems that regulate blood flow
Maja Braèiè Lotriè, November 1999.

Master Theses

Development of the SPY-COBBLE - an instrumented tracer for measuring dynamics of sediment transport in turbulent flows
Mojca Spazzapan, October 2001.

The bispectral analysis of cardiovascular oscillations
Janez Jamšek, April 2000.

Synchronization in cardiovascular system
Mario Hožiè, April 2000.

The impact of autonomic and somatic nervous system on the blood flow dynamics
Marko Èenèur, April 1997.

Diploma Theses

Cardiovascular dynamics after myocardiac infarction
Fabris Peruško, September 1998.

A new generation of automation processes controling programms
Boris Ilovar, June 1998.

Controlling general anasthesia
Boštjan Makovec, June 1998.

Cardiovascular dynamics in diabetic subjects
Robert Mavri, December 1997.

The response of pheripheral blood flow on vasodilating substances
Smpad Vladikoviæ, September 1997.

Multiresolution analysis in trend detection
Toni Braèiè, April 1997.

Wavelets analysis of peripheral blood flow in susbjects with Raynaud's phenomen
Domen Rakovec, October 1996.

Wavelets analysis of cardiovascular functions
Matej Hoèevar, July 1996.

Blood flow dynamics in subjects with Raynaud's phenomenon
Urša Teran, July 1996.

Analysis of sensory information during gate assisted by electrical stimulation
Alenka Flander, June 1996.

Static and dynamics of blood flow in sportsman and non-sportsman
Mojca Spazzapan, May 1995.

Methods for the estimation of time-varying frequency spectra of the blood flow signal
Blaž Voler, January 1995.

Dynamics of partial oxygen pressure on the skin
Marko Èenèur, December 1993.

Lyapunov exponents of blood flow
Maja Braèiè, September 1993.

Last update: 28 May 2002

Synchronization and direction of coupling from time-series: an information-theoretic approach

Milan Palus
Institute of Computer Science
Academy of Sciences of the Czech Republic
Prague, Czech Republic

Abstract: An information-theoretic approach for studying synchronization phenomena experimental bivariate time series is presented. "Coarse-grained'' information rates are introduced and their ability to indicate synchronization as well as to establish a `"direction of information flow'' between coupled systems, i.e. to discern the driving from the driven (response) system, is demonstrated.

Introduction to classical and quantum chaos in Hamiltonian systems

Marko Robnik
CAMTP - Center for Applied Mathematics
and Theoretical Physics, University of Maribor,
Krekova 2, 2000 Maribor, Slovenia

Abstract: We shall review the basic aspects of complete integrability and complete chaos (ergodicity) in classical Hamiltonian systems, as well as all the cases in between, the mixed type systems, where KAM Theory is applicable, and shall illustrate it using the billiard model systems. Then we shall proceed to the quantum chaos and its stationary properties, that is the structure and the morphology of the solutions of the underlying Schroedinger equation which in case of 2-dim billiards is just the 2-dim Helmholtz equation. We shall discuss the statistical properties of chaotic eigenfunctions, the statistical properties of the energy spectra, and show arguments and results in support of the so-called universality classes of spectral fluctuations, where in the fully chaotic case the Random Matrix Theory (RMT) is applicable. We shall mention the rich variety of applications in the domain of physics.

Modeling the Cardiovascular and Respiratory control systems

Jerry Batzel
Karl-Franzens University of Graz
Institute of Mathematics
Research Center on Optimization and Control
Heinrichstr. 36
A-8010 Graz, Austria

Abstract: In this talk we consider approaches to modeling the human cardiovscular and respiratory control systems. We include transport delays in the state equations for respiration. The effectiveness of the control of the ventilation rate V is influenced by such transport delays. The cardiovascular control system interaction between heart rate, blood pressure, cardiac output, and blood vessel resistance is complex. We will model the cardiovascular control mechanism as an optimal control. We will review a number of modeling approaches to clinical conditions which are of importance at the current time.

The normal form method in the theory of ordinary differential equations

Valery Romanovski
Center za uporabno matematiko in teoreticno fiziko
Univerza v Mariboru
Krekova 2, SI-2000 Maribor, Slovenia

Abstract: The normal form method of local analysis of solutions of ordinary autonomous differential equation will be briefly introduced. Then, main theorems of the Lyapunov function method will be presented and their application to investigation of local properties of solutions of differential equations will be demonstrated. The problem of periodic solutions for a system of few coupled oscillators will also be considered.

Large fluctuations, escape, and the control of chaos

Peter V.E. McClintock
Low Temperature Laboratory / Nonlinear Laboratory
Lancaster University
Lancaster, United Kingdom

Abstract: Most of the important events in fluctuating systems (eg. escape from an attractor) are due to occurrence of special larger-than-average fluctuations. Although they are very rare, and coming at random intervals, when they occur they do so in an almost deterministic way. The lecture will discuss the nature of large fluctuations, how they can be studied experimentally, and how they can sometimes be calculated analytically.

Discrete Heisenber Algebras and and Discrete Fourier Transforms

Andreas Ruffing
Technische Universität München
Zentrum Mathematik
Arcisstrasse 21, D-80333 München, Germany

Abstract: On 5 December 1901 Werner Heisenberg was born. One of his main contributions to quantum mechanics, the Heisenberg uncertainty principle, plays - apart from its meaning to physics - also a strong role in functional analysis: there, for instance, the deep connection between the Heisenberg algebra and the structure of Fourier transforms is of great interest. Starting from the classical Heisenberg algebra, we present a modification of this algebra which leads to a discrete Fourier transform on a one dimensional q-grid. We present the basic similarities between the Fourier transform and Schroedinger operators in the discrete scenario and in the continuous one. Both situations are compared and we will ask the question to what extent the presented q-Fourier transform might be applied to the analysis of signals, for instance in biomathematics.

Nonlinear dynamics of human bloodflow: computer analysis of cardiovascular data

Peter V. E. McClintock
Low Temperature Laboratory / Nonlinear Laboratory
Department of Physics, Lancaster University
Lancaster, UK

Abstract: The blood flows in accordance with the main rhythms of the human body, not just heartbeat and breathing, but many others too. Although it has been well-known for almost a century that these much slower rhythms also exist, it is only recently that the full picture has been revealed and clarified by Aneta Stefanovska and her collaborators in Ljubljana. She and Peter McClintock in Lancaster are working to under- stand how the various rhythms influence each other, and to see how they are affected by different diseases - and might thus be used to detect the onset of disease at an early stage.

Information rates for signal analysis

Milan Palus
Institute of Computer Science
AS CR
Prague, Czech Republic

Abstract: The concept of characterization of dynamical processes using entropy rates is common to the theory of stochastic processes and to information theory, and due to Kolmogorov also to the theory of dynamical systems. Entropy rates which quantify a rate of information creation by a system (or, in other words, the rate how quickly a system forgets its history) are measures suitable for quantifying dynamical "complexity" (or regularity and predictability) of a process under study. In real data applications, however, possibilities to estimate the exact entropy rate are limited to a few cases (Gaussian processes, finite state Markov chains). Instead, we introduce so called coarse-grained entropy rates (CER) suitable for a relative quantification of regularity and predictability of complex dynamical processes. The performance of CER in analyses of real data is compared to that of other dynamical measures, such as dimensions, Lyapunov exponents as well as other entropy measures. Extensions of CER into information rates for characterization of synchronization phenomena is also discussed.

Information rates for signal analysis

Michael Rosemblum
Nonlinear Dynamics Group at the Institute of Physics
University of Potsdam
Potsdam, Germany

Abstract: Brief introduction to synchronization theory will be presented on a qualitative level. Main effects, such as entrainment of an oscillator by external force, mutual synchronization of coupled systems, synchronization in noisy environment, synchronization in ensembles and in oscillatory media will be discussed and illustrated by results of experiments and observations.

Information rates for signal analysis

Peter A. Tass
Institute of Medicine (MEG) Research Centre Juelich
Germany

Abstract: The talk is about detecting and manipulating synchronization processes. Phase syncronization is a fundamental control mechanism in the nervous system. By means of the synchronization tomography it is possible to anatomically localize phase synchronization non-invasively in humans with magnetoencephalography. The method will be explained and applications to motor control as well as Parkinson's disease will be presented. Based on stochastic phase resetting stimulation techniques were designed which effectively desynchronize populations of interacting oscillators. This approach is used for the development of mild and efficient deep brain stimulation techniques for the therapy of neurological diseases like Parkinson's disease or essential tremor.

Optimal fluctuations and the control of chaos

Dmitrii G. Luchinsky
Department of Physics
Lancaster University
Lancaster, UK

Abstract: The energy-optimal migration of a chaotic oscillator from one attractor to another coexisting attractor is investigated via an analogy between the Hamiltonian theory of fluctuations and Hamiltonian formulation of the control problem. We demonstrate both on physical grounds and rigorously that the Wentzel-Freidlin Hamiltonian arising in the analysis of fluctuations is equivalent to the Pontryagin's Hamiltonian in the control problem with an additive linear unrestricted control. The deterministic optimal control function is identified with the optimal fluctuational force. Numerical and analogue experiments undertaken to verify these ideas demonstrate that, in the limit of small noise intensity, fluctuational escape from the chaotic attractor occurs via a unique (optimal) path corresponding to a unique (optimal) fluctuational force. Initial conditions on the chaotic attractor are identified. The solution of the boundary value control problem for the Pontryagin's Hamiltonian is found numerically. It is shown that this solution is very accurately approximated by the optimal fluctuational force found using statistical analysis of the escape trajectories. A second series of numerical experiments on the deterministic system (i.e. in the absence of noise) show that a control function of precisely the same shape and magnitude is indeed able to instigate escape. It is demonstrated that this control function minimizes the cost functional and the corresponding energy is found to be smaller than that obtained with some earlier adaptive control algorithms.

Aneta Stefanovska

Assistant Professor
Head of the Group of Nonlinear Dynamics and Synergetics
Faculty of Electrical Engineering
University of Ljubljana, Slovenia

Main page
Recent publications
Meetings

Group page

Recent publications

2003

P. V. E. McClintock and A. Stefanovska, Interaction and synchronization in the cardiovascular system, Fluctuations and Noise Letters, 3, L167-L176, 2003.

H. D. Kvernmo, A. Stefanovska and K. A. Kirkebøen, Enhanced endothelial activity reflected in the cutaneous blood flow oscillations of athletes, Eur. J. Appl. Physiol. 90, 16-22, 2003. PDF (372,111 bytes)

J. Jamšek, A. Stefanovska, P. V. E. McClintock and Igor A. Khovanov, Time-phase bispectral analysis, Phys. Rev. E. 68, 016201, 2003. PDF (1,430,876 bytes)

M. Paluš and A. Stefanovska, Direction of coupling from phases of interacting oscillators: An information-theoretic approach, Phys. Rev. E. 67, 055201(R), 2003. PDF (70,159 bytes)

P. Kvandal, A. Stefanovska, M. Veber, H. D. Kvernmo and K. A. Kirkebøen, Regulation of human cutaneous circulation evaluated by laser Doppler flowmetry, iontophoresis, and spectral analysis: importance of nitric oxide and prostaglandines, Microvascular Res., 65, 160-171, 2003. PDF (1,196,572 bytes)

T. Soderstrom, A. Stefanovska, M. Veber and H. Svensson, Involvement of sympathetic nerve activity in skin blood flow oscillations in humans, Am. J. Physiol. Heart Circ. Physiol., 284, H1638-H1646, 2003. PDF (250,649 bytes)

2002

A. Stefanovska, Cardiorespiratory interactions, Nonlinear Phenom. Complex Syst., 5, 462-469, 2002. PDF (911,861 bytes)

P. V. E. McClintock, A. Stefanovska, Noise and determinism in cardiovascular dynamics, Physica A 314, 69-76, 2002. PDF (389,100 bytes)

2001

M. Braèiè and A. Stefanovska, Paired Lyapunov Exponents Characterise blood flow dynamics in healthy subjects, Nonlinear Phenomena in Complex Systems, 4(3), 285-294, 2001.

A. Stefanovska, M. Braèiè Lotriè, S. Strle and H. Haken, The cardiovascular system as coupled oscillators? Physiol. Meas., 22, 535-550, 2001.

A. Stefanovska, D. G. Luchinsky and P. V. E. McClintock, Modelling couplings

among the oscillators of the cardiovascular system, Physiol. Meas., 22, 551-564, 2001.

2000 **A. Stefanovska, H. Haken, P. V. E. McClintock, M. Hožiè, F. Bajroviè and S. Ribariè, Reversible transitions between synchronization states of the cardiorespiratory system,** Phys. Rev. Lett. 85, 4831-4834, 2000. PDF (739,328 bytes)

M. Braèiè Lotriè, A. Stefanovska, D. Stajer and V. Urbanèiè-Rovan, Spectral components of heart rate variability determined by wavelet analysis, Physiol. Meas. 21, 441-457, 2000.

M. Braèiè, P. V. E. McClintock and A. Stefanovska, Characteristic frequencies of the human blood distribution system, In: D. S. Broomhead, E. A. Luchinskaya, P. V. E. McClintock and T. Mullin (Eds.), Stochastic and Chaotic Dynamics in the Lakes, American Institute of Physics, Melville, New York, 146-153, 2000.

F. Bajroviè, M. Èenèur, M. Hožiè, S. Ribariè and A. Stefanovska, The contribution of lumbar sympathetic neurones activity to rat's skin blood flow oscillations, Pflügers Archiv: Eur. J. Physiol. 439 Suppl, R158-R160, 2000.

M. Hožiè and A. Stefanovska, Karhunen-Loeve decomposition of peripheral blood flow, Physica A 280, 587-601, 2000. PDF (430,807 bytes)

A. Stefanovska and M. Hožiè, Spatial synchronization in the human cardiovascular system, Progress of Theoretical Physics 139, 270-282, 2000.

M. Braèiè Lotriè and A.Stefanovska, Synchronization and modulation in the human cardio-respiratory system, Physica A 283, 451-461, 2000. PDF (233,468 bytes)

1999 **A. Stefanovska and M. Braèiè, Physics of the human cardiovascular system,** Contemporary Physics 40, 31-55, 1999. PDF (1,143,529 bytes)

A. Stefanovska and M. Braèiè, Reconstructing cardiovascular dynamics, Control Engineering Practice 7, 161-172, 1999.

H. D. Kvernmo, A. Stefanovska, K. A. Kirkeboen and K. Kvernebo, Oscillations in the cutaneous blood flow in humans modified by endothelium-dependent and endothelium-independent vesodilators, Microvascular Research 57, 298-309, 1999.

A. Stefanovska, M. Braèiè, P. Leger, T. Braèiè, H. Boccalon and P. Bendayan, Linear and nonlinear analysis of resting blood flow signal in healthy subjects and subjects with Raynaud`s phenomenon, Technology and Health Care 7, 225-241, 1999.

A. Stefanovska, S Strle, M. Braèiè and H. Haken, Model synthesis of the coupled oscillators which regulate human blood flow dynamics, Nonlinear Phenomena in Complex Systems 2:2, 72-78, 1999.

M. Braèiè and A. Stefanovska, Wavelet analysis in studying the dynamics of blood circulation, Nonlinear Phenomena in Complex Systems 2:1, 68-77, 1999.

A. Stefanovska, M. Braèiè and H.D. Kvernmo, Wavelet analysis of oscillations in the peripheral blood circulation measured by laser Doppler technique, IEEE Transactions on Biomedical Engineering 46, 1230-1239, 1999.

N. Novakovski and A. Stefanovska, On the possible mechanical character of the respiratory frequency modulation of the heart rate, Phys. Maced. 49, 41-44, 1999.

1998 **H. D. Kvernmo, A. Stefanovska, M. Braèiè, K. A. Kirkeboen and K. Kvernebo, Spectral analysis of the laser Doppler perfusion signal in human skin before and**

after exercise, Microvascular Research 56, 173-182, 1998.

H. D. Kvernmo, A. Stefanovska, K. A. Kirkeboen, B. Osterud and K. Kvernebo, Enhanced endhothelial-dependent vasodilatation in human skin vasculature induced by physical conditioning, Eur. J. Appl. Physiol. 79, 30-36, 1998. PDF (179,537 bytes)

S. Ribariè, A. Stefanovska and I. Eržen, Direct current stimulation of crushed nerve increases capillary density in red muscle, Journal of Electro- and Magnetobiology 17, 243-254, 1998.

M. Braèiè and A. Stefanovska, Wavelet based analysis of human blood flow dynamics, Bulletin of Mathematical Biology 60, 919-935, 1998. PDF (1,225,681 bytes)

M. Braèiè and A. Stefanovska, Lyapunov exponents of simulated and measured quasi-periodic flows, A Chapter of A. Prochazka, J. Uhlir, P. J. Rayner and N.G. Kingsbury, Signal analysis and prediction, 479-488, Birkhauser, Boston, 1998.

M. Braèiè and A. Stefanovska, Nonlinear dynamics of the blood flow studied by Lyapunov exponents, Bulletin of Mathematical Biology 60, 417-433, 1998. PDF (326,571 bytes)

1997

M. Braèiè and A. Stefanovska, Local and global Lyapunov exponents of blood flow, Open Sys. & Information Dyn. 4, 435-456, 1997.

A. Stefanovska and P. Krošelj, Correlation integral and frequency analysis of cardiovascular functions, Open Sys. and Information Dyn. 4, 457-478, 1997.

A. Stefanovska, S.Strle and P. Krošelj, On the overestimation of the correlation dimension, Physics Letters A 235, 24-30, 1997. PDF (739,171 bytes)

1996

M. Braèiè and A. Stefanovska, Lyapunov exponents of quasi-periodic flows, Electrotehnical Review 63, 29-37, 1996.

J.J. Daly, E. B. Marsolais, L. M. Mendell, W. Z. Rymer, A. Stefanovska, J. R. Waplaw and C. Kantor, Therapeutic neural effects of electrical stimulation, IEEE Trans. Rehab. Eng. 4, 218-230, 1996.

1995

A. Stefanovska, P. Krošelj and S. Strle, Revealling oscillators - Calculation of dimension of attractors, Open Sys. and Information Dyn. 3, 149-178, 1995.

Last update: 25 Aug 2003

Aneta Stefanovska

Assistant Professor
Head of the Group of Nonlinear Dynamics and Synergetics
Faculty of Electrical Engineering
University of Ljubljana, Slovenia

Main page
Recent publications
Meetings

Group page

Organistion of meetings

International Workshop
Noisy Oscillators: Dynamics of Coupled Oscillatory and Complex Systems
Ljubljana, Slovenia, 10-13 December 2003

Fifth International conference
Simulations in Biomedicine
Ljubljana, Slovenia, 2-4 April 2003

International workshop
Fluctuations chaos and complexity in multistable systems
Lancaster University, UK, 1-7 August 2002

International summer school/conference
Let's face chaos through nonlinear dynamics
Ljubljana, Slovenia, September 1993 and August 1994
Maribor, Slovenia, June-July 1996, June-July 1999 and June-July 2002

International workshop
International Workshop on Fluctuations and Superfluidity
Lancaster, UK, 2-3 September 2000

Last update: 18 Jun 2002

Aneta Stefanovska – raziskovalna pot

Ko sem na programu študija na Univerzi v Ljubljani marca 1976 prebrala specialnost biokibernetika, v okviru študija na Fakulteti za elektrotehniko, sem bila prepričana, da je to tisto, kar sem si od nekdaj želela.

Profesor Vodovnik je več let preživel v Ameriki in se seznanil s področjem, ki je združevalo matematiko, fiziko, fiziologijo in medicino. To področje so pogosto poimenovali biokibernetika. Združevalo je vedenje o povratnozančnem delovanju sistemov, ki ga je nekaj desetletij prej matematik Wiener poimenoval kibernetika, in pa uporabnost teh spoznanj za razumevanje delovanja bioloških sistemov. Med vsemi biološkimi sistemi je bil takrat v ospredju sistem za gibanje, predvsem pri človeku, in razumevanje njegovega delovanja – od živca, prek živčno-mišične interakcije, preprostega gibanja enega sklepa, pa vse do hoje ali gibanja rok. Profesor Vodovnik je gojil področje, ki je zajemalo razumevanje gibanja in kontrole gibanja ter gradnjo matematičnih modelov na osnovi Wienerjevega kibernetskega pristopa z negativno povratnozančno regulacijo pri zdravih osebah in po spremembah, ki jih prinašajo poškodbe in bolezni živčno-mišičnega sistema. Te se, med drugim, izražajo kot hemiplegija, paraplegija, multipla skleroza, Friedrichova ataksija, Parkinsonova bolezen, mišična ali živčno-mišična distrofija.

S sodelavci, med katere sem celo desetletje sodila tudi jaz, je iskal možnosti za izboljšanje nekaterih izmed teh stanj. Pomanjkljivo kontrolo je poskušal popraviti z zunanjo kontrolo s pomočjo električnih tokov. Zaradi poškodb ali bolezni je živčni sistem izvajal omejeno kontrolo nad mišicami, ali pa kontrole sploh ni bilo, in zato je bilo gibanje bolnikov omejeno ali celo onemogočeno. V ozadju tega pristopa je bila zamisel, da je mogoče manjkajočo kontrolo živcev nad mišicami in sklepi nadomestiti ali premostiti z zunanjo kontrolo z električnimi tokovi. Le program kontrole in vrednotenje ustreznosti izvabljenega giba je bilo potrebno raziskati in ugotoviti. Gradil je torej svet visoko analitičnega pristopa, zgrajen na teoriji kibernetike, in pa popolnoma praktičen svet priprave orodij in naprav, s katerimi bi pomagali bolnikom.

Moje delo v okviru laboratorija za biokibernetiko je bilo vseskozi zaznamovano s to dvojnostjo: z željo po čimvečjem teoretičnem – matematičnem in fizikalnem – razumevanju in predstavitvi posameznih delov sistema za gibanje, ter hkrati praktičnim pristopom in izdelavo pripomočkov za izboljšanje bolezenskih stanj. Pri tem sem se nenehno spopadala z dejstvom, da je zelo težko povezati ta dva pristopa oziroma da med modeli in praktičnimi aplikacijami obstaja velik razkorak.

Na Fakulteti za elektrotehniko, v laboratoriju za biokibernetiko, sem formalno začela delati 1. aprila 1981, dejansko pa mesec dni prej. Čakala sem namreč na nastavitev na mesto stažistke-raziskovalke.

Med dodiplomskim študijem sem bila vseskozi usmerjena k biokibernetiki oziroma uporabi sistemske teorije za biološke sisteme. Na koncu četrtega letnika sem za šest tednov odšla na študijsko prakso v termoelektrično centralo Turbigo blizu Milana. Tam sem se seznanila z različnimi sistemi za regulacijo posameznih procesov. Vsem, ki so me bili pripravljeni poslušati, pa sem razlagala, kaj si želim delati. Tako da me je eden od inženirjev povezal s profesorjem Divietijem z Univerze v Milanu. Kmalu sem ga obiskala in od njega izvedela, da je možno z električnimi tokovi doseči spremembe tudi pri zdravih osebah, denimo pri športnikih. Delal je na programu, ki ga je nekaj let prej vpeljal ruski znanstvenik Kotz za jačanje mišic športnikov, predvsem pa mišic astronavtov med biva-

njem v breztežnostnem prostoru. Tam namreč hitro izgubijo mišično moč, ker se mišicam ni treba nenehno upirati gravitacijski sili, kot je to na Zemlji.

Spoznanja, ki sem jih pridobila med obiskom pri profesorju Divietiju, sem prinesla s seboj v Ljubljano in jih takoj posredovala profesorju Vodovniku, s katerim sem se že dogovorila, da bom pri njem delala diplomsko nalogo. Ni popolnoma verjel, da je mogoče kakorkoli vplivati na zdrav živčno-mišični sistem. Pred leti je namreč predlagal "balančno hipotezo", ki ima za osnovo delovanja živčno-mišičnega sistema ravnotežje med ekcitatornimi (dražilnimi) in inhibitornimi (zaviralnimi) dražljaji. Pri bolnikih je to ravnotežje porušeno, zato ga z zunanjimi električnimi tokovi lahko popravljamo, zdravo stanje pa je dovolj stabilno in ga ni mogoče dodatno spreminjati.

Dogovorila sva se, da bom s poskusi preverila, ali je možno vplivati na živčno-mišični sistem zdravih oseb, in če je, predlagala model na sinaptičnem nivoju, s katerim bi poiskala razlago za dosežene spremembe. Tako sem z diplomskim delom začela svojo pot, ki traja do danes: poskušati združiti eksperimentalni in teoretični pristop do določenega problema. Moj prvi članek je nastal na osnovi diplomskega dela, ki je kasneje privedlo do nekaj dodatnih študij in tudi več člankov.

Delo v okviru diplomske naloge me je še leta občasno pripeljalo med športnike, tako da sem sodelovala z raziskovalci na Fakulteti za šport in nekaterimi športniki. Poleg raziskav je šlo včasih le za pomoč. Na primer, smučarka Andreja Leskovšek si je pri padcu na smukaški tekmi pretrgala kolenske vezi, ki so jih z operacijo spet povezali. Ker kolena ni smela obremenjevati, ji je zelo hitro oslabela nadkolenska mišica quadriceps. V izometričnih razmerah, brez obremenitev za koleno, smo ji nekaj tednov dva do trikrat na teden z električnimi tokovi izvabljali kontrakcijo mišice in jo tako krepili. Z rezultati je bila zelo zadovoljna, in kot se spominjam, tudi njen trener in zdravnik.

Delo s športniki sem opravljala vzporedno z ostalim delom še nekaj let. S trenerjem atletov, Srdjanom Djordjevićem in Renato Karbo, mlado raziskovalko v laboratoriju za biokibernetiko smo sestavili program vadbe z električno stimulacijo, ki je jačal eksplozivno komponento gibanja. Do takrat so bile namreč vse študije usmerjene k jačanju vztrajnostne komponente, saj se je, ob povečani aktivnosti zaradi električne stimulacije težko izogniti mišičnemu utrujanju. Ko se pojavi utrujanje, se takoj vključi vztrajnostna komponenta, ki se krepi, eksplozivna pa ne več. Program smo preverili v skrbno načrtovani študiji, v kateri smo z daljšimi časovnimi presledki izvabljali kratko, a močno mišično kontrakcijo. Ugotovitve smo prikazali v znanstveni publikaciji. Program so hkrati vključili v trening skakalcev v višino in drugih atletov v eksplozivnih disciplinah.

Vmes sem intenzivno delala na problemu spastičnih mišic. To vprašanje sem obdelala za magistrsko nalogo. S pomočjo hidravlične merilne opornice, ki jo je za svoj doktorat razvil kolega Stanislav Reberšek, sem merila določene parametre med pasivnim gibanjem skočnega sklepa pri zdravih osebah in pri bolnikih z nekaterimi živčno-mišičnimi boleznimi, zaradi katerih je prihajalo do spastičnosti, ki se pojavlja kot posledica neinhibirane in nekontrolirane aktivnosti posameznih mišic. Na primer, med nategom mišice se aktivirajo mišična vretena in receptorji za nateg. Nato signal potuje do hrbtenjače, kjer je zaradi pomanjkljive regulacije, posledice bolezenskega stanja, slabo usmerjen in zato povzroči nekontrolirano in močno reakcijo mišice. Moja naloga je bila predlagati model, ki ponazarja stanje spastične mišice in daje primerljive oblike obnašanja, kot smo jih izmerili pri različnih bolnikih. Hkrati naj bi podala cenilke, s katerimi bi lahko ločili različne oblike in stopnje spastičnosti.

Torej sem se poglobila v študij fiziologije, patofiziologije in nevrofiziologije, in v študij

obstoječih modelov mišic in sklepov. Enosklepni sistem z mišicami je zelo nelinearen. Zato sem lahko izbrala nešteto različnih modelov, ki so vsi po vrsti le delno ponazarjali stvarnost. Modeliranje je navadno potekalo tako, da je bilo mogoče doseči izboljšave z višanjem reda modela ali vpeljavo dodatnih nelinearnih členov. Vendar le na račun obsežnosti modela, ki je v glavnem opisoval le neko specifično obliko delovanja sistema. Za novo obliko delovanja je bilo večinoma potrebno model znova razširjati.

S takim pristopom nisem bila zadovoljna in sem zato nenehno iskala povsem drugačno rešitev. takšno, ki bi že na začetku izhajala iz stališča, da je glavna lastnost sistema nelinearenost. Tako sem prišla do Volterra-Wienerjevega pristopa. Ta mi je prvič omogočail, da sem izhajala iz izmerjenih signalov in si z njihovo analizo pridobivala informacijo o nelinearnih dinamičnih lasnostih sistema. Z modelom, ki sem ga predlagala, sem na podlagi velikosti jeder prvega, drugega, tretjega in višjih redov lahko sklepala o stopnji nelinearnosti. Spastičnost sem zato izrazila kot spremembo jakosti posameznih jeder. To je bila osnova za mojo magistrsko nalogo.

Med pripravo magistrske naloge sem opravljala številne klinične študije v zvezi z vrednotenjem stopnje spastičnosti in različnih metod za njeno zmanjšanje, kot tudi študije na področju celjenja preležanin, rasti ali regeneracije živcev. Do magisterija sem s sodelavci napisala okoli 10 člankov, en pregledni članek in tri prispevke za monografijo. Veliko sem tudi potovala in se udeleževala različnih znanstvenih srečanj, tudi kot povabljena predavateljica.

Že pred tem, poleti 1982, je bila na neki vrtni zabavi tudi Olga, ki je zaradi spine bifide od rojstva na vozičku. V njenem življenju ni bilo opaziti nobene razlike, saj je hodila v službo, na zabave, v kino. Večkrat sem jo srečala sredi mesta, zabavna in polna življenja. Na zabavi se je kmalu poslovila. Rekla je, da ima preležanino in da je ne sme več obremenjevati s sedenjem. V meni se je takoj sprožil mehanizem 'pomagaj'. Ker sem sklepala, da so mišice zadnjice oslabele zaradi zmanjšane aktivnosti in ker sem že ugotovila, da je z električnimi tokovi možno mišice okrepiti, sem ji predlagala, da bi poskusili odpraviti njeno preležanino.

Privolila je, in jaz sem se nekaj mesecev temeljito posvetila izbiri parametrov in režima stimulacije. Poskus sem opravljala zasebno, saj mi ni bila pomembna znanost, temveč morebiten učinek. Ko sem zaprosila za izposojo stimulatorja, sem profesorju Vodovniku omenila, zakaj ga nameravam uporabljati. Profesor Vodovnik je bil takoj za to, in tako smo sestavili natančen protokol dela in izbrali nekaj metod za vrednotenje morebitnega učinka. S stimulacijo sva začeli proti koncu novembra, med prazniki za takratni Dan republike. Preležanine so namreč tako trdožive, da se vlečejo mesece ali celo leta, in se tudi rade ponavljajo. Medicinska sestra, ki je Olgo vsak dan prihajala previjati, nekaj dni, zaradi praznikov ni prišla, jaz pa sem ji rano stimulirala vsak dan. Že čez nekaj dni so bile spremembe očitne. Najbolj spodbudno je bilo to, da je bila sestra, ki ni vedela za moje delo, izrazito presenečena nad izboljšanjem, saj je bila pripravljena le na poslabšanje stanja.

Olgina zgodba nas je spodbudila, da smo napisali številne vloge za financiranje raziskav mehanizmov in učinkov električnih tokov na preležanine. To področje je kmalu postalo osrednje raziskovalno področje laboratorija za biokibernetiko.

Leta raziskav na področju funkcionalne električne stimulacije, to je uporabe tokov za izboljšanje gibov ali celo izvabljanjE osnovnega vzorca hoje, kot je med tem uspelo pri nekaj paraplegičnih bolnikih, so namreč prinesla izredno število evidenc, da je z 'elektriko' možno vplivati tudi na strukturo bioloških sistemov, na rast in regeneracijo tkiv.

Preležanine so se tudi izkazale kot odličen model za preverjanje teh opažanj in hkrati ponujale možnost za zelo široko uporabnost in koristnost rezultatov študije.

Zopet sem se znašla pri iskanju in gradnji modelov. Morala sem se učiti o fiziološkem ozadju delovanja tkiv, tkivni presnovi, mehanizmih interakcije tokovi-celice-tkiva, imunskih reakcijah in mehanizmih celjenja. Hkrati sem sodelovala pri študiju regeneracije živcev in se tudi tam ukvarjala z modeliranjem. Oba modela, 'rast mehkih tkiv' in 'regeneracija perifernih živcev', sta postajala izrazito kompleksna in pri modeliranju sem združevala opis z diferencialnimi enačbami s kvalitativnimi modeli. Modeliranje sem imela predvsem za orodje za sintezo obstoječega stanja, oziroma predstave o tem, kako potekajo procesi in kako se izvajajo posamezne funkcije. Zanesljive in jasne rezultate so prinašale le klinične in fiziološke eksperimentalne študije, saj je vsaka prinesla določeno trdno spoznanje, kamenček v mozaiku, ki je nastajal.

Čeprav se med rastjo in regeneracijo tkiv in celic odvijajo številni procesi, sem vedno verjela, da obstaja skupen mehanizem. Z vidika termodinamike sem si celice in tkiva predstavljala kot odprte sisteme. Za izboljšanje njihove rasti in regenerativnih lastnosti bi torej morali izboljšati proces dovajanja snovi in energije in odvajanja stranskih produktov celične presnove. Za dovajanje in odvajanje snovi v celice skrbi krvni obtok. Zato sem si za doktorsko disertacijo zastavila cilj: ugotoviti kako električni tokovi v bližini preležanine vplivajo na periferni krvni pretok.

Eksperimente sem skrbno načrtovala in poleg merjenja perifernega krvnega pretoka z laserskim Dopplerjevim merilnikom, sem vključila še merjenje srčne in dihalne aktivnosti. Hkrati sem beležila električno aktivnost srca (EKG) in spremembe obsega prsnega koša zaradi dihanja. Želela sem namreč izključiti možnost, da so spremembe, ki bi jih opazila v perifernem krvnem pretoku, posledica sistemskih sprememb, oziroma sprememb srčne in respiratorne aktivnosti. Čeprav so do takrat pretok obravnavali le kot neko enosmerno veličino, ki se sicer v času nekoliko spreminja in jo je zato treba povprečiti, sva s Petrom Krošljem izbrala analogni izhod inštrumenta, dogradila A/D pretvornik, iz katerega je bil možen direktni dostop do spomina na računalniku (DMA), in z njim zajemala 'čiste' signale pretoka EKG-ja in dihanja. Za vzorčno frekvenco sem izbrala 400 Hz (pri študiju posameznih segmentov P-Q-R-S-T kompleksa so signal EKG navadno zajemali s to ali podobno frekvenco), vendar o frekvenčni vsebini signalov takrat nisem veliko vedela.

Hitro se je izkazalo, da je signal pretoka zelo bogat – vsebuje različne komponente, ki oscilirajo na različnih časovnih skalah in da se ponavljanje ne dogaja striktno periodično, temveč variira okoli določene periode za posamezno komponento. Tudi učinki tokov se niso izražali kot povečanje ali zmanjšanje pretoka krvi v opazovano področje, temveč kot spremembe posameznih, skoraj oscilatornih komponent pretoka. Torej so se učinki pretežno izražali na dinamičnih lastnostih signalov pretoka in manj na statičnih.

Takoj sem se začela seznanjati z metodami za analizo nelinearnih dinamičnih sistemov. Prve eksperimente sem izvedla konec leta 1990, ko so bile raziskave s področja kaosa na višku. Številni raziskovalci so uporabljali algoritem Grasbergerja in Procaccia za izračun korelacijske dimenzije – eno izmed meril za vrednotenje stopnje kaotičnosti sistema. Prvotno sem sama predpostavljala, da bo stanje brez stimulacije najbrž bolj ali manj kaotično, kot stanje po stimulaciji, in da bo pretok v okolici preležanine glede na stopnjo celjenja imel večjo ali manjšo korelacijsko dimenzijo.

Vendar sem se začela spraševati, kako določiti optimalno vstavitveno dimenzijo za izmerjene signale, saj so bili rezultati zelo odvisni od vstavitvene dimenzije. Drugačno korelacijsko dimenzijo sem dobila, če sem signal vstavila v 16, 20, ali 30-dimenzionalni

prostor in izrazitega nasičenja ni bilo možno opaziti. Obstajal je sicer določen vzorec, vendar ga ni bilo možno zanesljivo 'ujeti'. Imela sem dve možnosti:

— zugotoviti, da signal pretoka nima končne dimenzije in da ima lastnosti podobne šumu, ali

— da ima končno dimenzijo, vendar je ne moremo nedvoumno določiti, ker se dinamične lastnosti pretoka časovno spreminjajo.

Če sprejmemo drugo možnost, to pomeni, da signali vsebujejo oscilatorne komponente, ki nimajo konstantne frekvence, temveč tudi frekvence oscilirajo, kot je to zlahka razvidno pri srčnem ritmu. Torej, sistem je najbrž neavtonomen in so zato metode v faznem prostoru, kjer izgubimo informacijo o času, neustrezne za njegovo analizo. V prid oscilatorne narave procesov je govorilo tudi nešteto fizioloških ugotovitev.

Ker sem tudi pri tej študiji, kot pri vseh prejšnjih, želela zgraditi matematični model fizioloških procesov in sistemov, ki sem jih opazovala, sem poiskala izvirne pristope za študij kompleksnih sistemov. Tako sem se seznanila z deli Prigogena in Hakena in se navdušila nad idejo, ki je bila v bistvu Hakenove sinergetike. Biološki sistemi so se mi zdeli naravnost sinergetski: vsak sistem ima v osnovi veliko število prostostnih stopenj, ko pa se izvaja določena funkcija sistema, se število prostostnih stopenj izrazito zmanjša na tiste, ki so vodilne – agonistične, in tiste ki nasprotujejo – antagonistične. Vse ostale stopnje prostosti pa postanejo sinergistične – združijo se bodisi z agonističnimi ali z antagonističnimi.

Profesorju Hakenu sem pisala marca 1991 in ga v začetku julija, po njegovem povabilu, obiskala v Stuttgartu. S seboj sem prinesla nešteto izmerjenih časovnih vrst in upanje, da bom iz njih prej ali slej razbrala osnovne lastnosti sistema, ki jih je 'ustvaril'. To prvo srečanje je bilo osnova za najino sodelovanje, ki traja še danes. Dogovorila sva se za daljši obisk in tako sem september in del oktobra istega leta preživela na inštitutu, ki ga je vodil. Takrat je bilo v njegovi skupini več kot 30 diplomantov, doktorandov in sodelavcev, s tem pa nešteto možnosti za razprave in nova spoznanja. Tesneje sem sodelovala z Wolfgangom Lorenzem, ki je analiziral signale EKG-ja in dihanja, ter poskušal določiti vzorce njihovih medsebojnih sklopitev.

Tudi sama sem z vidika sklopitev analizirala signale, ki sem jih prinesla s seboj. Ugotovila sem, da se srčna in dihalna komponenta nahajata tudi v signalu pretoka in da so pravzaprav vse frekvenčne komponente zastopane v vseh istočasno izmerjenih signalih kardiovaskularnega izvora.

Tako sem za doktorat predlagala model sklopljenih oscilatorjev, ki sodelujejo pri regulaciji krvnega pretoka. Na časovni lestvici okoli ene minute, kolikor je potrebno, da celotna količina krvi pri sproščenem človeku obkroži kardiovaskularni sistem, oziroma da jo srce prečrpa, deluje pet oscilatornih procesov. Ti so z različnimi amplitudami navzoči v vseh signalih kardiovaskularnega sistema.

Model je v osnovi fenomenološki, vendar nosi sporočilo, da je zdravo stanje določeno z enim izmed naborov amplitud in frekvenc posameznih oscilatorjev in njihovih medsebojnih sklopitev, ter da se patološka stanja, ki nastajajo zaradi obolenj, pa tudi vse spremembe v sistemu, odražajo kot spremenjene amplitude, frekvence in medsebojne sklopitve oscilatorjev. Za nadaljnjo nadgradnjo modela pa je bilo potrebno ugotoviti točno fiziološko naravo posameznih oscilatorjev in njihovih sklopitev.

Po doktoratu sem se povsem posvetila rekonstrukciji dinamike kardiovaskularnega sistema. Delo poteka vzporedno na treh področjih, ki se med seboj prepletajo:

— izbira ustreznih metod za analizo kardiovaskularnih signalov;

— študij fizioloških osnov oscilatorjev in njihovih medsebojnih sklopitev, kot tudi patofizioloških sprememb, ki jih vnašajo različne bolezni kardiovaskularnega sistema;

— izpopolnjevanje in analiza delovanja matematičnega modela, ki ponazarja sistem kot sistem sklopljenih oscilatorjev.

Po doktoratu sem ugotovila, da je analiza dinamičnih lastnosti signala EKG že prejmed znanstveniki, ki so se ukvarjali z analizo časovnih vrst, ki nastajajo kot rezultat delovanja nelinearnih dinamičnih sitemov izzvala veliko zanimanja . Večina teh študij je slonela na metodah za analizo v faznem prostoru, saj so tam definirane poglavitne lastnosti sistemov s kaotično dinamiko. Zato so bila vprašanja, ki so jih raziskovalci zastavljali, v tem: ali je sistem determinističen, kaotičen, ali morda stohastičen. Hkrati so iskali ustrezno metodo, ki bi omogočala ločitev bolezenskega od zdravega stanja sistema.

Z raziskavami, ki sem jih opravila v Ljubljani, in pri katerih se mi je pridružilo nekaj diplomantov, magistrantov in doktorandov, med njimi tudi Maja Bračič, sem vedno želela izluščiti klinično in fiziološko relevantne informacije o dinamiki sistema. Zato sem se tudi povezala z nekaterimi kliničnimi in fiziološkimi skupinami v Ljubljani, Oslu, Trømsi, Malmöju, Rigi, Touluseu, Odenseju in Baslu. Vedno smo skupaj načrtovali eksperimente in tudi sama sem bila večkrat navzoča, vsaj pri začetnih meritvah.

Poleg korelacijske dimenzije smo vpeljali še izračun lokalnih in globalnih Lyapunovih eksponentov, Karhunen-Loèvejevo dekompozicijo in druge metode v faznem prostoru. Vendar se je izguba informacije o času vedno odražala tako, da ni bilo mogoče enoumno določiti optimalne vstavitvene dimenzije prostora. Določitev ustrezne vstavitvene dimenzije za posamezne signale kardiovaskularnega izvora je po moji presoji še danes odprto vprašanje. Še več, iskazalo se je, da je treba časovno spremenljivost osnovnih frekvenc upoštevati kot poglavitno značilnost sistema in zato izbirati metode, ki omogočajo zajeti dinamične lastnosti sistema ob ohranitvi informacije o času.

Tako smo razvijali in preverjali uporabnost različnih časovno-frekvenčnih metod, kot so metoda periodogramov s Fourierjevo transformacijo, izračun spektrov na osnovi avtoregresijskih modelov izmerjenih signalov, selektivna Fourierjeva transformacija ali valčne transformacije. Valčna transformacija se je izkazala za izredno uporabno pri analizi oscilatornih komponent kardiovaskularnih signalov. Hkrati omogoča kvantitativno vrednotenje posameznih komponent in s tem ponuja možnost za oceno različnih vplivov in sprememb stanja sistema.

Z valčno tranformacijo dosežemo tudi logaritmsko frekvenčno rezolucijo, kar nam omogoča dobro oceno spektralnih komponent na nizkofrekvenčnem področju, na primer oscilacije s frekvenco okoli 0.01 Hz, ki je 100-krat nižja od srčne frekvence. Ob sodelovanju s kolegi iz Osla smo opravili več eksperimentov, s katerimi smo ugotovili, da oscilacije s to frekvenco odražajo endotelijsko aktivnost. Endotelij namreč sprošča imunske in citotoksične substance in s tem povzroča oscilacije premera žil. Amplitude ali energije, oscilatorne komponente s frekvenco okoli 0.01 Hz, nam omogočajo neinvazivno opazovanje delovanja biokemičnih procesov, ki so izrednega pomena za življenje.

Kolikor mi je znano, smo pokazali prvi, da se endotelijska aktivnost odraža oscilatorno, in tudi to, kje se nahaja njeno frekvenčno področje delovanja. Rezultate smo že objavili v dveh člankih. Z nadaljnimi raziskavami smo pokazali, da se endotelijska aktivnost značilno razlikuje pri športnikih v primerjavi s povprečno fizično aktivnimi zdravimi osebami, in o tem tudi napisali članek, ki smo ga že poslali v objavo. Tako je bilo z analizami, ki izhajajo iz osnov, ki jih podaja model sklopljenih oscilatorjev, možno kvantitativno pokazati, da je fizična aktivnost koristna za delovanje kardiovaskularnega sistema. Te študije so nam torej

dale jasne fiziološke rezultate in zaključke kliničnega pomena, ter tudi nazorno potrjujejo in dopolnjujejo model.

Obojestransko koristno in plodno sodelovanje s kolegi iz Osla pa poteka še naprej. Pravkar zaključujemo nekaj študij, s katerimi ugotavljamo vpliv določenih substanc na oscilacije, ki nastajajo z endotelijsko aktivnostjo. V ospredju našega trenutnega interesa je dušikov oksid, substanca, ki je v zadnjem desetletju vzbudila izredno pozornost med fiziologi, farmakologi in kliničnimi zdravniki. (Nobelovo nagrado za medicino so leto 1998 podelili raziskovalcem, ki so ugotovili, da je dušikov oksid tista substanca, ki jo sprošča endotelij, in vpliva na relaksacijo žil – učinek, ki so ga opazili že nekaj let prej). Če bomo določili vlogo dušikovega oksida pri oscilacijah perifernega krvnega obtoka, bomo lahko ponudili neinvazivno metodo za spremljanje njene aktivnosti *in vivo*. S tem bomo tudi odprli izredne možnosti za raziskave vpliva dušikovega oksida pri različnih obolenjih in pa za ugotavljanje vpliva različnih substanc in zdravil na njegovo aktivnost.

Posvetili smo se tudi ugotavljanju fiziološke osnove ostalih nizkofrekvenčnih oscilacij v kardiovaskularnih signalih, predvsem miogenega in nevrogenega izvora. Indirektno smo pokazali, da imajo oscilacije zaradi intristične aktivnosti gladkih mišic v stenah žil, oziroma miogene oscilacije, frekvenco okoli 0.1 Hz in smo tudi o tem objavili članek. O vpletenosti somatskega sistema v oscilacije kardiovaskularnih funkcij smo s kolegi iz Malmöja napisali članek in ga poslali v objavo. Podobne rezultate smo prej, s sodelovanju kolegov na Inštitutu za patofiziologijo v Ljubljani, dobili pri podganah in jih tudi že objavili.

Prispevke posameznih oscilatornih komponent smo analizirali pri bolnikih s kardiovaskularnimi obolenji, kot so osebe po akutnem infarktu srčne mišice, osebe z diabetesom tipa II, ali osebe z Raynauldovo boleznijo. Dokazali smo, da se prispevki nizkofrekvenčnih komponent, ki jih je zaenkrat mogoče ustrezno določiti le z valčno transformacijo, katero smo prvi vpeljali pri analizi kardiovaskularnih signalov, značilno spremenijo pri določeni bolezni. Rezultati, ki smo jih že objavili, podajajo nov vpogled v fiziologijo in patofiziologijo teh bolezni in tudi omogočajo vrednotenje stopnje nastalih sprememb in učinkov različnih zdravil. Na primer, v študiji, ki smo jo začeli med mojim bivanjem poleti 2000 v Lancastru, ugotavljamo vpliv β-blokatorjev na oscilacije v kardiovaskularnih funkcijah (spremenljivost srčnega ritma, spremenljivost sistoličnega, diastoličnega in srednjega krvnega pritiska, ter perifernega krvnega pretoka in temperature kože) pri bolnikih, s srčnim popuščanjem.

Dve podobni, zelo obsežni klinični študiji pravkar potekata tudi v Ljubljani. Hkrati zajemamo 12 različnih signalov kardiovaskularnega izvora. Rezultate obsežnih obdelav z metodami, ki jih razvijamo, bomo primerjali s številnimi kliničnimi preizkavami in podatki o bolnikih. Poiskati želimo značilne dinamične lastnosti in nastale spremembe kardiovaskularnih parametrov pri osebah po akutnem infarktu srčne mišice in pri bolnikih z diabetesom tipa II. Pri študijah sodelujejo tudi zdravniki internisti in diabetologi, dr. Dušan Štajer, dr. Vilma Urbančič-Rovan in dr. Katja Ažman Juvan. S skupino zdravih oseb, ki smo jih že izmerili za kontrolo, bomo v okviru teh dveh študij vključili okoli 300 oseb. Obe študiji sta zasnovani na zelo vzpodbudnih rezultatih obdelave signalov, ki smo jih pred časom izmerili na manjšem številu bolnikov z istimi obolenji.

Poleg časovno-frekvenčnih metod uporabljamo tudi metode za analizo sinhronizacije med posameznimi oscilatornimi komponentami. Pri tem uporabljamo novo medoto za analizo sinhronizacije med nestatcionarnimi, zašumljenimi in kaotičnimi procesi, ki je rezultat teoretičnih raziskav v zadnjih petih letih. Določamo časovni potek relativne medsebojne fazne razlike tako pri zdravih osebah kot pri obolelih oz. v različnih stanjih sistema. Eden od rezultatov je tudi ugotovitev, da je stopnja sinhronizacije med srčnim in

respiratornim ritmom med anestezijo povezana z globino anestezije. Še več, spremembe v relativni fazi, ki smo jih opazili med anestezijo, so podobne spremembam, ki so jih opazili v fizikalnih sistemih, kot so laserji. Naša študija kardiorespiratorne sinhronizacije med anestezijo ima torej, poleg izjemnega kliničnega pomena tudi dodaten pomen: nazorno kaže na to, da ima kardiovaskularni sistem lastnosti 'klasičnih' fizikalnih sistemov, četudi je zelo kompleksen.

Raziskave smo opravili na podganah in rezultate opisali v članku, ki je bil objavljen lani v PRL, odmevi na članek pa v decembrski številki Physics Today. Pred anestezijo se sistema le občasno sinhronizirata. Po vbrizgu anestetika pa opazimo serijo prehodov: najprej dva srčna utripa na eno periodo dihanja, nato trije, štirje in pet. Ko se vpliv anestetika zmanjša, se prehodi odvijajo v obratnem vrstnem redu in na koncu nastopi enako stanje kot pred vbrizgom anestetika. Prehodi so ponovljivi, in smo jih opazili tudi pri ponovni anesteziji teden dni pozneje.

Z nadaljnjimi poskusi nameravamo raziskati, ali je možno z določanjem stopnje sinhronizacije med srčnim, respiratornim in somatskim sistemom sproti ugotavljati in določati globino anestezije. Pokazali smo tudi, da je vzorec frekvenčne modulacije in sinhronizacije porušen pri bolnikih z diabetesom, spremenjen pri športnikih ali pa povsem izključen v komi.

V zadnjem času smo začeli tesno sodelovati z Oddelkom za fiziko na Univerzi v Lancastru. Kupili so dve napravi petkanalnih ojačevalnikov za kardiovaskularne signale, ki smo jih razvili v Ljubljani ob sodelovanju z Jankom Petrovčičem z Odseka za računalniško avtomatizacijo in regulacije na Inštitutu Jožef Stefan. Postavili so dva merilna sistema z enakimi senzorji kot jih že uporabljamo v Ljubljani in izvajajo podobne meritve in študije na zdravih osebah in na bolnikih s popuščanjem srca.

Hkrati smo model sklopljenih oscilatorjev razširili za vpliv fluktuacij in šuma ter raziskali nekatere njegove dinamične lastnosti. O tem smo naisali dva članka, ki smo jih že poslali v objavo. Pokazali smo, da je z modelom možno ponoviti osnovne značilnosti spektrov izmerjenih signalov. Na modelu smo tudi pokazali, da se dva oscilatorna sistema lahko sinhronizirata ob prisotnosti šuma in da gre v sistemu najbrž za kombinacijo med linearno in parametrično sklopitvijo med oscilatorji. Naravo mesebojnih sklopitev poskušamo določiti z dodatnimi eksperimentalnimi študijami in z analizo izmerjenih signalov, kot tudi z nadaljnjimi analizami modela.

Model sklopljenih oscilatorjev in rezultati analiz, ki nastajajo na osnovi predstave sistema, ki jo ponuja model, pridobivajo vse večjo odmevnost. Tako sem letos povabljena na pet znanstvenih srečanj, na enega skupaj z Majo Bračič.

Model postaja zelo zanimiv tudi za fizike in matematike. V okviru projekta Intas o dinamiki sklopljenih oscilatorjev, ki je pravkar sprejet, bomo poleg dinamike laserjev, kot primera tehnoloških oscilatornih sistemov obravnavali model sklopljenih kardiovaskularnih oscilatorjev kot primer naravnih oscilatornih sistemov. V projekt je vključenih 10 skupin, ki bodo raziskovale skupne značilnosti kompleksnega obnašanja oscilatornih sistemov. Številna vprašanja, ki jih bomo obravnavali, izhajajo iz analize signalov kardiovaskularnega izvora. S pridobljenimi spoznanji bomo analizirali in dograjevali model, ki podaja sintezo bogatih značilnosti kardiovaskularnega sistema kot sistema sklopljenih oscilatorjev.

Lancaster, 17. maja 2001

Maja Bracic Lotric

Group of Nonlinear Dynamics and Synergetics
Faculty of Electrical Engineering
University of Ljubljana, Slovenia

Main page
Research area
Publications

Research area

I am working on processing the signals of physiological origin, especially those related to the blood flow dynamics. To gain an insight into the dynamics of the cardiovascular system, both linear and nonlinear system theory are applied to measured time series. So far, the majority of my work is related to calculating the Lyapunov exponents of the system from the measured time series of blood flow, the wavelet based analysis of cardiovascular signals and the analysis of cardio-respiratory coupling.

The Lyapunov exponents

The Lyapunov exponents measure the rate of convergence or divergence of nearby trajectories in the phase space. They were first introduced by A.M. Lyapunov at the end of last century, but became widely used in the past decade. This is partly due to the development of very fast computers and partly to increasing interest in chaotic dynamics. Namely, a positive exponents indicates sensitive dependence on initial conditions. Learn more about the exponents

The existing algorithms for the estimation of Lyapunov exponents from time series have free parameters. Since there are no analytical criteria for parameter settings, we have analyzed the effect of each parameter to the results for various chaotic and quasi-periodic test signals.

For a wide range of parameter values the exponents of the blood flow signals of various subjects appear in pairs consisting of a positive and negative exponent. Typically, 4 or 5 pairs and a zero exponent are found. The presence of a zero exponent implies the deterministic nature of the cardiovascular system on the time scale of minutes.

Lyapunov exponents provide essential information for the system characterization from measured signal. However, the application of this algorithm to numerous signals is limited by the time-consuming parameter settings.

The wavelet analysis

It is known that cardiovascular control mechanisms manifest themselves through rhithmic activities. Various techniques of spectral analyses have been applied to blood pressure and heart rate variability (HRV) signals. Besides the respiratory (HF) fluctuations, fluctuations around 0.1 Hz (LF) and below 0.05 Hz (VLF) were revealed.

There are two major problems related to the frequency analysis of cardiovascular signals:

- the time-varying nature of characteristic frequencies which demands an analysis in the time-frequency domain, and
- the relatively broad frequency band on which characteristic peaks are expected which raises the problem of the time and frequency resolution.

In the time-frequency analysis, a window of fixed length is shifted along the signal to achieve time localization and the frequency content of each window is evaluated. The window length determines the time and frequency resolution. The choice window length

is a trade-off between time and frequency resolution. If both low and high frequencies with different time spans are to be simultaneously detected in a signal, the choice might be a puzzling one. To overcame this difficulty, the wavelet analysis was introduced.

The wavelet analysis is a scale-independent method. The window is not only translated along the signal, but it is also scaled. High frequency components are analyzed by a short window, while longer windows are used for low frequency components. In this way, good frequency resolution for low frequencies and good time resolution for high frequencies are obtained.

Some results of the wavelet analysis of cardiovascular signals are available on the group page.

Cardio-respiratory coupling

The cardiac and respiratory systems do not act independently, they influence each other by several mechanisms. For example, the heart rate increases during inspiration and decreases during expiration. This respiratory modulation of heart rate, known as respiratory sinus arrhythmia (RSA), was observed as early as in 1847. During the past few years, another phenomenon that arises from the coupling between both systems was revealed -- the adjustment of their rhythms or synchronisation.

We have found short episodes of synchronisation or entrainment of cardiac and respiratory rhythms in healthy relaxed subjects. We may infer that a coupling between heart and respiratory systems that enables synchronisation exist. Synchronisation, however, is not a state of the system, but a process of the adjustment of rhythms. The two interacting systems are not isolated and face the influence of other physiological systems. Their impact may change the stability or even existence of phase locked solutions.

More about the cardiorespiratory interaction can be found in my PhD thesis Couplings among subsystems that regulate blood flow.

Last update: 19 Mar 2001

Maja Bracic Lotric

Group of Nonlinear Dynamics and Synergetics
Faculty of Electrical Engineering
University of Ljubljana, Slovenia

Main page
Research area
Publications

Publications

Published Papers

M. Bracic and A. Stefanovska, Lyapunov exponents of quasi-periodic flows. Elektrotehnical Review 63, 29-37, 1996.

M. Bracic and A. Stefanovska, Local and global Lyapunov exponents of blood flow, Open Sys. & Information Dyn. 4: 435-456, 1997.

Abstract: The Lyapunov exponents are calculated from numerically simulated and measured time series. The existing algorithms for the estimation of Lyapunov spectra have free parameters. Hence, their influence is analysed on various chaotic and quasi-periodic simulated signals. Furthermore, the exponents of blood flow signal, measured on a healthy subject, are calculated over a wide range of parameter values. For embedding dimension d >= 10 two typical spectra are observed for both the global and the local Lyapunov exponents. Either we have 4 paired and 1 zero, or 5 paired exponents. At least one exponent equals zero within calculation error.

File: zip compressed: osljap.zip (433 kB)

M. Bracic and A. Stefanovska,Lyapunov exponents of simulated and measured quasi-periodic flows, A Chapter of A. Prochazka, J. Uhlir, P.J. Rayner, N.G. Kingsbury, Signal analysis and prediction, 479-488, Birkhauser, Boston, 1998.

Abstract: The Lyapunov exponents are calculated from numerically simulated and measured signals. The existing algorithms for their estimation have free parameters and their impact and the impact of noise are analysed on quasi-periodic simulated signals. Furthermore, calculation of the exponents of blood flow signal, measured on a healthy subject, is presented. Over a wide range of parameter values two typical patterns of both the global and the local Lyapunov exponents are obtained. Either we have four paired and one zero exponent, or five paired exponents. This may be an indication of the deterministic and almost conservative nature of the system governing the blood circulation on the time scale of minutes.

File: zip compressed: praga.zip (122 kB)

M. Bracic and A. Stefanovska, Nonlinear dynamics of the blood flow studied by Lyapunov exponents, Bulletin of Mathematical Biology, 60, 417-433, 1998.

Abstract: In order to gain an insight into the dynamics of the cardiovascular system throughout which the blood circulates, the signals measured from peripheral blood flow in humans are analysed by calculating the Lyapunov exponents. Over a wide range of algorithm parameters, paired values of both the global and the local Lyapunov exponents are obtained, and at least one exponent equals zero within the calculation error. This may be an indication of the deterministic nature and finite number of degrees of freedom of the cardiovascular system governing the blood flow dynamics on the time scale of minutes. A difference is observed in the Lyapunov dimension of controls and sportsmen.

File: zip compressed: bmbljap.zip (1.01 MB)

M. Bracic and A. Stefanovska, Wavelet based analysis of human blood flow dynamics,Bulletin of Mathematical Biology, 60, 919-935, 1998.

Abstract: To analyse signals measured from human blood flow in the time-frequency domain, we used the wavelet transform which gives good time resolution for high frequency components and good frequency resolution for low frequency components. We have introduced several time and spatially invariant measures which characterise the dynamics in the time-frequency domain. They were used to compare the time-frequency content of blood flow signals belonging to control subjects and

athletes. Some statistically significant differences between the two groups are discussed.

File: zip compressed: bmbwav.zip (679 kB)

H. D. Kvernmo, A. Stefanovska, M. Bracic K. A. Kirkeboen and K. Kvernebo, Spectral Analysis of the laser Doppler perfusion signal in human skin before and after exercise, Microvascular Research, 56, 173-182, 1998.

A. Stefanovska and M. Bracic, Physics of the human cardiovascular system, Contemporary Physics, 40, 31-55, 1999.

A. Stefanovska and M. Bracic, Reconstructing cardiovascular dynamics, Control Engineering Practice, 7, 161-172, 1999.

Abstract: The signals which originate from the human cardiovascular system were analysed using methods of both linear and nonlinear system theory. The analyses in the time domain and in the phase space revealed the deterministic and almost conservative nature of the cardiovascular control system on the time scale of minutes. Five characteristic frequencies were found in the signal of peripheral blood flow. Some of them were already found in other cardiovascular functions, the breathing, blood pressure, ECG and IHR. Each characteristic peak reflects the periodic action of one of the subsystems, involved in the regulation of the blood flow. These systems are mutually dependent via the couplings among them. Their strength plays an essential role in the performance of the system. In some cases their importance is indicated, thus pointing to the practical application in the diagnosis and prediction of cardiovascular functions.

File: zip compressed: cep.zip (1.40 MB)

A. Stefanovska, M. Bracic, P. Leger, T. Bracic, H. Boccalon and P. Bendayan, Linear and nonlinear analysis of resting blood flow signal in healthy subjects and subjects with Raynaud`s phenomenon, Technology and Health Care, 7, 225-241, 1999.

M. Bracic and A. Stefanovska, Wavelet analysis in studying the dynamics of blood circulation, Nonlinear Phenomena in Complex Systems, 2:1, 68-77, 1999.

Abstract: To analyse signals, related to the human cardiovascular system in the time-frequency domain, we used the wavelet transform which gives good time resolution for the high frequency components and good frequency resolution for the low frequency components. Peaks at approximatelly the same frequencies were found in all signals revealing their common origin. Further, we hypothessise that peaks which appear at exactly the same frequencies in all signals measured from the one subject reflect the action of central regulatory mechanisms, whilst other have a local origin.

File: zip compressed: oswav.zip (1.28 MB)

A. Stefanovska, S Strle, M. Bracic and H. Haken, Model synthesis of the coupled oscillators which regulate human blood flow dynamics, Nonlinear Phenomena in Complex Systems, 2:2, 72-78, 1999.

A. Stefanovska, M. Bracic and H.D. Kvernmo, Wavelet analysis of oscillations in the peripheral blood circulation measured by laser Doppler technique, IEEE Transactions on Biomedical Engineering, 46, 1230-1239, 1999.

Abstract: Oscillations in the peripheral blood flow signal, measured by laser Doppler flowmetry, extend over a wide frequency scale and their periods vary in time. Therefore, a time-frequency method with logarithmic frequency resolution, namely the wavelet transform, was used for their analysis. In this way, frequencies between 0.0095 Hz and 1.6 Hz were studied. On this scale, five characteristic oscillations were revealed resulting from both local and central regulatory mechanisms. We discuss endothelial activity as a possible mechanism of the rhythmic process with a characteristic frequency of around 0.01 Hz. Furthermore, we illustrate the potential of laser Doppler flowmetry combined with dynamics analysis for studies of both the micro- and macroscopic mechanisms of blood flow regulation in vivo.

M. Bracic, P. V. E. McClintock and A. Stefanovska, Characteristic frequences of the human blood distribution system, In: D. S. Broomhead, E. A. Luchinskaya, P. V. E. McClintock and T. Mullin, Stochastic and chaotic Dynamics in the lakes: STOCKAOS, AIP Conference Proceedings, Ambleside, United Kingdom, 146-153, 1999.

M. Bracic Lotric, A. Stefanovska, Synchronization and modulation in the human cardiorespiratory system, Physica A, 283, 451-461, 2000.

M. Bracic Lotric, A. Stefanovska, D. Stajer and V. Urbancic-Rovan, Spectral components of heart rate variability determined by wavelet analysis, Physiol. Meas., 21, 441-457, 2000.

Conference Papers

M. Bracic in A. Stefanovska, Dinamika krvnega pretoka. Zbornik delavnice Racunalniska analiza medicinskih podatkov CADAM -95, Bled, Slovenija, 27.-28. november 1995.

M. Bracic and A. Stefanovska, Lyapunov exponents of blood flow. Proccedings IEEE Engineering in Medicine and Biology, 18th Annual International Conference, Amsterdam, 31. october - 3. november 1996, ISBN 90-9010005-9(CD-ROM) SOE 9609001, Soetekouw Videoproductions, Nijmegen, The Netherlands.Amsterdam.

M. Bracic and A. Stefanovska, Lyapunov exponents of simulated and measured quasi-periodic flows, Proceedings of the first European Conference on Signal Analysis and Prediction, Praga 24. - 27. june 1997, 379-382.

A. Stefanovska, P. Kroselj and M. Bracic, Linear and nonlinear methods of signal analysis in reconstructing cardiovascular dynamics, Proceedings of the first European Conference on Signal Analysis and Prediction, Praga 24. - 27. june 1997, 427-430.

A. Stefanovska, P. Kroselj, M. Bracic and S. Strle, Reconstructing cardiovascular dynamics, The 3rd IFAC Symposium Modelling and Control in Biomedical Systems, University of Warwick, UK, 23. - 26. march 1997.

A. Stefanovska and M. Bracic, Evidences that coupled oscillators govern flow of blood in the human cardiovascular system, Proc. Nonlinear Phenomena in Complex systems, Minsk, Belorusija, 10. - 13. february 1997, invited lecture.

F. Perusko, D. Stajer, M. Bracic, A. Stefanovska, Periferni krvni pretok po srcnem infarktu , B. Zajc (ed.) Zbornik sedme Elektrotehniske in racunalniske konference ERK'98 Portoroz, Slovenija, 24. - 26. september 1998, volume B, 403-406.

R. Mavri, F. Perusko, M. Bracic, V. Urbanic-Rovan, D. Stajer, A. Stefanovska, Oscilacije v srcnem ritmu , B. Zajc (ed.) Zbornik sedme Elektrotehniske in racunalniske konference ERK'98 Portoroz, Slovenija, 24. - 26. september 1998, volume B, 407-410.

M. Bracic, A. Stefanovska, Dynamics of human blood distribution , Fifth SIAM conference on applications of dynamical systems, Snowbird, Utah, 23. - 27. may 1999, page 57.

Last update: 23 Dec 2000

Eur J Appl Physiol (2003) 90: 16–22
DOI 10.1007/s00421-003-0867-6

ORIGINAL ARTICLE

Hebe Désirée Kvernmo · Aneta Stefanovska
Knut Arvid Kirkebøen

Enhanced endothelial activity reflected in cutaneous blood flow oscillations of athletes

Accepted: 24 March 2003 / Published online: 29 May 2003

Abstract Functional alterations of vascular endothelial cells may be evaluated by analysing differences in effects of endothelium-dependent [acetylcholine (ACh)] and endothelium-independent [sodium nitroprusside (SNP)] vasodilators. We evaluated whether a dynamic approach using spectral analysis of the blood flow signal, resulting from the cutaneous red cell flux and recorded by the technique of laser Doppler flowmetry (LDF), can detect higher endothelial responsiveness in trained versus less trained individuals. There was a 1.6 times higher ACh-induced cutaneous perfusion in athletes than in controls ($P < 0.05$), both when evaluated as a mean value of the LDF signal or as the amplitudes of its spectral components. In the frequency interval from 0.009 to 1.6 Hz, ACh induced a 1.6 times higher average spectral amplitude ($P < 0.01$) in athletes compared with controls. ACh also induced a 1.6 times higher absolute spectral amplitude of the oscillator at around 0.01 Hz ($P < 0.05$) in the athletes compared with the controls, whereas the endothelial oscillation at around 0.01 Hz during basal unstimulated perfusion was 1.5 times higher ($P < 0.01$). There were no significant differences in absolute or relative amplitude during iontophoresis with SNP. These results indicate that athletes have higher endothelial activity than less trained individuals.

Keywords Acetylcholine · Endothelium-mediated vasodilatation · Oscillations · Spectral analysis · Wavelet transform

H. D. Kvernmo (✉)
Division for Hand and Microsurgery, Orthopaedic Department, National Hospital, 0027 Oslo, Norway
E-mail: hebe.kvernmo@rikshospitalet.no

A. Stefanovska
Faculty of Electrical Engineering, University of Ljubljana, 1000 Ljubljana, Slovenia

K. A. Kirkebøen
Institute for Experimental Medical Research and Department of Anaesthesia, Ullevål Hospital, 0407 Oslo, Norway

Introduction

The vascular endothelium plays an important role in the regulation of blood pressure and flow by releasing vasoactive substances, such as nitric oxide (NO) and prostaglandins (Vallance et al. 1989). In exercise-trained subjects, vascular responsiveness to endothelium-dependent vasodilators has been shown to be enhanced in skeletal muscle (Delp 1995; Kingwell et al. 1996) and in cutaneous vasculature (Kvernmo et al. 1998a).

Analysis of periodic oscillations in cutaneous blood flow as measured by laser Doppler flowmetry (LDF) is introduced for evaluation of microvascular control mechanisms (Intaglietta 1989; Stefanovska 1992; Bollinger et al. 1993; Stefanovska and Kroselj 1997; Kvernmo et al. 1998b, 1999). The fifth and slowest periodic oscillation (0.01 Hz) is considered to be modulated by the vascular endothelium, and may be assessed by the difference in effects of endothelium-dependent and endothelium-independent vasodilators on the blood flow oscillations of this frequency (Kvernmo et al. 1999).

The present study evaluates whether analysis of spectral amplitudes based on wavelet transformation can detect an enhanced vascular responsiveness to endothelium-dependent vasodilators in the cutaneous vasculature of exercise-trained subjects and whether this approach may increase information on mechanisms underlying blood flow regulation.

Methods

The study included nine male long-distance runners and a control group of nine healthy male soldiers (Table 1). The subjects had not taken any medication in the week prior to the study and were not smokers. Subjects with a history of chronic disease were not included. After being informed of the study design, the subjects gave written consent as approved by the local Ethics Committee.

Procedures

Maximal oxygen uptake ($\dot{V}O_{2max}$) was measured with the use of a Sensor Medics analyser (MMC Horizon System, USA). Heart rate was recorded using an electrocardiograph (Sirekust 341, Siemens, Germany). Subjects refrained from strenuous exercise for 24 h prior to the study. Food intake was a light meal 2 h prior to the test. LDF was carried out in a room with temperature at 22 (21–23)°C with the subject supine. At least 20 min were allowed for equilibration to the conditions. Skin temperature was measured using a digital skin thermometer (Fluke 2190, John Fluke, USA).

Laser Doppler flowmetry

LDF gives a semiquantitative assessment of microvascular red cell flux, which is expressed in arbitrary units (AU) (Nilsson et al. 1980). The LDF recorded from the skin of the forearm reflects perfusion in capillaries, arterioles, venules and dermal vascular plexa. A minor part of the signal reflects nutritive perfusion, while the major part is thermoregulatory perfusion (Bollinger et al. 1991). In the present study the perfusion was recorded with a single channel flowmeter (MBF 3D, Moor Instruments, Axminster, Devon, UK), by an optical fibreprobe (P10A, Moor Instruments) which has two fibres: one delivers light (a near-infrared laser diode with a power of 1.0 mW at a wavelength of 780 nm) to the site under observation, and the other fibre collects the backscattered light which contains the Doppler shifted frequency information. The signal is filtered with cut-off frequencies at 18 Hz and 22.5 kHz. A sampling frequency of 40 Hz and a time constant of 0.1 s were selected.

Iontophoresis

Iontophoresis allows polar drugs to cross the skin barrier by using a small direct current and assesses microvascular reactivity while perfusion is measured (Müller et al. 1987; Westermann et al. 1988; Andreassen et al. 1998; Kvernmo et al. 1998a). A probeholder for iontophoresis and perfusion measurement (Moor Instruments) was fixed with a double-sided adhesive tape on the volar side of the right forearm after the skin was cleaned. The probeholder had a chamber for deposition of the test substances in proximity to the laser Doppler probe (''direct chamber''). A battery powered constant current stimulator (MIC 1, Moor Instruments) was used. A 1% solution of acetylcholine (ACh) (E. Merck, Germany) or sodium nitroprusside (SNP) (E. Merck) was used. For ACh, anodal current was used, and for SNP, a cathodal current was applied (Müller et al. 1987; Westermann et al. 1988). The reference electrode was attached to the wrist of the right arm.

The dose of drugs administered by this technique is proportional to the total charge (Q) in millicoulombs (mC), i.e. product of current (I) in milliamperes (mA) and the duration (t). To avoid stimulation of sensory nerves, currents of less than 0.20 mA and total charge of less than 8 mC were used (Westermann et al. 1988). Dose–response curves were obtained for both ACh and SNP using charges in a sequence of 0.75 mC (0.075 mA for 10 s), 1.5 mC (0.15 mA for 10 s), 3.0 mC (0.15 mA for 20 s) and 6.0 mC (0.20 mA for 30 s) with a response period of 300 s after each dose. These charges produced a stepwise increase in laser Doppler perfusion, achieving a maximum response at 6.0 mC.

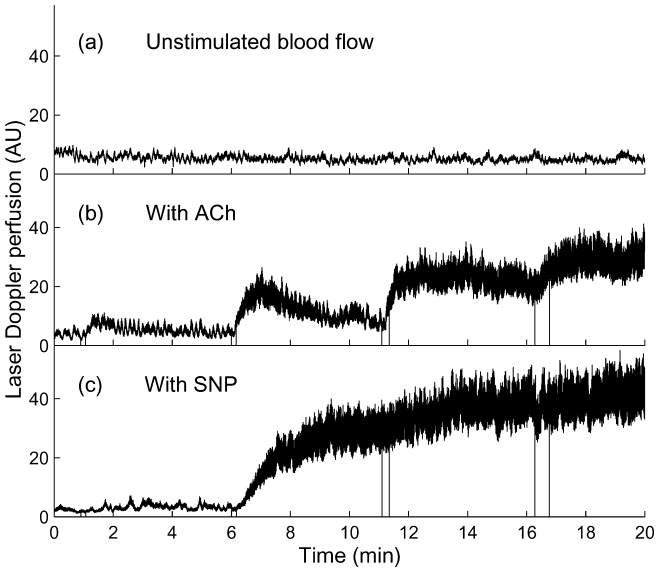

Fig. 1 A laser Doppler flowmetry recording on human forearm during **a** unstimulated blood perfusion, during iontophoresis with **b** acetylcholine (*ACh*) and **c** sodium nitroprusside (*SNP*) recorded over a period of 1,330 s in arbitrary units (*AU*)

Blood perfusion recordings were analysed during unstimulated conditions and during iontophoresis with ACh or SNP (Fig. 1). Each of the three recordings was of 1,330 s duration with 40 data points each second, giving a total of 53,200 measurements for each of the recordings. Prior to each measurement session, the LDF probe was calibrated using a standard aqueous suspension of microspheres (Flux Standard, Moor Instruments). ACh and SNP were applied at different sites separated by at least 5 cm. The chamber allowed a skin area of 0.64 cm^2 to be treated.

Spectral analysis

The oscillations of the microvascular blood perfusion signal can be divided into different components by spectral analysis (Meyer et al. 1988; Intaglietta 1989; Hoffmann et al. 1990; Stefanovska 1992; Bollinger et al. 1993; Mück-Weymann et al. 1996). From the LDF curve (Fig. 2a), a three-dimensional picture was obtained with frequency, amplitude (AU) and time as the axes (Fig. 2b). In addition, the time–frequency representation of the local maxima (Fig. 2c) and the time average of the amplitude as a function of frequency (Fig. 2d) were used. Analysis of short segment signal recordings (seconds) shows distinct frequency peaks

Table 1 Anthropometric and performance data of athletes and controls. $\dot{V}O_{2max}$ Maximal oxygen uptake; $\dot{V}O_{2\ 80\%}$ 80% of maximal oxygen uptake; *MAP* mean arterial blood pressure. Data are medians and ranges

	Athletes ($n=9$)	Controls ($n=9$)
Age (years)	26 (18–32)	20 (19–21)*
Body mass (kg)	76 (70–79)	75 (70–90)
Height (cm)	187 (171–192)	180 (176–197)
Heart rate (beats min^{-1})	51 (44–60)	57 (51–72)*
MAP (mmHg)	106 (87–113)	91 (79–100)*
Skin temperature (°C)	33.1 (32.3–34.9)	33.4 (32.1–34.4)
$\dot{V}O_{2max}$ (ml kg^{-1} min^{-1})	68.9 (62.0–73.0)	51.5 (44.4–61.4)#
Running velocity at $\dot{V}O_{2\ 80\%}$ (m min^{-1})	227 (217–243)	177 (143–198)#

*$P<0.05$ and #$P<0.0001$

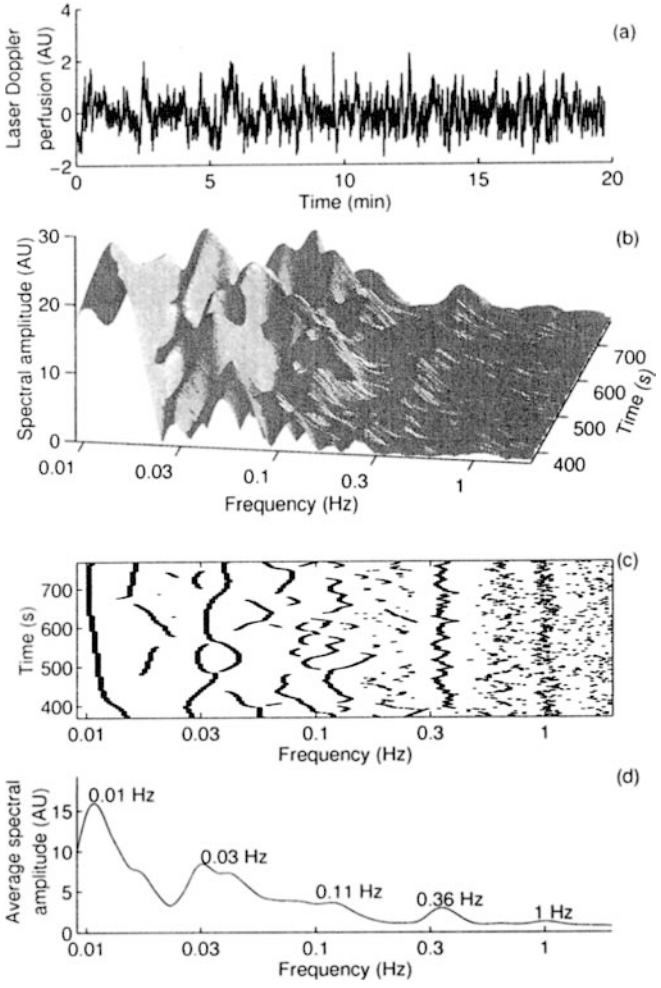

Fig. 2 The laser Doppler perfusion signal where the perfusion values are normalised to zero (**a**), the wavelet transform (**b**), local amplitude maxima (**c**) and average spectrum (**d**) of the laser Doppler perfusion signal recorded in arbitrary units (AU), where b–d are shown on a log scale

around 1 and 0.2 Hz. These represent the heart rate and the respiratory component of the blood flow signal. In analysis of longer recordings (minutes) these peaks spread out and appear less distinct due to natural variability in their generation. However, analysis of longer segment recordings improves low-frequency resolution. Wavelet analysis proposed by Morlet (1983) is a scale-independent method that involves an adjustable window length. Hence, the low frequencies are analysed using a long window and the higher frequencies using a shorter window. In the present study the wavelet transform of 22-min recordings was calculated and periodic oscillations with five characteristic frequency peaks were observed within the frequency interval 0.009–1.6 Hz. The position of each peak differs between subjects and changes with time in a given subject, but they are found to be within the following frequency intervals: 0.009–0.02, 0.02–0.06, 0.06–0.16, 0.16–0.4 and 0.4–1.6 Hz. The average amplitude of the oscillations of the total spectrum from 0.009–1.6 Hz and the absolute amplitude within each of the five frequency intervals were calculated. We then normalised the absolute amplitude within a particular frequency interval with respect to the average amplitude of the entire spectrum. In this way we defined the relative amplitude as the ratio between the absolute amplitude within a particular frequency interval and the average amplitude of the entire spectrum (Fig. 3).

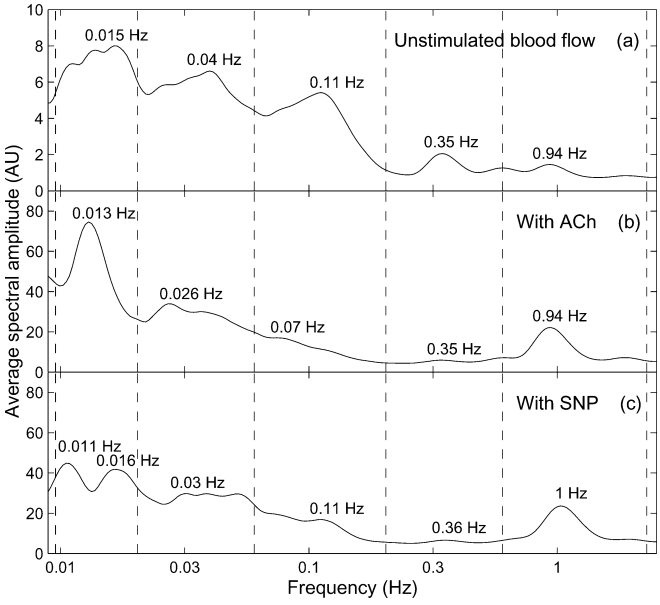

Fig. 3 An example of the spectrum of a laser Doppler perfusion during **a** unstimulated blood perfusion, during iontophoresis with **b** ACh and **c** SNP recorded over a period of 1,330 s in arbitrary units (AU). The vertical lines indicate the outer limits of each frequency interval

Statistical analysis

Data are presented either as median with range, or as box plots. The five horizontal lines shown in the boxes are the 10, 25, 50, 75 and 90th percentiles: Values above or below the 10th and 90th percentile are presented as data points. The Wilcoxon signed-rank test was used to evaluate differences in ACh and SNP responses, whereas differences between the groups in unstimulated blood flow and responses to ACh and SNP were evaluated by the Mann-Whitney test with two-sided critical values. Statistical significance was defined as $P < 0.05$.

Results

Resting heart rate was lower in the athletes compared with the controls, whereas mean arterial pressure was slightly higher. There was no significant difference in skin temperature between the two groups of subjects (Table 1).

Table 2 Average values and the average spectral amplitude in athletes and controls. The average values and the average spectral amplitude of the total spectrum from 0.009 to 1.6 Hz of the unstimulated cutaneous perfusion signal, and during iontophoresis with acetylcholine (*Ach*) and sodium nitroprusside (*SNP*), recorded in arbitrary units (*AU*). Data are given as medians and total ranges

	Athletes ($n=9$)	Controls ($n=9$)	P value
Average values			
Unstimulated	5.8 (3.7–9.2)	3.5 (2.4–5.3)	<0.001
With Ach	27.2 (14.3–45.1)	16.8 (5.9–26.6)	<0.02
With SNP	27.9 (9.4–36.3)	27.9 (14.8–50.8)	<0.5
Average spectral amplitude			
Unstimulated	0.72 (0.40–1.20)	0.28 (0.22–0.39)	<0.0001
With Ach	1.69 (1.01–2.54)	1.05 (0.42–1.71)	<0.01
With SNP	1.81 (0.76–2.56)	1.67 (0.77–3.46)	<0.5

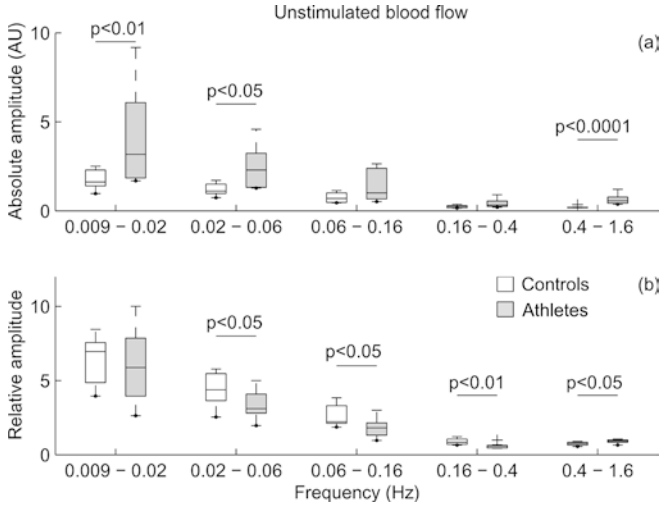

Fig. 4 The absolute (**a**) and relative (**b**) amplitude for five frequency intervals in the frequency spectrum from 0.009 to 1.6 Hz of the laser Doppler perfusion signal in less trained subjects (*open symbols*) and athletes (*filled symbols*) for unstimulated blood perfusion recorded in arbitrary units (AU). The five horizontal lines on the boxplot show the 10, 25, 50, 75 and 90th percentiles. The values above or below the 10th and 90th percentiles are represented as data points. *P* values are given on the figure

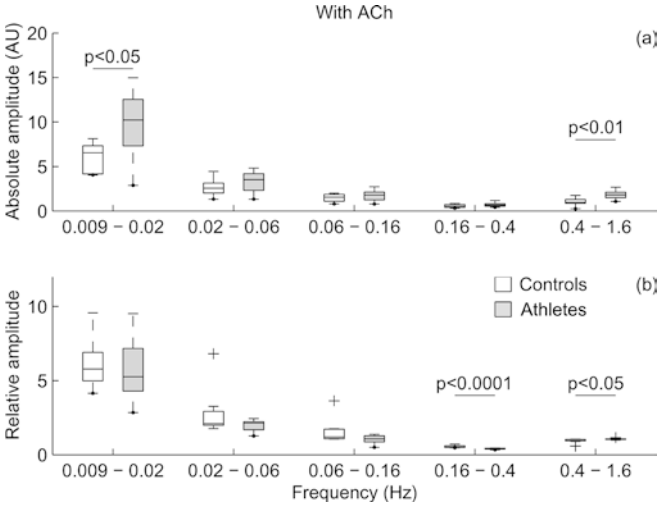

Fig. 5 The average (**a**) and relative (**b**) amplitude for all five frequency intervals in the frequency spectrum from 0.009 to 1.6 Hz of the laser Doppler perfusion signal in controls (*open symbols*) and athletes (*filled symbols*) during iontophoresis with ACh in arbitrary units (AU). The five horizontal lines on the boxplot show the 10, 25, 50, 75 and 90th percentiles. The values above or below the 10th and 90th percentiles are represented as data points. *P* values are given on the figure

Cutaneous perfusion

The athletes had higher unstimulated cutaneous perfusion than the controls (Table 2). Also the perfusion responses evoked by ACh increased to a higher level in the athletes than in the controls, whereas no significant difference was observed with respect to SNP (Table 2).

Spectral amplitudes of the LDF signal

Average spectral amplitude of the total spectrum from 0.009 to 1.6 Hz

The spectral amplitude under the unstimulated condition was higher in athletes than in controls ($P < 0.0001$) (Table 2). Likewise, ACh evoked higher values in athletes than in controls ($P < 0.01$), whereas no difference was observed with SNP stimulation.

Contribution of the different periodic oscillations

Under the unstimulated condition, athletes had higher absolute amplitude than the controls in the frequency bands with peak amplitudes at around 1, 0.04 and 0.01 Hz ($P < 0.0001$, $P < 0.05$ and $P < 0.01$, respectively) (Fig. 4a). The relative amplitudes under the unstimulated condition uncovered differences between the two groups at four of the periodic oscillations, where athletes had lower amplitudes of the oscillations with peak amplitude at around 0.3, 0.1 and 0.04 Hz ($P < 0.01$, $P < 0.05$ and $P < 0.05$, respectively) than controls, whereas athletes had higher values for oscillations with a peak amplitude at around 1 Hz ($P < 0.05$) (Fig. 4b). In addition, athletes had higher absolute amplitude during iontophoresis with ACh than the controls in the frequency band with peak amplitude around 1 and 0.01 Hz ($P < 0.01$ and $P < 0.05$) (Fig. 5a), whereas the relative amplitude of oscillations with a peak amplitude at around 0.3 Hz was lower ($P < 0.0001$) and for oscillation at around 1 Hz ($P < 0.05$) it was higher (Fig. 5b). We found no significant differences in absolute or relative amplitude during iontophoresis with SNP between the athletes and the controls (Fig. 6).

Discussion

This study indicates that enhanced responsiveness of the vascular endothelium is induced by physical training and that this enhanced endothelial activity may be evaluated by the dynamic approach of spectral analysis based on wavelet transformation of periodic oscillations in the cutaneous LDF signal.

Oscillations modulated by vascular endothelium

A major finding was a higher ACh-induced cutaneous perfusion both in average and dynamic values in the athletes compared with the controls. The latter was demonstrated by a higher average spectral amplitude and absolute amplitude of the oscillations at around 0.01 Hz in athletes compared with their controls.

ACh acts indirectly on vascular smooth muscle cells, via the production of endothelial factors, whereas SNP

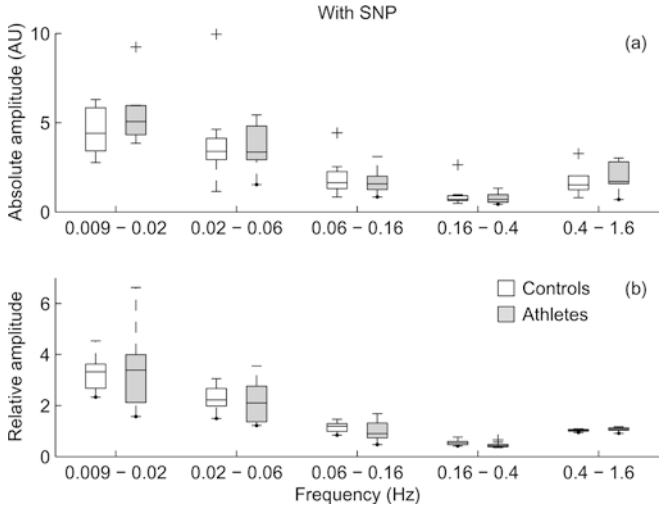

Fig. 6 The average (**a**) and relative (**b**) amplitude for all five frequency intervals in the frequency spectrum from 0.009 to 1.6 Hz of the laser Doppler perfusion signal in controls (*open symbols*) and athletes (*filled symbols*) during iontophoresis with SNP recorded in arbitrary units (AU). The five horizontal lines on the box show the 10, 25, 50, 75 and 90th percentiles. The values above or below the 10th and 90th percentiles are represented as data points. *P* values are given on the figure

is an endothelium-independent vasodilator that acts directly on smooth muscle cells (Rapoport et al. 1983). ACh has been used to demonstrate impaired endothelium-mediated vasodilatation in diabetes mellitus, essential hypertension, hypercholesterolaemia, heart failure and atherosclerosis (Drexler 1997; Andreassen et al. 1998). The higher ACh-induced cutaneous perfusion among the athletes compared with the controls seen in the present study is in agreement with enhanced endothelial responses among athletes compared with less trained subjects (Kvernmo et al. 1998a). These results indicate that regular exercise induces an enhanced endothelial capacity for vasodilatation, which in skeletal muscles may result in an enhanced oxygen delivery due to a decrease in vascular resistance.

Endothelial function may be evaluated non-invasively by analysing the periodic oscillations in the cutaneous circulation by spectral analysis based on a wavelet transformation (Kvernmo et al. 1999). Whereas the four fastest oscillations are influenced by the heart beat, respiration, intrinsic myogenic activity of vascular smooth muscle, and neurogenic activity on the vessel wall, the fifth and slowest oscillation (0.01 Hz) is modified by the microvascular endothelium (Kvernmo et al. 1999). This was revealed by Kvernmo et al. (1999) or in the present study by evaluating the effect of ACh and SNP on the periodic oscillations of the cutaneous perfusion. Our finding suggests that the activity of the vascular endothelium is an almost periodic phenomenon with a repetition time of approximately 1 min. The higher peak amplitude at around 0.01 Hz evoked by ACh indicates enhanced endothelial vasodilator properties among athletes. A higher peak amplitude of the endothelial oscillations at around 0.01 Hz in athletes was also demonstrated in unstimulated perfusion, which illustrates the consistency of the results.

To evaluate whether physical conditioning makes vascular smooth muscle cells more sensitive to NO, we compared the vasodilatation response to an NO donor (SNP) in athletes and controls. SNP evokes vascular relaxation by increasing guanosine 3′,5′-cyclic monophosphate (cGMP) in vascular smooth muscle cells (Rapoport et al. 1983), and the relaxation is not dependent on a intact vascular endothelium. Our data demonstrated no significant difference between the athletes and controls in response to SNP either in the static or in dynamic data, indicating no difference in the dilator capacity or vascularity between the groups. The data also indicated that the higher ACh-induced skin perfusion among athletes compared with controls, was not due to alterations in vascular smooth muscle relaxation via the cGMP mechanism, but rather due to increased levels of endothelial factors reaching vascular smooth muscle cells. This is in agreement with data from animals (Delp et al. 1993) and humans (Kingwell et al. 1996). An in vitro study of human subcutaneous resistance vessels suggested that both NO and prostaglandins are involved in ACh-induced relaxation (Richards et al. 1990). However, Morris and Shore (1996) concluded that mechanisms other than prostaglandins and sensory nerve activation may be involved in skin perfusion following iontophoresis with ACh. Kreidstein et al. (1992) who studied endothelium-dependent and endothelium-independent vasodilatation in skin flaps, proposed that ACh-induced vasodilatation is mediated by NO, since the response was reduced when an inhibitor of NO synthesis was administered. To what extent other substances, such as endothelium-derived hyperpolarisation factor, contribute to ACh-induced vasodilatation remains to be elucidated. The present results simply show that an endothelium-dependent vasodilator increases the cutaneous blood perfusion to a higher level among athletes compared with controls. However, the mechanisms for ACh-induced increase in perfusion are not determined, but may occur at any stage between the action of ACh on its receptors and the release of NO.

Other oscillators of the cutaneous blood perfusion

The LDF data we obtained during unstimulated condition demonstrated a higher absolute, but lower relative amplitude of the oscillations with a peak at around 0.04 Hz in athletes than in controls, whereas no difference was observed during iontophoresis with ACh and SNP. Oscillations at around 0.04 Hz disappear in humans after denervation, after local and ganglionic nerve blockade and after sympathectomy (Kastrup et al. 1989). Thus, our results suggest a higher total neurogenic contribution to the unstimulated blood flow in athletes than in the controls. Our results also suggest that the neurogenic component contributes relatively less to the blood flow than the other regulators of the

cutaneous blood flow in athletes than in controls, which may be explained by the relatively higher contribution of the heart beat oscillation (1 Hz) in the athletes.

The present study also demonstrated lower relative amplitudes of the oscillations with a peak amplitude at around 0.1 Hz among athletes than in controls under unstimulated condition. Oscillations at around 0.1 Hz are suggested to reflect the intrinsic myogenic activity of smooth muscle cells in resistance vessels (Salerud et al. 1983; Meyer et al. 1988; Intaglietta 1989, Kastrup et al. 1989; Hoffmann et al. 1990; Bollinger et al. 1991; Stefanovska 1992). Thus, these results may suggest that athletes have decreased vasomotion induced by the intrinsic activity of vascular smooth muscle cells than controls.

Periodic oscillations at around 0.3 Hz are synchronous with respiration (Stefanovska 1992; Bollinger et al. 1993; Mück-Weymann et al. 1996; Stefanovska and Kroselj 1997), and can be explained by a coupling between the respiratory and circulatory system mediated by the autonomic nervous system and by respiratory-dependent, left cardiac preload alterations (Schmid-Schönbein et al. 1992). The lower relative amplitude of the oscillations at around 0.3 Hz among athletes, of both cutaneous blood perfusion signals obtained during the unstimulated condition and during iontophoresis with ACh, indicate a lower contribution of the respiratory-dependent oscillations to the blood perfusion in athletes than in controls.

Finally, athletes had higher absolute and relative amplitudes of the oscillations at around 1 Hz both during unstimulated perfusion and during iontophoresis with ACh. Since these oscillatory changes are thought to reflect the pulsatile flow of the cardiac cycle (Stefanovska 1992; Bollinger et al. 1993; Mück-Weymann et al. 1996; Stefanovska and Kroselj 1997), the higher absolute amplitude of these oscillations in the trained subjects may reflect an increased stroke volume.

Conclusion

The present study demonstrated that the endothelium-dependent vasodilator ACh selectively enhances the amplitude of oscillations at around 0.01 Hz in the cutaneous LDF signal to a greater extent in athletes than in less trained subjects. The study also demonstrated enhanced amplitude of the oscillations at around 0.01 Hz in the unstimulated cutaneous LDF signal in athletes. Oscillation at around 0.01 Hz is considered to be modulated by the vascular endothelium. Therefore, the present results indicate that endothelium-mediated vasodilatation is manifested in the steady value of the LDF perfusion and also as an oscillatory activity. Importantly, our results suggest that the oscillatory activity of the endothelium may be evaluated by spectral analysis, and that this can provide complementary information about the mechanisms of microvascular regulation.

Acknowledgements We acknowledge Moor Instruments, UK, for providing the devices used in this study, with a special word of thanks to Rodney Gush. We are also grateful to Maja Bracic for technical assistance. A.S. was supported by the Slovenian Ministry of Education, Science and Sport. H.D.K. was supported by the Norwegian Research Council for Science and Humanities.

References

Andreassen AK, Kvernebo K, Jørgensen B, Simonsen S, Kjekshus J, Gullestad L (1998) Exercise capacity in heart transplant recipients: Relation to impaired endothelium-dependent vasodilatation of the peripheral microcirculation. Am Heart J 136:320–328

Bollinger A, Hoffmann U, Franzeck UK (1991) Evaluation of flux motion in man by the laser Doppler technique. Blood Vessels 28:21–26

Bollinger A, Yanar A, Hoffmann U, Franzeck UK (1993) Is high-frequency fluxmotion due to respiration or to vasomotion activity? In: Messmer K (ed) Progress in applied microcirculation. Karger, Basel, pp. 52–58

Delp MD (1995) Effects of exercise training on endothelium-dependent peripheral vascular responsiveness. Med Sci Sports Exerc 27:1152–1157

Delp MD, McAllister RM, Laughlin MH (1993) Exercise training alters endothelium-dependent vasoreactivity of rat abdominal aorta. J Appl Physiol 73:1354–1363

Drexler H (1997) Endothelial dysfunction: Clinical implications. Prog Cardiovasc Dis 4:287–324

Hoffmann U, Franzeck UK, Geiger M, Bollinger A (1990) Variability of different patterns of skin oscillatory flux in healthy controls and patients with peripheral arterial occlusive disease. Int J Microcirc Clin Exp 12:255–273

Intaglietta M (1989) Vasomotion and flow modulation in the microcirculation. In: Intaglietta M (ed) Progress in applied microcirculation, vol 15. Karger, Basel, pp 1–9

Kastrup J, Bühlow J, Lassen NA (1989) Vasomotion in human skin before and after local heating recorded with laser Doppler flowmetry. A method for induction of vasomotion. Int J Microcirc Clin Exp 8:205–215

Kingwell BA, Tran B, Cameron JD, Jennings GL, Dart AM (1996) Enhanced vasodilation to acetylcholine in athletes is associated with lower plasma cholesterol. Am J Physiol 270:H2008–H2013

Kreidstein ML, Pang CY, Carlsen LN, Xu N (1992) Evidence for endothelium-dependent and endothelium-independent vasodilation in human skin flaps. Can J Physiol Pharmacol 70:1208–1216

Kvernmo HD, Stefanovska A, Kirkebøen KA, Østerud B, Kvernebo K (1998a) Enhanced endothelium-dependent vasodilatation in human skin vasculature induced by physical conditioning. Eur J Appl Physiol 79:30–39

Kvernmo HD, Stefanovska A, Kirkebøen KA, Kvernebo K (1998b) Spectral analysis of the laser Doppler perfusion signal in human skin before and after exercise. Microvasc Res 56:173–182

Kvernmo HD, Stefanovska A, Kirkebøen KA, Kvernebo K (1999) Oscillations in the cutaneous blood flow signal modified by endothelium-dependent and endothelium-independent vasodilators. Microvasc Res 57:298–309

Meyer JU, Borgström P, Lindblom L, Intaglietta M (1988) Vasomotion patterns in skeletal muscle arterioles during changes in arterial pressure. Microvasc Res 35:193–203

Morlet J (1983) Sampling theory and wave propagation. In: Chen CH (ed) NATO ASI series, vol I, Issues in acoustic signal/image processing and recognition. Springer, Berlin Heidelberg New York

Morris SJ, Shore AC (1996) Skin blood flow responses to the iontophoresis of acetylcholine and sodium nitroprusside in man: possible mechanisms. J Physiol (Lond) 496:531–542

Mück-Weymann ME, Albrecht H-P, Hager D, Hiller D, Hornstein OP, Bauer RD (1996) Respiratory-dependent laser-Doppler flux motion in different skin areas and its meaning to autonomic nervous control of the vessels of the skin. Microvasc Res 52: 69–78

Müller PH, Keller R, Imhof P (1987) Laser Doppler flowmetry, a reliable technique for measuring pharmacologically induced changes in cutaneous blood flow. Methods Find Exp Clin Pharmacol 9:409–420

Nilsson GE, Tenland T, Öberg PÅ (1980) Evaluation of a laser Doppler flowmeter for measurement of tissue blood flow. IEEE Trans Biomed Eng 27:597–604

Rapoport RM, Draznin MB, Murad F (1983) Endothelium-dependent relaxation in rat aorta may be mediated through cyclic GMP-dependent protein phosphorylation. Nature 306:174–176

Richards NT, Poston L, Hilton L (1990) Cyclosporin A inhibits endothelium-dependent prostanoid-induced relaxation in human subcutaneous resistance vessels. J Hypertens 3:159–163

Rubanyi GM (1993) The role of endothelium in cardiovascular homeostasis and diseases. J Pharmacol 22 [Suppl 4]:S1–S4

Salerud EG, Tenland T, Nilsson GE, Öberg PÅ (1983) Rhythmical variations in human skin blood flow. Int J Microcirc Clin Exp 2:91–102

Schmid-Schönbein H, Ziege S, Rütten W, Heidtmann H (1992) Active and passive modulations of cutaneous red cell flux as measured by laser Doppler anemometry. Vasa [Suppl] 34: 38–47

Stefanovska A (1992) Self-organization of biological systems influenced by electrical current. Thesis, Faculty of Electrical Engineering, University of Ljubljana, Slovenia

Stefanovska A, Kroselj P (1997) Correlation integral and frequency analysis of cardiovascular functions. Open Sys Inform Dyn 4:457–478

Vallance P, Collier J, Moncada S (1989) Effects of endothelium-derived nitric oxide on peripheral arteriolar tone in man. Lancet 2:997–1000

Westerman RA, Widdop RE, Hannaford A, Low A, Roberts RGD, Kent P, Sideris K, Yip T, Hales JRS, Stephens FRN (1988) Laser Doppler velocimetry in the measurement of neurovascular function. Aust Phys Eng Sci Med 11:53–65

PHYSICAL REVIEW E **68**, 016201 (2003)

Time-phase bispectral analysis

Janez Jamšek,[1,2,3,*] Aneta Stefanovska,[1,3,†] Peter V. E. McClintock,[3,‡] and Igor A. Khovanov[3,4,§]
[1]*Group of Nonlinear Dynamics and Synergetics, Faculty of Electrical Engineering, University of Ljubljana, Tržaška 25, 1000 Ljubljana, Slovenia*
[2]*Department of Physics and Technical Studies, Faculty of Education, University of Ljubljana, Kardeljeva ploščad 16, 1000 Ljubljana, Slovenia*
[3]*Department of Physics, University of Lancaster, Lancaster LA1 4YB, United Kingdom*
[4]*Laboratory of Nonlinear Dynamics, Saratov State Unversity, 410026 Saratov, Russia*
(Received 8 January 2003; published 3 July 2003)

Bispectral analysis, a technique based on high-order statistics, is extended to encompass time dependence for the case of coupled nonlinear oscillators. It is applicable to univariate as well as to multivariate data obtained, respectively, from one or more of the oscillators. It is demonstrated for a generic model of interacting systems whose basic units are the Poincaré oscillators. Their frequency and phase relationships are explored for different coupling strengths, both with and without Gaussian noise. The distinctions between additive linear or quadratic, and parametric (frequency modulated), interactions in the presence of noise are illustrated.

DOI: 10.1103/PhysRevE.68.016201 PACS number(s): 05.45.Df, 02.70.Hm, 05.45.Xt

I. INTRODUCTION

Most real systems are nonlinear and complex. In general, they may be regarded as a set of interacting subsystems; given their nonlinearity, the interactions can be expected to be nonlinear too.

The phase relationships between a pair of interacting oscillators can be obtained from bivariate data (i.e., where the coordinate of each oscillator can be measured separately) by use of the methods recently developed for analysis of synchronization, or generalized synchronization, between chaotic and/or noisy systems. Not only can the interactions be detected [1], but their strength and direction can also be determined [2]. The next logical step in studying the interactions among coupled oscillators must be to determine the nature of the couplings: the methods developed for synchronization analysis are not capable of answering this question.

Studies of higher-order spectra, or polyspectra, offer a promising way forward. The approach is applicable to interacting systems quite generally, regardless of whether or not they are mutually synchronized. Following the pioneering work of Brillinger and Rosenblatt [3], increasing applications of polyspectra in a diversity of fields have appeared, e.g., telecommunications, radar, sonar, speech, biomedical, geophysics, imaging systems, surface gravity waves, acoustics, econometrics, seismology, nondestructive testing, oceanography, plasma physics, and seismology. An extensive overview can be found in Ref. [4]. The use of the bispectrum as a means of investigating the presence of second-order nonlinearity in interacting harmonic oscillators has been of particular interest during the last few years [5–8].

Systems are usually taken to be stationary. For real systems, however, the mutual interaction among subsystems often results in time variability of their characteristic frequencies. Frequency and phase couplings can occur temporally, and the strength of coupling between pairs of individual oscillators may change with time. In studying such systems, bispectral analysis for stationary signals, based on time averages, is no longer sufficient. Rather, the time evolution of the bispectral estimates is needed.

Priestley and Gabr [9] were probably the first to introduce the time-dependent bispectrum for harmonic oscillators. Most of the subsequent work has been related to the time-frequency representation and is based on high-order cumulants [10]. The parametric approach has been used to obtain approximate expressions for the evolutionary bispectrum [11]. Further, Perry and Amin have proposed a recursion method for estimating the time-dependent bispectrum [12]. Dandawaté and Giannakis have defined estimators for cyclic and time-varying moments and cumulants of cyclostationary signals [13]. Schack *et al.* [14] have recently introduced a time-varying spectral method for estimating the bispectrum and bicoherence: the estimates are obtained by filtering in the frequency domain and then obtaining a complex time-frequency signal by inverse Fourier transform. They assume, however, that the interacting oscillators are harmonic.

Millingen *et al.* [15] introduced the wavelet bicoherence and were the first to demonstrate the use of bispectra for studying interactions among nonlinear oscillators. They used the method to detect periodic and chaotic interactions between two coupled van der Pol oscillators, but without concentrating on time-phase relationships, in particular.

In this paper we develop an approach [16] that introduces time dependance to the bispectral analysis of univariate data. We focus on the time-phase relationships between two (or more) interacting systems. As we demonstrate below, the method enables us to detect that two or more subsystems are interacting with each other, to quantify the strength of the interaction, and to determine its nature, whether additive linear or quadratic, or parametric in one of the frequencies. It yields results that are applicable quite generally to any system of coupled nonlinear oscillators. Our principal motiva-

*Electronic address: janez.jamsek@pef.uni-lj.si
†Electronic address: aneta@osc.fe.uni-lj.si
‡Electronic address: p.v.e.mcclintock@lancaster.ac.uk
§Electronic address: igor@chaos.ssu.runnet.ru

tion has been to develop a technique for studying the human cardiovascular system [17], including the interactions among its subsystems, and the nature of these interactions. Here, however, we are concerned with basic principles, and in demonstrating (testing) the technique on a well-characterized simple model. Application to the more challenging problem posed by the cardiovascular system, currently in progress, will be described in a subsequent publication.

II. METHOD

A. Bispectral analysis

Bispectral analysis belongs to a group of techniques based on high-order statistics (HOS) that may be used to analyze non-Gaussian signals, to obtain phase information, to suppress Gaussian noise of unknown spectral form, and to detect and characterize signal nonlinearities [5]. In what follows we extend bispectral analysis to extract useful features from nonstationary data, and we demonstrate the modified technique by application to test signals generated from coupled oscillators.

The bispectrum involves third-order statistics. Spectral estimation is based on the conventional Fourier type direct approach, through computation of the third-order moments which, in the case of third-order statistics, are equivalent to third-order cumulants [5,18–21].

The classical bispectrum estimate is obtained as an average of estimated third-order moments (cumulants) $\hat{M}_3^i(k,l)$,

$$\hat{B}(k,l)=\frac{1}{K}\sum_{i=1}^{K}\hat{M}_3^i(k,l), \tag{1}$$

where the third-order moment estimate $\hat{M}_3^i(k,l)$ is performed by a triple product of discrete Fourier transforms (DFTs) at discrete frequencies k, l, and $k+l$:

$$\hat{M}_3^i(k,l)=X_i(k)X_i(l)X_i^*(k+l), \tag{2}$$

with $i=1,\ldots,K$ segments into which the signal is divided to try to obtain statistical stability of the estimates, see the Appendix.

Just as the discrete power spectrum has a point of symmetry at the folding frequency $f_s/2$, the discrete bispectrum has many symmetries in the (k,l) plane [22]. Because of these, it is necessary to calculate the bispectrum only in the nonredundant region, or principal domain, as shown in Fig. 1. The principal domain can be divided into two triangular regions in which the discrete bispectrum has different properties: the inner triangle (IT) and the outer one [23]. In the current work it is the IT that is of primary interest. Thus, it is sufficient to calculate the bispectrum over the IT of the principal domain defined in Refs. [5,7]: $0\leqslant l\leqslant k$, $k+l\leqslant f_s/2$.

The bispectrum $B(k,l)$ is a complex quantity, defined by magnitude A and phase ϕ,

$$B(k,l)=|B(k,l)|e^{j\angle B(k,l)}=Ae^{j\phi}. \tag{3}$$

Consequently, for each (k,l), its value can be represented as a point in a complex space, Re$[B(k,l)]$ versus Im$[B(k,l)]$,

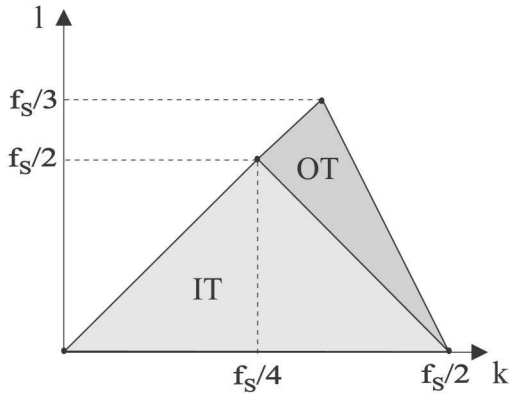

FIG. 1. The principal domain of the discrete bispectrum of a band-limited signal can be divided into two triangular regions, the inner triangle (IT) and the outer triangle (OT). k and l are discrete frequencies, f_S is the sampling frequency.

thus defining a vector. Its magnitude (length) is known as the biamplitude. The phase, which for the bispectrum is called the biphase, is determined by the angle between the vector and the positive real axis.

The bispectrum quantifies the relationships among the underlying oscillatory components of the observed signals. Specifically, bispectral analysis examines the relationships between the oscillations at two basic frequencies, k and l, and a harmonic component at the frequency $k+l$. This set of three frequencies is known as a triplet $(k,l,k+l)$. The bispectrum $B(k,l)$, a quantity incorporating both phase and power information, can be calculated for each triplet.

A high bispectrum value at bifrequency (k,l) indicates that there is at least frequency coupling within the triplet of frequencies k, l, and $k\pm l$. Strong coupling implies that the oscillatory components at k and l may have a common generator. Such components may synthesize a new component at the combinatorial frequency $k\pm l$ if a quadratic nonlinearity is present.

B. Time-phase bispectral analysis

The classical bispectral method is adequate for studying stationary signals whose frequency content is preserved over time. We now wish to encompass time dependance within the bispectral analysis. In analogy with the short-time Fourier transform, we accomplish this by moving a time window $w(n)$ of length M across the signal $x(n)$, calculating the DFT at each window position

$$X(k,n)\cong\frac{1}{M}\sum_{n=0}^{M-1}x(n)w(n-\tau)e^{-j2\pi nk/M}. \tag{4}$$

Here, k is the discrete frequency, n the discrete time, and τ the time shift. The choice of window length M is a compromise between achieving optimal frequency resolution and optimal detection of the time variability. The instantaneous biphase is then calculated: from Eqs. (2) and (3), it is

$$\phi(k,l,n)=\phi_k(n)+\phi_l(n)-\phi_{k+l}(n). \tag{5}$$

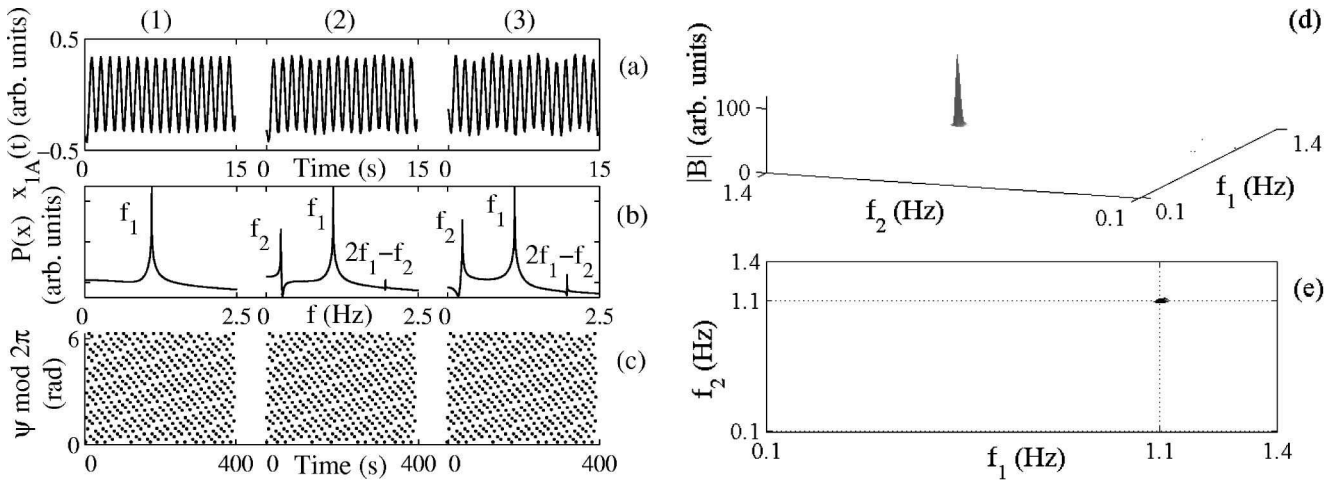

FIG. 2. Results in the absence of noise. (a) The test signal $x_{1A}(t)$, variable x_1 of the first oscillator with characteristic frequency $f_1 = 1.1$ Hz. The characteristic frequency of the second oscillator is $f_2 = 0.24$ Hz. The oscillators are unidirectionally and linearly coupled with three different coupling strengths: $\eta_2 = 0.0$ (1), 0.1 (2), and 0.2 (3). Each coupling lasts for 400 s at sampling frequency $f_s = 10$ Hz. Only the first 15 s are shown in each case. (b) The power spectrum and (c) synchrogram. (d) The bispectrum $|B|$, using $K = 33$ segments, 66% overlapping, and the Blackman window to reduce leakage and (e) its contour view.

If the two frequency components k and l are frequency and phase coupled, $\phi_{k+l} = \phi_k + \phi_l$, it holds that the biphase is 0 (2π) radians. For our purposes the phase coupling is less strict because dependent frequency components can be phase delayed. We consider phase coupling to exist if the biphase is constant (but not necessarily $= 0$ radians) for at least several periods of the lowest frequency component. Simultaneously, we observe the instantaneous biamplitude from which it is possible to infer the relative strength of the interaction. We thus hope to be able to observe the presence and persistence of coupling among the oscillators.

III. ANALYSIS

To illustrate the essence of the method, and to test it, we use a generic model of interacting systems whose basic unit is the Poincaré oscillator:

$$\dot{x}_i = -x_i q_i - \omega_i y_i + g_{x_i},$$

$$\dot{y}_i = -y_i q_i + \omega_i x_i + g_{y_i}, \tag{6}$$

$$q_i = \alpha_i(\sqrt{x_i^2 + y_i^2} - a_i).$$

Here x and y are vectors of the oscillator state variables, α_i, a_i and ω_i are constants, and $g_y(y)$ and $g_x(x)$ are coupling vectors. The activity of each subsystem is described by the two state variables x_i and y_i, where $i = 1, \ldots, N$ denotes the subsystem.

The form of the coupling terms can be adjusted to study different kinds of interaction among the subsystems, e.g., additive linear or quadratic, or parametric frequency modulation. Examples will be considered both without and with a zero-mean white Gaussian noise to obtain more realistic conditions.

Different cases of interaction are demonstrated for signals generated by the proposed model. In each case we analyze the x_1 variable of the first oscillator, recorded as a continuous time series. For the first 400 s, the interoscillator coupling strength was zero. It was then raised to a small constant value. After a further 400 s, it was increased again. The first 15 s and corresponding power spectrum for each coupling strength are shown in the figures for each test signal, in order to demonstrate the changes in spectral content and behavior caused by the coupling. For bispectral analysis the whole signal is analyzed as a single entity, but the transients caused by the changes in coupling strength are removed prior to processing. First the classical bispectrum is estimated. Bifrequencies where peaks provide evidence of possible frequency interactions are then further studied by the calculation of the biphase and biamplitude as functions of time. They were calculated using a window of length 100 s, moved across the signal in 0.3 s steps.

A. Linear couplings

Let us start with the simplest case of a linear interaction between coupled oscillators. We suppose model (6) to consist of only two oscillators, $i = 1,2$. The parameters of the model are set to $\alpha_1 = 1$, $a_1 = 0.5$ and $\alpha_2, a_2 = 1$. The coupling term is unidirectional and linear

$$g_{x_1} = \eta_2 x_2, \quad g_{y_1} = \eta_2 y_2. \tag{7}$$

The test signal $x_{1A}(t)$ is the variable x_1 of the first oscillator. It is presented in Fig. 2(a) with the corresponding power spectrum for three different coupling strengths: no coupling $\eta_2 = 0$ and weak couplings $\eta_2 = 0.1,0.2$. The peaks labeled as $f_1 = 1.1$ Hz and $f_2 = 0.24$ Hz are the independent harmonic components of the first and the second oscillator. These frequencies are deliberately chosen to approximately have a noninteger ratio. There is also at least one peak

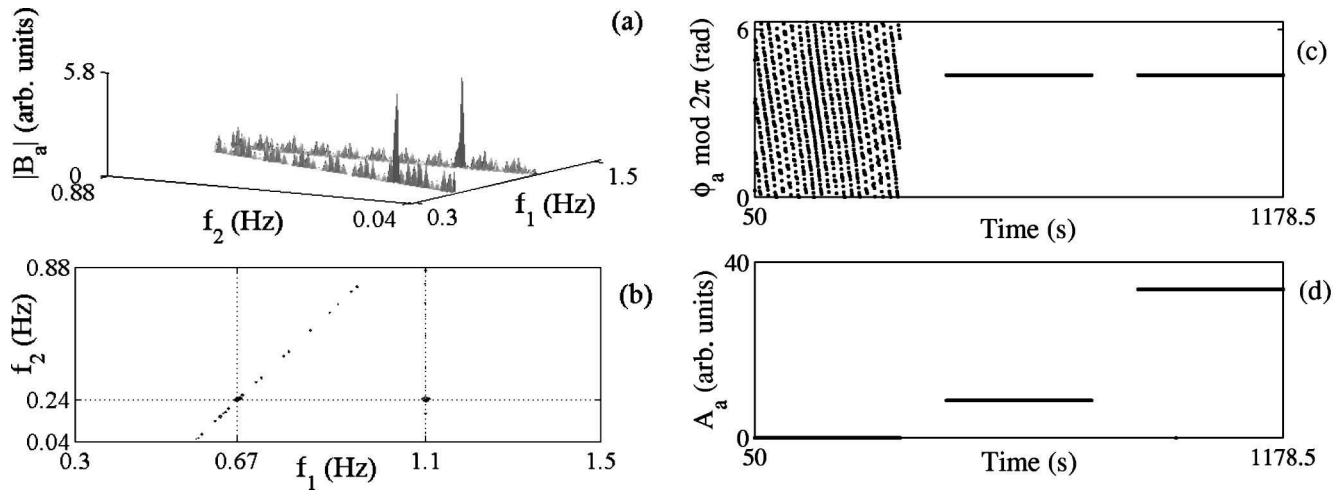

FIG. 3. (a) Adapted bispectrum $|B_a|$, calculated from the test signal x_{1A} using $K=34$ segments, 80% overlapping, and the Blackman window and (b) its contour view. Regions of the adapted bispectrum above $f_2>0.88$ Hz and below $f_1<0.3$ Hz are cut, because the triplets (1.1 Hz,1.1 Hz,1.1 Hz) and (0.24 Hz,0.24 Hz,0.24 Hz) produce high peaks that are physically meaningless. (c) Adapted biphase ϕ_a and (d) biamplitude A_a for bifrequency (1.1 Hz,0.24 Hz), using a 0.3-s time step and a 100-s-long Blackman window for estimating the DFT.

present at the harmonically related position $f_3=2f_1-f_2$ attributable to interaction between the two oscillators. It arises from the nonlinearity of the first oscillator, but is caused by the forcing of the second oscillator.

The principal domain of the bispectrum for the test signal x_{1A}, Fig. 2(d), shows one peak at the bifrequency (1.1 Hz, 1.1 Hz), the so-called self-coupling. No other peaks are present. Bispectral analysis examines the relationships between oscillations at the two basic frequencies f_1 and f_2, and a modulation component at the frequency $f_1\pm f_2$, which is absent from the power spectra in Fig. 2(b). Therefore, no peak is present at bifrequency (1.1 Hz,0.24 Hz). Thus, the method as it stands is incapable of detecting the presence of linear coupling between the oscillators by analysis of the test signal x_{1A}. Nonetheless, we still suggest the use of bispectral analysis to investigate the presence of nonlinearity, but based on an adapted way of calculating the bispectrum.

In general, the bispectral method can be used to examine phase and frequency relationships at arbitrary time. It is thus well suited for detecting the presence of quadratic couplings and frequency modulation, since they both give rise to frequency components at the sum and difference of the interacting frequency components.

To be able to detect linear couplings using the bispectral method, as proposed, it is necessary to change the frequency relation. Study of coupled Poincaré oscillators demonstrate the presence of a component at frequency $2k-l$ as a consequence of nonlinearity. This component was detected numerically, and is not necessarily characteristic of all nonlinear oscillators. By modifying the bispectral definition to

$$B_a(k,l)=E[X(k)X(l)X^*(2k-l)], \tag{8}$$

the biphase turns into

$$\phi_a(k,l)=\phi_k+\phi_l-\phi_{2k-l}-\phi_c, \tag{9}$$

where index a is introduced and will be used in what follows to indicate that the values are obtained using the adapted method. To obtain 0 radians in the case of phase coupling we have to correct the adapted biphase expression (9) by subtracting $\phi_c=2\phi_l-\phi_k$. In the presence of a harmonically related frequency component and phase coupling, the biphase will then be 0 radians.

The adapted bispectrum $|B_a|$ for the signal x_{1A} exhibits several peaks, as shown in Fig. 3(a). It peaks where $f_1=f_2$; a triple product (f_1,f_2,f_3) of power at frequencies $f_1=f_2=f$, and also $f_3=2f_1-f_2=f$, raises a high peak at the bifrequency (f,f). The self-coupling peak is physically meaningless, and it is therefore cut from the adapted bispectrum. It can be used for additional checking, since it strongly implies nonlinearity [6].

The peak of primary interest is at bifrequency (1.1 Hz, 0.24 Hz). There is also a high peak positioned at bifrequency (0.67 Hz,0.24 Hz) lying on the line where the third frequency in the triplet is equal to the frequency of the first oscillator and is therefore a consequence of the method. The small peaks present in the adapted bispectrum are the result of numerical rounding error and leakage effects due to the DFT calculation.

The peak (1.1 Hz,0.24 Hz) indicates that oscillations at those pairs of frequencies are at least linearly frequency coupled. Frequency coupling alone is sufficient for a peak in the bispectrum to occur. Although the situation can in principle arise by coincidence, frequency and phase coupling together strongly imply the existence of nonlinearities. To be able to distinguish between different possible couplings, we calculate the adapted biphase Fig. 3(c).

During the first 400 s of test signal x_{1A}, where no coupling is present, the adapted biphase changes continuously between 0 and 2π radians. For the same time of observation it can be seen that the adapted biamplitude is 0, Fig. 3(d). During the second and third 400 s of the signal x_{1A}, a constant adapted biphase can be observed indicating the pres-

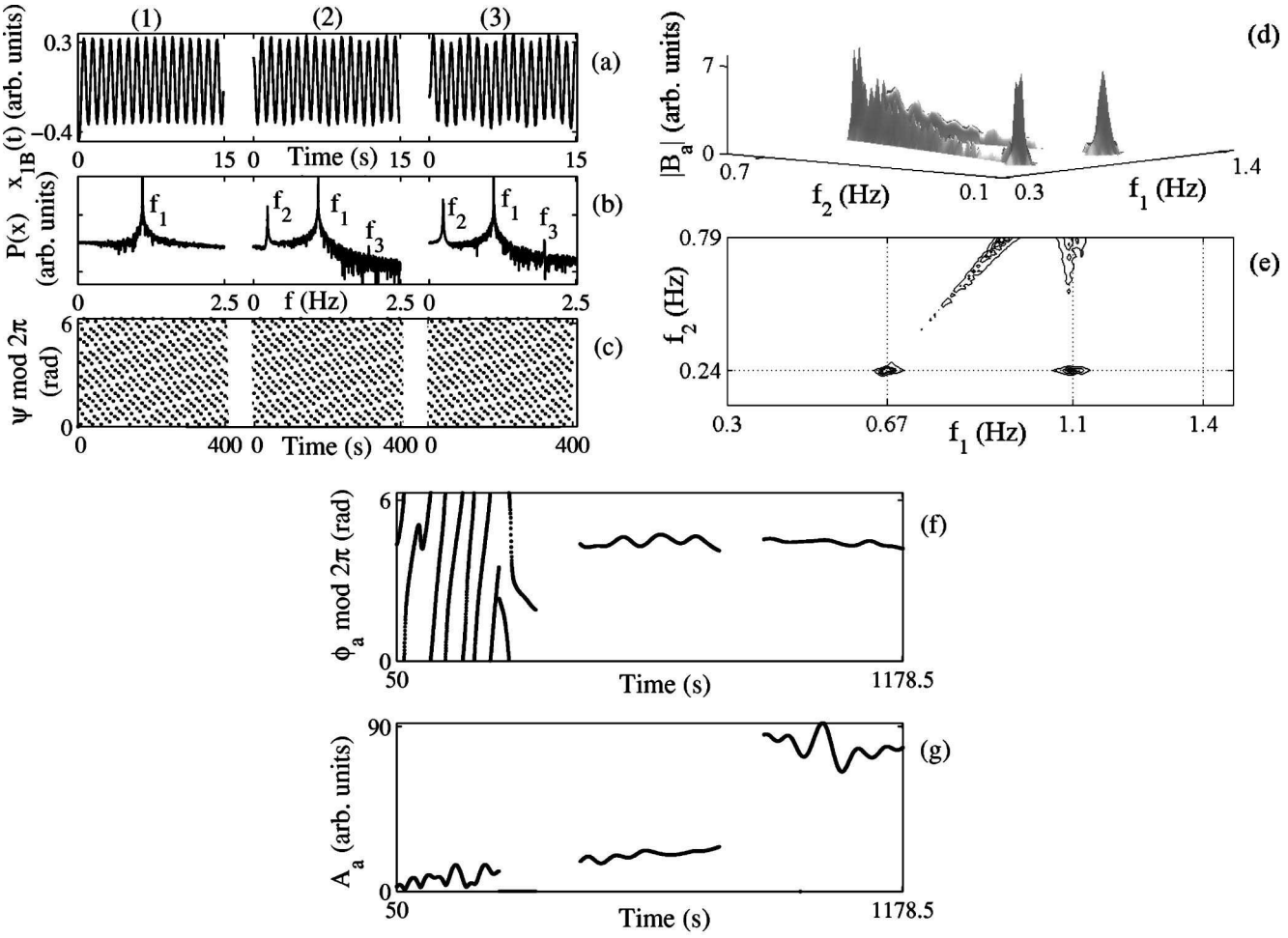

FIG. 4. Results in the presence of additive Gaussian noise. (a) Test signal x_{1B}, variable x_1 of the first oscillator with characteristic frequency $f_1=1.1$ Hz. The characteristic frequency of the second oscillator is $f_2=0.24$ Hz. The oscillators are unidirectionally and linearly coupled with three different coupling strengths; $\eta_2=0.0$ (1), 0.1 (2), and 0.2 (3). Each coupling lasts for 400 s at a sampling frequency $f_s=10$ Hz. Only first 15 s are shown in each case. (b) Its power spectrum and (c) synchrogram. (d) Adapted bispectrum $|B_a|$ using $K=33$ segments, 66% overlapping, and the Blackman window and (e) its contour view. The parts of the $|B_a|$ above $f_2>0.79$ Hz and below $f_1<0.3$ Hz are omitted because the triplets (1.1 Hz,1.1 Hz,1.1 Hz) and (0.24 Hz,0.24 Hz,0.24 Hz) produce a high peak that is physically meaningless. (f) Adapted biphase ϕ_a and (g) adapted biamplitude A_a for bifrequency (1.1 Hz,0.24 Hz), using a 0.3-s time step and a 100-s-long window for estimating the DFT using the Blackman window.

ence of linear coupling. The value of the adapted biamplitude is higher in the case of stronger coupling. The coupling constant η_2 can be obtained by normalization, and we are thus able to define the relative strengths of different couplings.

When the oscillators are coupled bidirectionally the frequency content of each of them changes and components $2f_1$ and $2f_2$ are generated. Both of these characteristic frequencies can be observed in the time series of each oscillator. Two combinatorial components are also present in their spectra, $2f_1-f_2$ and f_1-2f_2, assuming that $f_1>f_2$. In analyzing bidirectional coupling, the procedure described above can be extended and two combinatorial components should be analyzed in the same way.

Making use of the calculated instantaneous phases of both oscillatory components we also construct a synchrogram [Fig. 2(c)], as proposed by Schäfer *et al.* (see Ref. [1] and the references therein), and can immediately establish whether or not the coupling also results in synchronization.

The instantaneous phases can also be used to calculate the direction and strength of coupling, using the methods recently introduced by Schreiber, Rosenblum *et al.*, and Paluš *et al.* [2].

B. Linear couplings in the presence of noise

We now test the method for the case where noise is added to the variable x_1 of the first oscillator:

$$\dot{x}_1=-x_1q_1-\omega_1y_1+g_{x_1}+\xi(t),$$
$$\dot{y}_1=-y_1q_1+\omega_1x_1+g_{y_1}. \tag{10}$$

Here $\xi(t)$ is zero-mean white Gaussian noise, $\langle\xi(t)\rangle=0$, $\langle\xi(t),\xi(0)\rangle=D\delta(t)$, and $D=0.08$ is the noise intensity. In this way we obtain a test signal $x_{1B}(t)$, Fig. 4(a).

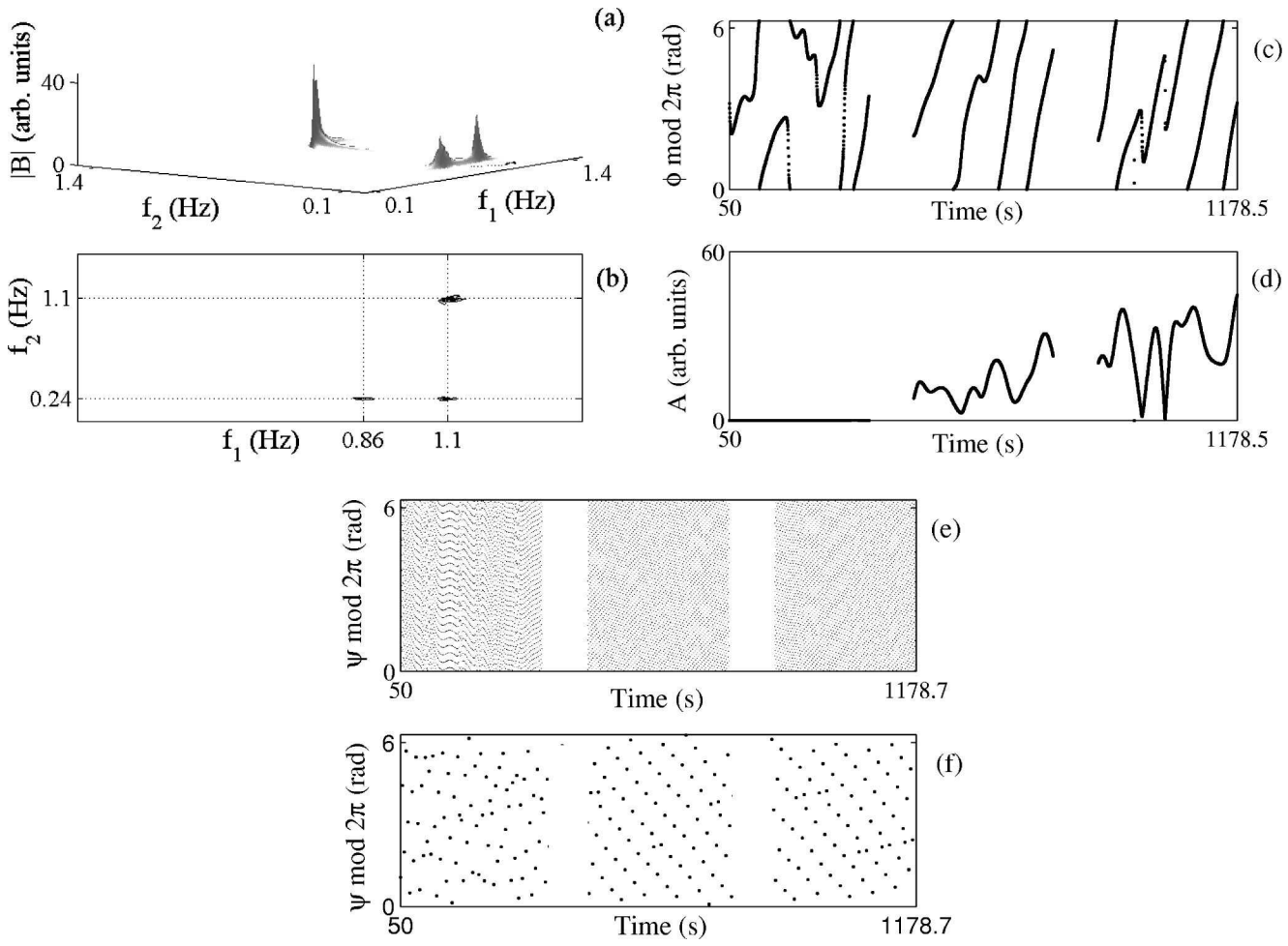

FIG. 5. Bispectrum $|B|$, calculated from the signal x_{1B} presented in Fig. 4(a), using $K=33$ segments, 66% overlapping, and the Blackman window to reduce leakage and (b) its contour view. (c) Biphase ϕ and (d) biamplitude A for bifrequency (1.1 Hz,0.24 Hz), using a 0.3-s time step and a 100-s-long window for estimating the DFTs using a Blackman window. (e) Phase difference ψ between ϕ_1 of the characteristic frequency component f_1 of the first oscillator and ϕ_2 of the characteristic frequency component f_2 of the second oscillator, for time step $1/f_s$ and (f) at each period of lowest frequency $1/f_2$ in the bifrequency pair (1.1 Hz,0.24 Hz), using interpolation and 100-s-long window for estimating DFTs using the Blackman window.

For nonzero coupling strength η_2, the component at frequency position f_3 can still be seen in the power spectrum, despite the noise, Fig. 4(b). The adapted biphase [Fig. 4(f)] can clearly distinguish between the presence and absence of coupling. When coupling is weaker, the adapted biamplitude [Fig. 3(g)] is lower and the adapted biphase is less constant.

The bispectrum for the signal x_{1B}, shown in Fig. 5(a), differs from that in the case of zero noise, Fig. 2(d). Noise raises two additional peaks positioned at (1.1 Hz,0.24 Hz) and (0.86 Hz,0.24 Hz). The former could be the result of interaction; the latter is due to the method: the sum of the frequencies in this bifrequency pair gives the frequency of the first oscillator.

Close inspection of the (0.24 Hz,1.1 Hz) peak by calculation of the biphase gives Fig. 5(c). When coupling is present, the characteristic frequency of the second oscillator appears in the power spectrum [Fig. 4(b)]. Two frequencies of high amplitude result in a small peak even if no harmonics are present at the sum and/or difference frequencies. The second peak is not of interest to us. It can easily be checked whether a phase coupling exists among the bifrequencies from the time evolution of the biphase.

In general, besides estimating bispectral values, one can also observe the time dependences of the phase and amplitude for each frequency component and their phase relationships. This applies particularly to frequencies that form a bifrequency giving a high peak in the bispectrum or adapted bispectrum. Synchrograms, Figs. 2(c) and 4(c), are obtained by first calculating the instantaneous phase of each oscillator and then their phase difference [1]. The phase difference in this case is between two fixed frequencies. We do not calculate their instantaneous frequencies, although it is possible to follow the frequency variation by calculating the phase difference at neighboring bifrequencies around the observed one and showing them simultaneously on the same plot. Examples of the phase difference $\psi=\phi_1-\phi_2$ between the phases of the first ϕ_1 and the second ϕ_2 interacting oscillators are shown in Figs. 5(e) and 5(f).

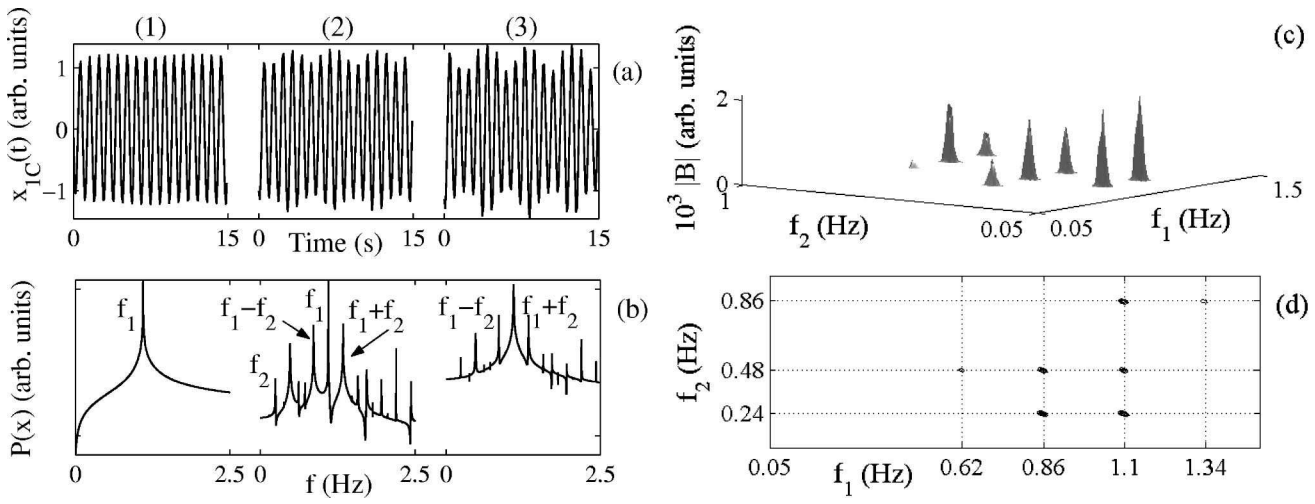

FIG. 6. Results for quadratic coupling in the absence of noise. (a) The test signal x_{1C}, variable x_1 of the first oscillator with characteristic frequency $f_1=1.1$ Hz. The characteristic frequency of the second oscillator is $f_2=0.24$ Hz. Oscillators are unidirectionally and quadratically coupled with three different coupling strengths: $\eta_2=0.0$ (1), 0.05 (2), and 0.1 (3). Each coupling lasts for 400 s at sampling frequency $f_s=10$ Hz. Only the first 15 s are shown in each case. (b) The power spectrum. (c) The bispectrum $|B|$, using $K=33$ segments, 66% overlapping, and the Blackman window to reduce leakage and (d) its contour view. The part of the bispectrum above $f_2>1.0$ Hz is cut, because triplet (1.1 Hz,1.1 Hz,1.1 Hz) produces a high peak that is not physically significant.

C. Quadratic couplings

We now assume that two Poincaré oscillators can interact with each other nonlinearly. A quadratic nonlinear interaction generates higher harmonic components in addition to the characteristic frequencies [5]. In order to study an example where the first $f_1=1.1$ Hz and second $f_2=0.24$ Hz oscillators are quadratically coupled, we change the coupling terms in model (6) to quadratic ones

$$g_{x_1}=\eta_2(x_1-x_2)^2, \quad g_{y_1}=\eta_2(y_1-y_2)^2. \tag{11}$$

Clearly, the test signal x_{1C} presented in Fig. 6(a) for three different coupling strengths [no coupling $\eta_2=0$ (1) and weak couplings $\eta_2=0.05$ (2), $\eta_2=0.1$ (3)] has a richer harmonic structure. In addition to the characteristic frequencies, it contains components with frequencies $2f_1$, $2f_2$, f_1+f_2, and f_1-f_2 [Fig. 6(b)]. Equation (11) also indicates that, as well as having a particular harmonic structure, the components of the signal x_{1C} also have related phases, $2\phi_1, 2\phi_2, \phi_1+\phi_2$, and $\phi_1-\phi_2$.

We expect several peaks [24] to arise in the bispectrum. The peak of principal interest is at bifrequency (1.1 Hz,0.24 Hz). As before, the self-coupling peaks are at (1.1 Hz,1.1 Hz) and (0.24 Hz,0.24 Hz) are of no interest, so they are cut from the bispectrum. Additional peaks appear at the bifrequencies (0.86 Hz,0.24 Hz), (0.62 Hz,0.48 Hz), (0.86 Hz,0.48 Hz), (1.1 Hz,0.48 Hz), (1.1 Hz,0.86 Hz), and (1.34 Hz,0.86 Hz). The triplet of harmonically related frequency components (f_1,f_2,f_3) would peak in the bispectrum when the power for all these frequencies differs from zero. The components 0.48 Hz,0.86 Hz,1.34 Hz, and 2.2 Hz resulting from quadratic couplings form such triplets that peak in the bispectrum: (0.86 Hz,0.24 Hz,1.1 Hz), (0.86 Hz,0.48 Hz, 1.34 Hz), and (1.34 Hz,0.86 Hz,2.2 Hz). Besides these, there are also other peaks, e.g., that at the bifrequency (0.62 Hz, 0.48 Hz) arising from the triplet (0.62 Hz,0.48 Hz,1.1 Hz); the sum-difference combination of such frequencies always give the characteristic frequency, or one that results from quadratic coupling. The existence of such peaks has no other meaning than as a strong indicator of second-order nonlinearity. Consequently, the biphase for all peaks due to possible nonlinear mechanisms in the bispectrum must have the same value, and same behavior, as shown, e.g., in Figs. 7(a) and 7(c). The biphase is constant in the presence of quadratic coupling. From the biamplitude, the coupling constant can be determined by normalization.

In the power spectrum there is a component at frequency $2f_1-f_2$, even although linear coupling is absent. It arises from nonlinearity in the Poincaré oscillator. The adapted bispectrum for the signal x_{1C} shows a peak at bifrequency (1.1 Hz,0.24 Hz), but the adapted biphase varies continuously: we may therefore exclude the possibility of linear coupling being present.

D. Quadratic couplings in the presence of noise

As in the case of linear coupling (Sec. II B) we add a noise term to the quadratic coupling g_{x_1} and obtain the test signal x_{1D}, presented in Fig. 8(a).

Using the bispectral and adapted bispectral methods, we find that we obtain results very similar to those in the absence of noise. The method is evidently noise robust. The results for nonzero coupling are quite different from those where coupling is absent, Fig. 8(e).

E. Frequency modulation in the presence of noise

We are also interested of being able to detect parametric frequency modulation and to distinguish it from quadratic coupling. Parametric modulation produces frequency components at the sum and difference of the characteristic fre-

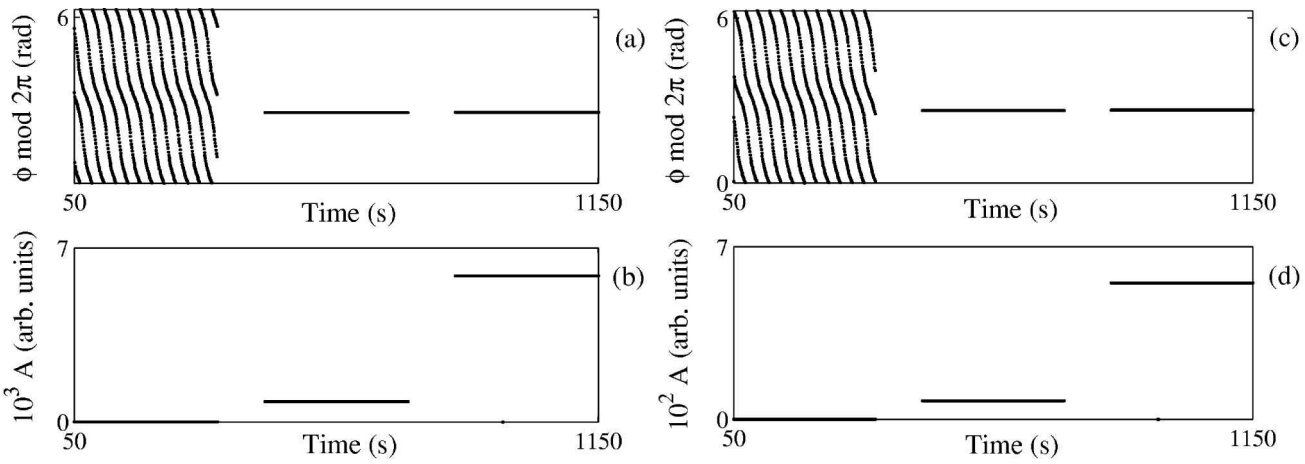

FIG. 7. (a) The biphase ϕ and (b) biamplitude A for the test signal x_{1C} for bifrequency (1.1 Hz,0.24 Hz), using 0.3-s time step and 100-s-long window for estimating DFT using the Blackman window. (c) Biphase and (d) biamplitude for the bifrequency (0.86 Hz,0.24 Hz), with a 0.3-s time step and a 100-s-long window for estimating DFT using the Blackman window.

quency and the modulation frequency, i.e., the same two frequency components that can also result from quadratic coupling. Let us now consider an example where the first oscillator $f_1 = 1.1$ Hz is frequency modulated by the second one $f_2 = 0.24$ Hz. For this purpose the equations of the first oscillator become

$$\dot{x}_1 = -x_1 q_1 - y_1(\omega_1 + \eta_m x_2) + \xi(t),$$
$$\dot{y}_1 = -y_1 q_1 + x_1(\omega_1 + \eta_m y_2). \tag{12}$$

The model parameters $\alpha_{1,2}$, $a_{1,2}$ and the noise intensity D are chosen to be the same as in the previous examples.

We thus obtain a test signal x_{1E}. It is the time evolution of the variable x_1 of the first oscillator, presented in Fig. 9(a) with the corresponding power spectrum 9(b) for three different parametric frequency modulation strengths: no modulation $\eta_m = 0$; and modulation $\eta_m = 0.1, 0.2$. The bispectrum of the test signal x_{1E}, Fig. 9(c), exhibits several high peaks. The highest are at bifrequencies (1.1 Hz,0.86 Hz), (0.86 Hz, 0.24 Hz), and (1.1 Hz,0.24 Hz), in addition to the (1.1 Hz, 1.1 Hz) peak. They also appear in the case of quadratic coupling. In general, however, the other peaks that appear for quadratic coupling are absent. The reason is that although the component of the second oscillator f_2 (one component of the triplet) is not present in the power spectrum, its value is not not exactly zero.

Observing the biphase, no epochs of constant biphase can be observed, although for strong frequency modulation the biphase is less variable. In the power spectrum, Fig. 9(b), no component rises above the noise level at frequency f_2, of the bifrequency pair, where the bispectrum peaks. This is an indication that there is parametric coupling between the oscillators, as there is a high value of biamplitude. The biphase changes runs between 0 and 2π, and is modulated in the absence of noise. There are also no rapid 2π phase slips of the kind that are normal if no modulation is present. In the absence of couplings and modulation, but in the presence of noise, there would be no such peaks in the power spectrum or bispectrum.

IV. SUMMARY AND CONCLUSIONS

We have extended the bispectral method to encompass time dependence and have demonstrated the potential of the extended technique to determine the type of coupling among interacting nonlinear oscillators. Time-phase couplings can be observed by calculating the bispectrum and adapted bispectrum and by obtaining the time-dependent biphase and biamplitude. The method has the advantage that it allows an arbitrary number of interacting oscillatory processes to be studied.

Recently introduced methods for synchronization analysis among chaotic and noisy oscillations (see Ref. [1] and references therein) have stimulated applications to a variety of different systems. Methods for quantifying the strength and identifying the direction of couplings, based on nonlinear dynamic or information theory approaches, have recently been proposed [2]. Here we have addressed the question of the type of coupling that may result in synchronization, and we have proposed a method for its analysis. It is applicable to both univariate data (a single signal from the coupled system) or multivariate data (a separate signal from each oscillator).

Millingen *et al.* [15] have analyzed multivariate data using a combined wavelet and bispectral method, and have discussed its application in the field of chaos analysis. Here we have concentrated on univariate data and illustrated the potential of the time-phase bispectral method for the detection of higher-order couplings in the presence of noise. The possibility of using univariate data is of particular importance when dealing with real signals, as in practice we often cannot observe and measure the separate subsystems directly, but only their combination, which is intrinsically difficult. Most of the methods proposed so far for synchronization analysis and detection of the direction of couplings are based

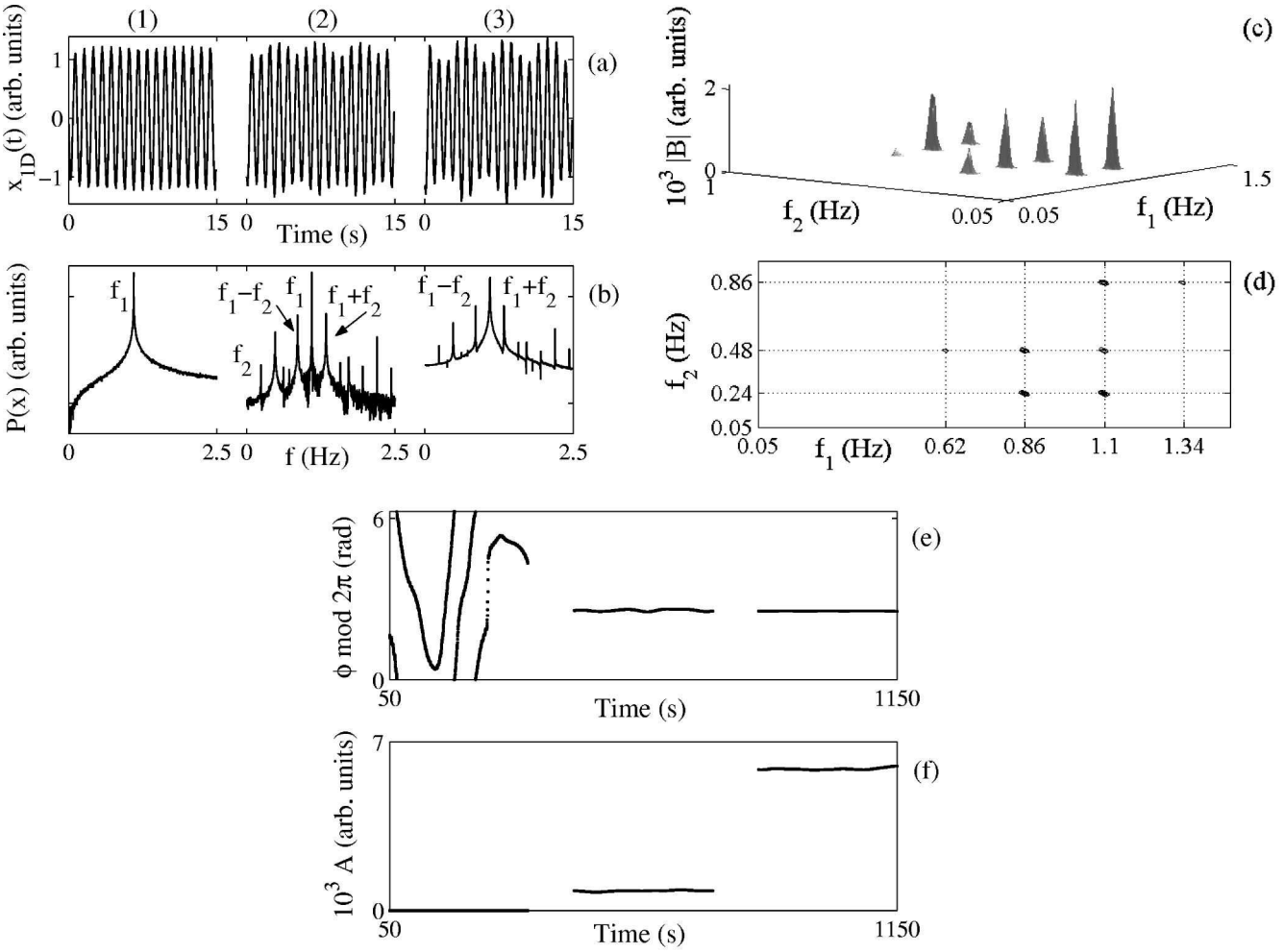

FIG. 8. Results for quadratic couplings in the presence of additive Gaussian noise. (a) The test signal x_{1D}, variable x_1 of the first oscillator with characteristic frequency $f_1=1.1$ Hz. The characteristic frequency of the second oscillator is $f_2=0.24$ Hz. The oscillators are unidirectionally and quadratically coupled with three different coupling strengths: $\eta_2=0.0$ (1), 0.05 (2), and 0.1 (3). Each coupling lasts for 400 s at a sampling frequency $f_s=10$ Hz. Only the first 15 s are shown in each case. (b) The power spectrum. (c) The bispectrum $|B|$ calculated with $K=33$ segments, 66% overlapping, and using the Blackman window to reduce leakage and (d) its contour view. The part of the bispectrum above $f_2>1.0$ Hz is cut, because the triplet (1.1 Hz,1.1 Hz,1.1 Hz) produce a high peak that is physically meaningless. (e) The biphase ϕ and (f) biamplitude A for bifrequency (1.1 Hz,0.24 Hz), with a 0.3-s time step and a 100-s-long window for estimating DFTs using the Blackman window.

on bivariate or multivariate data [1,2]. In conjunction with frequency or time-frequency filtering [27] or mode decomposition [28] to obtain two or more ''separate'' signals, these methods can be used for univariate data as well. Synchronization can also be detected in univariate data through an analysis of angles and radii [29] in return time maps [30].

The time-phase bispectral method proposed in this paper is not only applicable to the synchronization analysis of univariate data but also, at the same time, allows one to determine the nature of the couplings among the interacting nonlinear oscillators. Its benefits include (1) the possibility of observing the whole frequency domain simultaneously; (2) detecting that two or more subsystems are interacting with each other; (3) quantification of the strength of the interaction; and (4) determination of whether the coupling is additive linear or quadratic, or parametric in one of the frequencies. We have shown the method to be suitable for the analysis of noisy signals.

Although we have shown that the technique works effectively on a well-characterized simple model, there will be some difficulties to be faced and overcome in applying it to real problems, e.g., to data from the cardiovascular system. Understanding the content of the bispectrum and identification of the peaks of interest are not always straightforward. To appreciate which peaks are those to focus on, one has to be aware of the basic properties of the system and its fundamental frequencies. Distinguishing a quadratic interaction from parametric frequency modulation may be easy when the coupling (modulation) is relatively strong, but becomes more difficult in the case of relatively weak coupling (modulation). In the latter case, observing each phase in the triplet separately can be helpful. Also it is not always an easy task

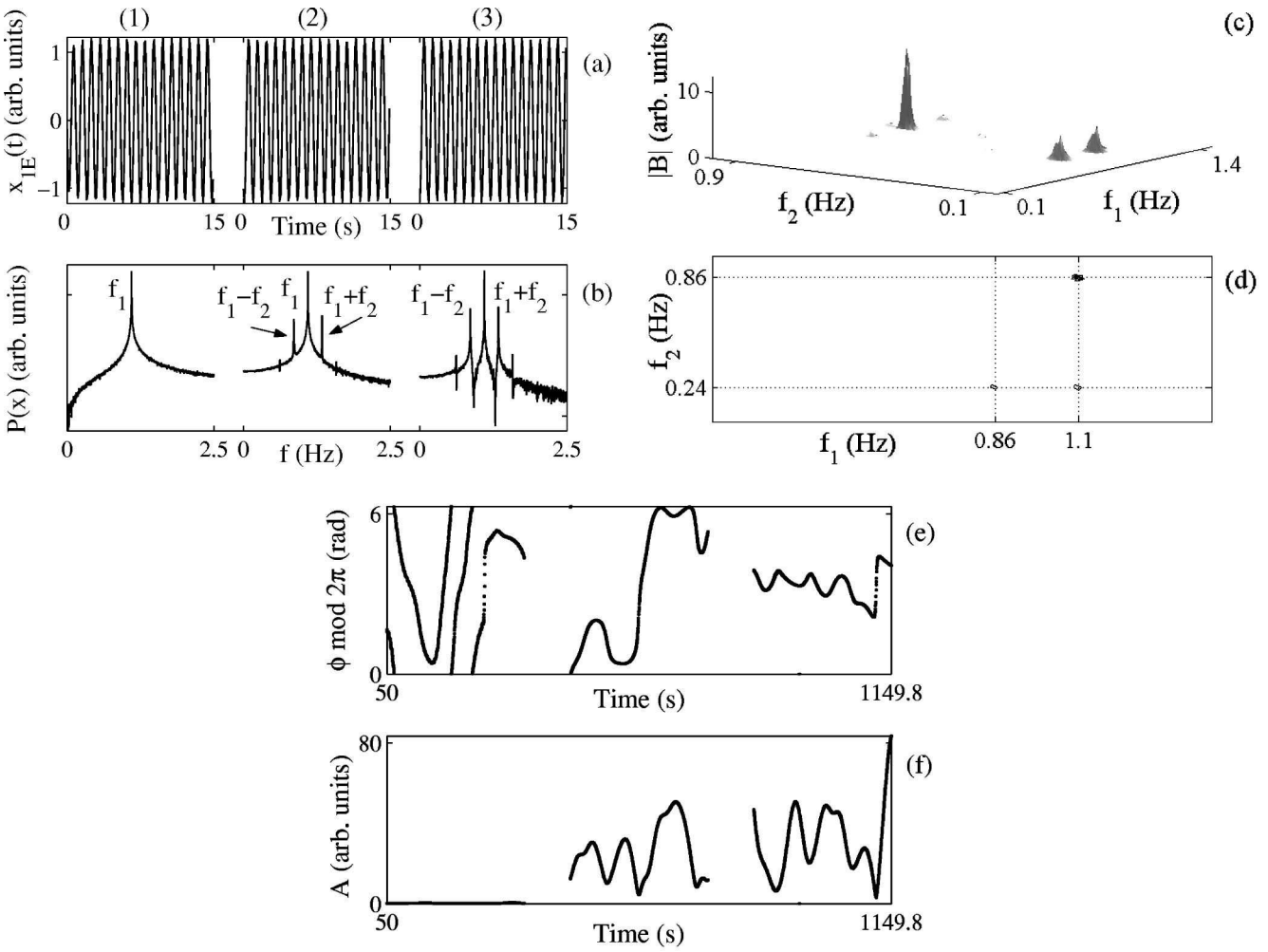

FIG. 9. Results for parametric frequency modulation in the presence of additive Gaussian noise. (a) The test signal x_{1E}, of variable x_1 of the first oscillator with characteristic frequency $f_1=1.1$ Hz frequency modulated by the second oscillator $f_2=0.24$ Hz with three different frequency modulation strengths: $\eta_m=0.0$ (1), 0.1 (2), and 0.2 (3). Each frequency modulation lasts for 400 s, at sampling frequency $f_s=10$ Hz. Only the first 15 s are shown in each case. (b) The power spectrum. (c) The bispectrum $|B|$ calculated with $K=33$ segments, 66% overlapping, and using the Blackman window to reduce leakage and (d) its contour view. The part of the bispectrum above $f_2>1.0$ Hz is cut, because the triplet (1.1 Hz,1.1 Hz,2.2 Hz) produces a high peak that is physically meaningless. (e) The biphase ϕ and (f) biamplitude A for bifrequency (1.1 Hz,0.24 Hz), with a 0.3-s time step and a 100-s-long window for estimating the DFTs using the Blackman window.

to distinguish between quadratic interaction and parametric frequency modulation in the cases when both of them occur simultaneously. Further, where the possible basic frequencies are relatively close, it will be hard to detect them separately. This could cause particular problems in the detection of quadratic phase couplings where frequency pairs are close together. Although it is possible in principle to study an arbitrary number of interacting oscillators, it is advisable in practice to study them in pairs: a knowledge of the basic frequency of each is necessary.

The time-dependent biphase-biamplitude estimate was estimated with a short-time Fourier transform (STFT), using a window of constant length. The optimal window length depends, however, on the frequency being studied. The effective length of the window used for each frequency can be varied by applying the wavelet transform, or the selective Fourier transform. For demonstration purposes above, the natural frequencies of the oscillators were chosen to lie within a relatively narrow frequency interval. A STFT was therefore sufficient for good time and phase (frequency) localization. With a broader frequency content, however, the wavelet transform or selective Fourier transform will need to be applied.

Higher-order spectral methods can be used to study arbitrary interactions among coupled oscillators: of quadratic, cubic, or even higher order. In this paper we have concentrated on the lowest one, using the third-order spectrum or bispectrum. For higher orders the volume of the calculations rises substantially, and the method becomes numerically increasingly demanding. At the same time, graphical presentation and interpretation of the results become increasingly difficult.

ACKNOWLEDGMENTS

We gratefully acknowledge valuable comments and discussions with Andriy Bandrivskyy, Justin Fackrell, Mounir

Ghogho, Fluvio Gini, Georgios B. Giannakis, Peter Husar, Dmitri G. Luchinsky, and Anathram Swami. The study was supported by the Slovenian Ministry of Education, Science and Sport, by INTAS, and by the Engineering and Physical Sciences Research Council (U.K.).

APPENDIX: VARIANCE OF THE BISPECTRUM ESTIMATE

In order to interpret bispectral values from a finite length time series, the statistics of bispectrum estimates must be known. To achieve statistical stability, the time series is divided into K segments for averaging [25]. When there is a large number of segments, the estimate gains statistical stability at the expense of power spectral and bispectral resolution. For a real signal, with a finite number of points, the compromise between bispectral resolution and statistical stability may be expected at K around 30. Estimates are subject to statistical error, such as bias and variance. An estimate must be consistent, that is the statistical error must approach zero in the mean-square sense as the number of realizations becomes infinite. Here we neglect the effects of finite time series length, we assume that they are sufficiently long. Let us consider the bias and the variance of the bispectrum estimate $\hat{B}(k,l)$. The expected value of $\hat{B}(k,l)$ will be

$$E[\hat{B}(k,l)]=\frac{1}{K}\sum_{i=1}^{K}E[X_i(k)X_i(l)X_i^*(l,k)]$$
$$=E[X(k)X(l)X^*(l,k)]=B(k,l), \qquad \text{(A1)}$$

as K becomes infinite, X_i is the DFT of the ith segment. Thus, $\hat{B}(k,l)$ can be taken as an unbiased estimate [29]. Its variance will be

$$\mathrm{var}(\hat{B})=E[\hat{B}\hat{B}^*]-E[\hat{B}]E[\hat{B}^*]$$
$$=\frac{1}{K}\{E[|X(k)|^2|X(l)|^2|X(k+l)|^2]-E|B(k,l)|^2\}. \qquad \text{(A2)}$$

Note that the variance is inversely proportional to K. From a mathematical statistics point of view, it is a nontrivial task to compute the quantity in the bracket in terms of low order spectra, but one may write a good approximation [26],

$$E[|X(k)|^2|X(l)|^2|X(k+l)|^2]=P(k)P(l)P(k+l), \qquad \text{(A3)}$$

in which case the variance will be

$$\mathrm{var}(\hat{B})=E[|\hat{B}(k,l)|^2]-E[\hat{B}(k,l)]^2$$
$$\approx\frac{1}{K}P(k)P(l)P(k+l)[1-b^2(k,l)]. \qquad \text{(A4)}$$

Note that it is a consistent estimate in the sense that the variance approaches zero as K becomes infinite. The variance is proportional to the product of the powers $[P(k)=E[X(k)X^*(k)]]$ at the frequencies k, l, and $k+l$. Consequently, a larger statistical variability is introduced in estimating larger values in the bispectrum. Finally, the variance is proportional to $[1-b^2(k,l)]$, where the bicoherence b^2 is a normalized bispectrum, $b^2(k,l)=E[\hat{B}(k,l)]^2/[P(k)P(l)P(k+l)]$. That is, when the oscillations at k, l, and $k+l$ are nonlinearly coupled ($b^2\approx 1$), the variance approaches zero, and when the components are statistically independent ($b^2\approx 0$), the variance is proportional to the power at each spectral component [26].

Brillinger and Rosenblatt [3] have investigated the asymptotic mean and variance of Fourier-type estimates of high-order spectra and proved that under certain assumptions the kth order spectral estimate is asymptotically unbiased and Gaussianly distributed and that estimates of different order are asymptotically independent. The variances of the real and imaginary parts of the bispectrum are asymptotically (i.e., for large K) Gaussian and are equal, $\mathrm{var}\{\mathrm{Re}[\hat{B}(k,l)]\}\cong\mathrm{var}\{\mathrm{Im}[\hat{B}(k,l)]\}$. For a perfect phase-coupled triplet, the variances of the real and imaginary parts are equal to zero. In the case of no coupling, there is an identical contribution to the variances from the real and imaginary parts of the estimate of the bispectrum.

The total variance is a sum of individual ($i=1,\ldots,K$) contributions, because different triplets are mutually statistically uncorrelated in the absence of phase coupling. Partial coupling can be expected to result in a combination of perfectly phase-coupled oscillations and oscillations with randomly changing phases.

[1] A.S. Pikovsky, M.G. Rosenblum, and J. Kurths, *Synchronization; A Universal Concept in Nonlinear Sciences* (Cambridge University Press, Cambridge, 2001).

[2] T. Schreiber, Phys. Rev. Lett. **85**, 461 (2000); M.G. Rosenblum and A.S. Pikovsky, Phys. Rev. E **64**, 045202 (2001); M.G. Rosenblum, L. Cimponeriu, A. Bezerianos, A. Patzak, and R. Mrowka, *ibid.* **65**, 041909 (2002); M. Paluš, V. Komárek, Z. Hrnčíř, and K. Štěbrová, *ibid.* **63**, 046211 (2001).

[3] D.R. Brillinger and M. Rosenblatt, *Spectral Analysis of Time Series* (Wiley, New York, 1967).

[4] A. Swami, G.B. Giannakis, and G. Zhou, Signal Process. **60**, 65 (1997).

[5] C.L. Nikias and A.P. Petropulu, *Higher-Order Spectra Anlysis: A Nonlinear Signal Processing Framework* (Prentice-Hall, Englewood Cliffs, 1993).

[6] G. Zhou and G.B. Giannakis, IEEE Trans. Signal Process. **43**, 1173 (1995).

[7] J.W.A. Fackrell, Ph.D. thesis, University of Edinburgh, 1996 (unpublished).

[8] Y.C. Kim, J.M. Beall, E.J. Powers, and R.W. Miksad, Phys.

Fluids **23**, 258 (1980); M.R. Raghuveer, IEEE Trans. Autom. Control **35**, 48 (1990); H. Parthasarathy, S. Prasad, and S.D. Joshi, IEEE Trans. Signal Process. **43**, 2346 (1995).

[9] M.B. Priestley and M.M. Gabr, *Multivariate Analysis: Future Directions* (North-Holland, Amsterdam, 1993).

[10] J.R. Fonollosa and C.L. Nikias, IEEE Trans. Signal Process. **41**, 245 (1993); B. Boashash and P.J. O'Shera, *ibid.* **42**, 216 (1994).

[11] T.S. Rao and K.C. Indukumar, J. Franklin Inst. **33**, 425 (1996).

[12] R.J. Perry and M.G. Amin, IEEE Trans. Signal Process. **43**, 1017 (1995).

[13] A.V. Dandawaté and G.B. Giannakis, IEEE Trans. Inf. Theory **41**, 216 (1995).

[14] B. Schack *et al.*, Clin. Neurophysiol. **112**, 1388 (2001).

[15] B.Ph. van Milligen, C. Hidalgo, and E. Sánchez, Phys. Rev. Lett. **74**, 395 (1995); B.Ph. van Milligen *et al.*, Phys. Plasmas **2**, 3017 (1995).

[16] J. Jamšek, M.Sc. thesis, University of Ljubljana, 2000.

[17] A. Stefanovska and M. Bračič, Contemp. Phys. **40**, 31 (1999).

[18] J.M. Mendel, Proc. IEEE **79**, 278 (1991).

[19] A.K. Nadi, IEE Proc. F, Commun. Radar Signal Process. **140**, 380 (1993).

[20] A.K. Nadi, *Higher-Order Statistics in Signal Processing* (Cambridge University Press, Cambridge, 1998).

[21] C.L. Nikias and J.M. Mendel, IEEE Signal Process. Mag. **7**, 10 (1993).

[22] L.A. Pflug, G.E. Ioup, and J.W. Ioup, J. Acoust. Soc. Am. **94**, 2159 (1993); **95**, 2762 (1994).

[23] M.J. Hinch, IEEE Trans. Acoust., Speech, Signal Process. **38**, 1277 (1990); I. Sharfer and H. Messer, IEEE Trans. Signal Process. **41**, 296 (1993); M.J. Hinch, *ibid.* **43**, 2130 (1995).

[24] Three and not four, because the triplet (f_1, f_2, f_1+f_2) has the same peak in the bispectrum as the triplet (f_1, f_2, f_1-f_2).

[25] The phases are random variables over $[0.2\pi)$. The phases of different segments are independent of each other.

[26] Y.C. Kin and E.J. Powers, IEEE Trans. Plasma Sci. **PS-7**, 120 (1979); V. Chandran, Ph.D. thesis, Washington State University, 1990; V. Chandran and S.L. Elgar, IEEE Trans. Signal Process. **19**, 2640 (1991).

[27] P. Tass, M.G. Rosenblum, J. Weule, J. Kurths, A. Pikovsky, J. Volkmann, A. Schnitzler, and H.-J. Freund, Phys. Rev. Lett. **81**, 3291 (1998); A. Stefanovska and M. Hožič, Prog. Theor. Phys. Suppl. **139**, 270 (2000).

[28] N.E. Huang, Z. Shen, S.R. Long, M.C. Wu, H.H. Shih, Q. Zheng, N. Yen, C.C. Tung, and H.H. Liu, Proc. R. Soc. London, Ser. A **454**, 903 (1998).

[29] N.B. Janson, A.G. Balanov, V.S. Anishchenko, and P.V.E. McClintock, Phys. Rev. E **65**, 036211 (2002).

[30] K. Suder, F.R. Drepper, M. Schiek, and H.H. Abel, Am. J. Physiol. Heart Circ. Physiol. **275**, H1092 (1998).

PHYSICAL REVIEW E **67**, 055201(R) (2003)

Direction of coupling from phases of interacting oscillators: An information-theoretic approach

Milan Paluš[1] and Aneta Stefanovska[2]
[1]*Institute of Computer Science, Academy of Sciences of the Czech Republic, Pod vodárenskou věží 2, 182 07 Prague 8, Czech Republic*
[2]*Group of Nonlinear Dynamics and Synergetics, Faculty of Electrical Engineering, University of Ljubljana, Tržaška 25, 1000 Ljubljana, Slovenia*

(Received 28 August 2002; published 27 May 2003)

A directionality index based on conditional mutual information is proposed for application to the instantaneous phases of weakly coupled oscillators. Its abilities to distinguish unidirectional from bidirectional coupling, as well as to reveal and quantify asymmetry in bidirectional coupling, are demonstrated using numerical examples of quasiperiodic, chaotic, and noisy oscillators, as well as real human cardiorespiratory data.

DOI: 10.1103/PhysRevE.67.055201 PACS number(s): 05.45.Xt, 05.45.Tp, 87.80.Tq

Cooperative behavior of coupled complex systems has recently attracted considerable interest from theoreticians as well as experimentalists (see, e.g., the monograph [1]), since synchronization and related phenomena have been observed not only in physical, but also in many biological systems. Examples include the cardiorespiratory interaction [2,3] and the synchronization of neural signals [4–9]. In such physiological systems it is important not only to detect synchronized states, but also to identify causal (driver-response) relationships between the systems studied. The problem of coupling direction in generalized synchronization [10] has been treated using amplitudes of the system observables and evaluating their mutual predictability [4,5] or mutual nearest neighbors in reconstructed state spaces [7,11]. Information-theoretic approaches [8,9,12] have also been successfully applied.

Considering weakly coupled oscillators the coupling properties of the systems studied can be inferred from an analysis of the interrelations between the instantaneous phases of the oscillators, $\phi_{1,2}(t)$. These can be estimated from (scalar) observable signals [1,13,14]. Several methods have been proposed for the detection and quantification of phase synchronization from the experimental data [1,6,14]. Rosenblum *et al.* [15,16] have also introduced methods for inferring directionality of coupling, based either on the Fourier approximation of phase increments or instantaneous periods as functions of the phases $\phi_{1,2}(t)$, or on mutual predictability of the instantaneous phases $\phi_{1,2}(t)$. Paluš *et al.* [8] have introduced an information-theoretic framework for the study of generalized synchronization in experimental time series based on evaluation of so-called coarse-grained transinformation rates (CTIRs). In this paper, CTIRs are developed and applied to instantaneous phases $\phi_{1,2}(t)$ of coupled oscillators.

The method introduced in Ref. [8] operates with information-theoretic tools, such as the well-known mutual information $I(X;Y)$ of two random variables X and Y, given as $I(X;Y)=H(X)+H(Y)-H(X,Y)$, where the entropies $H(X)$, $H(Y)$, $H(X,Y)$ are given in the usual Shannonian sense [8,17]. The conditional mutual information $I(X;Y|Z)$ of the variables X, Y given the variable Z is defined using the conditional entropies [8,17] as

$$I(X;Y|Z)=H(X|Z)+H(Y|Z)-H(X,Y|Z). \qquad (1)$$

Consider two time series $\{x(t)\}$ and $\{y(t)\}$ regarded as realizations of two stationary ergodic stochastic processes $\{X(t)\}$ and $\{Y(t)\}$, which represent observables of two possibly coupled systems. Dependence structures between the two processes (time series) can be studied using the simple mutual information $I(y;x_\tau)$, where we use y for $y(t)$ and x_τ for $x(t+\tau)$. $I(y;x_\tau)$ measures the average amount of information contained in the process $\{Y\}$ about the process $\{X\}$ in its future τ time units ahead (τ future thereafter). However, this measure as well as other dependence and predictability measures could also contain information about the τ future of the process $\{X\}$ contained in this process itself if the processes $\{X\}$ and $\{Y\}$ are not independent, i.e., if $I(x;y)>0$.

For inferring causality relations, i.e., the directionality of coupling between the processes $\{X(t)\}$ and $\{Y(t)\}$, we need to estimate the ''net'' information about the τ future of the process $\{X\}$ contained in the process $\{Y\}$ itself by using an appropriate tool—the conditional mutual information $I(y;x_\tau|x)$. It has been shown [8,9] that using $I(y;x_\tau|x)$ and $I(x;y_\tau|y)$ the coupling directionality can be inferred from time series measured in coupled, but not yet fully synchronized systems.

Consider now that the processes $\{X\}$ and $\{Y\}$ can be modeled by weakly coupled oscillators and that their interactions can be inferred by analyzing the dynamics of their instantaneous phases $\phi_1(t)$ and $\phi_2(t)$ [15,16]. The latter can be estimated from the measured time series $\{x(t)\}$ and $\{y(t)\}$, e.g., by application of the discrete Hilbert transform [1,13,14]. Rather than simply substituting the series $\{x(t)\}$ and $\{y(t)\}$ by the phases $\phi_1(t)$ and $\phi_2(t)$ (which are confined in interval $[0,2\pi)$ or $[-\pi,\pi)$), we consider phase increments

$$\Delta_\tau\phi_{1,2}=\phi_{1,2}(t+\tau)-\phi_{1,2}(t),$$

and the conditional mutual information $I(\phi_1(t);\Delta_\tau\phi_2|\phi_2(t))$ and $I(\phi_2(t);\Delta_\tau\phi_1|\phi_1(t))$, in a shorter notation $I(\phi_1;\Delta_\tau\phi_2|\phi_2)$ and $I(\phi_2;\Delta_\tau\phi_1|\phi_1)$. Now, in analogy with Rosenblum *et al.* [15,16] we define a directionality index

$$D(1,2)=\frac{i(1\to2)-i(2\to1)}{i(1\to2)+i(2\to1)}, \qquad (2)$$

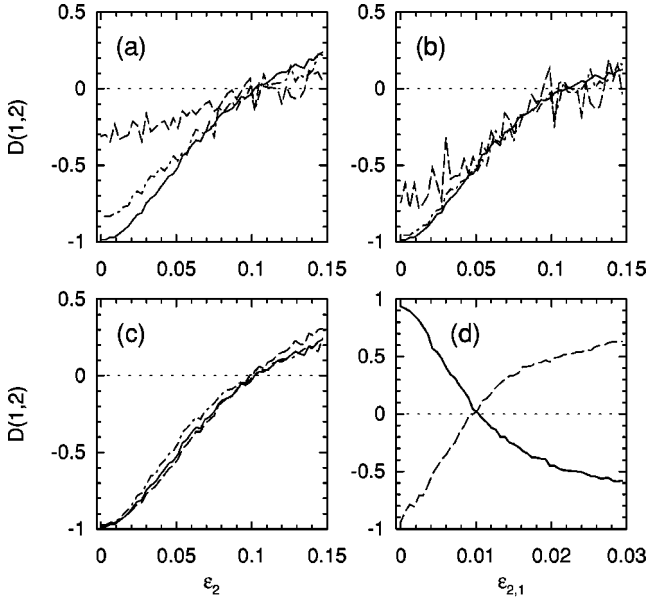

FIG. 1. (a)–(c) Directionality index $D(1,2)$ for noisy phase oscillators (3) for $\epsilon_1=0.1$ as a function of ϵ_2 computed using $q=8$ (a) and $q=4$ (b) equiprobable marginal bins and series length $N=1k$ (dashed line), $N=8k$ (dash-dotted line), and $N=128k$ samples (full line). (c) $D(1,2)$ for $N=128k$, $q=8$, averaged over time lags 1–5 (dashed line), 1–15 (full line), 1–150 (dash-dotted line). The integration step is $\pi/7$. (d) $D(1,2)$ for coupled Rössler systems (4) with $\epsilon_1=0.01$ as a function of ϵ_2 (dashed line) and with $\epsilon_2=0.01$ as a function of ϵ_1 (full line). $N=128k$, $q=8$, lags 1–15.

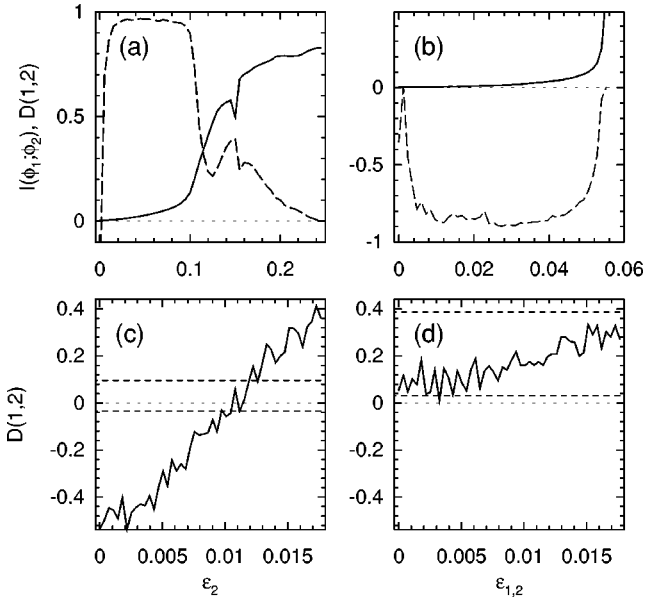

FIG. 2. (a),(b) Directionality index $D(1,2)$ (dashed line) and mutual information $I(\phi_1;\phi_2)$ (full line) of the phases of unidirectionally coupled Rössler systems (4) ($\epsilon_1=0$) as a function of ϵ_2 (a), and for $\epsilon_2=0$ as a function of ϵ_1 (b). $N=128k$, $q=8$, lags 1–15. (c),(d) $D(1,2)$ for noisy phase oscillators (3) (full line) with $\omega_1=0.1$ and $\omega_2=1.1$ (1:11) for $\epsilon_1=0.01$ as a function of ϵ_2 for lags 1–15 (c) and lags 10, 20, . . . , 150 (d). The horizontal dashed lines are ranges of the mean ± 2SD of $D(1,2)$ obtained from the surrogate data.

where the measure $i(1\to2)$ of how system 1 drives system 2 is either equal to the conditional mutual information $I(\phi_1;\Delta_\tau\phi_2|\phi_2)$ for a chosen time lag τ or equal to an average of $I(\phi_1;\Delta_\tau\phi_2|\phi_2)$ over a selected range of lags τ. (For motivation for averaging and the concept of the coarse-grained information rates see Refs. [8,18].) And in full analogy we define $i(2\to1)$ using $I(\phi_2;\Delta_\tau\phi_1|\phi_1)$. $D(1,2)$ should be positive if the driving from system 1 to system 2 prevails, and negative for the opposite case.

In order to test how well directionality index (2) works, we start with the same simple model of two coupled phase oscillators as has been used by Rosenblum and Pikovsky [15] and Rosenblum *et al.* [16]:

$$\dot{\phi}_1=\omega_1+\epsilon_1 f_1(\phi_1,\phi_2)+\xi_1(t),$$

$$\dot{\phi}_2=\omega_2+\epsilon_2 f_2(\phi_2,\phi_1)+\xi_2(t). \qquad (3)$$

Using $\omega_{1,2}=1\pm0.1$, $q_{1,2}=0$, $f_{1,2}=\sin(\phi_{2,1}-\phi_{1,2})$ and mutually independent Gaussian IID noises with zero mean and standard deviation $\sigma=0.2$ for $\xi_{1,2}$, with a fixed coupling parameter $\epsilon_1=0.1$, we generated time series of the phases $\phi_{1,2}(t)$ for 50 different values of the coupling parameter ϵ_2. The directionality indices $D(1,2)$ were obtained from coarse-grained estimates of the conditional mutual information. The latter were obtained by a simple box-counting algorithm based on equiprobable marginal bins (marginal equiquantization [18]). The dependence of $D(1,2)$ on the quantization and the series length can be seen in Figs. 1(a, b), and its dependence on time lags in Fig. 1(c).

Averaging $I(\phi_{1,2};\Delta_\tau\phi_{2,1}|\phi_{2,1})$ over a short range of lags decreases fluctuations of the estimates. For shorter time series ($N=1k=1024$ samples) more coarse ($q=4$) estimates have higher variance [Fig. 1(b), dashed line], while for $q=8$ the estimates have a higher bias for weaker coupling [Fig. 1(a), dashed line]. The results for series lengths $N=8k=8192$ (Figs. 1(a, b), dash-dotted line) and $N=128k=1.3\times10^5$ samples [Figs. 1(a, b), full line] reflect well the coupling asymmetry and smoothly changes with changing coupling parameter ϵ_2 [cf. the results in Ref. [15], Fig. 3(a).]

Let us now consider two coupled Rössler systems, the same as studied in Refs. [13,14], but with different coupling coefficients $\epsilon_1\neq\epsilon_2$:

$$\dot{x}_{1,2}=-\omega_{1,2}y_{1,2}-z_{1,2}+\epsilon_{1,2}(x_{2,1}-x_{1,2}),$$

$$\dot{y}_{1,2}=\omega_{1,2}x_{1,2}+0.15y_{1,2}, \qquad (4)$$

$$\dot{z}_{1,2}=0.2+z_{1,2}(x_{1,2}-10).$$

The frequencies $\omega_{1,2}$ are defined as $\omega_{1,2}=1\pm0.015$. The phases of the Rössler systems (4) have been obtained using the Hilbert transform by the same way as in Ref. [14], where the simple mutual information $I(\phi_1;\phi_2)$ was proposed for detecting phase synchronization. Here we repeat the numerical study of transients to phase synchronization, as in Ref. [14], but for unidirectional coupling, i.e., either $\epsilon_1=0$ [Fig.

2(a)], or $\epsilon_2 = 0$ [Fig. 2(b)]. We can see that $D(1,2)$ (dashed line) correctly identifies the driver from the response system [19] before the coupling parameter reaches the synchronization threshold [20]. The latter is detected by a steep increase of $I(\phi_1;\phi_2)$ [full line in Figs. 2(a, b)] [14].

Keeping the coupling parameters before the synchronization threshold we can repeat the same study as with the oscillators (3), when one of the coupling parameters was kept constant, i.e., $\epsilon_2 = 0.01$, and the other, ϵ_1, varies from 0 to 0.03 [dashed line, Fig. 1(d)], and vice versa [full line, Fig. 1(d)]. The directionality of coupling was exactly revealed also in this example of chaotic systems that were not studied yet from this point of view.

Let us return to phase oscillators (3). We have also studied the noise-free quasiperiodic system, as well as more complex noisy cases with larger differences in the natural frequencies, or with asymmetric coupling, as treated in Ref. [16]. In all cases the directionality index $D(1,2)$ identified the correct coupling direction.

Since we intend to study cardiorespiratory interactions during paced respiration, when the ratio of natural frequencies can be rather large, we have studied systems (3) with such frequency ratios as $\omega_1 : \omega_2 = 1:11$ [Figs. 2(c, d)]. For relatively short time lags τ the directionality index $D(1,2)$ detects the correct coupling directionality for the majority of the coupling parameter values [Fig. 2(c), the full line], while for long time lags [Fig. 2(d)] the directionality detection ability of $D(1,2)$ is lost. Looking back at the conditional mutual information $I(\phi_1;\Delta_\tau\phi_2|\phi_2)$ and $I(\phi_2;\Delta_\tau\phi_1|\phi_1)$, we can find that their values are very low, comparable with variance of their estimates. This leads to a large bias and variance of the directionality index $D(1,2)$. Therefore, we need to establish significance of $D(1,2)$ values by a statistical test.

We use the concept of surrogate data (see Ref. [14] and references therein). In this case the surrogate data can be a set of realizations (with different random initial conditions) of phases of uncoupled oscillators (3). Estimating the conditional mutual information and the directionality indices for these surrogate data sets, we can assess the fluctuations of these quantities for uncoupled data without any directionality of coupling. To present these fluctuations, we illustrate the ranges of the mean ± 2SD (standard deviations) of $D(1,2)$ for the surrogates by the dashed lines in Figs. 2(c, d). In the case of large time lags [Fig. 2(d)] the surrogates confirm the extremely large fluctuations of $D(1,2)$ and its bias to positive values. As a result, the directionality index of the coupled oscillators does not differ significantly from $D(1,2)$ of the surrogates, so in this case no directionality can be inferred [Fig. 2(d)]. In the case of small lags, fluctuations and bias of $D(1,2)$ are much smaller, although not negligible [Fig. 2(c), dashed lines]. The range of surrogate $D(1,2)$ fluctuations disqualifies values of $D(1,2)$ for the coupled oscillators for a small interval around the symmetry point $\epsilon_2 = 0.01$. Since we can see that the fluctuations of $D(1,2)$ estimated for the coupled systems [full line in Fig. 2(c)] are of similar magnitude to the surrogate mean ± 2SD range, comparison of the directionality index obtained from the studied data with its surrogate range saves us from making an unreliable inference of the directionality.

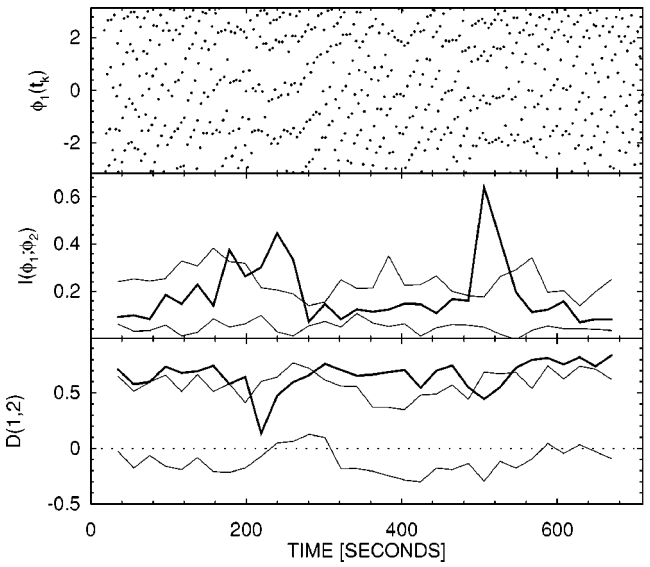

FIG. 3. Synchrogram (top panel), mutual information $I(\phi_1;\phi_2)$ (middle panel), and the directionality index $D(1,2)$ (bottom panel) for the phases of human cardiorespiratory data (respiration and heartbeat, full thick lines). The ranges of surrogate mean ± 2SD for $I(\phi_1;\phi_2)$ and $D(1,2)$ are depicted by thin lines in the respective panels.

In any experimental application, estimation of the directionality index should be accompanied by an assessment of its significance. Otherwise an incorrect directionality could be concluded due to either variance or bias in the estimate of the directionality index. The surrogate data test is one possible approach. In many practical applications, however, it is the only available one. Various types of bivariate surrogate data useful in the study of coupled systems are discussed in Ref. [14]. A special type related to a specific application is presented below, where we analyze data from human cardiorespiratory interactions.

The cardiorespiratory coupling during spontaneous and paced respiration was analyzed in a group of young healthy subjects. The data were noninvasively recorded for 12 min, while the subjects were lying comfortably. The cardiac activity was assessed by recording the electrocardiogram (ECG) and a piezoelectric sensor was used to measure excursions of the thorax and hence the respiratory activity. A sampling rate of 400 Hz was used for both signals. (For details of measurements see Ref. [21].) The phases of cardiac activity were estimated using the marked events method, by marking R peaks. The phases of the respiratory oscillations were obtained by application of the Hilbert transform to the respiratory signal. The results will be presented in detail elsewhere; here we briefly illustrate the potential of the proposed approach. The directionality index $D(1,2)$ (1—respiratory, 2—cardiac system) was estimated in moving 40-s windows with 50% overlap, using four quantization levels and time lags from 20 to 200, increased by 20 (samples).

In the same windows, but using 16 quantization levels, the simple mutual information $I(\phi_1;\phi_2)$ of the instantaneous phases $\phi_1(t), \phi_2(t)$ was calculated in order to assess presence of phase synchronization [14]. Significance levels

for both $D(1,2)$ and $I(\phi_1;\phi_2)$ were established using sets of 30 realizations of surrogate data. The latter were constructed by random permutations of *R*-*R* intervals, thus producing artificial heartbeat data with the same frequency histograms as the original data. Due to the randomization of the *R*-peak positions, however, any possible association with the respiratory rhythm was destroyed. The respiratory data remained unchanged, so that the significance levels depend on the character of the respiratory dynamics in each window.

The synchrogram [2], the mutual information $I(\phi_1;\phi_2)$, and the directionality index $D(1,2)$ for an example of spontaneous respiration are illustrated in Fig. 3. Two episodes of phase synchronization between the heartbeat and respiratory rhythms, visible in the synchrogram as almost horizontal lines (at times of approximately 240 and 500 s), are detected by $I(\phi_1;\phi_2)$ (thick line in Fig. 3, middle panel) lying outside from the surrogate range (mean$\pm$2SD of the surrogates, depicted by thin lines). The necessity of establishing the significance level (here as the mean plus two standard deviations of the surrogate set) is obvious—even relatively large positive values of $I(\phi_1;\phi_2)$ do not necessarily reflect the presence of synchronization (but the bias and variance of estimates) unless $I(\phi_1;\phi_2)$ is larger than the significance level given by the surrogate mean and variance.

The same holds also for the values of the directionality index $D(1,2)$ (thick line in Fig. 3, bottom panel), estimates of which are severely biased towards positive values, as confirmed by the surrogate mean $\pm$2SD ranges (thin lines). Nevertheless, in a large part of the recording, $D(1,2)$ is larger than its significance level, indicating that the respiration is driving the cardiac system, as was recently reported by Rosenblum *et al.* [16]. It is also noticeable that $D(1,2)$ falls into the surrogate range, i.e., no directionality can be inferred, in the two synchronous intervals [20], detected by $I(\phi_1;\phi_2)$ as well as seen in the synchrograms (Fig. 3).

Note that the tools introduced above have a firm mathematical basis in the information theory, and their coarse-grained estimates can be computed more efficiently [18,22] than measures used by other authors.

In conclusion, an information-theoretic approach for detecting the directionality of coupling from the phases of interacting oscillators has been proposed and tested. Its ability to reveal and quantify possible asymmetry in the coupling has been demonstrated, using both numerical and real data examples. The problem of assessing the significance of estimated directionality indices is discussed for the first time in this context and solutions were proposed.

The authors would like to thank Peter V. E. McClintock for comments and suggestions. The work was supported by the Czech Ministry of Education, Youth and Sports, and the Slovenian Ministry of Education, Science and Sport Cooperation Project No. 14-2003-04; and in part by GA CR (205/00/1055), IGA MZCR(NF6258-3/2000), and INTAS.

[1] A. Pikovsky, M. Rosenblum, and J. Kurths, *Synchronization, A Universal Concept in Nonlinear Sciences* (Cambridge University Press, Cambridge, 2001).

[2] C. Schäfer, M.G. Rosenblum, J. Kurths, and H.-H. Abel, Nature (London) **392**, 239 (1998); C. Schäfer, M.G. Rosenblum, H.-H. Abel, and J. Kurths, Phys. Rev. E **60**, 857 (1999).

[3] M. Paluš and D. Hoyer, IEEE Eng. Med. Biol. Mag. **17**, 40 (1998); A. Stefanovska, H. Haken, P.V.E. McClintock, M. Hožič, F. Bajrović, and S. Ribarič, Phys. Rev. Lett. **85**, 4831 (2000).

[4] S.J. Schiff, P. So, T. Chang, R.E. Burke, and T. Sauer, Phys. Rev. E **54**, 6708 (1996).

[5] M. Le Van Quyen, J. Martinerie, C. Adam, and F.J. Varela, Physica D **127**, 250 (1999).

[6] P. Tass, M.G. Rosenblum, J. Weule, J. Kurths, A. Pikovsky, J. Volkmann, A. Schnitzler, and H.-J. Freund, Phys. Rev. Lett. **81**, 3291 (1998).

[7] J. Arnhold, P. Grassberger, K. Lehnertz, and C.E. Elger, Physica D **134**, 419 (1999).

[8] M. Paluš, V. Komárek, Z. Hrnčíř, and K. Štěrbová, Phys. Rev. E **63**, 046211 (2001).

[9] M. Paluš, V. Komárek, T. Procházka, Z. Hrnčíř, and K. Štěrbová, IEEE Eng. Med. Biol. Mag. **20**, 65 (2001).

[10] N.F. Rulkov, M.M. Sushchik, L.S. Tsimring, and H.D.I. Abarbanel, Phys. Rev. E **51**, 980 (1995).

[11] R. Quian Quiroga, J. Arnhold, and P. Grassberger, Phys. Rev. E **61**, 5142 (2000).

[12] T. Schreiber, Phys. Rev. Lett. **85**, 461 (2000).

[13] M.G. Rosenblum, A.S. Pikovsky, and J. Kurths, Phys. Rev. Lett. **76**, 1804 (1996).

[14] M. Paluš, Phys. Lett. A **235**, 341 (1997).

[15] M.G. Rosenblum and A.S. Pikovsky, Phys. Rev. E **64**, 045202(R) (2001).

[16] M.G. Rosenblum, L. Cimponeriu, A. Bezerianos, A. Patzak, and R. Mrowka, Phys. Rev. E **65**, 041909 (2002).

[17] T.M. Cover and J.A. Thomas, *Elements of Information Theory* (Wiley, New York, 1991).

[18] M. Paluš, Physica D **93**, 64 (1996).

[19] With the exception of the uncoupled case, when $D(1,2)$ is biased to negative values.

[20] The impossibility of detecting the directionality of coupling from data in synchronized states is discussed in Ref. [8] as well as in Ref. [16].

[21] A. Stefanovska and M. Bračič, Contemp. Phys. **40**, 31 (1999); M. Bračič and A. Stefanovska, Physica A **283**, 451 (2000).

[22] See also http://www.cs.cas.cz/~mp/nlin0.html

ACADEMIC PRESS

Available online at www.sciencedirect.com

SCIENCE DIRECT®

Microvascular Research 65 (2003) 160–171

Microvascular Research

www.elsevier.com/locate/ymvre

Regulation of human cutaneous circulation evaluated by laser Doppler flowmetry, iontophoresis, and spectral analysis: importance of nitric oxide and prostaglandines

Per Kvandal,[a,b,*] Aneta Stefanovska,[c] Mitja Veber,[c] Hebe Désirée Kvermmo,[d] and Knut Arvid Kirkebøen[a,e]

[a] *Department of Anesthesiology, Ulleval University Hospital, 0407 Oslo, Norway*
[b] *Department of Intensive Care Medicine, Ulleval University Hospital, 0407 Oslo, Norway*
[c] *Faculty of Electrical Engineering, University of Ljubljana, 1000 Ljubljana, Slovenia*
[d] *Hand- and Microsurgery Department, National Hospital, 0407 Oslo, Norway*
[e] *Institute for Experimental Medical Research, Ulleval University Hospital, 0407 Oslo, Norway*

Received 26 September 2003

Abstract

Nitric oxide (NO) and prostaglandines (PGs) are important in regulation of vascular tone and blood flow. Their contribution in human cutaneous circulation is still uncertain. We inhibited NO synthesis by infusing N^G-monomethyl-L-arginine (L-NMMA) in the brachial artery (16 μmol/min for 5 min) and reversed it by intraarterial infusion of L-arginine (40 μmol/min for 7.5 min). PG synthesis was inhibited by the cyclooxygenase inhibitor aspirin (600 mg over 5 min intravenously). Basal cutaneous perfusion and perfusion responses during iontophoresis with the endothelium-dependent vasodilator acetylcholine (ACh) and the endothelium-independent vasodilator sodium nitroprusside (SNP) were recorded by laser Doppler flowmetry (LDF). We performed wavelet transforms of the measured signals. Mean spectral amplitude within the frequency interval from 0.0095 to 1.6 Hz and mean and normalized amplitudes of five intervals around 1, 0.3, 0.1, 0.04, and 0.01 Hz were analysed. The oscillations with frequencies around 1, 0.3, 0.1, and 0.04 Hz are influenced by the heartbeat, the respiration, the intrinsic myogenic activity of vascular smooth muscle, and the neurogenic activity of the vessel wall, respectively. We have previously shown that the oscillation with a frequency around 0.01 Hz is modulated by the vascular endothelium. L-NMMA reduced mean value of the LDF signal by ≈20% ($P = 0.0067$). This reduction was reversed by L-arginine. Mean value of the LDF signals during ACh and SNP iontophoresis did not change after infusion of L-NMMA. Aspirin did not affect mean value of the LDF signal or the LDF signal during ACh or SNP iontophoresis. Before interventions the only significant difference between the effects of ACh and SNP was observed in the frequency around 0.01 Hz, where ACh increased normalized amplitude to a greater extent than SNP. L-NMMA abolished this difference, whereas it reappeared after infusion of L-arginine ($P = 0.0084$). Aspirin did not affect this difference ($P = 0.006$). We conclude that basal cutaneous blood flow and the endothelial dependency of the oscillation around 0.01 Hz are partly mediated by NO, but not by endogenous PGs. Other aspects of human cutaneous circulation studied are not regulated by NO or PGs.

Keywords: Acetylcholine; Cutaneous blood flow dynamics; Endothelium; Nitric oxide; Oscillations; Prostaglandins; Sodium nitroprusside; Spectral analysis; Wavelet transform

Introduction

The vascular endothelium modulates smooth muscle tone by releasing several vasoactive substances. Nitric oxide (NO) is involved in regulation of vascular tone and plays an important role in regulation of blood pressure and blood flow distribution (Vallance et al., 1989). It is released during basal conditions in response to chemical stimuli, such as acetylcholine (ACh) (Furchgott and Zawadzki, 1980; Ignarro et al., 1987), and in response to mechanical stimuli, such as shear stress (Koller and Kaley, 1991). The terminal guanidino nitrogen of the amino acid L-arginine is the pre-

* Corresponding author. Department of Intensive Care Medicine, Ulleval University Hospital, 0407 Oslo, Norway. Fax: +4722119634.
E-mail address: per.kvandal@ulleval.no (P. Kvandal).

0026-2862/03/$ – see front matter © 2003 Elsevier Science (USA). All rights reserved.
doi:10.1016/S0026-2862(03)00006-2

cursor of NO (Palmer et al., 1988). L-arginine analogues, such as N^G-monomethyl-L-arginine (L-NMMA), inhibit the synthesis of NO.

Abnormalities of vascular prostaglandin (PG) synthesis have been implicated in a number of pathophysiological states. Prostacyclin contributes to the tromboresistant and dilatory properties of blood vessels and opposes the constrictor and protrombotic effects of thromboxane (Moncada and Vane, 1978; Roth and Caverley, 1994). Endogenous PGs modulate reactive and functional hyperemia (Kilbom and Wennmalm, 1976). Bhagat et al. (1995) demonstrated that local generation of PGs in human vessels in vivo alters vascular tone. The importance of PGs can be investigated by using the cyclooxygenase inhibitor aspirin (Heavy et al., 1985), which irreversibly acetylates the active site of the enzyme.

ACh-induced vasodilation depends on intact vascular endothelium (Furchgott and Zawadzki, 1980), whereas sodium nitroprusside (SNP) acts directly on vascular smooth muscle cells (Rapoport et al., 1983). Endothelial dysfunction can therefore be evaluated by comparing ACh- and SNP-induced vasodilation. ACh and SNP may be introduced transdermally by iontophoresis, and the increases in perfusion may be quantified by the laser Doppler flowmetry (LDF) technique. ACh-induced vasodilation may be mediated by generation of NO (Vallance et al., 1989), PGs (Zellers et al., 1994), or endothelial-derived hyperpolarizing factor (Garland et al., 1995). The relative contribution of these mediators varies between tissues and the contributions of these factors in human skin are unclear.

Endothelial activity may also be evaluated by the dynamics of the blood perfusion signal. Periodic oscillations of five characteristic frequencies have been revealed in the human cutaneous circulation (Bracic and Stefanovska, 1998; Kvernmo et al., 1998b; Stefanovska et al., 1999). These oscillations represent the influence of the heartbeat, the respiration, the intrinsic myogenic activity of vascular smooth muscle, and the neurogenic activity on the vessel wall, with frequencies around 1, 0.3, 0.1, and 0.04 Hz, respectively (Salerud et al., 1983; Kastrup et al., 1989; Hoffmann et al., 1990; Stefanovska, 1992; Bollinger et al., 1993; Mück-Weymann et al., 1996). In addition, we have demonstrated an oscillation with a period of around 1 min (0.01 Hz) (Kvernmo et al., 1998b), which is modulated by the endothelium (Kvernmo et al., 1999).

Based on these findings and the fact that NO and PGs are important in the physiological and pathophysiological regulation of vascular tone, we hypothesized that these two mediators might modulate parts of the dynamics of the blood perfusion signal in human cutaneous circulation. The specific aims of the present study were to investigate the importance of endogenous NO and PGs for: (1) basal cutaneous blood flow, evaluated by its mean value; (2) the blood flow recorded during iontophoretic application of ACh and SNP, evaluated by its mean value; and (3) the five oscillatory components of the blood perfusion signal, during basal conditions and during iontophoretic application of ACh and SNP. We tested these variables in healthy male volunteers (1) before and after inhibition of NO synthesis with L-NMMA and after reversing inhibition of NO synthesis with L-arginine and (2) before and after the inhibition of PG synthesis with aspirin.

Table 1
Anthropometric data of the three groups

	NO Group	PG Group	Control
Age (years)	32 (28–39)	32 (29–43)	37 (31–39)
Body mass (kg)	84 (74–110)	80 (70–110)	82 (70–91)
Height (cm)	185 (174–203)	181 (176–203)	182 (174–197)
Room temperature (°C)	23.6 (23.0–24.2)	24 (23–25)	23.8 (22.5–25.0)

Note. Data are given as median and total range. NO, nitric oxide; PG, prostaglandin.

Material and methods

Subjects

Sixteen healthy male volunteers were recruited for the NO group, 15 healthy males volunteered for the PG part, and 7 healthy male volunteers served as controls. All subjects gave informed consent and the study was approved by the local Ethics Committee. The subjects had not taken any medication the last week prior to the study. None of the subjects were smokers, and they refrained from alcohol and caffeine-containing drinks at least 4 h prior to the study. Exclusion criteria were a history of cardiovascular disease or other illness. For anthropometric data of the three groups see Table 1.

Experimental procedure

The study was performed with subjects in the supine position in a quiet room with the temperature kept at 23 to 24°C. The experimental procedure started after an acclimatization period of 20 min. In all groups two probes for basal LDF recordings (MP1 probes, Moor Instruments, Axminster, Devon, UK), and two probes for combined iontophoresis and LDF recordings (DP1T probes, Moor Instruments) were positioned with double-sided adhesive tape. One basal probe was positioned on the upper arm, and the other probes were placed on the forearm distal to the cubital fossa (Fig. 1). The probes were positioned at least 5 cm apart, avoiding superficial veins and broken skin areas. To avoid residual effects of the drugs the position of the probes for combined iontophoresis and LDF recordings were changed to untreated skin after each of the measurements.

Skin temperature was measured by temperature sensors in the laser Doppler probes. Invasive blood pressure was measured in the NO group and noninvasive blood pressure

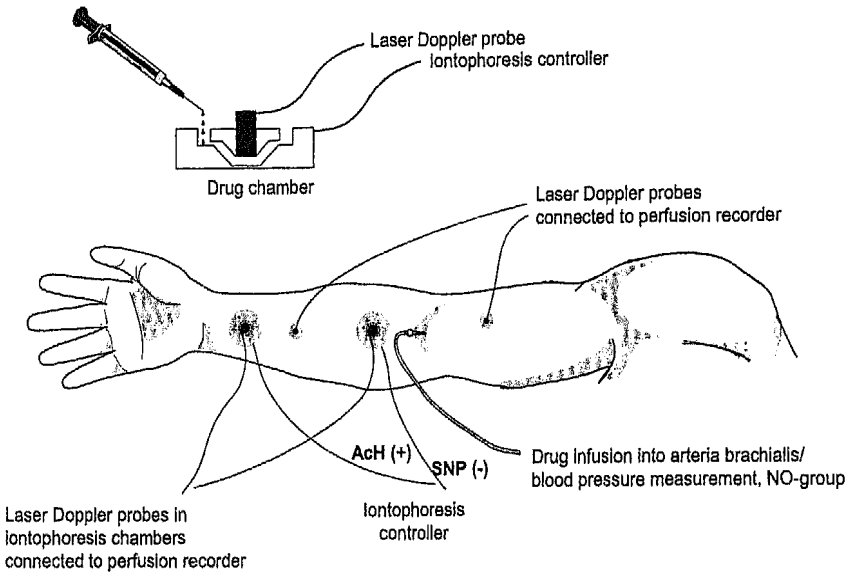

Fig. 1. Experimental setup for laser Doppler perfusion recordings and iontophoresis with acetylcholine (ACh) and sodium nitroprusside (SNP). In the nitric oxide (NO) group, arteria brachialis was cannulated and L-NMMA and L-arginine were infused into the artery. In the prostaglandin (PG) group aspirin was infused through a venous catheter placed in a superficial vein on the volar part of the opposite hand (not shown). Arteria brachialis was not cannulated in the PG group.

was measured in the PG and control groups. Heart rate was continuously monitored by the electrocardiograph signal and respiratory rate was counted.

NO group (n = 16)

The brachial artery was cannulated under local anaesthesia (1% lidocaine) with a 20-gauge/1.0 mm × 45 mm intravascular over-the-needle catheter. The catheter was connected to a pressure transducer (Baxter Healthcare Corp., USA) for direct measurement of arterial blood pressure, and to an infusion pump (Graseby 3200, Graseby Medical, UK) for drug infusion. Basal blood perfusion and blood perfusion responses during iontophoresis with ACh and SNP were simultaneously recorded for 30 min (Fig. 2, top panel). L-NMMA (16 μmol/min for 5 min) was then infused into the brachial artery, followed by simultaneous recordings of basal blood perfusion and blood perfusion responses during iontophoresis with ACh and SNP for 30 min. Thereafter, L-arginine (40 μmol/min for 7.5 min) was infused into the brachial artery, again followed by simulta-

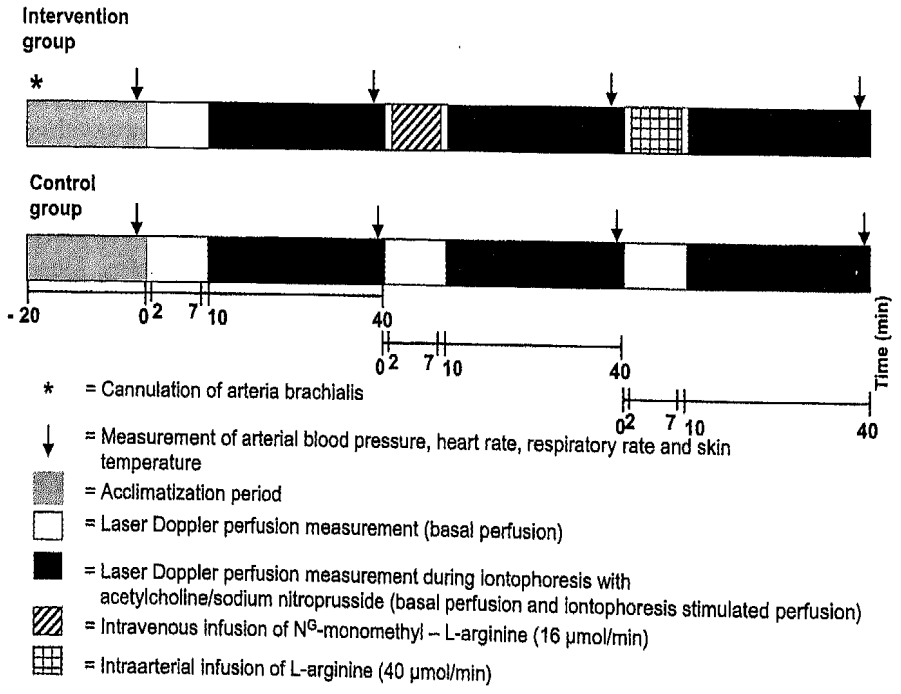

Fig. 2. Experimental procedure for the NO group and the control group.

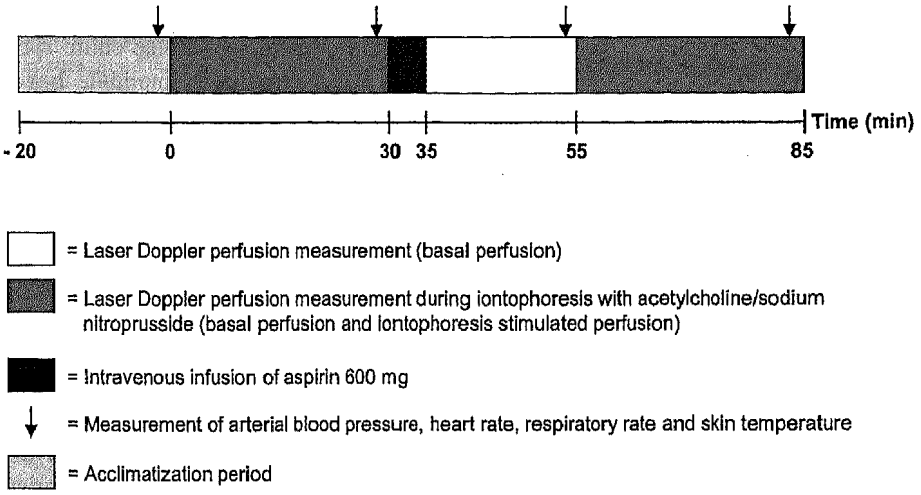

Fig. 3. Experimental procedure for the PG group.

neous recordings of basal blood perfusion and blood perfusion responses during iontophoresis with ACh and SNP for 30 min.

PG group (n = 15)

Basal blood perfusion and blood perfusion responses during iontophoresis with ACh and SNP were recorded for 30 min (Fig. 3). Aspirin (600 mg over 5 min) was then administered by an infusion pump (Graseby 3200, Graseby Medical) connected to a intravenous catheter (internal diameter 1.1 mm) in a superficial vein on the arm opposite to the probes. Twenty minutes after the end of the infusion basal blood perfusion and blood perfusion responses during iontophoresis with ACh and SNP were recorded for 30 min.

Control group (n = 7)

To evaluate the reproducibility of our methods three consecutive periods of basal blood perfusion recordings (same skin areas) and blood perfusion recordings during iontophoresis with ACh and SNP (different skin areas) were performed. The setup and experimental protocol were identical to the NO group, except that L-NMMA and L-arginine were not infused (Fig. 2, bottom panel).

Laser Doppler flowmetry

LDF gives a semiquantitative assessment of microvascular blood perfusion, which is expressed in arbitrary units (AU) (Nilson et al., 1980; Leahy et al., 1999). LDF measurements from the skin reflect perfusion in capillaries, arterioles, venules, and dermal vascular plexa. A minor part of the signal reflects nutritive perfusion and a major part thermoregulatory perfusion (Bollinger et al., 1991). The LDF measurements were obtained with a two-channel flowmeter (MoorLAB server/satellite, Moor Instruments) for reference recordings, and a two-channel flowmeter (DRT 4, Moor Instruments) for recordings during iontophoresis with ACh and SNP. Both instruments deliver light generated by a semiconductor laser diode operating at a wavelength of 780 to 820 nm and with a maximum accessible power of 1.6 mW. The probe has two fibers: one delivers light to the site under observation, and the other collects the backscattered light which contains the Doppler-shifted frequency information. The signal is then filtered with a band-pass filter with cut-off frequencies at 18 Hz and 22.5 kHz. A sampling frequency of 40 Hz and a time constant of 0.1 s were selected.

Iontophoresis

Iontophoresis allows transdermal delivery of polar drugs by means of a small electrical current. Thus, it is possible to assess microvascular reactivity when blood perfusion is measured simultaneously in the same area (Morris and Shore, 1996; Gardner-Medwin et al., 1997; Andreassen et al., 1998). A combined probeholder for iontophoresis and perfusion measurement was fixed with a double-sided adhesive tape on the volar side of the right forearm after the skin was cleaned with isopropyl alcohol and left to dry. The Perspex probeholder has a small chamber for deposition of the test substance which is in direct proximity to the laser Doppler probe ("direct chamber"). A battery-powered constant current stimulator (MIC 1, Moor Instruments) was used to provide a direct current for the drug iontophoresis. The active electrode is made of platinum. By using a second chamber containing a drug of opposite polarity an electrical current is completed. This is the case with both ACh and SNP.

The dosages of the drugs delivered were directly proportional to the total charge (Q) in millicoulombs (mC) which migrates through the skin surface, determined by the product of constant current (I) measured in milliamperes (mA) and the duration (t) of current flow in seconds. We used a charge of 2 mC (100 μA for 20 s) followed by a 240-s response measurement period after each iontophoresis. The iontophoresis was repeated seven times. The statistical anal-

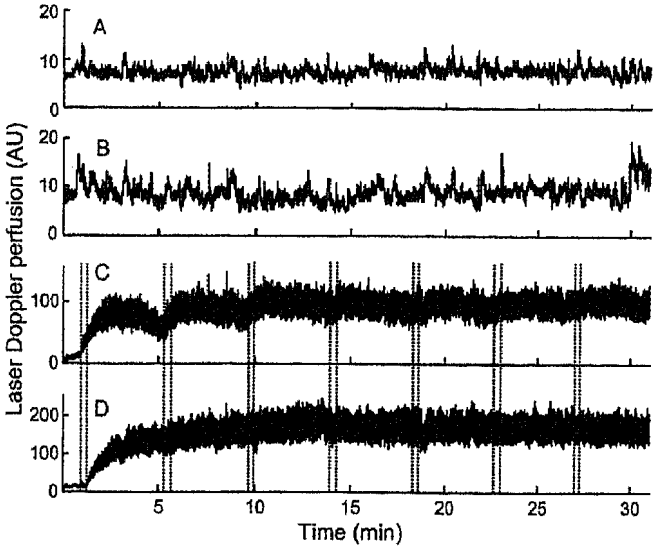

Fig. 4. A typical laser Doppler flowmetry recording during unstimulated perfusion (A and B) and during iontophoresis with acetylcholine (C) and sodium nitroprusside (D). Amplitudes are given in arbitrary units (AU). The short periods between the interrupted vertical lines denotes iontophoresis periods (20-s stimulation with a current of 100 μA repeated seven times).

ysis is based on the mean value of the seven periods. A typical laser Doppler flowmetry recording during basal conditions and during iontophoresis with ACh and SNP is demonstrated in Fig. 4. The magnitude of the applied current avoids vasodilation due to stimulation of local sensory nerves (Westerman et al., 1988). The chamber used in all experiments allowed a skin area of 0.71 cm^2 to be treated.

Spectral analysis

The oscillations of the microvascular blood perfusion signal can be divided into different components by spectral analysis (Meyer et al., 1988; Intaglietta, 1989; Hoffmann et al., 1990; Stefanovska, 1992; Bollinger et al., 1993; Mück-Weymann et al., 1996). Wavelet analysis proposed by Morlet (1983) is a scale-independent method comprising an adjustable window length. Hence, the low frequencies are analysed using a long window and the higher frequencies using a shorter window. The wavelet transform of 30-min recordings was calculated. Periodic oscillations with five characteristic frequency peaks were observed within the frequency interval 0.005–2 Hz. The position of each peak differs between subjects and changes with time in a given subject, but in healthy subjects responses are found to be within the following frequency intervals: 0.0095–0.021, 0.021–0.052, 0.052–0.145, 0.145–0.6, and 0.6–1.6 Hz. The mean amplitude of the oscillations of the total spectrum from 0.0095 to 1.6 Hz and the mean amplitude of each particular frequency interval were calculated. We then normalized the amplitude of the particular frequency interval with respect to the mean amplitude of the entire spectrum. The normalized amplitude was defined as the ratio between the mean amplitude at a particular frequency interval and the mean amplitude of the entire spectrum from 0.0095 to 1.6 Hz. Normalized amplitude has also previously been described as relative amplitude (Kvernmo et. al., 1999).

Drugs

L-NMMA and L-arginine (Alexis Biochemicals, Switzerland) were dissolved in 0.9% sterile saline into solutions containing 16 μmol/ml (L-NMMA) and 40 μmol/ml (L-arginine). Aspirin (Aspegic, Synthelabo Pharma, Lausanne, Switzerland) was dissolved in sterile water into a solution containing 100 mg/ml. ACh and SNP (E. Merck, Germany) were dissolved in deionized water to 1% solutions immediately before the start of the experimental protocol.

Statistical analysis

Data are presented either as group median with total range or as box plots. The five horizontal lines at the boxes are the 10th, 25th, 50th, 75th, and 90th percentiles. Values above or below the 10th or the 90th percentiles are presented as data points. The Wilcoxon signed rank test for comparison of dependent samples and the Friedman's test (Conover, 1980) was used to evaluate statistical differences. A P value of < 0.05 was considered statistically significant.

Results

Effects of L-NMMA, L-arginine, and aspirin on hemodynamics, respiratory rate, and skin temperature

Intraarterial infusion of L-NMMA produced no significant alterations in heart rate, invasive blood pressure, or respiratory rate (Table 2). After infusion of L-arginine mean arterial blood pressure increased by 4.9% ($P = 0.00096$) and systolic blood pressure increased by 4.3% ($P = 0.029$). There were no alterations in diastolic blood pressure or heart rate. The only alteration measured in the skin temperature throughout the experimental procedure was a ~ 2% ($P = 0.02$) decrease measured in the ACh iontophoresis chamber. Intravenous infusion of aspirin produced no significant changes in heart rate, blood pressure, respiratory rate, or skin temperature throughout the experimental procedure (Table 2).

Effects of L-NMMA, L-arginine, and aspirin on basal skin perfusion

Mean value of basal skin perfusion measured by LDF above the elbow (proximal to the injection site of L-NMMA) was unaltered throughout the experimental procedure. Mean value of basal skin perfusion measured by LDF below the elbow (distal to the injection site of L-NMMA) was reduced by ≈20% ($P = 0.0067$) after L-

Table 2
Hemodynamic data, respiratory rate, and skin temperature in the nitric oxide, prostaglandin, and control group throughout the procedure

NO Group	Before L-NMMA	After L-NMMA	After L-arginine
MAP	84 (74–99)	86 (73–102)	90 (69–108)*
SBP	119 (108–133)	120 (105–145)	126 (108–149)**
DBP	67 (57–81)	68 (57–81)	73 (63–91)
HR	57 (43–71)	58 (47–78)	57 (48–78)
RR	16 (12–20)	16 (12–20)	15 (12–20)
Skin temp.[1]	30.7 (29.6–32.6)	30.1 (27.1–33.2)***	30.0 (27.1–31.7)
Skin temp.[2]	30.8 (29.3–33.1)	30.4 (28.3–31.8)	29.7 (27.8–31.9)

PG group	Before Aspirin iv	20 min after Aspirin iv	50 min after Aspirin iv
MAP	85 (77–95)	88 (74–102)	90 (77–108)
SBP	119 (103–135)	122 (108–141)	123 (105–144)
DBP	69 (60–80)	74 (61–85)	74 (50–90)
HR	60 (50–70)	60 (47–70)	60 (50–70)
RR	16 (12–20)	16 (12–16)	16 (12–20)
Skin temp.[1]	29.9 (29.3–32.8)	30.0 (28.3–32.9)	30.6 (28.8–33.0)
Skin temp.[2]	30.8 (29.6–32.4)	30.6 (29.4–32.5)	30.8 (29.9–32.9)

Control	Before Recording 1	Before Recording 2	Before Recording 3
MAP	84 (80–87)	83 (76–90)	84 (79–89)
SBP	119 (114–124)	120 (110–132)	120 (111–127)
DBP	70 (63–78)	69 (61–77)	71 (64–75)
HR	56 (47–60)	55 (50–60)	56 (50–60)
RR	13 (12–16)	14 (12–16)	13 (12–16)
Skin temp.[1]	30.3 (29.3–32.3)	30.2 (29–31.2)	30.5 (28.4–32.9)
Skin temp.[2]	29.9 (29.2–31.3)	29.9 (28.9–30.8)	29.8 (28.5–31.1)

Note. Data are given as median and total range, iv, intravenous; MAP, mean arterial blood pressure; DBP, diastolic blood pressure; SBP, systolic blood pressure; HR, heart rate; RR, respiratory rate; Skin temp.[1,2], skin temperature measured in the two iontophoresis chambers; NO, nitric oxide; PG, prostaglandin.

* $P < 0.001$.

** $P < 0.03$.

*** $P < 0.05$.

NMMA (Fig. 5, left). L-arginine reversed the reduction in skin perfusion induced by L-NMMA. L-NMMA reduced mean value of skin perfusion below vs above the elbow ($P = 0.035$) and L-arginine reversed this difference.

Basal skin perfusion measured by LDF was not significantly altered after aspirin ($P = 0.46$ for the probe above and $P = 0.49$ for the probe below the elbow) (Fig. 5, right).

Effects of L-NMMA, L-arginine, and aspirin on skin perfusion in response to iontophoresis with ACh and SNP

LDF perfusion during iontophoresis with ACh or SNP was not significantly altered after L-NMMA or L-arginine

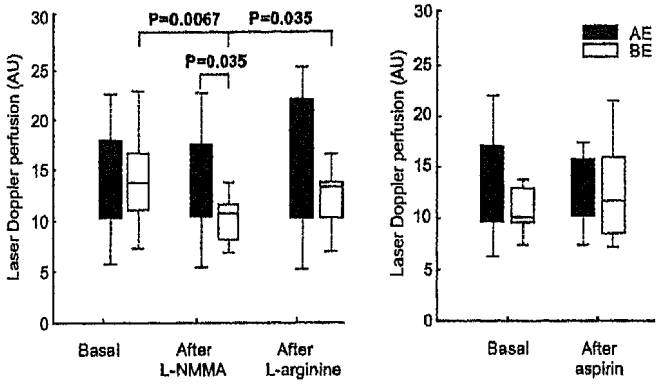

Fig. 5. Mean values of the laser Doppler perfusion signal in arbitrary units (AU) measured in skin probes above (AE) and below (BE) the elbow. (Left) Before and after intraarterial infusion of N^G-monomethyl-L-arginine (L-NMMA) and after intraarterial infusion of L-arginine. (Right) Before and after intravenous infusion of aspirin.

(overall $P = 0.57$ for ACh and $P = 0.87$ for SNP) (Fig. 6, left) or after intravenous infusion of aspirin (overall $P = 0.33$ for ACh and $P = 0.06$ for SNP) (Fig. 6, right). When comparing the responses to iontophoresis with ACh vs SNP, no significant alterations were found after L-NMMA or L-arginine or after aspirin.

When skin perfusion during iontophoresis with ACh or SNP was evaluated by mean spectral amplitude of the frequency interval from 0.0095 to 1.6 Hz, no significant effects of L-NMMA, L-arginine ($P = 0.76$ for ACh and $P = 0.91$ for SNP), or aspirin ($P = 0.71$ for ACh and $P = 0.2$ for SNP) were seen.

Effects of L-NMMA, L-arginine, and aspirin on the mean amplitude of the total spectrum and on the mean spectral amplitudes within each of the five frequency intervals during basal perfusion

When basal skin perfusion was evaluated by mean amplitude of the total spectrum from 0.0095 to 1.6 Hz, no significant effects of L-NMMA or L-arginine (overall $P = 0.7$) or aspirin (overall $P = 1.0$) were seen.

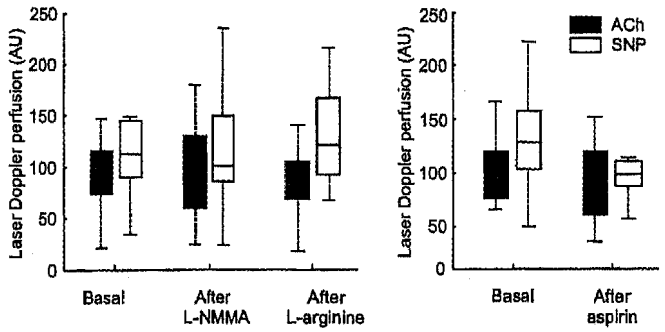

Fig. 6. Mean values of the laser Doppler perfusion signal in arbitrary units (AU) during iontophoresis with acetylcholine (ACh) and sodium nitroprusside (SNP) before and after intraarterial infusion of N^G-monomethyl-L-arginine (L-NMMA) and after intraarterial infusion of L-arginine (left) and before and after the intravenous infusion of aspirin (right).

There were no significant differences in either of the five frequency intervals after L-NMMA or L-arginine (overall $P = 0.44$ in the 0.0095–0.021 Hz interval, $P = 0.31$ in the 0.021–0.052 Hz interval, $P = 0.53$ in the 0.052–0.145 Hz interval, $P = 0.53$ in the 0.145–0.6 Hz intervals, and $P = 0.53$ in the 0.6–1.6 Hz interval) or after aspirin ($P = 0.68$ in the 0.0095–0.021 Hz interval, $P = 0.68$ in the 0.021–0.052 Hz interval, $P = 0.25$ in the 0.052–0.145 Hz interval, $P = 0.33$ in the 0.145–0.6 Hz interval, and $P = 0.68$ in the 0.6–1.6 Hz interval).

Effects of L-NMMA, L-arginine, and aspirin on normalized spectral amplitudes within each of the five frequency intervals in response to iontophoresis with ACh and SNP

None of the normalized spectral amplitudes in each of the five frequency intervals in response to iontophoresis with either ACh or SNP were altered by L-NMMA, L-arginine, or aspirin. Normalized amplitude of the oscillation with a frequency around 0.01 Hz increased to a greater extent in response to ACh iontophoresis than to SNP iontophoresis before L-NMMA ($P = 0.025$) and before aspirin ($P = 0.01$). This difference was abolished after L-NMMA, whereas it reappeared after L-arginine ($P = 0.0084$) (Fig. 7A). Aspirin did not alter this relationship ($P = 0.0058$) (Fig. 7B). The response to ACh vs SNP iontophoresis was not significantly altered by L-NMMA, L-arginine, or aspirin in any of the four other frequency intervals.

Control group

Hemodynamics, respiratory rate, and skin temperature were not significantly altered throughout the experimental protocol (Table 2). There were no significant alterations in basal skin perfusion measured by LDF or by mean value of the total spectrum from 0.0095 to 1.6 Hz among the three measurements (Table 3). Perfusion during iontophoresis with ACh or SNP, performed at three different sites, showed no significant differences among the three measurements. Normalized amplitude of spectral components, either during basal perfusion or during iontophoresis with ACh or SNP, did not show significant differences among the three measurements (Table 3).

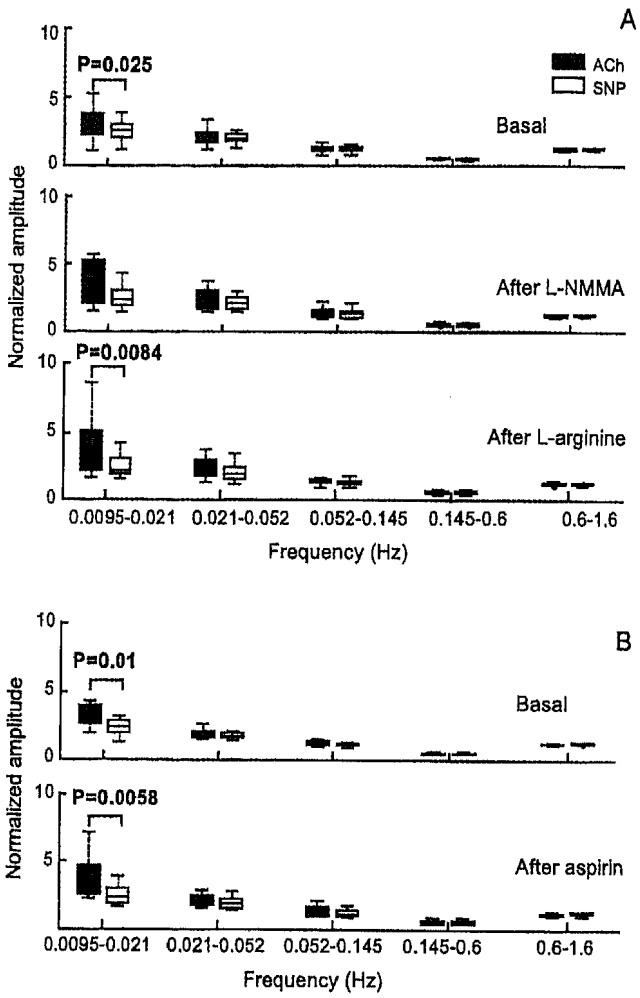

Fig. 7. Amplitudes of each of the five frequency intervals, normalized to the mean amplitude of the total spectrum from 0.0095 to 1.6 Hz during iontophoresis with acetylcholine (ACh) and sodium nitroprusside (SNP). In (A) data are given before and after intraarterial infusion of N^G-monomethyl-L-arginine (L-NMMA) and after intraarterial infusion of L-arginine. In (B) data are given before and after the intravenous infusion of aspirin.

Discussion

The human cutaneous circulation has provided important information regarding the pathophysiology of several diseases, such as hypertension (Heagerty et al., 1988), diabetes (Rayman et al., 1986), and heart failure (Angus et al., 1993). In heart failure and hypercholesterolemia, basal and stimulated release of endothelium-derived factors are impaired in the microcirculation, but not in conduit vessels (Drexler et al., 1992; Hayoz et al., 1995). A relation between exercise capacity and endothelium-dependent vasodilation measured by the LDF/iontophoresis technique has been described in heart transplant recipients (Andreassen et al., 1998). Skin perfusion can be monitored easily and noninvasively by LDF.

Methodological considerations

To inhibit NO synthesis we used the specific, competitive inhibitor L-NMMA (Rees et al., 1989). A total of 16 μmol/min L-NMMA was infused into the brachial artery for 5 min. In previous studies infusion rates of L-NMMA into the brachial artery have varied from 1 to 16 μmol/min (Vallance et al., 1989; Endo et al., 1994; Noon et al., 1996; Gilligan et al., 1994) for a period of 5 min. The dose of L-NMMA we used might have been insufficient to induce total inhibition of NO synthesis in the skin microcirculation. However, in studies on effects of L-NMMA on arterial circulation it has been shown that lower doses cause flow reduction in the brachial artery by 40–50% (Vallance et al.,

Table 3
Mean values of laser Doppler perfusion signals, mean amplitudes, and normalized amplitudes of each oscillatory component in three consecutive measurements in different skin areas in the control group

	Measurement 1	Measurement 2	Measurement 3	n	P123
Basal perfusion 1 (AU)	11.4 (9.9–16.8)	10.8 (8.7–13.9)	9.7 (8.8–11.6)	5	0.247
Basal perfusion 2 (AU)	9.5 (5.8–20.6)	11.3 (5.9–29.8)	12.9 (6.1–30.4)	6	0.223
Perfusion with ACh (AU)	98.1 (69.2–196.6)	95.4 (10.5–187.7)	67.9 (28.7–111.5)	7	0.050
Perfusion with SNP (AU)	99.3 (47.0–173.1)	88.8 (48.3–147.4)	87.8 (23.7–126.3)	7	0.651
P ACh/SNP	0.706	0.706	0.059		
Mean amplitude in the frequency interval from 0.095 to 1.6 Hz					
Basal perfusion 1	303.4 (57.7–475.2)	281.7 (139.8–410.5)	195.8 (120.1–372.4)	5	0.5488
Basal perfusion 2	162.3 (62.7–603.8)	200.8 (86.73–972.9)	199.6 (105.0–610.5)	6	0.1353
Perfusion with ACh	313.2 (200.7–488.7)	286.8 (41.8–502.9)	206.2 (83.7–342.7)	7	0.3679
Perfusion with SNP	194.3 (160.7–466.1)	296.2 (155.0–496.0)	261.2 (79.1–324.9)	7	0.6514
P ACh/SNP	0.257	0.706	0.706		
Normalized amplitudes of oscillatory components					
Basal perfusion 1					
0.0095–0.021	10.3 (8.7–16.0)	9.5 (7.6–16.4)	10.2 (8.7–16.0)	5	1.000
0.021–0.052	9.9 (5.6–10.1)	8.7 (3.9–11.2)	9.9 (5.6–10.1)	5	0.091
0.052–0.145	4.1 (2.6–10.1)	4.7 (1.6–5.7)	4.1 (2.6–5.0)	5	0.819
0.145–0.6	0.7 (0.6–1.1)	0.6 (0.6–1.2)	0.7 (0.6–1.1)	5	0.165
0.6–1.6	0.6 (0.4–0.6)	0.5 (0.3–0.7)	0.5 (0.4–0.6)	5	0.247
Basal perfusion 2					
0.0095–0.021	8.6 (6.0–12.6)	7.8 (4.8–13.1)	8.6 (6.0–12.6)	6	0.513
0.021–0.052	6.6 (4.2–10.5)	6.1 (3.5–11.1)	6.6 (4.2–10.5)	6	0.513
0.052–0.145	4.7 (2.8–5.8)	4.9 (2.2–5.2)	4.7 (2.8–5.8)	6	0.311
0.145–0.6	0.8 (2.8–5.8)	0.9 (0.6–1.3)	0.8 (0.7–1.1)	6	0.847
0.6–1.6	0.5 (0.3–0.7)	0.5 (0.4–0.9)	0.5 (0.3–0.7)	6	0.311
Perfusion with ACh					
0.0095–0.021	4.9 (2.8–10.4)	4.2 (2.7–7.7)	3.6 (2.8–10.4)	7	0.867
0.021–0.052	2.3 (1.7–3.4)	2.7 (1.3–5.2)	2.3 (1.7–3.4)	7	0.498
0.052–0.145	1.3 (0.9–1.9)	1.2 (0.7–2.7)	1.2 (0.9–1.9)	7	0.867
0.145–0.6	0.6 (0.5–0.8)	0.6 (0.4–0.9)	0.5 (0.5–0.8)	7	0.651
0.6–1.6	1.1 (1.0–1.2)	1.1 (0.8–1.2)	1.1 (1.0–1.2)	7	0.565
Perfusion with SNP					
0.0095–0.021	2.4 (1.7–7.5)	2.8 (1.7–5.7)	2.4 (1.7–7.5)	7	0.8669
0.021–0.052	1.9 (1.5–3.7)	2.0 (1.4–3.8)	1.9 (1.5–3.7)	7	0.6514
0.052–0.145	1.1 (0.9–2.9)	1.3 (0.7–2.0)	1.1 (1.5–3.7)	7	0.6514
0.145–0.6	0.5 (0.5–0.8)	0.6 (0.4–0.9)	0.5 (0.5–0.8)	7	0.5647
0.6–1.6	1.1 (0.9–1.2)	1.1 (1.0–1.2)	1.1 (0.9–1.2)	7	0.8669

Note. Data are given as median and total range. ACh, acetylcholine; SNP, sodium nitroprusside; AU, arbitrary units; P123, overall P value between measurements 1, 2, and 3. The basal blood perfusion signals were recorded on the same skin area for all three sets, while the blood perfusion responses to iontophoresis with ACh/SNP were recorded on different skin areas for each set.

1989) and almost abolish the radial response to ACh (Joannides et al., 1995). Higher doses of L-NMMA were not infused in order to avoid increased systemic blood pressure and vasoconstriction in other vascular beds. By using a lower dose of L-NMMA than in the present study Vallance et al. (1989) induced an increase in forearm vascular resistance, lasting at least 30 min after the infusion was stopped. Thus, we consider that NO was inhibited throughout the recording period of 30 min.

To inhibit PG synthesis we infused intravenously the cyclooxygenase inhibitor aspirin (600 mg over 5 min). This dose of aspirin, given either intravenously (Heavy et al., 1985) or orally (Barrow et al., 1987), has been shown to produce a rapid and substantial inhibition of PG synthesis. Heavy et al. (1985) showed that 600 mg of aspirin given over 5 min intravenously inhibited bradykinin-induced production of prostacyclin maximally at 30 min. Ninety minutes after aspirin administration bradykinin-induced production of prostacyclin was still 70% inhibited. Recovery of prostacyclin production was complete after 6 h. This dose of aspirin also maximally inhibited platelet thromboxane A_2 production. Thirty minutes after administration it was inhibited by more than 99% and it remained inhibited for at least 6 h.

Iontophoresis with ACh and SNP, combined with laser Doppler perfusion measurements, has emerged as a widely used method (Westerman et al., 1988; Kvernmo et al., 1998a, 1998b, 1999; Morris and Shore, 1996; Morris et al., 1995). A nonspecific vasodilation during iontophoresis has been demonstrated (Morris and Shore, 1996; Morris et al.,

1995). Åsberg et al. (1999) found that high molar concentrations of NaCl to the iontophoresis solutions attenuated the nonspecific vasodilation. However, the variability was higher using a hyperosmolar vehicle. Based on these findings we dissolved ACh and SNP in deionized water. To avoid possible nonspecific vasodilatory responses caused by galvanic currents we used a charge of 2.0 mC (100 μA for 20 s), followed by a 240-s registration period, repeated seven times.

Laser Doppler flowmetry recordings may show spatial variation due to the restricted area of skin in contact with the optical fibre and variations in anatomy of the skin areas examined (Kubli et al., 2000). On the volar part of the forearm both basal and iontophoretically increased LDF perfusion show small site-to-site variability (Gardner-Medwin et al., 1997). We evaluated the reproducibility of our data in a separate control group, with identical setup and experimental protocols as the NO group, except that L-NMMA and L-arginine were not administered. We found no significant alteration in basal skin perfusion, data from iontophoresis with ACh and SNP, or data from spectral analysis of the signals among the three measurement periods. Thus, our findings in the NO group cannot be explained by time-dependent or site-dependent variability in the methods used.

Basal skin perfusion

During basal conditions L-NMMA decreased the LDF signal by ~20%. This illustrates the major role of basal NO release in human skin, which keeps the dermal microvasculature in a dilated state. This is in agreement with human skin microdialysis experiments showing that addition of an inhibitor of NO synthesis to the perfusate caused a reduction in resting tissue NO (Clough, 1999), which was reversed by L-arginine. Thus the alterations seen are due to an NO-specific effect and not due to nonspecific effects unrelated to the L-arginine–NO axis. As far as we are aware, the reversibility with L-arginine has only been established for total brachial flow (Vallance et al., 1989), not for the skin microcirculation.

The role of NO in regulation of basal cutaneous vascular tone in humans is controversial. NO has been shown to contribute to the basal dilator tone on the dorsal finger skin and the forearm skin (Khan et al., 1996; Coffman, 1994), which is in accordance with our findings. However, our findings are in contrast to the findings of Noon et al. (1996), who showed that L-NMMA had no effect on resting vascular tone on the dorsal surface of the finger, but had an effect in the pulp where thermoregulatory arteriovenous anastomoses are present. Additionally, neither Khan et al. (1997) (3 mg/kg L-NMMA intravenously for 60 min) or Noon et al. (1998) (4 μmol/min L-NMMA in the brachial artery for 30 min) found any effect of L-NMMA on basal perfusion in human forearm skin measured by LDF. L-NMMA in these two studies was administered in much lower concentrations than in the present study.

The reason for the smaller effect of L-NMMA on skin perfusion in our study (~20%), compared to the reduction in brachial flow (~50%) found by Vallance et al. (1989), might relate to differences in blood flow in the two different perfusion areas. Substantially more L-NMMA might be delivered to the muscles than to the skin of the forearm. Alternatively, NO might play a more important role for flow in human skeletal muscle than in the skin microcirculation. Higher flow rates to the muscles of the forearm may result in a greater flow-dependent release of NO during basal conditions and thus a greater effect of L-NMMA.

Prostaglandins such as PGE_2, PGI_2 and PGD_2 are potent dilatators produced in the vessel wall, which theoretically might keep the skin microvasculature in a dilated state. However, in the present study aspirin did not alter the LDF signal during basal conditions. We cannot be completely certain that aspirin reached the cutaneous microcirculation in a concentration sufficient to completely inhibit a potential basal PG synthesis, but as discussed under methodological considerations, this is not very likely. Our results are in agreement with Noon et al. (1998), who found that 30 min after an intravenous bolus injection of 600 mg aspirin, LDF perfusion on the volar aspect of the forearm was unaltered. Additionally, Khan et al. (1997) demonstrated that administration of 600 mg/day of oral aspirin for 3 days did not alter basal LDF perfusion on the volar aspect on the forearm. Berghoff et al. (2002) found that four different doses of chewable aspirin (81, 648, 972, or 1944 mg) did not affect basal LDF perfusion on the forearm. These and our results indicate that basal cutaneous vascular tone in humans is not dependent on the production of endogenous PGs.

Iontophoresis with ACh and SNP

In rabbit skin ACh injected locally causes a dose-dependent increase in microvascular blood flow, which is abolished by inhibition of either PG or NO synthesis, indicating that both mediators might be important in ACh-induced vasodilation (Warren et al., 1994). However, in the present study the LDF signal during iontophoresis with ACh and SNP did not change after L-NMMA or aspirin, indicating that neither NO nor PG synthesis is important for ACh-induced vasodilation in our model. We cannot be completely certain that L-NMMA and aspirin reached the cutaneous microcirculation in concentrations sufficient to inhibit potential ACh-induced NO or PG production, but as discussed under methodological considerations, this is not very likely.

Morris and Shore (1996) performed iontophoresis with ACh and SNP dissolved in deionized water to a 1% solution on the forearm skin. Their iontophoresis protocol included seven charges of 2 mC and one charge of 4 mC. They found no significant difference in LDF perfusion before and after oral intake of 600 mg aspirin. Noon et al. (1998) performed

iontophoresis on the forearm skin with ACh and SNP dissolved in 2% methylcellulose gel to a 2% solution with charges of 1, 2, 4, and 8 mC, and found that intravenous infusion of 600 mg aspirin significantly reduced the LDF responses to ACh at charges of 2, 4, and 8 mC. Khan et al. (1997) found that oral intake of 600 mg aspirin/day for 3 days reduced the vasodilator response to forearm iontophoresis of ACh and SNP 1% dissolved in deionized water at a charge of 4 mC. The results from our study and the studies discussed above present conflicting results. Vasodilation induced by iontophoresis with ACh is dose-dependent. A significant reduction in LDF perfusion during ACh iontophoresis after treatment with aspirin seems to occur either at higher concentrations of ACh (2%) or higher iontophoretic charges (4 and 8 mC). A possible explanation for the discrepancy between different studies might be that aspirin inhibits PG-mediated vasodilation only in the higher cholinergic dose range. However, this explanation was not supported by Berghoff et al. (2002), who performed ACh iontophoresis on the forearm skin with charges from 0.06 to 56 mC without finding any change after chewable aspirin.

Spectral analysis of the LDF signal

Even though basal skin perfusion measured by LDF was reduced by ~20% after L-NMMA, there were no significant differences in mean amplitude of either of the five frequency intervals. Potential explanations for this discrepancy might be that differences in one or more intervals are too small to be detected by our methods. Alternatively, a steady constriction in the skin microvasculature might have occurred, but magnitudes of oscillations of the five analysed components have remained constant. When basal skin perfusion was evaluated by the mean amplitude of the total spectrum from 0.0095 to 1.6 Hz we did not find significant effects of L-NMMA. This finding is in accordance with unaltered LDF signal during basal conditions. These results indicate that the mean value of the basal skin LDF perfusion is a more sensitive variable to detect small alterations during intervention studies, compared to spectral analysis of the perfusion signal using mean amplitude of the total spectrum. Aspirin had no significant effects on either of the five frequency intervals within the total spectrum during basal perfusion.

Before L-NMMA and aspirin a significant difference in the effects of ACh and SNP was observed only for the oscillation, with a peak amplitude at around 0.01 Hz. In this frequency interval ACh increased the normalized amplitude to a greater extent than SNP. This finding has previously been demonstrated by Kvernmo et al. (1999). The main new finding in the present study is that L-NMMA abolished this difference and L-arginine reestablished it. Aspirin did not affect the difference. To the best of the authors' knowledge, this is the first time that the endothelial dependency of the oscillation with a frequency around 0.01 Hz has been shown to be at least partly mediated by NO, but not PGs. This finding implies that the oscillation with a repetition time of 1 min (0.01 Hz) may reflect either the rate of endothelial release of NO or the rhythmical response of an oscillator in the vascular smooth muscle cells to NO.

Slow oscillations that can be blocked by inhibition of NO synthesis have been described in the microcirculation of different species. In the cat optic nerve head Buerk and Riva (1998) reported NO activity manifested as low-frequency oscillations. They measured blood flow with LDF and NO simultaneously with electrochemical sensors. The lowest peak at around two cycles/min (or 0.03 Hz) in the NO signal decreased after administration of NO synthase inhibitors. By analysing time segments of a few minutes using Fourier transform, they were not able to correlate these changes in NO oscillations to oscillations in blood flow. Longer time segments with higher sampling frequency and better low-frequency resolution might have clarified the frequency characteristics of NO oscillations and their correlation to blood flow oscillations. Bertuglia and Colantuoni (1997) made LDF perfusion recordings in arterioles and venules in the hamster cheek pouch microcirculation during hemorrhagic shock. By characterizing the LDF signal with fast Fourier transform and autoregressive modeling they found that hemorrhagic shock induced large amplitude, low-frequency flowmotion exclusively in the venules with a frequency of around 3 cycles/min. This pattern was abolished by L-NMMA. A study on mesenteric small arteries has suggested that the release of NO from the endothelium, and subsequent generation of cyclic GMP in vascular smooth muscle cells, activates oscillations in membrane potential and tension and that the oscillator itself appears to be located within the smooth muscle cells (Gustafsson et al., 1993).

The NO dependency of the oscillation with a peak at around 0.01 Hz was only detected when we compared the responses between ACh and SNP iontophoresis. None of the five normalized spectral amplitudes of the blood flow signal measured during iontophoresis with ACh or SNP were altered either by L-NMMA or by L-arginine. One reason we did not find changes in response to ACh or SNP iontophoresis individually after inhibition of NO synthesis might be that we changed the site of the probes before each intervention, to avoid residual effects of ACh and SNP. Minor differences in the vascular structure of the skin or skin barrier might have given site-to-site differences in the responses to the drugs.

Other research groups have not reported periodic oscillations with a frequency of around 0.01 Hz in the signal of human cutaneous blood flow measured by LDF. Using spectral analysis based on windowed Fourier transform (Stefanovska, 1992; Stefanovska and Kroselj, 1997), or wavelet transform (Bracic and Stefanovska, 1998; Kvernmo et al., 1998b), we have shown that the oscillations with characteristic frequency around 0.01 Hz can be detected both in the cutaneous flow signal and in the heart rate signal. We have also demonstrated that these oscillations are

present both under resting conditions (Bracic and Stefanovska, 1998) and in postexercise hyperemia (Kvernmo et al., 1998b). The main reason why this frequency has not been revealed by other groups is that they analyzed shorter signals (up to some minutes only) and applied Fourier transform or autoregressive methods. For these reasons they did not obtain low-frequency resolution and missed the characteristic frequencies in the low-frequency region.

Acknowledgments

The experiments were performed at the Institute for Experimental Research, Ulleval University Hospital, Oslo, Norway. The authors are indebted to the head of the institute, Professor Ole M. Sejersted, for providing excellent conditions for our experiments. We also acknowledge Moor Instruments, Devon, UK, with special thanks to Rodney Gush. The study was funded by The Slovenian Ministry of Education, Science and Sport, The Research Forum of Ulleval Hospital, The Ulleval Foundation, The Family Blix Foundation, The Institute for promotion of Anaesthesiological Research, The University of Oslo Foundation (UNIFOR), and The Norwegian Air Ambulance Research Foundation.

References

Andreassen, A.K., Kvernebo, K., Jorgensen, B., Simonsen, S., Kjekshus, J., Gullestad, L., 1998. Exercise capacity in heart transplant recipients: relation to impaired endothelium-dependent vasodilation of the peripheral circulation. Am. Heart J. 136, 320–328.

Angus, J.A., Ferrier, C.P., Krishnankutty, S., Kaye, D.M., Jennings, G.L., 1993. Impaired contraction and relaxation in skin resistance arteries from patients with congestive heart failure. Cardiovasc. Res. 27, 204–210.

ÅAsberg, A., Holm, T., Vassbotn, T., Andreassen, A.K., Hartman, A., 1999. Nonspecific microvascular vasodilation during iontophoresis is attenuated by application of hyperosmolar saline. Microvasc. Res. 58, 41–48.

Barrow, S.E., Cockcroft, J.R., Ritter, J.M., Salvidge, T.T., 1987. Effects of aspirin and salicylate on bradykinin-stimulated prostacyclin production in man. J. Physiol. 398, 83P [Abstract].

Berghoff, M., Kathpal, M., Kilo, S., Hilz, M.J., Freeman, R., 2002. Vascular and neural mechanisms of ACh-mediated vasodilation in the forearm cutaneous microcirculation. J. Appl. Physiol. 92, 780–788.

Bertuglia, S., Colantuoni, A., 1997. Venular oscillatory flow during hemorrhagic shock and NO inhibition in hamster cheek pouch microcirculation. Microvasc. Res. 54, 233–242.

Bhagat, K., Collier, J., Vallance, P., 1995. Vasodilation to arachidonic acid in humans. An insight into endogenous prostanoids and effects of aspirin. Circulation 92, 2113–2118.

Bollinger, A., Hoffmann, U., Franzeck, U.K., 1991. Evaluation of flux motion in man by the laser Doppler technique. Blood Vessels 28, 21–26.

Bollinger, A., Hoffmann, U., Franzeck, U.K., 1993. Is high-frequency fluxmotion due to respiration or to vasomotion activity?, in: Messmer, K. (Ed.), Progress in Applied Microcirculation, Karger, Basel, pp. 52–58.

Bracic, M., Stefanovska, A., 1998. Wavelet based analysis of human blood flow dynamics. Bull. Math. Biol. 60, 919–935.

Buerk, D.G., Riva, C.E., 1998. Vasomotion and spontaneous low-frequency oscillations in blood flow and nitric oxide in cat optic nerve. Microvasc. Res. 55, 103–112.

Clough, G.F., 1999. Role of nitric oxide in the regulation of micro vascular perfusion in human skin in vivo. J. Physiol. 516, 549–557.

Coffman, J.D., 1994. Endothelium-derived nitric oxide on the skin and digital flow in humans. Am. J. Physiol. 267, H2087–H2090 (Heart Circ. Physiol. 36).

Conover, W.J., 1980. Practical Non-parametric Statistics, Second ed. Wiley, New York, pp. 299–300.

Drexler, H., Hayoz, D., Münzel, T., Burckhardt, H., Just, H., Brunner, H.R., Zelis, R., 1992. Endothelial function in chronic congestive heart failure. Am. J. Cardiol. 69, 1596–1601.

Endo, T., Imaizumi, T., Tagawa, T., Shiramoto, M., Ando, S., Takeshita, A., 1994. Role of nitric oxide in exercise induced vasodilation of the forearm. Circulation 90, 2886–2890.

Furchgott, R.F., Zawadski, J.W., 1980. The obligatory role of endothelial cells in the relaxation of arterial smooth muscle by acetylcholine. Nature 288, 373–376.

Gardner-Medwin, J.M., Taylor, J.Y., Macdonald, I.A., Powell, R.J., 1997. An investigation into variability in micro vascular skin blood flow and the responses to transdermal delivery of acetylcholine at different sites in the forearm and hand. Br. J. Clin. Pharmacol. 43, 391–397.

Garland, C.J., Plane, F., Kemp, B.K., Cocks, T.M., 1995. Endothelium-dependent hyperpolarisation: a role in the control of vascular tone. Trends Pharmacol. Sci. 16, 23–30.

Gilligan, D.M., Panza, J.A., Kilcoyne, C.M., Waclawiw, M.A., Cascino, P.R., Quyyumi, A.A., 1994. Contribution of endothelium-derived nitric oxide to exercise-induced vasodilation. Circulation 90, 2853–2858.

Gustafsson, H., Mulvany, M.J., Nilsson, H., 1993. Rhythmic contractions of isolated small arteries from rat: influence of the endothelium. Acta Physiol. Scand. 148, 153–163.

Hayoz, D., Weber, R., Rutschmann, B., Darioli, R., Burnier, M., Waeber, B., Brunner, H.R., 1995. Postischemic blood flow response in hypercholesterolemic patients. Hypertension 26, 497–502.

Heagerty, A.M., Bund, S.J., Aalkjaer, C., 1988. Effects of drug treatment on human resistance arteriole morphology in essential hypertension: direct evidence for structural remodeling of resistance vessels. Lancet 2, 1209–1212.

Heavy, D.J., Barrow, S.E., Hickling, N.E., Ritter, J.M., 1985. Aspirin causes short-lived inhibition of bradykinin-stimulated prostacyclin production in man. Nature 318, 186–188.

Hoffmann, U., Franzeck, U.K., Geiger, M., Bollinger, A., 1990. Variability of different patterns of skin oscillatory flux in healthy controls and patients with peripheral arterial occlusive disease. Int. J. Microcirc. Clin. Exp. 12, 255–273.

Ignarro, L.J., Byrns, R.E., Buga, G.M., Wood, K.S., 1987. Endothelium-derived relaxing factor from pulmonary artery and vein possesses pharmacological and chemical properties identical to those of nitric oxide radical. Circ. Res. 61, 866–879.

Intaglietta, M., 1989. Vasomotion and flow modulation in the microcirculation, in: Intaglietta, M. (Ed.), Progress in Applied Microcirculation, Vol. 15, Karger, Basel, pp. 1–9.

Joannides, R., Richard, V., Haefeli, W.E., Linder, L., Lüscher, T.F., Thuillez, C., 1995. Role of basal and stimulated release of nitric oxide in the regulation of radial artery caliber in humans. Hypertension 26, 327–331.

Kastrup, J., Bühlow, J., Lassen, N.A., 1989. Vasomotion in human skin before and after local heating recorded with laser Doppler flowmetry. A method for induction of vasomotion. Int. J. Microcirc. Clin. Exp. 8, 205–215.

Khan, F., Cohen, R.A., Ruderman, N.B., Chipkin, S.R., Struthers, A.D., Coffman, J.D., 1996. Vasodilator responses in the forearm skin of patients with insulin-dependent diabetes mellitus. Vasc. Med. 1, 187–193.

Khan, F., Davidson, N.C., Littleford, R.C., Litchfield, S.J., Struthers, A.D., Belch, J.J.F., 1997. Cutaneous vascular responses to acetylcholine are

mediated by a prostanoid-dependent mechanism in man. Vasc. Med. 2, 82–86.

Kilbom, A, Wennmalm, A, 1976. Endogenous prostaglandines as local regulators of blood flow in man: effect of indomethacin on reactive and functional hyperemia. J. Physiol. 257, 109–121.

Koller, A., Kaley, K., 1991. Endothelial regulation of wall shear stress and blood flow in skeletal muscle microcirculation. Am. J. Physiol. 260, H862–H868 (Heart Circ. Physiol. 29).

Kubli, S., Waeber, B., Dalle-Ave, A., Feihl, F., 2000. Reproducibility of laser Doppler imaging of skin blood flow as a tool to assess endothelial function. J. Cardiovasc. Pharmacol. 36, 640–648.

Kvernmo, H.D., Stefanovska, A., Bracic, A., Kirkebøen, K.A., Kvernebo, K., 1998b. Spectral analysis of the laser Doppler perfusion signal in human skin before and after exercise. Microvasc. Res. 56, 173–182.

Kvernmo, H.D., Stefanovska, A., Kirkebøen, K.A., Kvernebo, K., 1999. Oscillations in the human cutaneous blood perfusion signal modified by endothelium-dependent an endothelium-independent vasodilators. Microvasc. Res. 57, 298–309.

Kvernmo, H.D., Stefanovska, A., Kirkebøen, K.A., Østerud, B., Kvernebo, K., 1998a. Enhanced endothelium-dependent vasodilation in human skin vasculature induced by physical conditioning. Eur. J. Appl. Physiol. 79, 30–36.

Leahy, M.J., de Muhl, F.F.M., Nilsson, G.E., Maniewski, R., 1999. Principles and practice of the laser-Doppler perfusion technique. Tech. Health Care 7, 143–162.

Meyer, J.U., Borgstrøm, P., Lindblom, L., Intaglietta, M., 1988. Vasomotion patterns in skeletal muscle arterioles during changes in arterial pressure. Microvasc. Res. 35, 193–203.

Morlet, J., 1983. Sampling theory and wave propagation, in: Chen, C.H. (Ed.), NATO ASI Series: Issues in Acoustic Signal/Image Processing and Recognition, Vol. 1, Springer-Verlag, Berlin.

Moncada, S., Vane, J.R., 1978. Unstable metabolites of arachidonic acid and their role in haemostasis and thrombosis. Br. Med. Bull. 34, 129–135.

Morris, S.J., Shore, A.C., 1996. Skin blood flow responses to the iontophoresis of acetylcholine and sodium nitroprusside in man: possible mechanisms. J. Physiol. 496, 531–542.

Morris, S.J., Shore, A.C., Tooke, J.E., 1995. Responses of the skin microcirculation to acetylcholine and sodium nitroprusside in patients with NIDDM. Diabetologia 38, 1337–1344.

Mück-Weymann, M.E., Albrecht, H-P., Hager, D., Hiller, D., Hornstein, O.P., Bauer, R.D., 1996. Respiratory-dependent laser Doppler flux motion in different skin areas and its meaning to autonomic nervous control of the vessels of the skin. Microvasc. Res. 52, 69–78.

Nilsson, G.E., Tenland, T., Öberg, P.Å, 1980. Evaluation of a laser Doppler flowmeter for measurement of tissue blood flow. IEEE Trans. Biomed. Eng. 27, 597–604.

Noon, J.P., Haynes, W.G., Webb, D.J., Shore, A.C., 1996. Local inhibition of nitric oxide generation in man reduces blood flow in finger pulp but not in hand dorsum skin. J. Physiol. 490, 501–508.

Noon, J.P., Walker, B.R., Hand, M.F., Webb, D.J., 1998. Studies with iontophoretic administration of drugs to human dermal vessels in vivo: cholinergic vasodilation is mediated by dilator prostanoids rather than nitric oxide. Br. J. Pharmacol. 45, 545–550.

Palmer, R.M.J., Ferrige, A.G., Moncada, S., 1988. Vascular endothelial cells synthesize nitric oxide from L-arginine. Nature 333, 664–666.

Rapoport, R.M., Draznin, M.B., Murad, F., 1983. Endothelium-dependent relaxation in rat aorta may be mediated through cyclic GMP-dependent protein phosphorylation. Nature 306, 174–176.

Rayman, G., Hassan, A., Tooke, J.E., 1986. Blood flow in the skin of the foot related to posture in diabetes mellitus. Br. Med. J. 292, 87–90.

Roth, G., Caverley, D.C., 1994. Aspirin, platelets, and thrombosis: theory and practice. Blood 83, 885–898.

Salerud, E.G., Tenland, T., Nilsson, G.E., Öberg, P.Å., 1983. Rhythmical variations in human skin blood flow. Int. J. Microcirc. Clin. Exp. 2, 91–102.

Stefanovska, A., 1992. Self-Organization of Biological Systems Influenced by Electrical Current, Thesis, Faculty of Electrical Engineering, University of Ljubljana, Slovenia.

Stefanovska, A., Bracic, M., Kvernmo, H.D., 1999. Wavelet analysis of oscillations in the peripheral blood circulation signal measured by laser Doppler technique. IEEE Trans. Biomed. Eng. 46, 1230–1239.

Stefanovska, A., Kroselj, P., 1997. Correlation integral and frequency analysis of cardiovascular functions. Open Syst. Inf. Dyn. 4, 457–478.

Vallance, P., Collier, J., Moncada, S., 1989. Effects of endothelium-derived nitric oxide on peripheral arteriolar tone in man. Lancet 2, 997–1000.

Warren, J.B., Loi, R.K., Wilson, A.J., 1994. PGD_2 is an intermediate in agonist-stimulated nitric oxide release in rabbit skin microcirculation. Am. J. Physiol. 266, H1846–H1853 (Heart Circ. Physiol. 35).

Westerman, R.A., Widdop, R.E., Hannaford, A., Low, A., Roberts, R.G.D., Kent, P., Sideris, K., Yip, T., Hales, J.R.S., Stephens, F.R.N., 1988. Laser Doppler velocimetry in the measurement of neurovascular function. Aust. Phys. Eng. Sci. 11, 53–65.

Zellers, T.M., McCormick, J., Wu, Y., 1994. Interaction among ET-1, endothelium-derived nitric oxide, and prostacyclin in pulmonary arteries and veins. Am. J. Physiol. 267, H139–H147 (Heart Circ. Physiol. 36).

Am J Physiol Heart Circ Physiol 284: H1638–H1646, 2003;
10.1152/ajpheart.00826.2000.

Involvement of sympathetic nerve activity in skin blood flow oscillations in humans

Torbjörn Söderström,[1] Aneta Stefanovska,[2] Mitja Veber,[2] and Henry Svensson[1]

[1]*Department of Plastic and Reconstructive Surgery, Malmö University Hospital, S-205 02 Malmö, Sweden; and* [2]*Group of Nonlinear Dynamics and Synergetics, Faculty of Electrical Engineering, University of Ljubljana, 1000 Ljubljana, Slovenia*

Submitted 25 August 2000; accepted in final form 4 November 2002

Söderström, Torbjörn, Aneta Stefanovska, Mitja Veber, and Henry Svensson. Involvement of sympathetic nerve activity in skin blood flow oscillations in humans. *Am J Physiol Heart Circ Physiol* 284: H1638–H1646, 2003; 10.1152/ajpheart.00826.2000.—We have used the wavelet transform to evaluate the time-frequency content of laser-Doppler flowmetry (LDF) signals measured simultaneously on the surfaces of free microvascular flaps deprived of sympathetic nerve activity (SNA), and on adjacent intact skin, in humans. It was thereby possible to determine the frequency interval within which SNA manifests itself in peripheral blood flow oscillations. The frequency interval from 0.0095 to 2 Hz was examined and was divided into five subintervals: *I*, ~0.01 Hz; *II*, ~0.04 Hz; *III*, ~0.1 Hz; *IV*, ~0.3 Hz; and *V*, ~1 Hz. The average value of the LDF signal in the time domain as well as the mean amplitude and total power in the interval from 0.0095 to 2 Hz and amplitude and power within each of the five subintervals were significantly lower for signals measured on the free flap ($P < 0.002$). The normalized spectral amplitude and power in the free flap were significantly lower in only two intervals: *I*, from 0.0095 to 0.021 Hz; and *II*, from 0.021 to 0.052 Hz ($P < 0.05$); thus indicating that SNA is manifested in at least one of these frequency intervals. Because *interval I* has recently been shown to be the result of vascular endothelial activity, we conclude that we have identified SNA as influencing blood flow oscillations in normal tissues with repetition times of 20–50 s or frequencies of 0.02–0.05 Hz.

blood flow variability; time-frequency analysis; wavelet transform; autoregulation; microvascular free flaps

SYMPATHETIC NERVOUS SYSTEM activity provides one of the fundamental mechanisms for the control of blood flow and pressure. In contrast to somatic nerve activity, sympathetic nerves (SN) are continuously active. They rhythmically discharge so that all innervated blood vessels are under some degree of continuous contraction and relaxation. Their control of the blood distribution to the end cells or organs is exerted in several frequency bands, including rhythms related to the cardiac and respiratory cycles. Whereas the rhythmical discharge of SN at higher frequencies does not appear directly to induce oscillations in innervated vasculature, slower frequencies appear to be directly responsible for oscillations in the blood flow (30).

However, it is still unclear which frequency band(s) manifest the effect of sympathetic innervation on the blood flow oscillation in humans. One of the reasons is certainly connected with difficulties in obtaining good low-frequency resolution. Moreover, not one, but several oscillatory components were observed in the blood flow signal spanning from the cardiac frequency (~1 Hz in healthy humans) down to endothelium-related oscillations with frequencies ~0.01 Hz (25, 47). Like the cardiac frequencies, the others are also nonconstant, but rather vary in time. That is why, in studying various oscillatory components in the blood flow signal, a method for time-frequency analysis with logarithmic frequency resolution is required. With the use of Morlet's mother wavelet (17, 34), the wavelet transform was shown to meet these requirements (8, 46, 47).

In this study, clinical cases of microvascular free flaps were used to study the role of sympathetic oscillations in the peripheral blood flow. The flaps were transferred from a suitable donor site to the defected site. During surgery, the free flap is completely detached from its donor site, and the blood perfusion of the flap is restored by means of microvascular anastomoses. Normally, one supplying artery and one draining vein were used. Because all SN fibers are cut in this type of operation, there is no residual sympathetic control of the blood flow to the flap. The aim of the present study was to analyze the frequency content of blood flow signals simultaneously recorded on the free flap and on the intact skin. Any differences may thus be taken as an indication of the characteristic frequency of blood flow oscillations where sympathetic control is manifested.

METHODS

Patients

The investigation was conducted according to the Helsinki Declaration of 1975 (Revised 1983). Eight patients, all female, with transferred musculocutaneous flaps were included in the study (median age 50.6 yr, range 45–57 yr).

Address for reprint requests and other correspondence: T. Söderström, Dept. of Plastic and Reconstructive Surgery, Malmö Univ. Hospital, S-205 02 Malmö, Sweden (E-mail: t@soderstrom.nu).

The costs of publication of this article were defrayed in part by the payment of page charges. The article must therefore be hereby marked "*advertisement*" in accordance with 18 U.S.C. Section 1734 solely to indicate this fact.

Measurements

A laser-Doppler flowmeter (model PeriFlux PF-3, Perimed; Järfälla, Sweden) was used for the measurements of the skin blood perfusion. The method is noninvasive and allows for continuous recordings (38). The speed of blood cells moving within the measured volume is estimated from the frequency shift between the emitted and scattered light, with some chosen time constant. A time constant of 0.03 s was selected. Each blood perfusion signal was sampled at a frequency of 32 Hz and stored in a personal computer. Although the signal cannot be expressed in other than arbitrary units (AU) (26), in what follows we will refer to it either as blood perfusion or blood flow, because our main interest is cantered on its dynamical properties where only the relative changes are relevant.

The signals were recorded after free-flap surgery. The recordings started 2–10 h after reperfusion and continued overnight at the intensive care unit. Two probes functioning simultaneously were used. The first probe collected the signal from the revascularized free flap, whereas the second probe collected the signal from intact skin in the immediate vicinity of the free flap.

The exposed part of the flap was a free-flap skin (musculocutaneous flaps). Its size varied from ~10×15 cm up to ~20 × 30 cm. The flap probe was placed in the exposed center of the flap. The comparison probe, which collected signals from adjacent skin, was placed close to the flap, but out of range from the operation field to ensure that nondenervated skin was monitored, thereby avoiding undermined or compromised skin, and on scar-free skin supported by intact subcutaneous tissue. A common distance to the probe was ~10 cm from the wound and the border of the free flap.

The recordings were motivated clinically as well as experimentally. Namely, early detection of any disturbances of the flap perfusion is of paramount importance because a reoperation can usually save the flap if undertaken without delay. Therefore, the level of blood perfusion was continuously monitored for immediate detection of possible complications. At the same time, data were stored for later spectral analysis. However, movement artifacts are unavoidable in recordings taken over several hours. Consequently, only the segments without artifacts were extracted from each recording. A time interval of 20 min was chosen to achieve the weak stationarity of the signals necessary for calculation of the wavelet transform. This time interval allows for reliable estimation of the spectrum in the broad frequency interval where we expect sympathetic activity to be manifested, namely from 0.0095 to 2.0 Hz. The same time interval was selected for both signals (Fig. 1) and the spectral characteristics of signals measured on free flaps were compared with those of signals measured on intact skin.

Time-Frequency Analysis

Methods of frequency and time-frequency analysis are based on the theory of Fourier transform (12), a mathematical tool that connects representation of a signal in time and frequency domain. However, the Fourier analysis is inappropriate for dealing with signals that contain time-variable frequency content. Moreover, any abrupt change in time is spread out over the whole observed frequency interval. To obtain localization in time, a short-time Fourier transform was proposed (14). By using this method, a window $w(u)$ of fixed length is shifted along the signal to obtain information about the time and a standard Fourier transform is performed within this window to extract the current frequency content. However, when both low and high frequencies with different time spans are to be detected simultaneously in a signal, the short-time Fourier transform fails either to follow the time evolution of quick events or to estimate the frequency content within the low-frequency band. The method of wavelet analysis offers a solution to this problem. In the wavelet transform, at a particular time instant, each frequency is estimated for a corresponding window. The window, $\Psi(u)$, is called the mother wavelet and is scaled (dilated and constricted) in time, thus allowing for frequency localization. In this way, a family of generally nonorthogonal basis functions

$$\Psi_{s,t} = |s|^{-1/2}\psi\left(\frac{u-t}{s}\right) \quad (1)$$

is obtained, where t is time, s is scale related to the frequency f as $f = f_0/s$, and f_0 determines the current frequency resolution. By choosing $f_0 = 1$, we obtain the simple relation $f = 1/s$.

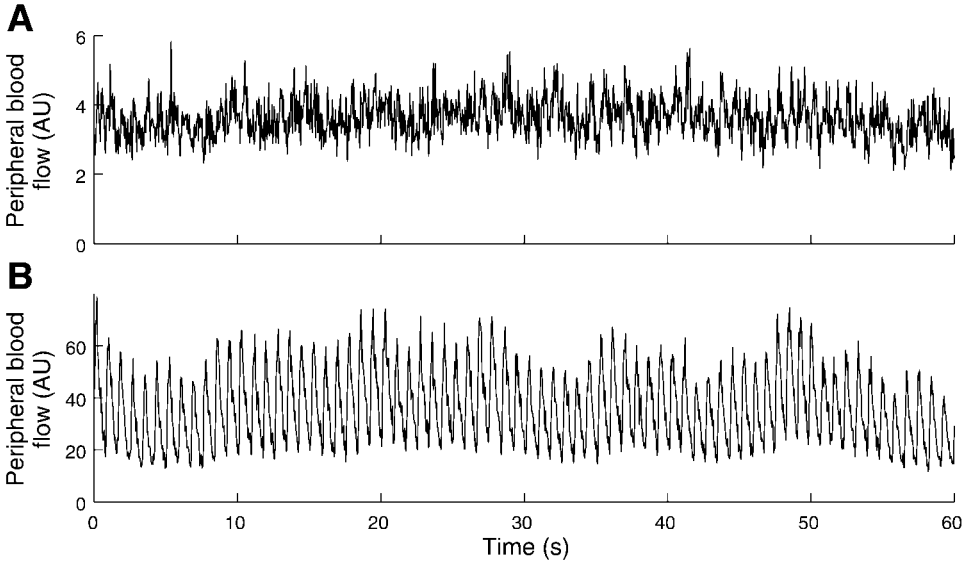

Fig. 1. A typical laser-Doppler flowmetry signal measured simultaneously on a free flap (*A*) and on intact skin (*B*). Segments of 60 s are displayed. AU, arbitrary units.

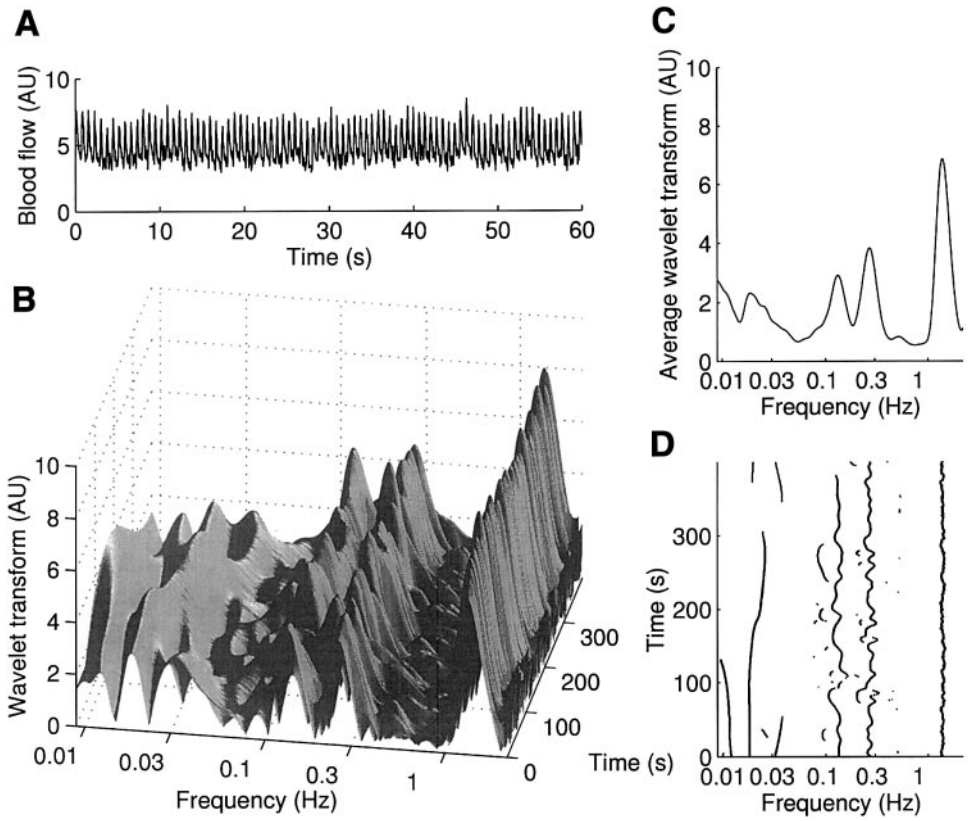

Fig. 2. *A*: laser-Doppler perfusion signal in AU. For the calculation of the wavelet transform (*B*), the signal is normalized to zero in the time domain. The wavelet transform averaged over time (*C*) and automatically detected amplitude peaks projected onto the time-frequency plane (*D*).

The continuous wavelet transform of a signal $g(u)$ is then defined as

$$\tilde{g}(s, t) = \int_{-\infty}^{+\infty} \bar{\Psi}_{s,t}(u) g(u)\, \mathrm{d}u \qquad (2)$$

It is a mapping of the function $g(u)$ onto the time-frequency plane.

By choosing a mother wavelet well concentrated in both time and frequency, we can precisely detect the frequency content within a given time interval. Here we are only restricted by the uncertainty principle. Namely, to detect a frequency, the signal must be observed over at least one period of this frequency. Hence, we cannot say exactly at which instant in time the signal had this frequency. The best time-frequency localization, within the limits given by the uncertainty principle, can be obtained by using the Morlet wavelet. It is a Gaussian function modulated by sine wave. The wavelet transformation of a signal (Fig. 2*A*) yields a three-dimensional plot (Fig. 2*B*), which can then be projected in two dimensions, averaging over either time (Fig. 2*C*) or amplitude (Fig. 2*D*). Before calculation of the wavelet transform, the average value of each signal was subtracted, normalizing its mean value to zero. The frequency content <0.0095 Hz, which manifests as a trend, was also removed by use of a moving average.

Quantitative measures. An oscillatory component in a signal can be characterized by its instantaneous frequency and corresponding amplitude or power. To compare many signals, quantitative measures were introduced (8). The frequency interval is divided into several intervals (Fig. 3), and the power and average amplitude within each interval are used to characterize the spectral components. In the blood flow signal, five oscillatory components were demonstrated to exist in the interval between 0.0095 and 2.0 Hz. In resting subjects, their frequencies are centered at ~0.01, 0.04, 0.1, 0.3, and 1 Hz. The outer limits for each characteristic frequency were determined and are presented in Table 1. Time-averaged wavelet transforms obtained from signals measured on the free flap and on intact skin are presented in Fig. 3, *A* and *B*, respectively. The frequency intervals for each oscillatory component are indicated.

Power of spectral components. In a given frequency interval, the average power can be determined as

$$\epsilon_i(f_{i1}, f_{i2}) = \frac{1}{t_w} \int_0^{t_w} \int_{1/f_{i1}}^{1/f_{i2}} \frac{1}{s^2} |\tilde{g}(s, t)|^2 \, \mathrm{d}s \, \mathrm{d}t \qquad (3)$$

where ϵ_i is the total power with the ith frequency interval and ds and dt are the derivatives of scale and time, respectively. The frequencies f_{i1} and f_{i2} are the lower and upper bounds of the ith frequency interval. The power is averaged over the time t_w, for which the wavelet transform was calculated.

To obtain the relative contribution of a particular spectral component, the normalized power was also introduced

$$e_i(f_{i1}, f_{i2}) = \frac{\epsilon_i(f_{i1}, f_{i2})}{\epsilon_{\text{total}}} \qquad (4)$$

where e_i is normalized power within the ith frequency interval and ϵ_{total} is the total power of the signal in the entire frequency range of interest, i.e., between 0.0095 and 2.0 Hz in our case.

The average amplitude of a spectral component in a given frequency interval can be determined as

$$A_i(f_{i1}, f_{i2}) = \frac{1}{t_w} \int_{1/f_{i1}}^{1/f_{i2}} \frac{1}{s^2} \tilde{g}(s, t) \, \mathrm{d}s \, \mathrm{d}t \qquad (5)$$

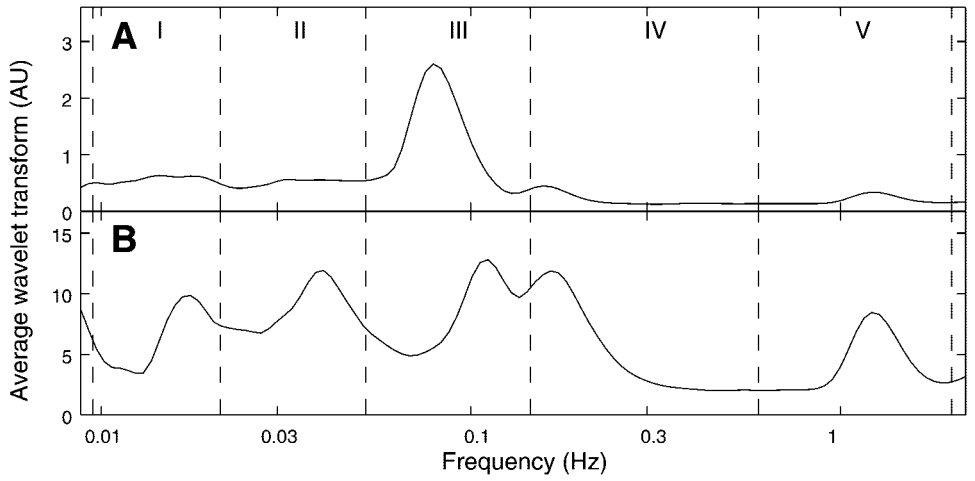

Fig. 3. A typical example of time-averaged wavelet transform calculated from a signal measured on a free flap (*A*) and on intact skin (*B*) simultaneously. Frequency *intervals I–V* are depicted, where average amplitude and spectral power are calculated.

The relative amplitude, or normalized amplitude, is then

$$a_i(f_{i1}, f_{i2}) = \frac{A_i(f_{i1}, f_{i2})}{A_{\text{total}}} \quad (6)$$

where a_i is the normalized average amplitude within the ith frequency interval and A_{total} is the average amplitude obtained over the entire frequency range under observation.

Statistical Analysis

Data are presented either as group medians within the total range or as box plots. The five horizontal lines at the boxes are the 10%, 25%, 50%, 75%, and 90%. Values below or above the 10% and 90% level are presented as data points. The Mann-Whitney test with two-sided critical values was applied. Statistically significant differences are defined as $P < 0.05$.

RESULTS

Average Values of Blood Flow Signal

For each 20-min signal, an average value was calculated. Data for both groups of signals, measured simultaneously on the flap ($n = 8$) and on intact skin in the immediate vicinity ($n = 8$), are presented as box plots in Fig. 4*A*. The median of average values of the blood perfusion signals from free flaps is 4.3 (1.4–10.6) AU and 36.9 (6.8–60.3) AU for signals collected from intact skin, thus demonstrating a significantly lower level of blood flow in the flaps ($P < 0.0003$).

Table 1. *Frequency intervals used in quantitative analysis of wavelet transforms of blood flow signals*

Subintervals	Frequency Intervals, Hz
I	0.0095–0.021
II	0.021–0.052
III	0.052–0.145
IV	0.145–0.6
V	0.6–2

Frequency intervals are given in cycles per second (Hz) used in quantitative analysis of wavelet transforms of laser-Doppler perfusion (LDP) signals. The wavelet transform was calculated for the frequency interval of 0.0095–2 Hz, which was then subdivided into the five subintervals (*I–V*) listed. The amplitude and power within each of the subintervals was then calculated as discussed in the text.

Average Spectral Amplitude

The mean values of the average spectral amplitude in the frequency range from 0.0095 to 2.0 Hz for signals obtained from free flaps is 0.30 (0.12–0.70) and 4.00 (0.42–6.84) on intact skin. The differences are significant ($P < 0.0003$). Box plots for both groups are presented in Fig. 4*B*.

Total Spectral Power

The total power in the entire frequency range, i.e., from 0.0095 to 2.0 Hz, was calculated for each signal. The box plots for groups of signals are presented in Fig. 4*C*. The mean value for signals obtained on flaps is 0.35 (0.04–1.45), and it is 74.92 (0.54–152.30) for signals obtained on intact skin. Again, the differences are significant ($P < 0.0003$), hence demonstrating that not only the level of flow but also the power of its oscillations is lower on free flaps.

Spectral Amplitude Within Each Frequency Interval

Median values and total ranges of spectral amplitude in each frequency interval are summarized in Table 2.

The amplitude of each oscillatory component is significantly smaller for signals measured on free flaps. To resolve whether the decrease in amplitude in any of the frequency intervals is relatively more pronounced we also present normalized amplitudes. Box plots for both groups of signals are presented in Fig. 5*A*. The normalized amplitude is significantly decreased in *intervals I* and *II*. The median value of normalized amplitude contributed by *interval I* for signals obtained on flaps is 1.46 (0.99–2.06) and for signals obtained on intact skin 3.16 (1.17–6.01), with $P < 0.04$. The median value of normalized amplitude within *interval II* is 1.38 (1.13–2.14) for flaps and 2.54 (1.10–5.18) for intact skin, with $P < 0.05$.

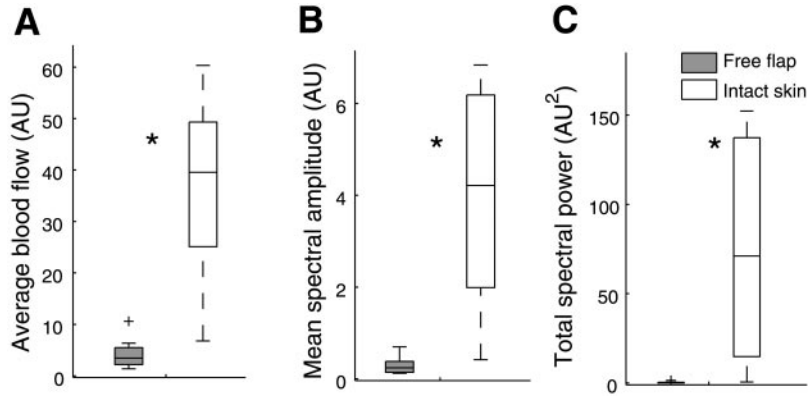

Fig. 4. Box plots obtained from 20-min signals measured on free flaps and on intact skin simultaneously. The average blood flow (*A*) is obtained as a time-average of each laser-Doppler signal. The average spectral amplitude (*B*) is calculated from the time-averaged wavelet transform in the interval from 0.0095 to 2 Hz. The total spectral power (*C*) is calculated for the same interval. All three values are significantly lower for signals measured on free flaps. *$P < 0.0003$.

Spectral Power Within Each Frequency Interval

Median values and the total range of spectral power in each frequency interval are summarized in Table 3.

The power of each oscillation is significantly smaller for signals measured on free flaps. Again, to see whether the spectral power in some of the intervals is changed more than in others, we also present the normalized power contributed by each frequency interval to the total power. Box plots for both groups of signals are presented in Fig. 5*B*. Here, we see that a great decrease in spectral power with respect to the total power occurs for flaps in frequency *intervals I* (0.0095–0.021 Hz) and *II* (0.021–0.052 Hz). The median value of normalized power contributed by *interval I* is 0.012 (0.005–0.025) for flaps and 0.048 (0.006–0.128) for intact skin, with $P < 0.03$. The median value of normalized power within *interval II* is 0.026 (0.015–0.058) for flaps and 0.083 (0.015–0.229) for intact skin, with $P < 0.05$.

DISCUSSION

We have presented an analysis of blood flow measured on free flaps and on intact skin within first 24 h after transplantation. Only flaps with no disturbances in perfusion were included in the study. Therefore, two main differences between the intact skin and the free flap were to be expected: *1*) the absence of sympathetic control of the vessels in the flap, and *2*) reduced endothelium-mediated metabolic activity in the flap.

The blood flow level in free flaps was significantly lower than in intact skin. In addition, the power and amplitude of oscillations in the frequency range from 0.0095 to 2.0 Hz were dramatically lowered. However, the most pronounced decreases, as manifested in normalized values of power and amplitude, were observed in two frequency intervals: *interval I*, from 0.0095 to 0.021 Hz; and *interval II*, from 0.021 to 0.052 Hz. These results imply that the sympathetic and endothelium-

Table 2. *Mean amplitude in each frequency interval of five spectral components*

Interval	Range, Hz	Free Flap	Intact Skin
I	0.0095–0.021	0.47 (0.12–1.45)	14.00 (1.18–36.28)
II	0.021–0.052	0.45 (0.14–1.50)	10.25 (1.47–30.81)
III	0.052–0.145	0.62 (0.10–1.63)	7.81 (0.80–17.77)
IV	0.145–0.6	0.23 (0.06–0.64)	2.78 (0.33–4.93)
V	0.6–2	0.29 (0.13–0.64)	3.95 (0.39–7.34)

With the use of the wavelet transform, the spectral power is calculated from two LDP signals measured simultaneously on the free flap and intact skin. The data are from eight patients, all female, with transferred musculocutaneous flaps. The numbers in parentheses refer to the total range. In each frequency interval (*I*–*V*), the average amplitude is significantly higher in the LDP signal measured on the intact skin compared with values obtained on the free flap ($P < 0.002$ for each interval).

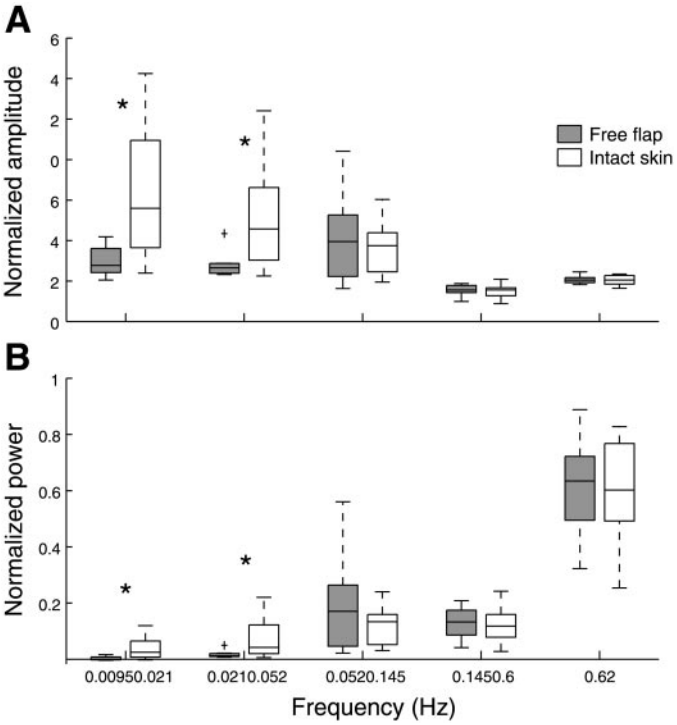

Fig. 5. *A*: spectral amplitude within each frequency interval normalized to the average spectral amplitude in the frequency interval from 0.0095 to 2 Hz. *B*: normalized spectral power is obtained by dividing the spectral power within each frequency interval by the total power in the interval from 0.0095 to 2 Hz. Both the normalized amplitude and normalized power are significantly lower in free flaps in two frequency intervals: *I*, from 0.0095 to 0.021 Hz; and *II*, from 0.021 to 0.052 Hz. *$P < 0.05$.

Table 3. *Mean power in each frequency interval*

Interval	Range, Hz	Free Flap	Intact Skin
I	0.0095–0.021	0.01 (0.00–0.03)	4.71 (0.02–19.51)
II	0.021–0.052	0.02 (0.00–0.08)	6.97 (0.08–34.84)
III	0.052–0.145	0.08 (0.00–0.32)	11.90 (0.08–37.87)
IV	0.145–0.6	0.06 (0.00–0.31)	8.66 (0.07–20.13)
V	0.6–2	0.19 (0.03–0.70)	42.68 (0.28–108.57)

With the use of the wavelet transform, the spectral power is calculated from two LDP signals measured simultaneously on the free flap and intact skin. The data are from eight patients, all female, with transferred musculocutaneous flaps. In each frequency interval (*I–V*), the power is significantly higher in the LDP signal measured on the intact skin compared to values obtained on the free flap ($P < 0.002$ for each interval).

mediated metabolic activity manifest in either or both of these two frequency intervals.

Oscillations in Blood Flow

The oscillations recorded in the blood flow reflect both vasomotion and flow motion. The vasomotion is usually defined as rhythmic changes in the diameter of the small blood vessels, produced by contraction and relaxation of the muscular components in their walls. The flow motion results from the motion of the blood cells and their interaction with the vessel walls.

The cardiac frequency (~1 Hz in a resting, healthy subject) and the respiratory frequency (~0.3 Hz) have been reported in the peripheral blood flow signal, measured by laser-Doppler flowmetry (8, 18, 25, 42, 46). They were also demonstrated in simultaneous measurements of ECG, respiration, and peripheral blood flow recorded at different sites of human skin (7, 46). The essential source of the blood flow, also in the peripheral vessels, is therefore the pressure difference generated by the heart and lung pumps. For example, ~50% of the normalized spectral power in the blood flow is contributed by the heart, both in the intact skin and the free flap (see Fig. 5*B*). However, there are also peripheral mechanisms that contribute to the oscillations observed in the blood flow.

Endothelium-mediated oscillations. The layer of endothelial cells that lines the entire vascular system acts not only as a passive barrier keeping cells and proteins from escaping freely into the tissue, but also as a source of several vasoactive substances. After Furchgott and Zawadzki (13) showed that the rabbit aorta dilates in response to the application of ACh only in the presence of intact endothelium, several studies were initiated to identify the vasoactive substances and their involvement in metabolic, immune, and cytotoxic activity (33). The application of iontophoretically an endothelium-dependent (ACh) and an endothelium-independent (sodium nitroprusside) vasodilator recently demonstrated that endothelial involvement in blood flow oscillations is manifested in the frequency interval from 0.0095 to 0.021 Hz (25, 47).

Oscillations with a period of ~1 min are significantly reduced in flaps. This may be taken as evidence that the contribution of endothelium-mediated metabolic activity to the blood flow oscillations of the flap is lower than to those of the intact skin. This may be on account of the smaller number of vessels, and hence the smaller area of endothelium involved in the perfusion, during the early stage after transplantation. The release of mediators from ischemic areas in the transplanted flap, such as oxygen-free radicals or nitric oxide, and the exposure of other metabolites after ischemia-reperfusion injury, may well contribute to decreased endothelial activity.

Sympathetic regulation of peripheral blood flow oscillations. Apart from frequency *interval I*, from 0.0095 to 0.021 Hz, the only significant difference between the normalized power and amplitude of oscillations in flaps and in intact skin was observed in the frequency *interval II*, from 0.021 to 0.052 Hz. Therefore, we may take the results of the present study as evidence that sympathetic control of the peripheral vasculature is involved in oscillations in this frequency interval.

The results obtained are in agreement with the findings of Kastrup et al. (23) and Golenhofen and Hildebrandt (15). With the use of a laser-Doppler flowmeter, Kastrup et al. (23) have identified rhythmical variations in the blood flow of the human skin with median frequencies of 6.8 min^{-1} (0.11 Hz) and 1.5 min^{-1} (0.025 Hz). They named these α-oscillations and β-oscillations, respectively. The β-oscillations correspond to our *interval II*, whereas α-oscillations correspond to *interval III*. They showed that the β-oscillations disappeared after local and ganglionic blockade or chronically sympathectomized tissue. Furthermore, they suggested that β-oscillations are a vascular reaction of pure neurogenic origin.

By using the wavelet transform, which facilitates good low-frequency resolution, we have confirmed the results of Kastrup et al. (23), obtained by observing periodicities in the time domain. It is difficult, however, in the time domain to visualize more than two oscillations. This could be the reason they concentrated only on those two particular oscillations.

The conclusion that the SN activity (SNA) influences skin blood flow in the frequency band of 0.02–0.05 Hz contrasts with the results of the study by Stauss et al. (43). In their investigations, the SN fibers were electrically stimulated at different frequencies and the responses in skin blood flow were recorded with the laser-Doppler method. In that study, sympathetic modulation of human skin blood flow was found to be most effective in the frequency range of 0.075–0.1 Hz. However, in the present study, we have collected signals from reliably denervated postischemic tissue and made comparative studies with intact tissue in its physiological state in the same individual without stimulation of any frequency. One possible explanation for the differences in the results obtained is that, as observed in the oscillations of the blood flow, the basic activity of the sympathetic nervous system differs from that induced by electrical stimulation via major peripheral nerves. Furthermore, the two studies differ with respect to the methods used for spectral estimation. We have used continuous wavelet transform, which allows for loga-

rithmic frequency resolution (which is of particular importance for the low-frequency content), whereas in the study by Stauss et al. (43) spectra were estimated using the fast Fourier transform.

There are several studies indicating that the oscillations at 0.1 Hz are due to resonance in the baroreceptor pathway (4). However, in our study, no difference was observed in the normalized spectral power at 0.1 Hz. Bernardi et al. (5) have argued that SNA to the skin displays an oscillation at 0.1 Hz, which directly induces an oscillation in the vasculature. However, what they failed to appreciate was that if blood pressure also displayed an oscillation at 0.1 Hz, then it would be apparent in the blood flow via a simple pressure to flow relationship. It was shown that the major parts of skin nerve activity controlling skin temperature are composed of baroreceptor-independent components (35). This, besides the improved low-frequency resolution compared with the previous studies, may be a possible explanation why in our study the skin SNA was not found to be dominantly influencing the 0.1-Hz oscillation. Yet it remains to be clarified whether or not the frequency of mechanical oscillations in the blood flow is synchronized with the discharge frequency of SNs. It might be that SNA only allows for the skin vascular oscillations to exist through the production of generalized tone, and the resultant frequency of oscillation could well be lower than that of the SN discharge. In fact, the clear-cut divergences in both setups and the results between Stauss et al. (43) and our study do indicate that this assumption may be correct.

Recently, Macefield and Wallin (28) demonstrated that the discharge of human cutaneous sympathetic neurons is modulated by the respiratory and cardiac frequencies. This might be taken as evidence that in its control of the stiffness of the peripheral vessels, sympathetic activity is also governed by the state of the cardiac and respiratory rhythms. However, the basic frequency of its autonomous discharge will only be established by analysis of the low-frequency content of the spontaneous sympathetic neural activity.

The differences between free flaps and intact skin may also be due to the different skin temperature. It was shown that skin temperature contains several oscillatory components in the frequency interval of <0.05 Hz (41), with the dominant frequency components lying <0.01 Hz (27). Because cutaneous nerve activity also controls skin temperature, a decrease in the temperature oscillations of the flaps could be expected as a consequence rather than a cause of the observed differences. However, the interplay between skin temperature oscillations, blood flow oscillations and adjacent SNA remains to be established by detailed analysis of all three simultaneously recorded signals.

Oscillations of local origin. Interval III, from 0.051 to 0.145 Hz, corresponds to α-oscillations as defined by Kastrup et al. (23). Rhythmical variations with the frequency ~0.1 Hz were reported already in the early studies of oscillations in the laser-Doppler signal of the blood flow (39).

Kastrup et al. (23) have shown that the α-oscillations were unchanged during local and ganglionic nerve blockade and preserved in chronically sympathectomized tissue, and they suggested their local nonneurogenic origin. Johansson and Bohr (21) demonstrated that isolated small subcutaneous vessels show rhythmic contraction. Furthermore, they proposed that this rhythmic behavior must be due to synchronization of contraction of many smooth muscle cells, indicating that the separate cells are able to communicate with each other. The passive local regulation of the blood flow is often named the myogenic response (11, 22, 40). It is a response to intravascular pressure elevation mainly mediated by stretch-sensitive ion channels in the smooth muscle cells. The oscillations with frequency ~0.1 Hz were shown to be preserved in free flaps immediately after transplantation (42). The results of the present study might be taken as a further evidence for the frequency interval at which the myogenic activity manifests in human cutaneous blood flow. Namely, the normalized spectral power and amplitude in the frequency interval ~0.1 Hz did not differ in flaps compared with intact skin, thus illustrating that the underlying mechanism of these oscillations is probably of local myogenic origin.

Oscillations Observed in Other Hemodynamic Parameters

It has long been recognized that the blood pressure is characterized by several spontaneous oscillations, or waves (32, 36). Besides the cardiac and respiratory waves, slower waves were also detected. Different terms are used in the literature to describe those waves. Traube, Hering, and Mayer, in separate studies, were the first to describe slow waves in blood pressure and the designation Traube-Hering-Mayer waves is often used for all waves slower than respiration. Attempts to identify and classify the waves also resulted in their ordering: cardiac, respiratory, and slow waves are also called waves of the first, second, and third order. After it was shown that the heart rate, cardiac contractility, and venous volume might fluctuate with the same rhythms, several studies (1, 9, 24, 36, 48) were initiated to distinguish these waves according to their origin. Many investigations (3, 16, 19, 20, 29, 31, 37, 44, 45, 49) have been performed to resolve the involvement of the vasomotor component and/or sympathetic control; however, the origin of third-order waves is unknown. Here, we show that oscillations with the same frequencies can also be observed in the peripheral blood flow signal. Moreover, applying the wavelet transform that allows for good low-frequency resolution, we were also able to show that waves slower than the third-order wave can be well distinguished in the blood flow fluctuations. However, their relation to the waves observed in blood pressure and heart rate still remains to be clarified as well as the question of whether waves with the same frequencies observed in other hemodynamic parameters share a common physiological origin.

Physiological and Clinical Implications

Vascular endothelial dysfunction has become a key issue in cardiovascular biology, in particular with respect to its role in the pathogenesis of arteriosclerosis, essential hypertension, diabetes mellitus, and heart failure (2, 10). Recently, the spectral analysis of laser-Doppler signals from peripheral blood flow measurements was shown to enable an in vivo noninvasive evaluation of endothelial function (25, 46). Our present study indicates that vascular sympathetic activity may also be evaluated in a similar way. The role of SN influence on the spatial distribution and level of skin perfusion has been graphically demonstrated with the laser-Doppler imaging technique (8). This study, however, strongly indicates that the presence of vascular sympathetic activity in tissue, at any time point, can be evaluated by examining the low-frequency domain of collected laser-Doppler signals. This possibility is of great interest for several diagnostic and therapeutic purposes, the identification and distributive pattern of SN degeneration in patients with diabetes mellitus being only one example.

In conclusion, in the absence of neurogenic control, but with a restored microcirculatory blood flow, the clinical free flap transfer was used as a model for studying the physiological origin of oscillations observed in the peripheral blood flow signal. The difference between spectral properties of blood perfusion signals measured on intact skin and free flap is manifested in the frequency interval <0.05 Hz. Besides oscillations in the frequency interval ~ 0.01 Hz, which were recently demonstrated to result from endothelial activity (25), it was shown that the main difference between the free flap and intact skin occurred in the frequency interval between 0.021 and 0.052 Hz. The compelling explanation is that the sympathetic control of blood flow oscillations are expressed with a repetition time between 20 and 50 s. Furthermore, our results feature a noninvasive technique for evaluation of sympathetic control of peripheral vascular activity, which may be important both for diagnostic and for therapeutic purposes.

The measurements were performed at the Department of Plastic and Reconstructive Surgery, Malmö University Hospital, Malmö, Sweden, within the European Concerted Action "Laser-Doppler Flowmetry for Microcirculation Monitoring."

T. Söderström and H. Svensson were supported by grants from Lund University and The European Commission. A. Stefanovska and M. Veber were supported by a grant from the Slovenian Ministry of Education, Science, and Sport, and A. Stefanovska was also partially supported by the Royal Society of London.

REFERENCES

1. **Akselrod S, Gordon D, Ubel FA, Shannon DC, Berger AC, and Choen RJ.** Power spectrum analysis of heart rate fluctuation: a quantitative probe of beat-to-beat cardiovascular control. *Science* 213: 220–222, 1981.
2. **Andreassen AK, Kvernebo K, Jørgensen B, Simonsen S, Kjekshus J, and Gullestad L.** Exercise capacity in heart transplant recipients: relation to impaired endothelium-dependent vasodilatation of the peripheral microcirculation. *Am Heart J* 136: 320–328, 1998.
3. **Bajrović F, Čenčur M, Hožič M, Ribarič S, and Stefanovska A.** The contribution of lumbar sympathetic neurones activity to rat's skin blood flow oscillations. *Pflügers Arch* 439: R158–R160, 2000.
4. **Bertram D, Berrès Cuisinaud G, and Julien C.** The arterial baroreceptor reflex of the rat exhibits positive feedback properties at the frequency of Mayer waves. *J Physiol* 513: 251–261, 1998.
5. **Bernardi L, Radaelli A, Solda PL, Coats JS, Reeder M, Calciati A, Garrard CS, and Sleight P.** Autonomic control of skin microvessels: assessment by power spectrum of photopletysmographic waves. *Clin Sci (Lond)* 90: 345–355, 1996.
6. **Bornmyr S, Svensson H, Söderström T, Sundkvist G, and Wollmer P.** Finger skin blood flow in response to indirect cooling in normal subjects and in patients before and after sympathectomy. *Clin Physiol* 18: 103–107, 1998.
7. **Bračič M, McClintock PVE, and Stefanovska A.** Characteristic frequencies of the human blood distribution system. In: *Stochaos: Stochastic and Chaotic Dynamics in the Lakes*, edited by Broomhead DS, Luchinskaya EA, McClintock PVE, and Mullin T. Melville, NY: American Institute of Physics, 2000, p. 146–153.
8. **Bračič M and Stefanovska A.** Wavelet based analysis of human blood flow dynamics. *Bull Math Biol* 60: 919–935, 1998.
9. **DeBoer RW, Karemaker JM, and Strackee J.** Hemodynamic fluctuations and baroreflex sensitivity in humans: a beat-to-beat model. *Am J Physiol Heart Circ Physiol* 253: H680–H698, 1987.
10. **Drexler H.** Endothelial dysfunction: clinical implications. *Prog Cardiovasc Dis* 4: 287–324, 1997.
11. **Folkow B.** Description of the myogenic hypothesis. *Circ Res* 15, *Suppl* I: 279–285, 1964.
12. **Fourier JBJ.** Théorie analytique de la chaleur. In: *Oeuvres de Fourier, Tome Premier*, edited by Darboux G. Paris: Gauthies-Villars, 1888.
13. **Furchgott RF and Zawadski JW.** The obligatory role of endothelial cells in the relaxation of arterial smooth muscle by acetylcholine. *Nature* 288: 373–376, 1980.
14. **Gabor D.** Theory of communication. *J IEE* 93: 439–457, 1946.
15. **Golendhofen K and Hildebrandt G.** Die Beziehungen des Blutdruckrhythmus zu Atmung und Peripherer Durchblutung. *Pflügers Arch* 267: 27–45, 1958.
16. **Golubinskaya V, Tarasova O, Borovik A, and Rodionov I.** Low-frequency blood pressure oscillations in mesenteric vessels in conscious rats. *J Vasc Res* 36: 528–531, 1999.
17. **Grossmann A and Morlet J.** Decomposition of Hardy functions into square-integrable wavelets of constant shape. *SIAM J Math Anal* 15: 723–736, 1984.
18. **Hoffman U, Yanar A, Franzeck UK, Edvards JM, and Bollinger A.** The frequency histogram: a new method for the evaluation of laser Doppler flux motion. *Microvasc Res* 40: 293–301, 1990.
19. **Janssen BJA, Oosting J, Slaaf DW, Persson PB, and Struijker-Boudier AJ.** Hemodynamic basis of oscillations in systemic arterial pressure in conscious rats. *Am J Physiol Heart Circ Physiol* 269: H62–H71, 1995.
20. **Japundzic N, Grichois ML, Zitoun P, Laude D, and Elghozi JL.** Spectral analysis of blood pressure and heart rate in conscious rats: effects of autonomic blockers. *J Auton Nerv Syst* 30: 91–100, 1990.
21. **Johansson B and Bohr D.** Rhythmic activity in smooth muscle from small subcutaneous arteries. *Am J Physiol* 210: 801–806, 1966.
22. **Johnson PC.** The myogenic response. *News Physiol Sci* 6: 41–42, 1991.
23. **Kastrup J, Bühlow J, and Lassen NA.** Vasomotion in human skin before and after local heating recorded with laser Doppler flowmetry. A method for induction of vasomotion. *Int J Microcirc: Clin Exp* 8: 205–215, 1989.
24. **Kitney RI, Fulton T, McDonald AH, and Linkens DA.** Transient interactions between blood pressure, respiration and heart rate in man. *J Biomed Eng* 7: 217–224, 1985.
25. **Kvernmo HD, Stefanovska A, Kirkebøen KA, and Kvernebo K.** Oscillations in the human cutaneous blood perfu-

sion signal modified by endothelium-dependent and endothelium-independent vasodilators. *Microvasc Res* 57: 298–309, 1999.
26. **Leahy MJ, de Mul FFM, Nilsson GE, and Manievski R.** Principles and practice of the laser-Doppler perfusion technique. *Technology and Health Care* 7: 143–162, 1999.
27. **Mabuchi KT, Chinzei T, Nasu Y, Yonezawa T, Fujimasa I, and Atsumi K.** Frequency analysis of skin temperature and its application for clinical diagnosis. *Biomed Thermol* 9: 30–33, 1989.
28. **Macefield VG and Wallin BG.** Respiratory and cardiac modulation of single sympathetic vasoconstrictor and sudomotor neurones to human skin. *J Physiol* 516.1: 303–314, 1999.
29. **Malliani A, Pagani M, Lombardi F, and Cerutti S.** Cardiovascular neural regulation explored in the frequency domain. *Circulation* 84: 482–492, 1991.
30. **Malpas SC.** The rhythmicity of sympathetic nerve activity. *Prog Neurobiology* 56: 65–96, 1998.
31. **Malpas SC, Hore TA, Navakatikyan M, Lukoshkova E, Kiong Nguang S, and Austin PC.** Resonance in the renal vasculature evoked by activation of the sympathetic nerves. *Am J Physiol Regul Integr Comp Physiol* 276: R1311–R1319, 1999.
32. **Miyakawa K, Koepchen HP, and Polosa C.** *Mechanisms of Blood Pressure Waves*. Berlin: Springer, 1984.
33. **Moncada S, Palmer RMJ, and Higgs EA.** Nitric oxide: physiology, pathophysiology and pharmacology. *Pharmacolog Rev* 43: 109–142, 1991.
34. **Morlet J.** Sampling theory and wave propagation. In: *Issues in Acoustic Signal/Image Processing and Recognition*, edited by Chen CH. NATO ASI Series. Berlin: Springer-Verlag, vol. 1, 1983.
35. **Ninomiya I, Irisawa A, and Nisimaru N.** Nonuniformity of sympathetic nerve activity to the skin and kidney. *Am J Physiol* 224: 256–264, 1973.
36. **Peňáz J.** Mayer waves: history and methodology. *Automedica* 2: 135–141, 1978.
37. **Persson PB, Stauss H, Chung O, Wittmann U, and Unger T.** Spectrum analysis of sympathetic nerve activity and blood pressure in conscious rats. *Am J Physiol Heart Circ Physiol* 263: H1348–H1355, 1992.
38. **Nilsson GE, Tenland T, and Öberg PA.** Evaluation of a laser Doppler flowmeter for measurement of tissue blood flow. *IEEE Trans Biomed Eng* 27: 597–604, 1980.
39. **Salerud EG, Tenland T, Nilsson GE, and Öberg PA.** Rhythmical variations in human skin blood flow. *Int J Microcirc: Clin Exp* 2: 91–102, 1983.
40. **Schmid-Schönbein H, St. Ziege W, Rütten W, and Heidtmann H.** Active and passive modulation of cutaneous red cell flux as measured by laser Doppler anemometry. *Vasa* 34, *Suppl*: 38–47, 1992.
41. **Shusterman V, Anderson KP, and Bernea O.** Spontaneous skin temperature oscillations in normal human skin. *Am J Physiol Regul Integr Comp Physiol* 273: R1173–R1181, 1997.
42. **Söderström T, Svensson H, Koop T, and Möller KA.** Processing of laser-Doppler signals from free flaps. *Technology and Health Care* 7: 219–223, 1999.
43. **Stauss HM, Anderson EA, Haynes WG, and Kregel KC.** Frequency response characteristics of sympathetically mediated vasomotor waves in humans. *Am J Physiol Heart Circ Physiol* 274: H1277–H1283, 1998.
44. **Stauss HM and Kregel KC.** Frequency response characteristic of sympathetic-mediated vasomotor waves in conscious rats. *Am J Physiol Heart Circ Physiol* 271: H1416–H1422, 1996.
45. **Stauss HM, Mrowka R, Nafz B, Patzak A, Unger T, and Persson PB.** Does low frequency power of arterial blood flow pressure reflect sympathetic tone? *J Auton Nerv Syst* 54: 145–154, 1995.
46. **Stefanovska A and Bračič M.** Physics of the human cardiovascular system. *Contemporary Physics* 40: 31–55, 1999.
47. **Stefanovska A, Bračič M, and Kvernmo HD.** Wavelet analysis of oscillations in the peripheral blood circulation measured by laser Doppler technique. *IEEE Trans Biomed Eng* 46: 1230–1239, 1999.
48. **Task Force of the European Society of Cardiology and the North American Society of Pacing Electrophysiology.** Heart rate variability: standards of measurement, physiological interpretation and clinical use. *Circulation* 93: 1043–1065, 1996.
49. **Yip K, Holstein-Rathlou NH, and Marsh DJ.** Mechanisms of temporal variation in single-nephron blood flow in rats. *Am J Physiol Renal Fluid Electrolyte Physiol* 264: F427–F434, 1993.

Cardiorespiratory interactions

Aneta Stefanovska

Nonlinear Dynamics and Synergetics Faculty of Electrical Engineering, University of Ljubljana
Tržaška 25, 1000 Ljubljana, SLOVENIA
E-mail: aneta@osc.fe.uni-lj.si

(Received 02 December 2002)

The cardiac and respiratory systems each function in an oscillatory manner, providing a nice example of coupled biological oscillators. The modulation of the cardiac frequency, called respiratory arrhythmia, has long been known. Synchronization analyses have recently confirmed that, in a conscious healthy subject at rest, the two systems can synchronize for a short episodes of time. In experiments with paced respiration we show that the synchronization and modulation can coexist. The respiratory system is the driving system at all respiration frequencies, whether paced or spontaneous.

Key words: biological oscillators, synchronization, modulation, direction of coupling, cardiovascular system

PACS numbers: 05.45.Xt; 87.80.Vt, 05.40.-a, 87.19.Hh

1 Introduction

Biological oscillators can be found at every level of complexity, and for almost every living system [1]. Single cell activity is characterised by oscillations. As cells cluster to form more complex systems, up to the level of tissues and organs, the activity of these complex structures remains oscillatory. With increasing complexity, the number of possible interactions rapidly increases and, in a biological system, the cluster of oscillators at the microscopic level usually contains almost infinitely many units. At the next higher level of complexity, however, their collective activity can still manifest as a single oscillatory unit. This functional organisation is typical of complex systems. The ideas were formulated for the case of lasers by Haken [2, 3] and, following his pioneering work, can now be understood to apply to complex systems quite generally, including biological ones.

Complex systems are self-organised at many levels and, for us their observers, the most difficult unsolved task is how to distinguish appropriately between each level of complexity. Understanding and revealing the organisational structure of a complex system is a challenging task. Basically, following the principles of synergetics, we seek clear signatures of the organisational units that characterise some given level of complexity, and then trace their interactions. Here, we come again to the oscillator as the basic unit for a complex dynamical system. In a living system, for example, the regulation of a variable is maintained through a dynamic balance between activation (or excitation) and deactivation (or inhibition) – a basic principle of an oscillator. Although, the field of coupled oscillators and their application to complex systems is still at an early stage, many pioneering models in biology have already been proposed [4, 5, 6, 7, 8, 9, 10].

One of the most interesting physiological complex systems – which at the same time is essential for the function of the human organism – is the cardiovascular system. It includes the heart, which pumps the blood into a huge network of vessels. Before returning back to the left heart, the blood is oxygenated in the lungs. At the macroscopic level, the heart, the lungs and the vessels can be considered as the basic organisational structures involved in transport of the blood. The vessels are not rigid tubes

but, rather, they play an active role in blood transport. Although a detailed understanding of the basic units of the vascular regulation of blood flow has yet to be reached, several organisational structures have already been proposed. Here the main difficulty is that of distinguishing between the organisational units and their interactions. Many systems are active in the transport of information within the cardiovascular system, and it is often difficult to separate them from the basic functional units.

The vascular regulation of blood flow, considered on a time scale corresponding to one blood circulation time, appears to involve myogenic, neurogenic and endothelial activity. In a healthy subject at rest, this time scale is around one minute, within which the heart pumps an amount of blood equivalent to the total amount in the organism. In what follows, I shall review recent developments in the understanding of the interactions between two of the oscillatory systems involved in the regulation of blood flow: the cardiac and the respiratory. My interest in cardiovascular interactions was greatly influenced by Hermann Haken. In the course of our collaboration, which started at the beginning of the 1990s while I was still a PhD student, he introduced me to the world of coupled oscillators and the possible outcomes of their many types of interaction. The introduction of a coupled oscillator model to describe cardiovascular dynamics [11, 12, 13] then followed naturally. It is therefore a great pleasure for me to dedicate to Hermann Haken the discussion of cardiovascular interactions that follows below.

2 Instantaneous phases

To monitor cardiac action, signals corresponding to its electrical activity (ECG) may be monitored. By an appropriate choice of electrode placement (e.g. two electrodes on the shoulders, and one on the lowest left rib) the amplitude and sharpness of the R-peak can be maximised, thereby minimising uncertainties in its timing. Placing the electrodes over bony prominences also minimizes noise resulting from electrical activity of the surrounding muscular, nervous or soft tissue. To record respiratory activity, various types of sensor have been used. An optimal compromise between the comfort of the subject and the quality of the signal can be obtained with piezo, or infrared sensors. The sensor is inserted in a rigid tape fastened around the thorax, and its excursions are then monitored. A typical sample of ECG and respiratory signals thus obtained from a resting healthy subject is presented in Fig. 1.

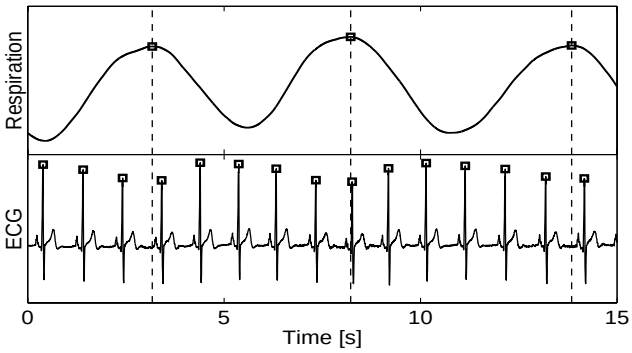

FIG. 1. A sequence of respiration and ECG signals recorded simultaneously. Maxima in the respiration signal, and R-peaks in the ECG, are marked to obtain instantaneous phases and frequencies.

Studies of the cardiorespiratory phase relations were introduced by Koepchen, Hildebrandt and Raschke (see [14, 15] and the references therein), and Kenner and his collaborators [16]. Hildebrandt reported preferred time delays between the onset of inspiration and the preceding heart beat, and the occurrence of an integer number of heartbeats per respiratory cycle. The preference of integer ratios existed only in statistical terms. Raschke investigated phase and frequency coordination in different states of the system and reported strong phase coordination between the cardiovascular and respiratory systems during sleep, which was diminished under conditions of strain or disease. Both Hildebrandt and Raschke proposed that synchronization, or frequency and phase coordination as they named it, establishes a system of economical co-action and thus favours the functional economy of the organism.

The notion of synchronization was for a long time restricted to periodic oscillations. More recently, new studies of cardiorespiratory synchronization were initiated by the introduction of methods for de-

tecting phase synchronization between non-regular or chaotic oscillators (see [17] and the references therein). In a broad sense, synchronization can be treated as the appearance of some relationship between the states of interacting systems $\mathbf{u_1}(t), \mathbf{u_2}(t)$, characterised by their phases Φ_1, Φ_2 and their generalised phase difference, $\phi_{n,m} = n\Phi_1 - m\Phi_2$. A weaker condition of phase locking

$$|n\Phi_1 - m\Phi_2 - \delta| < \text{const}\,, \qquad (1)$$

was proposed, in which case n:m phase locking manifests as a variation of $\phi_{n,m}$ around a horizontal plateau. The amplitudes of phase synchronized oscillators can be quite different, and need not be related. Phase synchronization is understood as the appearance of a peak in the distribution of the cyclic relative phase

$$\Psi_{n,m} = \phi_{n,m} \bmod 2\pi\,, \qquad (2)$$

and interpreted as the existence of a preferred stable value of phase difference between the two oscillators.

Two methods are often used to detect instantaneous phases, Φ_i, of the interacting oscillators from measured data: (i) marked events, and (ii) the Hilbert transform. By the first method events that characterise a cycle of an oscillator are first determined. Phases are then usually interpolated using linear interpolation, which introduces an approximation. A 2π increase in the phase is attributed to interval between subsequent marked events. Within this interval, the instantaneous phase is

$$\Phi(t) = 2\pi\frac{t - t_k}{t_{k+1} - t_k} + 2\pi k\,,\ \ t_k \le t < t_{k+1} \qquad (3)$$

where t_k is the time of kth marked event. Thus obtained, the phase is a monotonically increasing piecewise-linear function defined on the real line. The second method, based on the Hilbert transform, depends strongly on the quality of the measured signal representing the dynamics of the observed oscillator. In most living system, measured signals are an approximation of the dynamics of the oscillatory process under observation, and are often corrupted by interfering activity of other physiological processes and noise. In both cases, therefore, phase detection involves compromise, and probably both methods should be applied before one reaches a final interpretation of a set of measurements.

The introduction of nonlinear methods, and the concepts of generalised and phase synchronization, further illuminated the problem and confirmed that in the waking state of healthy humans cardiorespiratory synchronization usually occurs as brief episodes [18, 19]. It was found that the synchronization episodes at rest were ∼10 times longer (∼1000 s) in athletes [18] than non-athletes [19]. From these results it may reasonably be inferred that the inter-oscillator coupling strength, as revealed by the lengths of the synchronization episodes, constitutes a useful piece of information about the state of the organism. This idea is apparently confirmed by measurements on a critically ill patient in coma [13], where there is absolutely no synchronization at all.

Another physiological state where synchronization phenomena are of particular importance is that of anæsthesia [20]. Very long episodes of synchronization (>10 minutes) were found to occur in anæsthetised rats: phase-transition-like phenomena were observed when the synchronization ratio changed in stages from 1:2 to 1:5 as the anæsthesia deepened; and the same sequences was then followed in reverse as the anæsthetic wore off again. If the same phenomenon occurs in humans, then there is obvious potential in using measures of synchronization for a noninvasive evaluation of the depth of anæsthesia.

2.1 Quantifying synchronization

The problem of detection synchronization from real data is however still burdened with many difficulties. Noise plays an essential role. In the presence of weak noise, $\phi_{n,m}$ fluctuates around a constant value, and the condition of frequency locking is only fulfilled on average, i.e. $n\langle f_1\rangle = m\langle f_2\rangle$. Strong noise can also induce phase slips. In such cases, the question of whether the oscillators are synchronous, or not, cannot be answered uniquely, but only in a statistical sense. Note that in the case of cardiorespiratory interactions, the noise originates not only from measurements and external disturbances, but also from the fact that there are other subsystems that

are active in the cardiovascular control [12] whose influence is considered as noise in synchronization analysis.

Two tools have been introduced to improve the reliability of synchronization analyses: (i) synchrograms [18]; and (ii) synchronization indices [21].

Synchrograms

By definition, m:n phase synchronization can be detected by plotting the generalised phase difference $\phi_{n,m}$ versus time and looking for horizontal plateaus. For noisy systems the cyclic relative phase $\Psi_{n,m}$ is used instead, to avoid the impact of noise induced phase slips. There are however two problems with this approach: (i) the integers n and m can only be obtained through trial and error, by checking a wide range of values; and (ii) if several synchronization regimes exist, the method cannot reveal them, nor the transitions between them.

To overcome these problems, the cardiorespiratory synchrogram was introduced [18] (see also [17]). It is constructed by plotting the normalized relative phase of a heartbeat within m respiratory cycles

$$\Psi_m(t_k) = \frac{1}{2\pi}(\Phi_r(t_k) \bmod 2\pi m)\,, \qquad (4)$$

where t_k is the time of the kth heart beat and Φ_r is the instantaneous phase of respiration. Φ_r is defined on the real line and is observed stroboscopically at times t_k. In perfect n:m phase locking, $\Psi_m(t_k)$ exhibits n horizontal stripes. In the presence of noise, the stripes become broadened. By this technique only one integer, m, need be chosen by trial, and several different sequential regimes can be identified within a single plot.

Fig. 2 (left column) shows five cardiorespiratory synchrograms obtained from a young healthy subject at rest. The ECG and respiration were recorded during spontaneous respiration (top synchrogram), and during paced respiration with the respiration frequency kept constant below (second and third plots) and above (fourth and fifth plots) the frequency of spontaneous respiration. To obtain a constant respiratory frequency the subject was asked to follow the tick of a metronome. The results will be presented in detail elsewhere; here we illustrate the various synchronization ratios that can be obtained during paced respiration.

Indices of synchronization

Two indices have been proposed for the quantitative evaluation of synchronization based on: (i) Shannon entropy; and (ii) conditional entropy [21]. For the data presented in Fig. 2 (right column, dashed lines) the conditional probability was used and we shall now describe it briefly. Accordingly, the phase of the second oscillator is observed at fixed values of the first oscillator, $\Phi_1 \mathrm{mod} 2\pi m$. We divide the interval of each phase, $[0, 2\pi m]$ for $\Phi_1(t_k)$, and $[0, 2\pi n]$ for $\Phi_2(t_k)$, into N bins and calculate

$$r_l(t_k) = \frac{1}{M_l} \sum e^{i\Phi_2(t_k)} \;\; l = 1, \ldots, N\,, \qquad (5)$$

for all k such that $\Phi_1(t_k)$ belongs to bin l and M_l is the number of points in this bin. If there is a complete mutual interdependence between the two phases, $|r_l(t_k)| = 1$, whereas it is zero if there is no dependence at all. Finally, we calculate the average over all bins

$$\lambda = \frac{1}{N} \sum |r_l(t_k)|\,, \qquad (6)$$

which measures the conditional probability of Φ_2 to have a certain value provided Φ_1 is in a certain bin.

As different values for the frequency of respiration were chosen in our experiments, several synchronization regimes were obtained. Therefore, a range of synchronization indices was calculated, for $m = 1$ and $n = 4, \ldots, 10$. Maximal values are presented in figure 2 (right column, dashed lines). Typically, other values were close to zero. From presented results we may infer that a tendency towards synchronization exists, which appears in episodes, both during spontaneous, as well as during paced respiration.

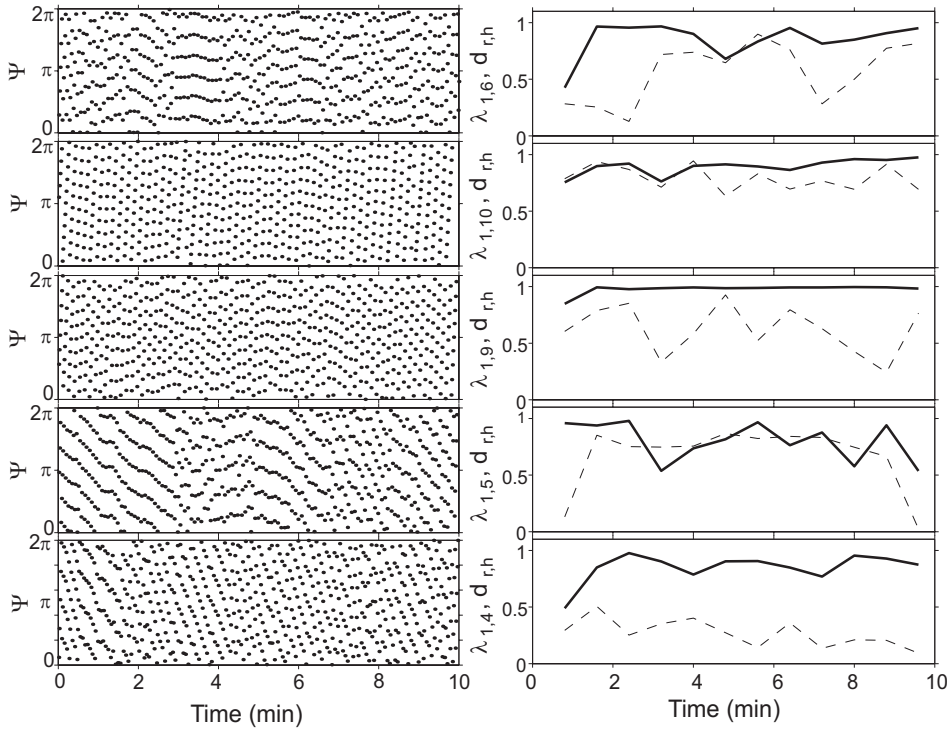

FIG. 2. Synchrograms (left column), indices of synchronization (right column, dashed lines) and direction of coupling (right column, solid lines) between the cardiac and respiratory oscillations during spontaneous (top) and paced respiration. Lover (second and third raw) and higher (fourth and fifth raw) than spontaneous frequency of respiration were selected for paced respiration (for values of frequencies see Fig. 3). While the pattern of synchronization slightly changes with the frequency of paced respiration, in all cases, during spontaneous, or paced respiration, the respiration appears to be the driving system.

Here, however, we should point that the indices are calculated as an average value within a chosen window. In our case a 80 s window was used, slid with an overlap of 0.6. This window was chosen to cover 8 periods of the slower oscillator – the respiration. As quite low values of the respiratory frequency were also chosen, ∼0.1 Hz being the minimum, it was these values that dictated the choice of window length. At the higher respiration frequencies e.g. ∼0.27 Hz (see Fig. 3, left column), however, such a window contains a large number of periods, ∼21 in this example. Within this interval the level of synchronization changes so that the indices represent averages only. A shorter window would have been inappropriate for the lower frequencies of respiration and the obtained value would be unreliable. The problem described here is of a quite general nature and is associated with the fact that the cardiovascular system has time-variable dynamical properties. In analysing time series related to it we therefore face the fact that the length of an optimal window within which we can analyse its dynamics, or the dynamics of its subsystems in this case, changes with time.

2.2 Direction of coupling

Having estimated the time series of the phases of our interacting oscillators, $\Phi_{1,2}(t_k)$, with δt as a sampling interval and $t_k = k\delta t$, we may ask another question: whether the phase dynamics of one oscillator is influenced by the phase of the other, or their influence is mutual? Several numerical methods have been recently proposed, both, based on information theory approach [22, 24], or phase dynamics approach [23], for detecting direction of coupling in interacting oscillators. Here, we present results using phase dynamics

approach. A comparative study, using several methods, will be presented elsewhere.

In phase dynamics approach, we first compute for each time point the increment $\Delta_{1,2} = \Phi_{1,2}(t_k + \tau) - \Phi_{1,2}(t_k)$. The choice of time delay was shown not to be important [23]. This increment is then considered as generated by some unknown two-dimensional noisy map $\Delta_{1,2}(k) = F_{1,2}(\Phi_{1,2}(k), \Phi_{2,1}(k)) + \eta_{1,2}(k)$. Several methods have been proposed to estimate the dependence of Δ on Φ_1 and Φ_2 and coefficients c_1 and c_2, which represent the cross-dependence of phase dynamics of the two systems were obtained. In this way an index of the direction of coupling was proposed, which can be written for the cardiac and respiratory systems in the form

$$d_{r,h} = \frac{c_r - c_h}{c_r + c_h}\,. \tag{7}$$

Normalized in this way the index varies from 1 in the case of unidirectional coupling ($r \to h$) to -1 in the opposite case ($h \to r$). Vanishing index $d_{r,h} = 0$ corresponds to symmetric bidirectional coupling.

The index of the direction of couplings is strictly > 0.5 in all considered cases, with spontaneous or paced respiration, indicating that in awaken healthy subjects at rest the interaction between the two systems is unidirectional.

3 Instantaneous frequencies

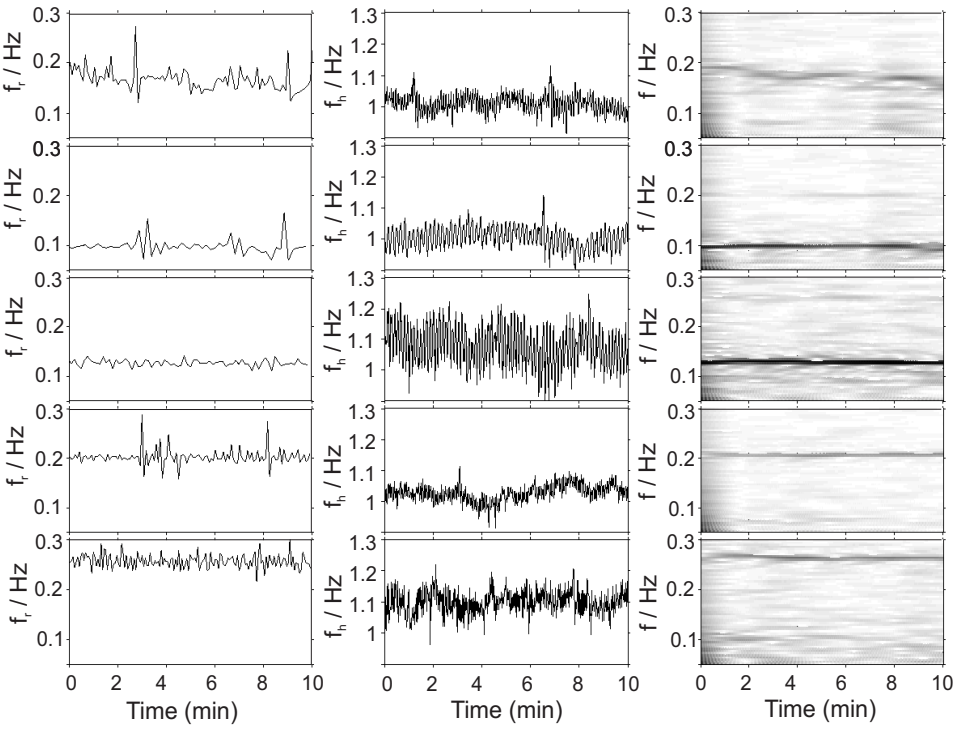

FIG. 3. Instantaneous respiratory f_r, (left column) and cardiac, f_h (middle) frequencies, obtained in five measurements on a young healthy subject. The subject was first asked to breath spontaneously (top). Four recordings with paced respirations were then performed, two with frequency lower (second and third rows) and two with frequency higher (fourth and fifth rows) than the spontaneous frequency of respiration. To keep the respiration constant the subject was asked to follow the tick of a metronome. The respiratory frequency can also be observed in the time-frequency plot of the instantaneous heart frequency (right), due to modulation of cardiac frequency by the respiration.

Another type of interaction between the respiratory and cardiac oscillations has been known since the 18th century when Hales carried out his celebrated experiments [25] on a horse. He found that the heart rate increased on inspiration and decreased on expiration. This frequency modulation phenomenon, known as respiratory sinus arrhythmia, has been studied extensively [26, 27] since then.

Where the coupling between the oscillators is strong, it can give rise either to strong modulation or to strong synchronization; but these are competing processes that by definition cannot occur simultaneously. Which of them is manifested must depend on the conditions. By analogy with the classical theory of synchronization [28], one may infer that the coupling gives rise to synchronization if the parameters are such that the working point lies within an Arnold tongue but that, otherwise, it produces modulation.

In reality, however, the cardio-respiratory interaction seems to function in a more complex way. Frequency modulation of the heart by respiration can be detected during spontaneous as well as paced respiration (Fig. 3). The fact that the frequency modulation of the heart rate by respiratory rhythm, known as respiratory sinus arrhythmia (RSA), can coexist with synchronization between the two rhythms may be interpreted in at least two ways. First, at least two different types of coupling may coexist between the cardiac and the respiratory systems. An adjustment of the two rhythms seems to be conducted by the central nervous system. The RSA on the other hand appears to be result of a mechanical coupling between respiration and the cardiac function, as discussed earlier [26]. Although there is currently no clear and unique understanding of the mechanisms of cardiorespiratory interaction, two different mechanisms of coupling have often been reported. Galletly has noted that the sinus arrhythmia appears to persist at all levels of cognitive arousal, whereas phase coupling is seen best during relaxation, sleep and anæsthesia [29]. Secondly, our result may also be taken as illustration that more than two rhythms are involved in the cardiovascular regulation.

4 Summary

Cardiovascular interactions, and the coexistence of synchronization with modulation, have been illustrated through experiments with paced respiration, yielding the results summarized in Fig. 4. It was shown that the respiratory system is the driving system, whether paced or spontaneous. Time-variability is one of the key features of the system. It is the non-stationarity of the frequency that presents the most challenging unsolved problem associated with the analysis of dynamical properties from measured time series.

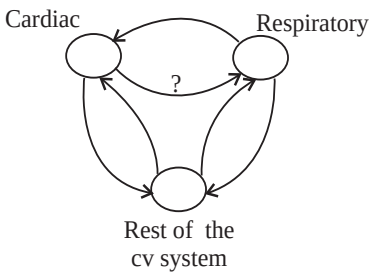

FIG. 4. Results obtained during paced respiration show that, for conscious subjects in repose, respiratory activity influences the cardiac system directly. Whether the cardiac system can influence respiratory activity directly is at present unclear. It is evident, however, that indirect interaction between the two systems exists, either via the higher centres, or via the other peripheral oscillatory processes (related to the myogenic, nurogenic or endothelial activity), or both.

Interactions and couplings characterize the state of the system. An important future aim must be the development of a coupled oscillator model that can provide a description of the different states of the system, thereby quantifying the couplings, and some initial progress has already been made [30] in this direction.

Acknowledgments

This work has been supported by the Slovenian Ministry of Education, Science and Sport, the EPSRC (UK) and INTAS. The author would like to thank Michael Rosenblum for his algorithm for calculation the index of coupling direction and to Bojan Musizza for his help in preparing figures.

References

[1] P.E. Rapp. Atlas of cellular oscillators. J. Exp. Biol. **81**, 281-306 (1979).

[2] H. Haken. A nonlinear theory of laser noise and coherence I and II. Z. Phys. **181**, 96 (1964), **182**, 346 (1965).

[3] H. Haken. *Synergetics - An Introduction.* (Springer-Verlag, Berlin, 1977).

[4] A.T. Winfree. *The Geometry of Biological Time.* (Springer, New York, 1980).

[5] Y. Kuramoto. *Chemical Oscillations, Waves, and Turbulence* (Springer, Berlin, 1984).

[6] S.H. Strogatz, I. Stewart. Coupled oscillators and biological synchronization. Sci. Am. **269**(6), 102-109 (1993).

[7] H. Haken, *Principles of Brian Functioning. A Synergetic Approach to Brain Activity, Behavior, and Cognition.* (Springer, Berlin, 1995).

[8] V.K. Jirsa, H. Haken. Field theory of electromagnetic brain activity. Phys. Rev. Lett. **77**, 960-963 (1996).

[9] P.C. Bresloff, S. Coombes, and B. De Souza. Dynamics of a ring of pulse-coupled oscillators: a group theoretic approach. Phys. rew. Lett. **79**, 2791-2794 (1997.

[10] P.A. Tass. *Phase Resetting in Medicine and Biology - Stochastic Modelling and Data Analysis* (Springer, Berlin, 1999).

[11] A. Stefanovska, S. Strle, M. Bračič, H. Hakenl. Model synthesis of the coupled oscillators which regulate human blood flow dynamics. Nonlin. Phen. in Compl. Sys. **2**(2), 72-78 (1999).

[12] A. Stefanovska, M. Bračič. Physics of the human cardiovascular system. Contemp. Phys. **40**, 31-55 (1999).

[13] A. Stefanovska, M. Bračič Lotrič, S. Strle, H. Haken. The cardiovascular system as coupled oscillators? Physiol. Meas. **22**, 535-550 (2001).

[14] *Temporal Disorder in Human Oscillatory Systems.* Edited by L. Resing, U. an der Heiden, M.C. Mackey. (Springer, Berlin, 1987).

[15] *Rhythms in Physiological Systems.* Edited by H. Haken, H.P. Koepchen. (Springer, Berlin, 1991).

[16] T. Kenner, H. Passenhofer, G. Schwaberger. Method for the analysis of the entrainment between heart rate and ventilation rate. Pflügers Archiv. **363**, 263-265 (1976).

[17] A. Pikovsky, M. Rosenblum, J. Kurths. *Synchronization - A Universal Concept in Nonlinear Sciences.* (Cambridge University Press, 2001).

[18] C. Schäfer, M.G. Rosenblum, J. Kurths. Heartbeat synchronised with respiration. Nature. **392**, 239-240 (1998).

[19] M. Bračič Lotrič, A. Stefanovska. Synchronization and modulation in the human cardiorespiratory system. Physica A **283**, 451-461 (2000).

[20] A. Stefanovska, H. Haken, P.V.E. McClintock, M. Hožic, F. Bajrović, S. Ribarič. Reversible transitions between synchronization states of the cardiorespiratory system. Phys. Rev. Lett. **85**, 4831-4834 (2000).

[21] P. Tass, M.G. Rosenblum, J. Weule, J. Kurths, A. Pikovsky, J. Volkmann, A. Schnitzler, H.-J. Freund. Detection of n:m phase locking from noisy data: Application to magnetoencephalography. Phys. Rev. Lett. **81**, 3291-3294 (1998).

[22] T. Schreiber. Measuring information transfer. Phys. Rev. Lett. **85**, 461-464 (2000).

[23] M.G. Rosenblum, A.S. Pikovsky. Detecting direction of coupling in interacting oscillators. Phys. Rev. E **64**, 045202(R) (2001).

[24] M. Paluš, A. Stefanovska. Direction of coupling from phases of interacting oscillators: An information-theoretic approach. Phys. Rev. E. submitted. (2003).

[25] S. Hales. Statistical Essays II, Hæmastatisticks. (Innings Manby, London, 1773).

[26] C.T.M. Davies,J.M.M. Neilson. Sinus arrhythmia in men at rest. J. Appl. Physiol. **22**, 947-955 (1967)

[27] J.A. Hirsch, B. Bishop. Respiratory sinus arrhythmia in humans: How breathing pattern modulates heart rate. Am. J. Physiol.: Herat Circ. Physiol. **241**, H620-H629 (1981).

[28] R.L. Stratonovich. *Topics in Theory of Random Noise, vol. 2.* (Gordon and Breach, New York, 1967).

[29] D.C. Galletly, P.D. Larsen. Cardioventilatory coupling during anaesthesia. Brit. J. Anæsth. **79**, 35-40 (1997).

[30] A. Stefanovska, D.G. Luchinsky, P.V.E. McClintock. Modelling couplings among the oscillators of the cardiovascular system. Physiol. Meas. **22**, 551-564 (2001).

ELSEVIER

Physica A 314 (2002) 69–76

PHYSICA A

www.elsevier.com/locate/physa

Noise and determinism in cardiovascular dynamics

Peter V.E. McClintock[a,*], Aneta Stefanovska[b,a]

[a] *Department of Physics, Lancaster University, Lancaster, LA1 4YB, UK*
[b] *Nonlinear Dynamics and Synergetics, Faculty of Electrical Engineering, University of Ljubljana, Trzaska 25, 1000 Ljubljana, Slovenia*

Abstract

Signals derived from the human cardiovascular system are well known to exhibit highly complex, nearly periodic, oscillatory behaviour whose nature is something of an enigma. It has, for example, been variously described as chaotic, fractal, stochastic, and subject to $1/f$ fluctuations—and its true nature is still the subject of vigorous debate. We review and describe some recent experiments that illuminate the problem and discuss a combination of noise and almost periodic frequency modulation as a signature of the system dynamics.

PACS: 87.22As; 87.45.Hw; 05.40+j

Keywords: Cardiovascular system; Nonlinear oscillators; Synchronization; Couplings; Frequency modulation; Stochastic processes

1. Introduction

Physiological signals derived from humans are extraordinarily complex—faithfully reflecting their origin in what is arguably the most complicated mechanism ever to have existed. Because they must reflect ongoing processes that normally occur unseen, within the interior of the body, such signals repay close attention. In particular, they can be used to diagnose incipient pathophysiological conditions before symptoms become obvious. A well-known example is the electrocardiogramme (ECG) signal, representing the electrical activity of the heart. ECG measurements have been used for diagnostic purposes for almost a century. For the first several decades of such measurements, attention was focussed mainly on the detailed *shape* of the approximately periodic

* Corresponding author. Tel.: +44-1524-593073; fax: +44-1524-844037.
E-mail address: p.v.e.mcclintock@lancaster.ac.uk (P.V.E. McClintock).

0378-4371/02/$ - see front matter
PII: S0378-4371(02)01165-2

pulses seen in the signal. More recently, however, attention has shifted to the *separation* of the pulses because it has become apparent that the heart of a healthy human in repose does not beat at a constant rate. Rather, the cardiac frequency varies in time, a phenomenon known as heart-rate variability (HRV).

Gene Stanley and his group have probably done more than anyone to try to characterise and analyse cardiovascular signals, so it is a particular pleasure to have been invited to present a paper on this topic in Messina. Approaches to the problem introduced by different authors have included, for example, studies of: Fourier spectra [1]; chaotic behaviour [2,3]; wavelet spectra [4–6]; Karhunen–Loève decomposition [7]; scaling properties [8–13]; Lyapunov exponents [14]; multifractal properties [15,16]; correlation integrals [17]; 1/f spectra [18–20]; and synchronization properties [21–25]. The two extreme perceptions of HRV consider it to be deterministic in origin, e.g. sometimes resulting in deterministic chaos [2,3], or stochastic [26]. It is not immediately obvious which of these several diverse approaches is the most promising: the criteria to be met, presumably, are that the technique of analysis should (i) be able to deal successfully with time variations of characteristic frequencies and amplitudes, and that (ii) it should yield some insight into the physiological processes responsible for the HRV, so that (iii) their individual function—normal or pathological—can be evaluated separately for diagnostic purposes.

In this paper we focus on the results obtained through use of one of the techniques mentioned above, wavelet analysis [4,27], and we point out that it apparently meets all three criteria. In Section 2 we summarise the experimental information obtained by this method and, in Section 3 we show how it can be accounted for in terms of mutually interacting oscillatory processes each of which appears to relate to a distinct physiological mechanism. In Section 4 we report the present status of attempts to model the cardiovascular system as a set of coupled oscillators, showing that important features of the measured signals can be reproduced by the model. In Section 5 we draw conclusions and try to point the way forward.

2. Cardiovascular signals

Many different protocols have been used for acquiring cardiovascular data, one of the most thorough being that described in Ref. [27] where ECG, blood pressure, and blood flow rate are recorded simultaneously over a period of about 20 min. Interest centres on the bloodflow circulatory control mechanisms, and so any processes occurring on timescales longer than about 1 min (the average circulation period) are ignored. For healthy subjects in repose, the results are typically as in Fig. 1(a); Fig. 1(b) shows the averaged wavelet transform of the same data, but calculated over the full 20 min. A detailed discussion of such results is presented in Ref. [27], but it is immediately evident that

- There are (at least) *five* characteristic spectral peaks.
- Remarkably, the *same*, or almost the same, peaks appear in all the spectra, regardless of where or how the corresponding signals were recorded, though there are considerable differences in amplitude.
- All the peaks are *broadened.*

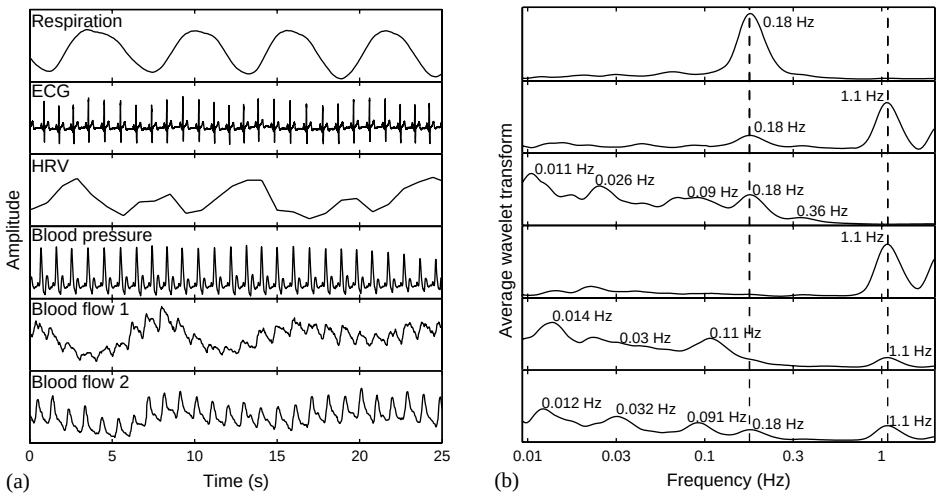

Fig. 1. Samples of cardiovascular signals (a) and time averages of their wavelet transforms (b). The positions of the peaks are almost the same for all signals, while the corresponding amplitudes may be considerably different. After Ref. [27].

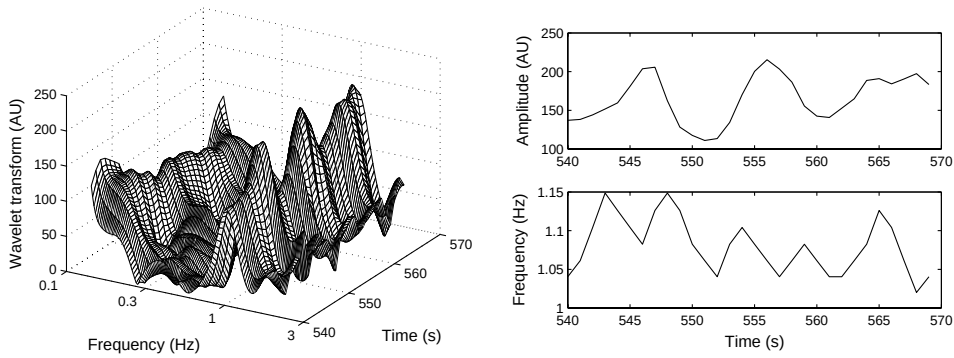

Fig. 2. A segment of the wavelet transform of the blood flow signal in the time-frequency plane (left). Peaks at the heart (~ 1.1 Hz) and respiration rates (~ 0.18 Hz) are visible. On the right are plotted the amplitude and frequency variations of the heartrate peak. After Ref. [5].

A clue to the origin of some of the broadening can be found by inspection of the full time-frequency wavelet spectrum, part of which is shown in Fig. 2. It can be seen that both the instantaneous amplitudes and central frequencies vary in time, giving rise to a considerable part of the broadening observed in the averaged spectra of Fig. 1(b).

What is the origin of this frequency and amplitude wandering? It appears that the instantaneous frequency of any given spectral peak oscillates. It does so at the frequency of the spectral peak next-lowest in frequency, with contributions coming from all of the other oscillatory processes too. HRV, for example, is a signal representing the variations of the cardiac frequency, and from Fig. 1(b) we can see (third spectrum

from the top) that its oscillations are also modulated by the processes with frequencies near 0.011, 0.026, 0.10, and 0.18 Hz (as well as its own second harmonic at 0.036 Hz). Such observations can be construed as evidence that the five oscillatory processes are mutually coupled. They seem to influence each other via couplings at least some of which are parametric, thus giving rise to the observed frequency modulation.

3. Interacting oscillatory processes

With varying degrees of confidence, all of the oscillatory processes can now be related to underlying physiological mechanisms. Their characteristic average frequencies vary slightly between individuals, and, in some cases, between different measurement locations, but in each case they lie within definite limits. The physiological origins of the peaks at 1 Hz (heart beat), and 0.2 Hz (respiration) are obvious. It is reasonably well established that the peak at 0.1 Hz is attributable to intrinsic myogenic activity of smooth muscles [28–30]. The 0.03 Hz peak is apparently connected to autonomous nervous control [31,32] (neurogenic), and there is strong evidence that the 0.01 Hz peak arises from metabolically related endothelial activity [33,34].

Thus wavelet analysis of signals from the cardiovascular system provides a noninvasive technique for acquiring information about these distinct physiological processes. Additional information, yielding deeper insight into the dynamics, can also be inferred from the *couplings* between the processes. These can manifest themselves either through mutual modulation (Fig. 2) or through synchronization between two or more of the processes. Which of these phenomena occurs in any given case probably depends partly on the strength of the coupling and partly on how close in frequency low harmonics of the processes would be to each other in the absence of coupling. In practice, measurements on healthy subjects show transient episodes of cardio-respiratory synchronization lasting typically a few tens of seconds. The average length of these episodes depends on the physiological state, and differs between, e.g. athletes, sedentary individuals, and patients with pathological conditions such as diabetes.

Synchronization effects are potentially of particular interest because of the information they carry about the couplings. But, with the exception of the cardio-respiratory coupling, they have not yet been closely studied. A major difficulty is that, unlike the heart and respiration, the lower-frequency processes do not give rise to separate signals that can be acquired noninvasively. In practice, therefore, it is necessary to infer the existence or absence of synchronization from univariate time series. This challenging problem is already being approached in three distinct ways: (i) filtration of the univariate data to create two "separate" signals that can then be tested for mutual synchronization [23] using established techniques such as synchrogrammes [21] or synchronization indices [35]; (ii) the use of angles-of-return-time maps [25,36]; and (iii) bispectral analysis [37]. In each case, it has been possible to derive information about the presence or absence of synchronization between the 0.1 Hz (myogenic) process and respiration or heartbeat. Problems of resolution—in time, frequency and phase—have so far made it impossible to obtain synchronization information for the 0.03 Hz (neurogenic) and 0.01 Hz (endothelial) processes.

Note that the three lower frequencies are derived in each case from spatially distributed processes. Within each of them, there must be significant global synchronization because, if this were not the case, low frequency oscillations would be undetectable in centrally measured quantities such as HRV (Fig. 1(b)) because they would all have averaged out.

To make further progress, it is necessary to develop a model to which the cardiovascular data can be fitted. One may then hope to characterise different physiological and pathophysiological conditions quantitatively in terms of the model parameters.

4. A coupled oscillator model of the cardiovascular system

Given the clear evidence of (a) well-defined spectral peaks (implying the presence of oscillatory processes) and (b) amplitude and frequency modulation, and synchronization effects (all indicating the existence of inter-oscillator interactions), it is natural to try to model the system with a set of oscillators [38] whose couplings [39] can be adjusted to try to reproduce the observed phenomena.

Little experimental information exists yet about either the nature of the couplings or the details of the oscillators. So we have used [38] the Poincaré oscillator

$$\dot{x}_i = -x_i q_i - \omega_i y_i + g_{x_i}(\mathbf{x}),$$

$$\dot{y}_i = -y_i q_i + \omega_i x_i + g_{y_i}(\mathbf{y}), \quad q_i = \alpha_i(\sqrt{x_i^2 + y_i^2} - a_i), \tag{1}$$

where, $\mathbf{x}$, $\mathbf{y}$ are vectors of the oscillator state variables, α_i, a_i, and ω_i are constants and $g_{yi}(\mathbf{y})$ and $g_{xi}(\mathbf{x})$ are linear coupling vectors. Although to some extent this choice is arbitrary, (1) possesses properties of structural stability, robustness and symmetry consistent with physiological understanding and the analyses of measured time series.

Using a numerical simulation [39] of five coupled oscillators (1), with characteristic frequencies chosen to accord with measured data (Fig. 1), and amplitudes set initially to unity, we find that we can generate signals that to the eye seem in many respects to resemble those from the cardiovascular system. We were especially interested to establish whether frequency and amplitude modulation would occur with short episodes of synchronization at random intervals, as observed in the experiments. The investigations are still at an early stage, but we have already established: (a) that the observed depth of modulation requires parametric couplings (as expected); (b) that with appropriately chosen parameter values parametric modulation indeed gives rise to episodes of synchronization, but of course in a totally deterministic fashion with equal intervals between the episodes; and (c) with purely linear couplings, and added noise (random fluctuations), the synchronization episodes occur briefly and randomly just as observed in reality. An example showing the modelling of cardiorespiratory synchronization is shown in Fig. 3. It appears, therefore, that both linear and parametric couplings exist and that it is essential to take into account the influence of stochastic effects resulting from the (unmodelled) rest of the system.

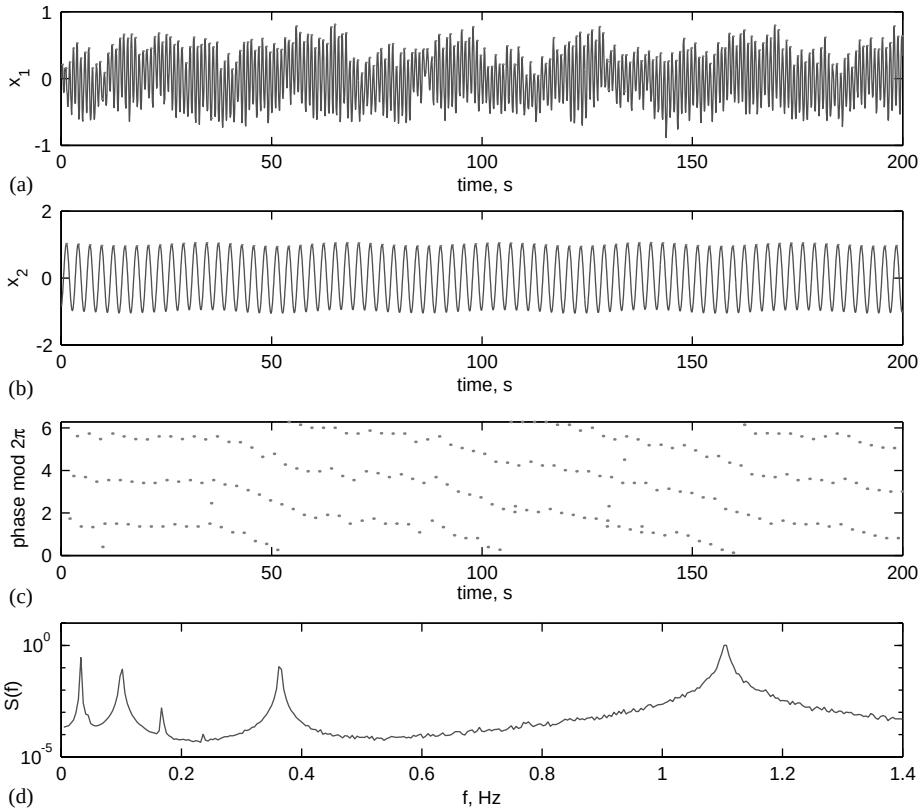

Fig. 3. Results of modelling with linear couplings, in the presence of fluctuations. (a) and (b) The time series showing the rhythmic activities of the cardiac and respiratory flow components. (c) The corresponding cardio-respiratory synchrogram. (d) Power spectrum of oscillation in the blood flow generated by the cardiac activity. After Ref. [39].

5. Conclusions

Information derived from analysis of cardiovascular signals in the time-frequency and time-phase domains has led to a coupled oscillator model able to reproduce many features seen in the data. From the model, we conclude that cardiovascular signals have a strong deterministic element, but that random noise (i.e. external influences and all effects not explicitly considered) also plays a crucially important role. Our approach meets all three of the criteria mentioned in Section 1. In particular, it relates the underlying physiological processes to particular spectral peaks and thus allows them to be studied individually. Furthermore, it promises quantitative evaluation of the couplings between them. The latter feature is potentially of particular interest for diagnosis and treatment because it enables the function and health of the cardiovascular system as a whole to be evaluated.

Acknowledgements

It is a pleasure to acknowledge valuable discussions with Fajko Bajrović, Alexander Balanov, Maja Bračič Lotrič, Peter Clarkson, Hermann Haken, Natalia Janson, Igor Khovanov, Peter Krošelj, Knut-Arvid Kirkebøen, Hebe Kvernmo, Mitya Luchinsky, Janko Petrovčič, Samo Ribarič, Misha Rosenblum, Carstin Schäfer, Sašo Strle, Dušan Štajer, Peter Tass, Vilma Urbančič-Rovan and Aleš Založnik. The research has been supported by the Ministry of Education, Science and Sport (Slovenia), the Engineering and Physical Sciences Research Council (UK), the Medical Research Council (UK), the Leverhulme Trust (UK), and INTAS, and the British Council.

References

[1] S. Akselrod, D. Gordon, F.A. Ubel, D.C. Shannon, A.C. Barger, R.J. Cohen, Science 213 (1981) 220.
[2] A. Babloyantz, A. Destexhe, Biol. Cybernet 58 (1988) 203.
[3] C.S. Poon, C.K. Merrill, Nature 389 (1997) 492.
[4] M. Bračič, A. Stefanovska, Bull. Math. Biol. 60 (1998) 919.
[5] M. Bračič, P.V.E. McClintock, A. Stefanovska, Characteristic frequencies of the human blood distribution system, in: D.S. Broomhead, E.A. Luchinskaya, P.V.E. McClintock, T. Mullin (Eds.), Stochastic and Chaotic Dynamics in the Lakes, American Institute of Physics, Melville, New York, 2000, pp. 146–153.
[6] M. Bračič-Lotrič, A. Stefanovska, D. Štajer, V. Urbančič-Rovan, Physiol. Meas. 21 (2000) 441–457.
[7] M. Hožič, A. Stefanovska, Physica A 280 (2000) 587.
[8] P.C. Ivanov, M.G. Rosenblum, C.K. Peng, J.E. Mietus, H.E. Stanley, A.L. Goldberger, Physica A 249 (1998) 587.
[9] L.A.N. Amaral, A.L. Goldberger, P.C. Ivanov, H.E. Stanley, Phys. Rev. Lett. 81 (1998) 2388.
[10] S. Havlin, S.V. Buldyrev, A.L. Goldberger, P.C. Ivanov, C.K. Peng, H.E. Stanley, Physica A 273 (1999) 46.
[11] S. Havlin, L.A.N. Amaral, Y. Ashkenazy, A.L. Goldberger, P.C. Ivanov, C.K. Peng, H.E. Stanley, Physica A 274 (1999) 274.
[12] Y. Ashkenazy, P.C. Ivanov, S. Havlin, C.K. Peng, A.L. Goldberger, H.E. Stanley, Phys. Rev. Lett. 86 (2001) 1900.
[13] P. Bernaola-Galván, P.C. Ivanov, L.A.N. Amaral, H.E. Stanley, Phys. Rev. Lett. 87 (2001) 168105.
[14] M. Bračič, A. Stefanovska, Bull. Math. Biol. 60 (1998) 417.
[15] P.C. Ivanov, L.A.N. Amaral, A.L. Goldberger, S. Havlin, M.G. Rosenblum, Z.R. Struzik, H.E. Stanley, Nature 399 (1999) 461.
[16] L.A.N. Amaral, P.C. Ivanov, N. Aoyagi, I. Hidaka, S. Tomono, A.L. Goldberger, H.E. Stanley, Y. Yamamoto, Phys. Rev. Lett. 86 (2001) 6026.
[17] A. Stefanovska, P. Krošelj, Open Systems Inform. Dyn. 4 (1997) 457.
[18] M. Kobayashi, T. Musha, IEEE Trans. Biomed. Eng. 29 (1982) 456.
[19] C.K. Peng, J. Mietus, J.M. Hausdorff, S. Havlin, H.E. Stanley, A.R. Goldberger, Phys. Rev. Lett. 70 (1993) 1343.
[20] P.C. Ivanov, L.A.N. Amaral, A.L. Goldberger, S. Havlin, M.G. Rosenblum, H.E. Stanley, Z.R. Struzik, Chaos 11 (2001) 641.
[21] C. Schäfer, M.G. Rosenblum, J. Kurths, Nature 392 (1998) 239.
[22] A. Stefanovska, H. Haken, P.V.E. McClintock, M. Hožič, F. Bajrović, S. Ribarič, Phys. Rev. Lett. 85 (2000) 4831.
[23] A. Stefanovska, M. Hožič, Prog. of Theor. Phys. (Suppl.) 139 (2000) 270.
[24] M. Bračič Lotrič, A. Stefanovska, Physica A 283 (2000) 451.
[25] N.B. Janson, A.G. Balanov, V.S. Anishchenko, P.V.E. McClintock, Phys. Rev. Lett. 86 (2001) 1749.
[26] P.C. Ivanov, L.A.N. Amaral, A.L. Goldberger, H.E. Stanley, Europhys. Lett. 43 (1998) 363.

[27] A. Stefanovska, M. Bračič, Contemporary Phys. 40 (1999) 31.
[28] P.C. Johnson, News Physiol. Sci. 6 (1991) 41.
[29] S. Bertuglia, A. Colantuoni, M. Intaglietta, Microcirc. Res. 48 (1994) 68.
[30] H.D. Kvernmo, A. Stefanovska, M. Bračič, K.A. Kirkebøen, K. Kvernebo, Microvasc. Res. 56 (1998) 173.
[31] J. Karstrup, J. Bühlow, N.A. Lassen, Int. J. Microcirc.: Clin. Exp. 8 (1989) 205.
[32] T. Söderström, A. Stefanovska, M. Veber, H. Svenson, Am. J. Physiol., in press.
[33] H.D. Kvernmo, A. Stefanovska, K.A. Kirkebøen, K. Kvernebo, Microvasc. Res. 57 (1999) 298.
[34] A. Stefanovska, M. Bračič, H.D. Kvernmo, IEEE Trans. Biomed. Eng. 46 (1999) 1230.
[35] P. Tass, M.G. Rosenblum, J. Weule, J. Kurths, A.S. Pikovsky, J. Volkmann, A. Schnitzler, H.-J. Freund, Phys. Rev. Lett. 81 (1998) 3291.
[36] N.B. Janson, A.G. Balanov, V.S. Anishchenko, P.V.E. McClintock, Phys. Rev. E 65 (2002) 036211 and 036212.
[37] J. Jamšek, A. Stefanovska, Bispectral analysis of cardiovascular oscillations, Phys. Rev. E., submitted for publication.
[38] A. Stefanovska, M. Bračič Lotrič, S. Strle, H. Haken, Physiol. Meas. 22 (2001) 535.
[39] A. Stefanovska, D.G. Luchinsky, P.V.E. McClintock, Physiol. Meas. 22 (2001) 551.

Reversible Transitions between Synchronization States of the Cardiorespiratory System

A. Stefanovska,[1] H. Haken,[2] P. V. E. McClintock,[3] M. Hožič,[1] F. Bajrović,[4] and S. Ribarič[4]

[1]*Group of Nonlinear Dynamics and Synergetics, Faculty of Electrical Engineering, University of Ljubljana, Tržaška 25, 1000 Ljubljana, Slovenia*

[2]*Center of Synergetics, Institute of Theoretical Physics 1, University of Stuttgart, Pfaffenwaldring 57, 70550 Stuttgart, Germany*

[3]*Department of Physics, University of Lancaster, Lancaster LA1 4YB, United Kingdom*

[4]*Institute of Pathophysiology, Faculty of Medicine, University of Ljubljana, Zaloška 4, 1000 Ljubljana, Slovenia*

(Received 30 June 2000)

Phase synchronization between cardiac and respiratory oscillations is investigated during anesthesia in rats. Synchrograms and time evolution of synchronization indices are used to show that the system passes reversibly through a sequence of different phase-synchronized states as the anesthesia level changes, indicating that it can undergo phase transitionlike phenomena. It appears that the synchronization state may be used to characterize the depth of anesthesia.

PACS numbers: 87.19.Hh, 05.45.Tp, 05.45.Xt, 87.19.Uv

Whenever two or more oscillatory processes are weakly coupled, there exists the possibility of their becoming synchronized. It is a scenario that is ubiquitous in nature, including living systems where rhythmic processes take place on widely differing time scales, ranging from milliseconds for single cell activity up to years for ecological changes.

Living systems are becoming increasingly accessible to mathematical modeling using the methods of dynamical systems theory. However, they are inherently nonstationary, being characterized by many oscillatory processes whose frequencies also change in time. The fact that they are quasiperiodic (with several characteristic frequencies) and nonstationary makes them difficult to study since, strictly, most of the methods for linear and nonlinear time series analysis require stationarity. The recently proposed concept of phase-synchronization analysis of noisy nonstationary bivariate data [1,2] provides a promising method for reconstructing their dynamics.

In this Letter we use the concept of synchronization to analyze interactions between cardiac and respiratory oscillations during general anesthesia in rats. Under resting conditions, the cardiovascular-respiratory system has been shown to be characterized by oscillatory processes on multiple time scales in both humans [3] and rats [4]. It has long been recognized that heart and respiratory activity interact, leading, e.g., to frequency modulation of the heart rate by respiration, known as respiratory arrhythmia [5]. The adjustment of the rhythms of the two oscillators may be expected to give rise to synchronization.

Early studies of the dynamics of coordinated activity between the respiratory and cardiovascular systems [6,7] assumed they behaved as almost periodic oscillators. Histograms of ratios of their periods were analyzed and, for example, an n:1 synchronization between the cardiac and respiratory rhythms was found in healthy subjects during sleep [7]. Entrainment was also found to occur in anesthetized rabbits [6] and humans [8]. It was proposed that synchronization (or, as named, frequency and phase coordination) establishes a system of economical coaction and thus favors the functional economy of the organism [7]. In another study, however, only weak coupling between cardiac and respiratory rhythms was found and it was concluded that the two rhythms are generally not phase locked [9].

The development of nonlinear methods has brought new attention to this problem [10]. Recently, using the concept of synchronization analysis in chaotic, noisy, and nonstationary oscillators, episodes of phase synchronization between cardiac and respiratory oscillations were observed in resting humans [11]. Cardiorespiratory synchronization during paced respiration [12] and heart synchronization to external stimuli [13] were also demonstrated. It appears that the degree of synchronization at rest differs in athletes (synchronization periods $\sim$1000 s [11]) and nonathletes ($\sim$100 s [14]), and is inversely related to the extent of frequency modulation of the heart rate. Therefore, we may expect that a better understanding of phase and frequency relations among the oscillatory processes involved in blood circulation may lead to deeper insight into the state of the system, with corresponding diagnostic possibilities.

Here we investigate phase synchronization during the state of anesthesia in rats, which in practice can be studied under more precisely controlled conditions than are usually possible for humans. It has been shown that the dynamics of the cardiovascular-respiratory system in rats [4] possesses similar features to those observed in humans, despite the cardiac and respiratory rhythms in rats being approximately 4 times faster than in humans. Moreover, during anesthesia in rats, respiration need not be assisted. This is an important point, as paced respiration has already been shown to influence the state of cardiorespiratory synchronization [12].

The electric activity of the heart (EKG) and excursions of the thorax, which are proportional to respiratory activity [15], were noninvasively recorded (Fig. 1) while the breathing remained spontaneous and unassisted. Using a 16 bit A/D converter, each time series was digitized at

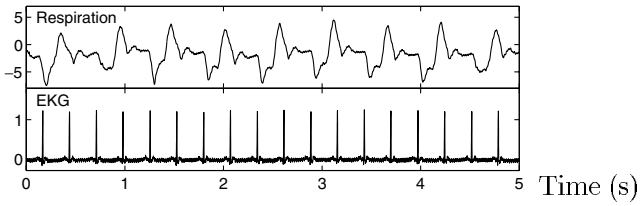

FIG. 1. Extracts from typical respiratory and EKG signals recorded from a rat in anesthesia. The y axes are in arbitrary units.

a sampling rate of 2000 Hz and recorded over the entire duration of anesthesia (~120 min). Recording started 5–10 min after anesthetic drugs [16] were injected and ended 5–10 min after the first signs of recovered reflex responses, detected by a skin pinch test [17], were observed. Five rats were recorded in the same way. On each animal the recording was repeated after one week, using the same anesthetics and concentrations. The synchronization analysis presented below revealed the same pattern in all animals and was well reproduced in the second recording in each case.

The instantaneous cardiac, f_h, and respiratory, f_r, frequencies and their ratio were first calculated. To calculate the instantaneous frequency the marker events method was used. The times of R peaks in the EKG signal and maxima of inspiration were taken as markers. Peaks were detected automatically and also manually checked. One oscillatory cycle was determined as the interval between two consecutive peaks in each time series, at times t_k and t_{k+1}. The instantaneous frequency was taken to be $f(t) = \frac{1}{t_{k+1}-t_k}$, and set constant within one cycle. In this paper, we use the same method to calculate the relative cyclic phase.

Both frequencies were found to undergo dramatic changes during the anesthesia (Fig. 2). During the first ~25 min, f_h decreases from 4 to 3.2 Hz; it then increases and decreases again and, after ~70 min, varies randomly between 3.5 and 4.5 Hz. The f_r slowly decreases from 2 to ~0.8 Hz until at ~40 min, it begins to increase again; it returns to its initial value of 2 Hz at ~70 min, at which point it becomes highly variable, between 1 and 4 Hz. Consequently, f_h/f_r first increases, from 2 to 5, then decreases back to 2 (top graph in Fig. 3), and as the effect of the anesthetic drugs vanishes it becomes highly variable, spanning a wide amplitude range, between 1 and 4.

The instantaneous cyclic relative phase between cardiac and respiratory activity was then calculated. This quantity has been discussed in several recent papers [1,2,11,18] but, briefly, the underlying idea is as follows. Classically, synchronization of two periodic nonidentical oscillators is understood as an adjustment of their rhythms, or locking (entrainment) of their phases, $\varphi_{n,m} = n\phi_1 - m\phi_2 =$ const, where ϕ_1 and ϕ_2 are phases (here defined on the whole real line and not on the circle $[0, 2\pi]$), n and m are integers, and $\varphi_{n,m}$ is the generalized phase difference, or relative phase. In this simplest case, the condition for phase locking is equivalent to the notion of frequency

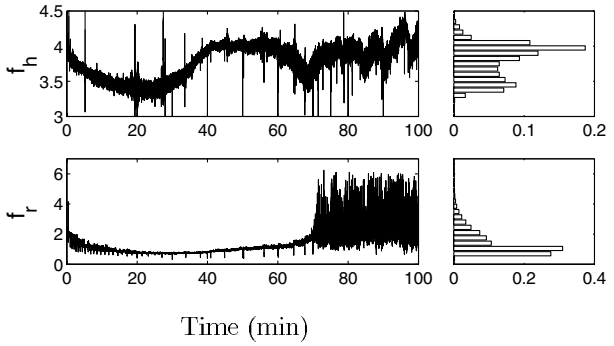

FIG. 2. Evolution of the instantaneous cardiac and respiratory frequencies during the period of anesthesia. The right-hand column shows the corresponding distributions.

locking $nf_1 = mf_2$, where $f_{1,2} = \langle \dot{\phi}_{1,2} \rangle$ and the brackets mean time averaging. If n periods of the first oscillator have exactly the same duration as m periods of the second one, the rhythms are n:m entrained.

Recently, the concept of synchronization was generalized to chaotic systems [19] and synchronizationlike

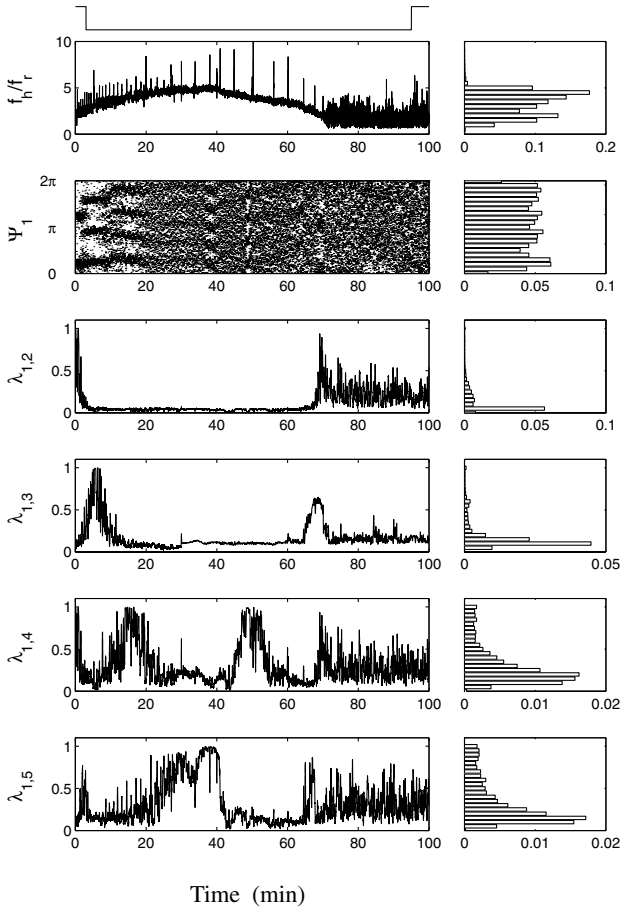

FIG. 3. Evolution of phase-synchronization measures during anesthesia. Top to bottom: frequency ratio, cardiorespiratory synchrogram, and 1:2, 1:3, 1:4 and 1:5 synchronization indices, respectively. Occurrence of 1:n synchronization is demonstrated both by the appearance of n plateaus in Ψ_1 and by $\lambda_{1,n}$ approaching unity. The reflex responsiveness from the skin pinch test [17] is given at the top.

phenomena have also been reported in purely stochastic systems, where the noise controls a characteristic time scale [20]. For noisy, chaotic systems and/or systems with modulated natural frequencies a weaker condition of phase synchronization, $|\varphi_{n,m}| = |n\phi_1 - m\phi_2 - \delta| < \text{const}$, where δ is some (average) phase shift, was introduced [1,2]. Accordingly, synchronization is understood as the appearance of peaks in the distribution of cyclic relative phase $\Psi_{n,m} = \varphi_{n,m} \bmod 2\pi$ and interpreted as the existence of a preferred stable value of phase difference between two oscillators. In such a case, the n:m phase locking is manifested as a time variation of $\Psi_{n,m}$ around a horizontal plateau.

In analyzing synchronization, the integers n and m should both be determined. In the case of two interacting noisy oscillatory processes, n and m change in time. One possibility (similar to an earlier proposed method of entrainment analysis [6]), known as the phase stroboscope, or synchrogram, is to fix the value of m and observe changes of n in time [11]. Accordingly, the cardiorespiratory synchrogram is constructed by plotting the normalized relative phase of a heartbeat within m respiratory cycles, $\Psi_m = \frac{1}{2\pi}(\phi_r(t_k) \bmod 2\pi m)$, where t_k is the time of kth heartbeat and ϕ_r is the instantaneous phase of respiration.

Here we focus on phase synchronization for $m = 1$ since, for most of the time, an integer value of the instantaneous frequency ratio was observed. We calculated the normalized relative phase, Ψ_1, directly from the measured data, exploiting the fact that both signals contain sharp peaks that clearly mark the instantaneous cycles (see Fig. 1). Each successive peak was marked as an equivalence of one oscillatory cycle, corresponding to which a 2π increment was added. The instantaneous phase is then

$$\phi(t) = 2\pi \frac{t - t_k}{t_{k+1} - t_k} + 2\pi k, \qquad t_k \le t < t_{k+1}, \quad (1)$$

where t_k is time of kth marker event. Defined in this way the phase is a monotonically increasing piecewise-linear function of time defined on the real line.

Usually, the first step in searching an n:m locking is to look for horizontal plateaus in Ψ_1, revealing the value of n in cases when synchronization exists. The distribution of $\Psi_{n,m}(t)$ is then a δ function, smeared in the presence of noise. For strongly nonlinear oscillators it can be nonuniform even in the absence of noise [2]. To characterize the strength of synchronization we therefore need a robust quantitative measure. Since in noisy systems phase synchronization can be understood in a statistical sense as the existence of preferred values of generalized phase difference, measures based on quantifying the distribution of phases

$$\eta = \phi_2 \bmod 2\pi n|_{\phi_1 \bmod 2\pi m = \theta} \quad (2)$$

were proposed. We will use an index based on conditional probability which was introduced in [18] and was shown to facilitate reliable detection of synchronous epochs of different order n:m [21]. Accordingly, the phase of the second oscillator is observed at fixed values of the phase of the first oscillator, θ. The interval of each phase ϕ_1 and ϕ_2, $[0, 2\pi m]$ and $[0, 2\pi n]$, respectively, is divided into N bins. The values of $\phi_1 \bmod 2\pi m$ that belong to bin l are denoted as θ_l, while the number of points inside this bin is denoted as M_l, and, by using Eq. (2), M_l values of $\eta_{j,l}$, $j = 1, \ldots, M_l$, are calculated.

If there is no synchronization between the oscillators, a uniform distribution of $\eta_{j,l}$ can be expected on the interval $[0, 2\pi n]$, or else it clusters around a certain value resulting in a unimodal distribution. Hence, the distribution is quantified as $r_l(t_k) = \frac{1}{M_l(t_k)} \sum_{i=1}^{M_l(t_k)} e^{i\phi_2(t_j)}$ for each j when $\phi_1(t_j)$ belongs to the lth bin and $t_k - t_p/2 \le t_j < t_k + t_p/2$. $M_l(t_k)$ is the number of points in this bin at the kth instant. An average over 10 periods, t_p, of the slower oscillator was used [18]. Where the phases are completely locked, or completely unlocked we obtain $|r_l(t_k)| = 1$ or $|r_l(t_k)| = 0$, respectively.

To improve reliability, we also calculate the average over all bins and obtain the index of synchronization $\lambda_{n,m}(t_k) = \frac{1}{N} \sum_{l=1}^{N} |r_l(t_k)|$. Accordingly, $\lambda_{n,m}$ is a measure of the conditional probability that ϕ_2 has a certain value within lth bin when ϕ_1 belongs to this bin.

Some typical results are shown in Fig. 3. The synchrogram, $\Psi_1(t)$, indicates immediately that several phase-synchronization states occur during anesthesia. This is confirmed by time evolutions of the synchronization indices, $\lambda_{1,n}$, which were obtained using a sliding window with $t_p = 8$ s. Three distinct stages during anesthesia may be distinguished from the evolutions of f_h/f_r, Ψ_1, $\lambda_{1,2}$, $\lambda_{1,3}$, $\lambda_{1,4}$, and $\lambda_{1,5}$. Stage 1, 0–40 min from the start of recording, may be defined as the interval during which the frequency ratio increases. Stage 2 of the recording (40–70 min) is where the frequency ratio decreases again. Stage 3 consists of the interval (70–100 min) in which the frequency ratio is hugely variable around a steady value. These same three stages were observed in all recordings, which lasted between 70 and 130 min (until the rat started to run freely).

During stage 1 all four states of synchronization, 1:2, 1:3, 1:4, and 1:5, are clearly present and gradually switch one into the other. The 1:2 phase-locked state seems to be observed for as long as a reflex response (tested by skin pinch test [17]) can still be obtained (depicted at the top of the figure). Approximately at the time when the reflex disappears, the transition to 1:3 phase locking starts, which then changes into 1:4 locking, followed by 1:5 locking. One possible explanation is that nerve conductivity decreases during this initial state of anesthesia, and this causes changes of the overall nervous control of the cardiorespiratory system, which then results in a series of phase-synchronized states.

As the effect of the drugs starts to decline, the phase-synchronization states switch back in reverse order. The strength of phase synchronization is slightly weaker on the way out of anesthesia than during entry. Shortly before the

end of anesthesia (stage 3), phase synchronization becomes very weak.

In conclusion, we have shown that the cardiac and respiratory systems possess dynamical properties and couplings that can synchronize their oscillations in a hierarchy of different phase-locked states. Kinetic phase transition phenomena between these states are reminiscent of those seen and analyzed in detail for physical systems such as lasers [22]. During the course of anesthesia, the transitions are found to occur in a reproducible sequence, suggesting that the state of synchronization may provide a potentially useful measure of the depth of anesthesia at any moment. Given the similarities in cardiorespiratory dynamics, in f_h/f_r, and in other characteristic frequency ratios for humans and rats [3,4], it seems plausible that similar results may also apply to humans.

This study was supported by the Slovenian Ministry of Science and Technology, and the Slovenian-German Scientific-Research Project Collaboration. A. S. was partially supported by the Royal Society of London. We thank P. A. Tass for valuable comments on the manuscript.

[1] A. S. Pikovsky, M. G. Rosenblum, and J. Kurths, Europhys. Lett. **34**, 165 (1996); M. G. Rosenblum, A. S. Pikovsky, and J. Kurths, Phys. Rev. Lett. **76**, 1804 (1996); M. G. Rosenblum, A. S. Pikovsky, and J. Kurths, *ibid.* **78**, 4193 (1997); A. S. Pikovsky, M. G. Rosenblum, G. V. Osipov, and J. Kurths, Physica (Amsterdam) **104D**, 219 (1997).

[2] M. G. Rosenblum, A. S. Pikovsky, C. Schäfer, P. Tass, and J. Kurths, in *Handbook of Biological Physics,* edited by S. Gielen and F. Moss [Elsevier Science, New York (to be published)].

[3] P. Ch. Ivanov, L. A. N. Amaral, A. L. Goldberger, S. Havlin, M. G. Rosenblum, Z. Struzik, and H. E. Stanley, Nature (London) **399**, 461 (1999); A. Stefanovska and M. Bračič, Contemp. Phys. **40**, 31 (1999); M. Bračič, P. V. E. McClintock, and A. Stefanovska, in *Stochastic and Chaotic Dynamics in the Lakes,* edited by D. S. Broomhead, E. A. Luchinskaya, P. V. E. McClintock, and T. Mullin (AIP, New York, 2000), pp. 146–153.

[4] F. Bajrović, M. Čenčur, M. Hožič, S. Ribarič, and A. Stefanovska, Eur. J. Phys. **439**, R158 (2000).

[5] S. Hales, *Statistical Essays II, Haemastatisticks* (Innings Manby, London, 1773); C. Ludwig, Arch. Anat. Phys. **13**, 242 (1847); C. T. M. Davies and J. M. M. Neilson, J. Appl. Phys. **22**, 947 (1967); J. A. Hirsch and B. Bishop, Am. J. Phys. **241**, H620 (1981).

[6] H. Passenhofer and T. Kenner, Pflügers Archiv. **355**, 77 (1975); T. Kenner, H. Passenhofer, and G. Schwaberger, *ibid.* **363**, 263 (1976).

[7] G. Hildebrandt, in *Temporal Disorder in Human Oscillatory System,* edited by L. Rensing, U. an der Heiden, and M. C. Mackey (Springer, Berlin, 1987), pp. 160–174; F. Raschke, *ibid.,* pp. 152–158; F. Raschke, in *Rhythms in Physiological Systems,* edited by H. Haken and H. P. Koepchen (Springer, Berlin, 1991), pp. 155–164.

[8] D. C. Galletly and P. D. Larsen, Br. J. Anaesth. **79**, 35 (1997).

[9] M. C. Mackey and L. Glass, *From Clocks to Chaos: The Rhythms of Life* (Princeton University, Princeton, NJ, 1988).

[10] D. Hoyer, O. Hader, and U. Zwiener, IEEE Eng. Med. Biol. **16**, 97 (1997); M. Schiek, F. R. Drepper, R. Engbert, H.-H. Abel, and K. Suder, in *Nonlinear Analysis of Physiological Data,* edited by H. Kantz, J. Kurths, and G. Mayer-Kress (Springer, Berlin, 1998), pp. 191–209.

[11] C. Schäfer, M. G. Rosenblum, J. Kurths, and H. H. Abel, Nature (London) **293**, 239 (1998); C. Schäfer, M. G. Rosenblum, H. H. Abel, and J. Kurths, Phys. Rev. E **60**, 857 (1999).

[12] H. Seidel and H. P. Herzel, IEEE Eng. Med. Biol. **17**, 54 (1998).

[13] V. S. Anishchenko, A. G. Balanov, N. B. Janson, N. B. Igosheva, and G. V. Bordyugov, in *Stochastic and Chaotic Dynamics in the Lakes,* edited by D. S. Broomhead, E. A. Luchinskaya, P. V. E. McClintock, and T. Mullin (AIP, New York, 2000), pp. 162–167.

[14] M. Bračič Lotrič and A. Stefanovska, Physica (Amsterdam) **283A**, 451 (2000).

[15] A piezoelectric sensor was inserted into a rigid strap which was wrapped around the thorax.

[16] Experiments were performed on adult male Wistar rats under general anesthesia with ketaminhydrochlorid 100 mg/kg b.w. and xylazinhydrochorid 20 mg/kg b.w., administered in a bolus, intraperitoneally. During the recording the animal was placed on a homeothermic operating table that enabled the body temperature to be kept constant at 37 °C.

[17] The depth of anesthesia was assessed at 5-min intervals, starting from the moment at which the drugs were applied, by the animal's response to touch and to painful stimulus with the skin pinch test. The plantar surface of the animal's hind paws was stroked with the tip of a pair of tweezers (touch stimulus) or pinched (pain stimulus). The tests were considered positive if the animal responded by flexing its fingers or withdrawing its limb and were not perturbative to any of the quantities analyzed (see Figs. 2 and 3).

[18] P. Tass, M. G. Rosenblum, J. Weule, J. Kurths, A. S. Pikovsky, J. Volkmann, A. Schnitzler, and H.-J. Freund, Phys. Rev. Lett. **81**, 3291 (1998).

[19] L. M. Pecora and T. L. Carroll, Phys. Rev. Lett. **64**, 821 (1990); L. Kocarev and U. Parlitz, *ibid.* **74**, 5028 (1995); N. F. Rulkov, M. M. Sushchik, L. S. Tsimring, and H. D. I. Abarbanel, Phys. Rev. E **51**, 980 (1995).

[20] A. Neiman, Phys. Rev. E **49**, 3484 (1994); B. Shulgin, A. Neiman, and V. Anishchenko, Phys. Rev. Lett. **75**, 4157 (1995); A. Longtin and D. R. Chialvo, *ibid.* **81**, 4012 (1998).

[21] R. Mrowka, A. Patzak, and M. Rosenblum, Int. J. Bifurcation Chaos Appl. Sci. Eng. (to be published).

[22] H. Haken, *Laser Theory* (Springer, Berlin, 1970); H. Haken, *Synergetics, An Introduction* (Springer, Berlin, 1983).

ELSEVIER

Physica A 280 (2000) 587–601

PHYSICA A

www.elsevier.com/locate/physa

Karhunen–Loève decomposition of peripheral blood flow signal

Mario Hožič[a,*], Aneta Stefanovska[a,b]

[a] *Faculty of Electrical Engineering, University of Ljubljana, Group of Nonlinear Dynamics and Synergetics, Tržaška 25, 1000 Ljubljana, Slovenia*

[b] *Center for Synergetics Pfaffenwaldring, University of Stuttgart, Institute for Theoretical Physics I, 57 IV, D-70550 Stuttgart, Germany*

Received 26 October 1999

Abstract

The Karhunen–Loève expansion is applied to scalar signals and the effect of window length (t_w), time lag (τ) and embedding dimension (d) is analysed for periodic signals and for signals modeled by the Lorenz equations. For $\tau \neq k/2f_i$ (f_i are characteristic frequencies of the signal, k is positive integer), we obtain $2m$ modes from an m-periodic signal. For a large set of parameters a finite number of modes was not obtained from the Lorenz system. It is further shown that, on the time scale of a minute, the peripheral blood flow signal contains oscillatory modes that occur in pairs thereby confirming that the blood flow through the cardiovascular system is oscillatory. Some of the difficulties of applying Karhunen–Loève expansion to scalar signals are pointed out.

PACS: 87.45−k; 05.90.+m; 02.50.Sk; 05.40+j

Keywords: Karhunen–Loève decomposition; Peripheral blood flow; Oscillations

1. Introduction

Cardiovascular control mechanisms manifest themselves through rhythmic activities [1,2] on several scales [3–7]. Analysis of such rhythms may, therefore, provide an essential contribution to the understanding of physical and physiological properties of cardiovascular system. On a time scale of minutes continuous wavelet transformation, using the Morlet mother wavelet which enables good low-frequency resolution, has revealed five characteristic peaks in the blood pressure, blood flow, respiration and

* Corresponding author. Fax: +386-61-1264-630.
E-mail address: mario@osc.fe.uni-lj.si (M. Hožič)

0378-4371/00/$ - see front matter
PII: S0378-4371(00)00070-4

heart-rate variability (HRV) signals [8]. The signals were simultaneously measured at different sites of the human body. Two peaks were located at heart-beat ($\sim$1.0 Hz) and respiratory frequencies ($\sim$0.2 Hz), respectively, resulting from centrally mediated regulation of blood distribution. The other three peaks were typically located around 0.1, 0.04 and 0.01 Hz [8]. They originate from peripheral, spatially distributed subsystems. They are hypothesized to result from the myogenic, neurogenic and endothelial-related regulation of the blood circulation through the cardiovascular system [9].

Both the peripheral and central regulatory processes are reflected in the peripheral blood flow signal, independently of the measurement site [8,10]. The blood flow signal was shown to be highly deterministic [8,11] and to contain paired Lyapunov exponents [12]. From signals analysed on time scales of minutes, either four pairs and one zero exponent, or five pairs, were obtained, pointing to the almost conservative nature of the blood distribution system on this time scale. Using different kinds of data-processing techniques, statistical differences were shown to exist between blood flow signals measured in healthy humans, sportsmen or subjects with various cardiovascular diseases [8,10].

The next challenging problem in the process of reconstructing cardiovascular dynamics is the extraction of parts of the blood flow signal which result from the activity of a particular physiological process involved in the regulation of blood circulation. A knowledge of the dynamics of each of the relevant modes provides a basis for modeling of the underlying system. Such knowledge is also necessary in studying the physiological origin and characteristics of processes involved in cardiovascular control, as well as in clinical studies where different modes are expected to be changed by certain cardiovascular diseases, such as myocardial infarction, diabetes, etc. However, at present it is not possible to obtain directly the time series of each of the processes involved in blood circulation. The reasons are technical and systemic:

(1) No measurement techniques are available for recording the activity of the slower periodic components, the myogenic, neurogenic and metabolic.

(2) All processes are mutually coupled and their activities interfere in all measured signals.

An often used method for signal decomposition is known as principal component analysis (PCA) [13] or Karhunen–Loève expansion (KL) [14,15]. Generally, the KL expansion is applied to analyse the spatio-temporal patterns emerging from complex systems [16–18]. Multi dimensional data, such as EEG or MEG data in physiology, are measured and spatial modes are calculated based on maximizing signal-projections of those modes. The KL decomposition leads to orthogonal spatial and temporal modes and gives a measure for the contribution of each mode to the signal. Modes with a signal-contribution above a certain threshold are considered as relevant, those below the threshold as irrelevant.

The peripheral blood flow signal is obtained from a Doppler shift of laser light directed on the measured area [19]. The technique of blood flow measurement allows for only a few simultaneously measured signals, while for the reconstruction of its spatial dynamics one would need a greater number of signals. In addition, the

cardiovascular system is complex system and the understanding of both its spatial and temporal dynamics at once is difficult. Therefore, at present, we restrict our interest to the temporal characteristics of the blood flow signal. The procedure of decomposition of the blood flow signal thus begins with its embedding in the phase space. Once the signal is appropriately embedded, its KL decomposition is performed in the same way as with multidimensional data.

2. Method

2.1. KL decomposition of a scalar signal

The Karhunen–Loève decomposition of the $d \times w$ matrix $\mathbf{A}$ is given by

$$\mathbf{A} = \mathbf{HV}\,, \tag{1}$$

where $\mathbf{H} \in \Re^{d\times w}$, $\mathbf{V} \in \Re^{w\times w}$ and $\mathbf{V}$ is a matrix of eigenvectors $\mathbf{V}^{\mathrm{T}}\mathbf{V} = \mathbf{I}$.

The idea is to describe a given statistical ensemble with the minimum number of modes. The number of modes equals the number of degrees of freedom. The matrix $\mathbf{A}$ is composed so that the rows of the matrix represent time-dependent signals at a specific place, and the columns represent spatially dependent signals at a specific time (or vice versa). But for a purely temporal (or spatial) signal, the matrix must be composed differently. We use the time-delay embedding method.

Let $x(t_n)$ be the measured signal. The time t_n is discrete and is determined by the sampling frequency $t_n = nt_s = n/f_s$, $n = 1,\ldots,N$, where N is the number of samples in the signal. The scalar time series $x(t_n)$ can be embedded in d-dimension phase space $\mathbf{x}(t_n) = [x(t_n), x(t_n+\tau), \ldots, x(t_n+(d-1)\tau)]$, where the time lag $\tau = Tt_s$. The embedding procedure can also be repeated by choosing windows, w, within the signal, where $w \leqslant N$. In what follows the window length is presented in continuous time, $t_w = wt_s$. The meaning of each of these parameters will be discussed in detail below. For a given window we compose the matrix $\mathbf{A}$

$$\mathbf{A} = \begin{bmatrix} x(t_1) & x(t_2) & \cdots & x(t_w) \\ x(t_1+\tau) & x(t_2+\tau) & \cdots & x(t_w+\tau) \\ \vdots & \vdots & & \vdots \\ x(t_1+(d-1)\tau) & x(t_2+(d-1)\tau) & \cdots & x(t_w+(d-1)\tau) \end{bmatrix}.$$

Then, we compute the correlation matrix

$$\mathbf{C} = \mathbf{A}^{\mathrm{T}}\mathbf{A}\,, \tag{2}$$

its eigenvalues λ_i and eigenvectors $\mathbf{v}_i$

$$\mathbf{C}\mathbf{v}_i = \lambda_i \mathbf{v}_i \tag{3}$$

and sort the eigenvalues by size: $\lambda_1 \geqslant \lambda_2 \geqslant \cdots \geqslant \lambda_d$. At the same time we sort the corresponding eigenvectors. Eigenvalues correspond to the energies of the modes. Since

the modes are determined by maximizing λ (the energy of a mode), the series converges rapidly. This means that it gives rise to an optimal set of basis functions from all possible sets. We calculate the matrix $\mathbf{H}$ from the matrix of eigenvectors

$$\mathbf{H} = \mathbf{A}\mathbf{V}^{\mathrm{T}}\,, \tag{4}$$

where $\mathbf{V}$ is the matrix of vectors $\mathbf{v}_i$. The rows of matrix $\hat{\mathbf{A}}_i$

$$\hat{\mathbf{A}}_i = \mathbf{h}_i\mathbf{v}_i^{\mathrm{T}} \tag{5}$$

represent ith mode of the signal.

If we have $p<d$ dominant eigenvalues, most of the information is included in

$$\hat{\mathbf{A}} = \sum_{i=1}^{p} \mathbf{h}_i\mathbf{v}_i^{\mathrm{T}}\,, \tag{6}$$

where $\mathbf{h}_i$ and $\mathbf{v}_i$ are the columns of matrices $\mathbf{H}$ and $\mathbf{V}$, respectively.

The first orthogonal function, i.e., mode of the KL method, is optimized in such a way that it contains the largest proportion of the kinetic energy of the signal and the successive modes contain decreasing proportions. By choosing a decomposition of this form, the characteristics of a signal associated with the mean kinetic energy can be represented by the fewest possible terms. This is in contrast to a Fourier type decomposition where the orthogonal functions are predetermined and are not necessarily reflective of the signal; therefore many orthogonal functions must be utilized to represent the signal [20].

In summary, the Karhunen–Loève expansion results in a generalized coordinate system defined by the eigenfunctions of the correlation matrix. It is optimized so that:

(1) The mean-square error between the signal and its KL representation is minimized such that, for any fixed p:

$$\left[\mathbf{A} - \sum_{i=1}^{p} \mathbf{h}_i\mathbf{v}_i^{\mathrm{T}}\right]^2 \to \min\,. \tag{7}$$

(2) It has the minimum representation entropy property.

(3) The number of modes needed to describe the signal for a given error may be minimized.

The optimality of KL method allows one to reduce the amount of information about the signal, or process, down to a reasonable number of independent eigenfunctions, which represent important characteristic features of the signal.

2.2. Embedding

The embedding is a transformation from one component of the state vector into a phase space with more dimensions [21]. The space in which a given signal is transformed is the embedding space and its dimension is the embedding dimension. We use the method of delays by which the vector is constructed taking components of scalar signal delayed in time. To construct the input matrix for the KL method one must

choose the appropriate embedding dimension d, window length $t_w = wt_s$ and time lag $\tau = Tt_s$.

It is more common to choose the embedding dimension than to choose the window length [22]. Takens [23] and Mañé [24] showed that the embedding dimension should be $d \geqslant (2m+1)$, where m is the system dimension, i.e., the number of system degrees of freedom. Since we do not know it in advance, we must take d large enough, so that the inequality is valid for the largest estimate of m. However, as we will see below, the window length strongly influences the results. Once the window length is fixed, the embedding dimension can be determined such that the whole signal is covered. The window length can also be determined by the length of the reconstructed signal. A short window does not give enough information, whereas the longer the window the more information we obtain. Therefore, the number of significant eigenvalues grows. When $t_w \to \infty$ the method becomes discrete Fourier transformation [22]. Obviously, some criteria must be met when choosing window length t_w.

When time lag τ is too small, all vector components obtained by embedding are nearly equal and consequently strongly correlated, which means that successive modes have monotonically distributed energies. The role of noise becomes dominant. If τ is too long, the vector components become spaced wide apart and thus statistically highly independent. The vectors are displaced in phase space, resulting again in higher dimension.

3. Applications to simulated data sets

To illustrate the role of each of the parameters we now present an analysis of simulated signals. First, we analyse periodic and quasi-periodic signals, for two basic reasons:

(1) For periodic signals the choice of the embedding parameters is straightforward, and

(2) Their time and frequency domain characteristics resemble the characteristics of a measured blood flow signal.

Then, we apply KL decomposition to signals obtained from the Lorenz equations.

3.1. Periodic signals

A simple sine signal, sampled at $t_s = 0.01$ s, has a period $t_p = 1$ s and lasts $t_{\mathrm{obs}} = 50$ s (Fig. 1 top). The window length was chosen to observe at least one period of the oscillations, that is $t_w = 5$ s ($500t_s$). Results obtained at two time lags, $\tau = 0.1$ s and $\tau = 0.5$ s, are presented in Fig. 1.

By decomposition of a sine signal one expects to obtain one mode only. However, as shown in Fig. 1(a), at $\tau = 0.1$ s two modes are obtained. This can be attributed to the embedding procedure. The embedding of a sine is two-dimensional, and the

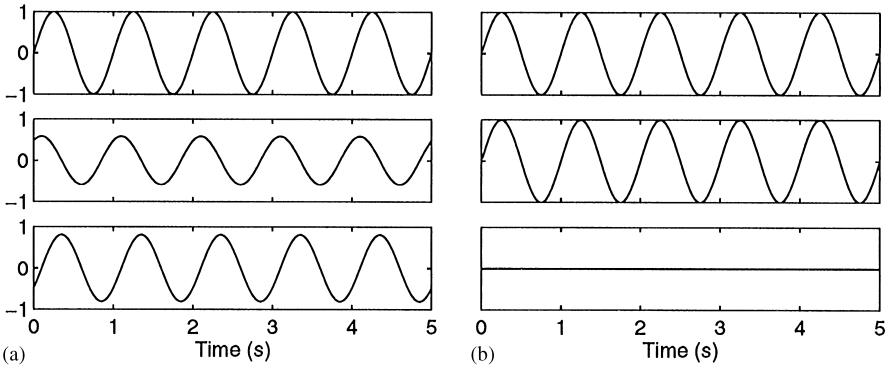

Fig. 1. On top the original sine signal with period $t_p = 1$ s, underneath the first and the second mode at (a) $\tau = 0.1$ s, and (b) $\tau = 0.5$ s; all other modes are equal to zero.

decomposition therefore results in two modes. The rows of the input matrix $\mathbf{A}$ are sines, successively translated by $\frac{1}{10}$ of a period and are not co-dependent. The matrix of a mode $\hat{\mathbf{A}}_i$ has rank 1, meaning that rows in this matrix are co-dependent. Hence, they have the same and reverse phase (translated by π) respectively. Therefore, two phase-shifted modes are necessary to describe a sine.

Fig. 1(b) shows only one mode as a result. For this example the time lag that equals a multiplier of the half period, $\tau = k/2t_p$, where k is positive integer, is chosen. In this case the input matrix $\mathbf{A}$ also has rows that are co-dependent – with the same and reverse phase. Consequently, only one mode is obtained.

3.2. Quasi-periodic signals

The same effect may be obtained for any m-periodic signal. For $\tau \neq k/2f_i$ (f_i are characteristic frequencies of the signal), $2m$ modes are obtained. Here, we face the problem of achieving an appropriate embedding of a scalar signal. For a m-periodic signal, with an incommensurate ratio of the characteristic frequencies, there will always be some frequency f_i for which $\tau \neq k/2f_i$. Therefore, the strengths of each of the two modes that result from a single period of the signal can not be unambiguously determined.

The eigenvalue of each of the modes depends on the value of τ chosen. The normalized eigenvalues σ_i [25]

$$\sigma_i = \lambda_i \Big/ \sum_{k=1}^{d} \lambda_k \,, \tag{8}$$

obtained at different τ for a sum of sine functions

$$x(t) = \sum_{i=1}^{5} \frac{1}{f_i} \sin(2\pi f_i t) \,, \tag{9}$$

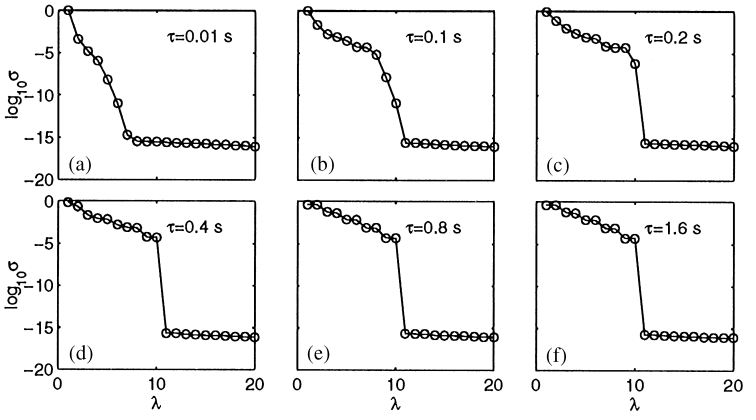

Fig. 2. Normalized eigenvalues obtained from (9) at $t_w = 80$ s, $d = 100$ and different τ. Small τ results in underestimation of the number of interacting modes (a). For τ around the value of the minimal repetition time in the quasi-periodic signal, $\tau \geqslant t_{min}/10$, a constant number of interacting mode is obtained (b)–(f).

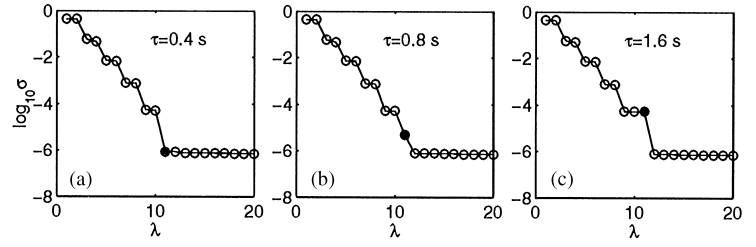

Fig. 3. (a–c) Normalized eigenvalues obtained from (9), at $t_w = 80$ s and $d = 100$. An uniformly distributed noise is added, with amplitude which is 30% of the maximal amplitude in (9). As a result of noise an extra mode is obtained and its normalized eigenvalue increases at large time delay.

where the frequencies f_i are 0.0123, 0.0349, 0.0951, 0.2943 and 1.1193 Hz, are presented in Fig. 2. Too small embedding time, compared to the repetition time of the fastest oscillation, underestimates both the eigenvalues of most of the modes as well as the number of modes involved (Fig. 2(a)). As the embedding time increases, the number of relevant modes is unambiguously determined, however the eigenvalues of each of them vary for different τ (Fig. 2(b)–(f)). If we further increase the embedding time, i.e., $\tau > t_{\min}$ (where $t_{\min}$ is the minimal repetition time in the quasi-periodic signal; in (9) taken as 0.84 s), the estimated number of interacting modes remains constant.

However, at large embedding time the noise structures may become dominant. In Fig. 3 eigenvalues obtained at large τ, from (8) with 30% of uniform noise added, are presented. As τ increases over one half of the $t_{\min}$ a new mode is obtained. There is another effect of the added noise. The normalized eigenvalues for non-relevant modes increase, so that the distinction between relevant and non-relevant modes is no longer sharp.

The value of embedding time is thus crucial for an appropriate estimation of the number of interacting modes. It should be expected to fall in a narrow window determined

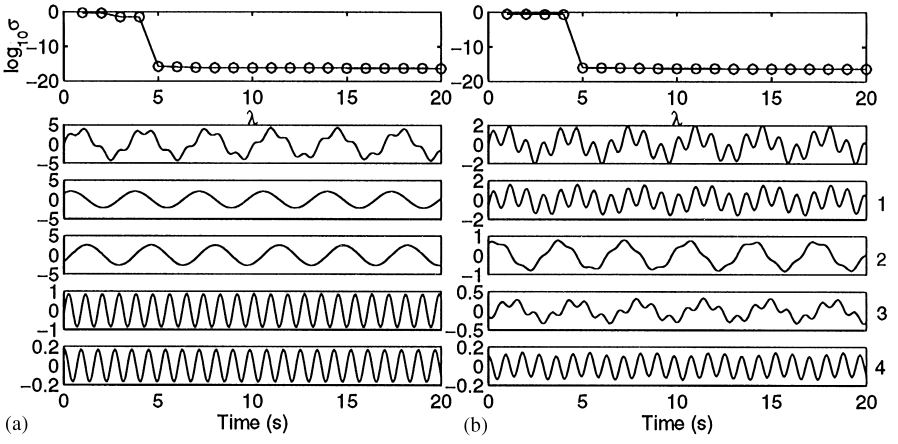

Fig. 4. The first 20 eigenvalues (top), the sum of two sine signals (2nd row) with $f_1 = 0.2943$ Hz and $f_2 = 1.1193$ Hz, (a) $A_1 = 1/f_1$; $A_2 = 1/f_2$ and (b) $A_1 = A_2 = 1$ and the first four modes obtained at $\tau = 0.4$ s, $t_w = 20$ s and $d = 100$. In each case, in the interests of clarity only 20 s are illustrated.

by the dynamics inherent in the signal. However, even for a simple quasi-periodic signals the reconstructed modes do not necessarily resemble the original components. Fig. 4 presents first four modes calculated for a sum of two sines with (a) different and (b) the same amplitudes. At different amplitudes, with both sines contributing the same energy, all components are reconstructed correctly, while sines originally with the same amplitudes become modulated after the reconstruction.

3.3. Lorenz equations

The next example deals with data obtained from the Lorenz system

$$\begin{aligned} \dot{x} &= a(x - y)\,, \\ \dot{y} &= cx - y - xz\,, \\ \dot{z} &= -bz + xy\,, \end{aligned} \tag{10}$$

with $a = 10$, $b = 8/3$, $c = 28$, $x(0) = y(0) = z(0) = 1$. The equations were integrated using the fourth-order Runge–Kutta method. The solutions were recorded at time intervals of 0.003 s with double precision.

At the chosen parameter values the system undergoes turbulent dynamics. The time evolution is organized by two unstable foci and an intervening saddle point. Using the Karhunen–Loève decomposition and the embedding procedure, Broomhead and King [22] and Mees et al. [25] have analysed data obtained from the Lorenz model, under their conditions.

In performing the subsequent calculations, we followed the Broomhead–King protocol, which was also repeated by Mees et al. [25]. Varying the embedding time

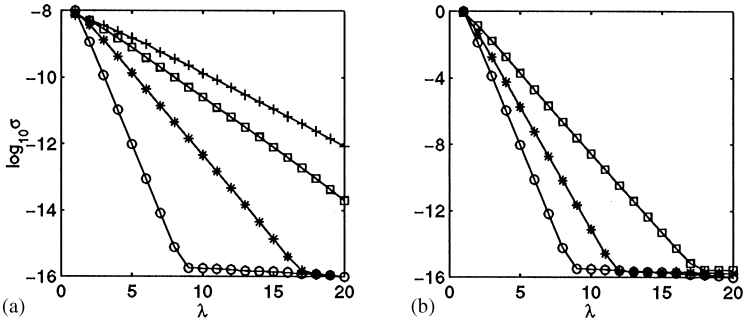

Fig. 5. Normalized eigenvalues for data generated by the Lorenz equations. The window length is $t_w = 12$ s in each case. (a) The embedding time τ is varied, 0.003, 0.012, 0.024 and 0.036 s from the bottom to the top, and the embedding dimension is fixed, $d = 25$. (b) The embedding time is fixed, $\tau = 0.003$ s and the embedding dimension is varied, 25, 50 and 100 from the bottom to the top.

and the embedding dimension at the same time, they repeated the calculations of normalized eigenvalues. Using single precision, Broomhead and King obtained four relevant modes, before arriving at what they term "the horizontal noise floor". Mees et al. [25] showed that this finite value resulted from the small precision used. Increasing the precision of the step of integration of the differential equation, they obtained an increase in the corresponding number of relevant modes.

We performed two sets of numerical experiments. Firstly, we analysed the effect of embedding time, at a constant embedding dimension (Fig. 5(a)). Secondly, at a fixed embedding time we repeated the calculations by varying the embedding dimension (Fig. 5(b)). In both sets of experiments, no constant number of relevant modes can be detected. The number of modes differs for different embedding times and embedding dimensions. It is therefore clear that, using the KL method and the time-delay embedding procedure, a turbulent flow in the Lorenz system cannot be decomposed into a finite number of modes. We infer that the results apply more generally.

4. Blood flow signal

Let us now see how much information we can extract from a real signal, namely the signal of peripheral blood flow, using the KL method. It was measured with a laser Doppler flowmeter (Perimed, Sweden) [19] for $t_{\mathrm{obs}} = 650$ s, sampled with $f_s = 200$ Hz and then resampled to $f_s = 40$ Hz using a moving average. This was the only preprocessing before KL was applied. The blood flow signal in the time domain and the phase plane, its autocorrelation function and power spectrum are presented in Fig. 6. The autocorrelation function reveals several periodic components and does not vanish in time (Fig. 6(c) and (d)). The time averaged power spectrum, calculated using the Morlet mother wavelet [10], in the frequency interval from 0.0095 to 2 Hz contains five characteristic frequencies. A number of processes are involved in the regulation

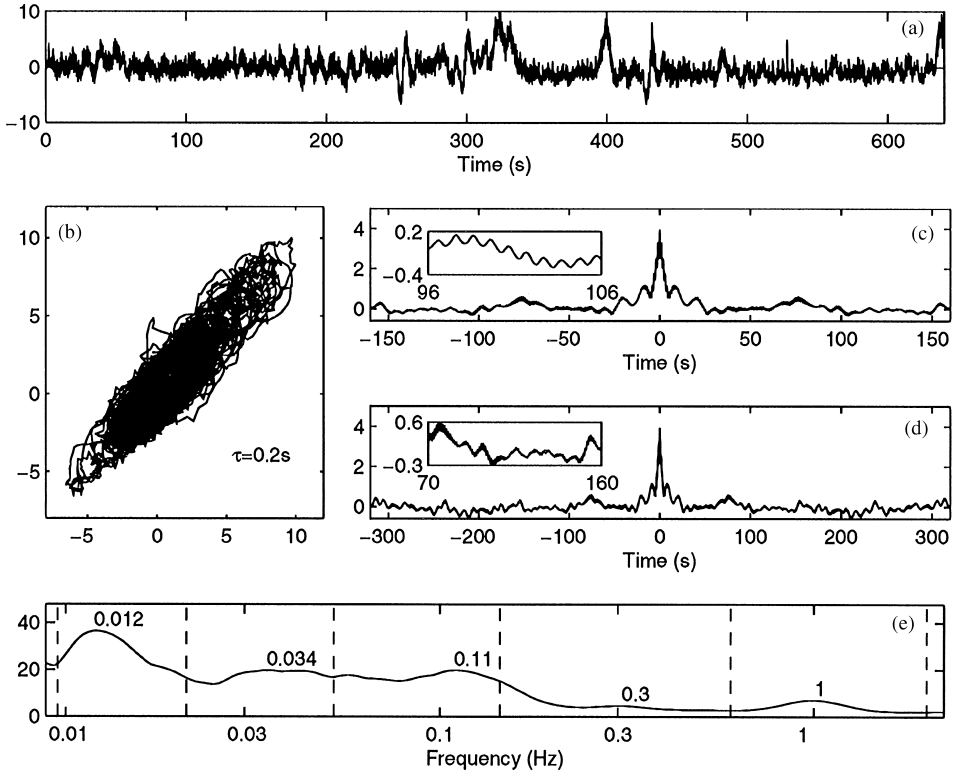

Fig. 6. The blood flow signal of a healthy subject in (a) the time domain and (b) the phase plane. The phase plane was reconstructed using the embedding time $\tau=0.2$ s. The autocorrelation function was obtained by use of a window t_w (c) 160 s and (d) 320 s in length taken from the middle of the signal and translated forward and backward along the whole signal. The power spectrum (e) was estimated by wavelet transformation using the Morlet wavelet.

of peripheral blood flow and their characteristic frequencies vary in time and their corresponding peaks are widened.

For the blood flow signal we need long window so that a relatively large amount of information can be observed. Then we need to determine a value of τ, such that we can capture all modes of the signal.

The window length is determined by the slowest period of oscillations in the blood flow. Because we are interested in the dynamics of one cycle of blood through the cardiovascular system, window lengths that reliably exceed the average circulation time of the blood ($\sim$1 min), i.e., $t_w = 160$ s and $t_w = 320$ s, were chosen.

First, we analyse the signal at $t_w=160$ s. The embedding time, τ, is determined by the shortest period of interest in the signal. The fastest oscillatory process in the peripheral blood flow and in other signals obtained by non-invasive measurements of cardiovascular functions [8] comes from the beating of the heart. Its frequency in a healthy resting person is around 1 Hz; therefore we choose time lags τ of $0.02, 0.1, 0.2, 0.3, 0.6$

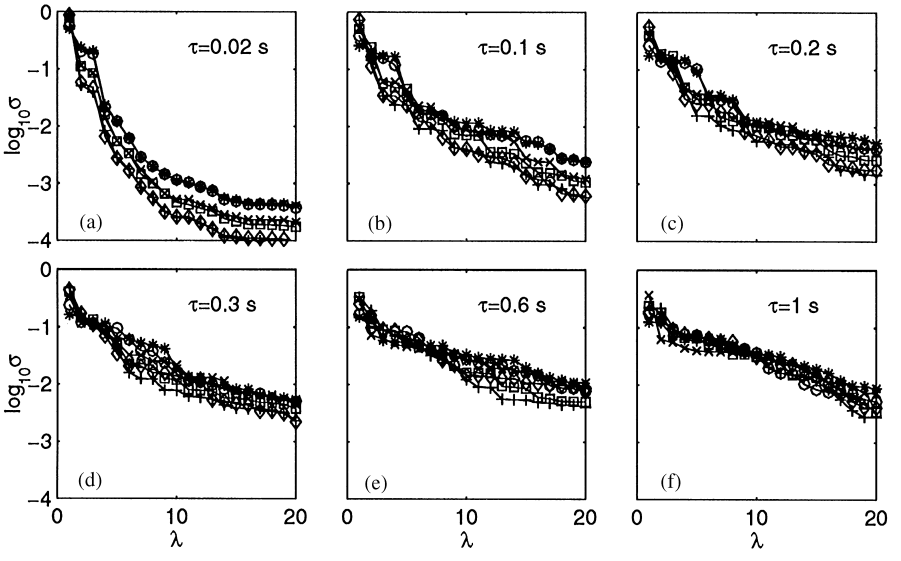

Fig. 7. (a–f) The first 20 normalized eigenvalues calculated at $d = 50$ and different time lags. The time window was $t_w = 160$ s and was repeatedly moved along the signal by 80 s, so that the calculations were repeated six times.

and 1 s. To estimate an optimal embedding time the calculations were repeated at an embedding dimension of $d = 50$.

The method was used similarly to the windowed Fourier transformation, where the spectrum is the average of the spectra of single-time windows, which are sequentially translated for half of the length of the window. At each set of parameters the eigenvalues and eigenvectors were calculated for several windows translated along the signal for 80 s. Since the signal is 650 s long, we made six calculations.

Fig. 7 shows the first 20 normalized eigenvalues. The other normalized eigenvalues are around 0 and are not shown. The first normalized eigenvalues decrease with increasing time lag. At small time lags the successive vectors are strongly correlated, so only the first few modes dominate. There are two knees at the fifth and the 10th eigenvalue at $\tau = 0.2$ s, while the further values are negligible. A similar pattern can be observed at $\tau = 0.3$ s. As the time lag increases the normalized eigenvalues of the higher modes increase, because the correlation is weaker. Therefore, time lags around $\tau = 0.2$ s were chosen for further calculations.

Next, we observed the effect of window length and embedding dimension on decomposition at $\tau = 0.2$ s and 0.24 s. Calculations were repeated at window lengths $t_w = 160$ s and 320 s and embedding dimensions $d = 50$ and 100. The normalized eigenvalues are presented in Fig. 8. Comparing the results obtained at same window length $t_w = 160$ s and different embedding dimensions $d = 50$ (Fig. 8(a) and (d)) and $d = 100$ (Fig. 8(b) and (e)), we see that by increasing embedding dimension the contribution of the first eigenvalues decrease and the contribution of the higher modes increases. A tendency

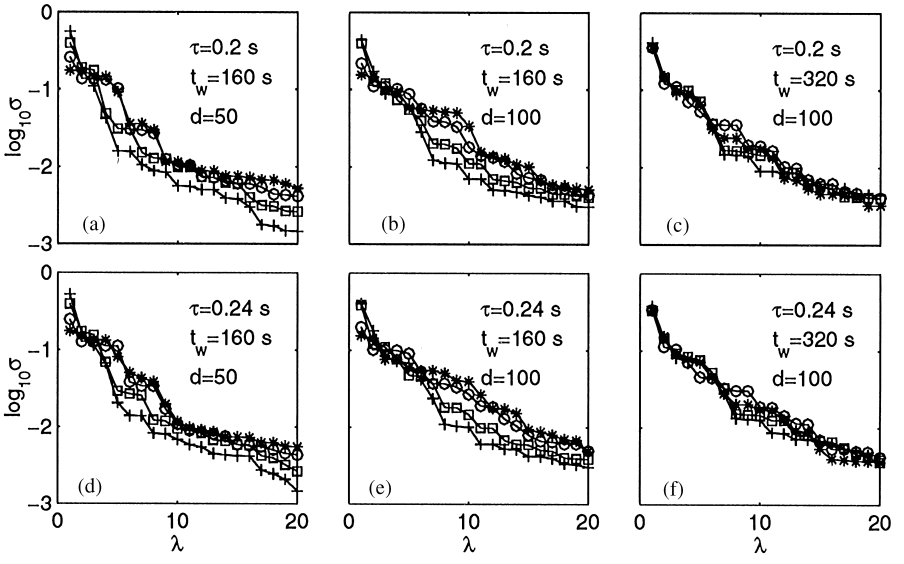

Fig. 8. The first 20 eigenvalues at $\tau = 0.2$ s (a)–(c) and $\tau = 0.24$ s (d)–(f). The window length and the embedding dimension are varied. At each set of parameters the window was moved along the signal for four times. At both embedding times the eigenvalues are comparable. For different section of the signal their difference is minimal at $n = 320$ s and $d = 50$ (c) and (d).

towards plateaux starting at $\lambda = 10$, with small differences between the values obtained for different windows, can be observed at $t_w = 160$ s and $d = 50$, for both the time lags $\tau = 0.2$ s (Fig. 8(a)) and $\tau = 0.24$ s (Fig. 8(d)). This tendency becomes less pronounced at $d = 100$ (Fig. 8(b) and (e)). If we also increase the window length, the variations in normalized eigenvalues between one window and another become minimal, (Fig. 8(c) and (f)).

With this knowledge of the effects of the embedding parameters, we make KL decomposition of one segment of the signal. The decomposition at two different sets of parameters: (a) $\tau = 0.24$ s, $t_w = 160$ s and $d = 50$ and (b) $\tau = 0.24$ s, $t_w = 320$ s and $d = 100$ is presented in Fig. 9. On the top are first 20 normalized eigenvalues and below is a section of the blood flow signal followed by the first 10 modes. For the sake of clarity, sections 80 s in length are plotted. In both cases several pairs of modes, with equal frequency contents can be observed. The existence of modes in pairs (see above) illustrates the oscillatory nature of the blood flow signal. For example, at $t_w = 160$ s (Fig. 9(a)), the main frequency of the ninth and the 10th mode coincides with the respiratory frequency (around 0.3 Hz), which also occurs in the Fourier [11] or wavelet transforms [8] of the blood flow.

Comparing Figs. 9(a) and (b), we see dramatic differences. At the decomposition with larger dimension and window length, the slower modes dominate. Furthermore, at larger window length greater number of modes becomes dominant. The appearance of additional, slower, modes corresponds to the existence of periodic components with

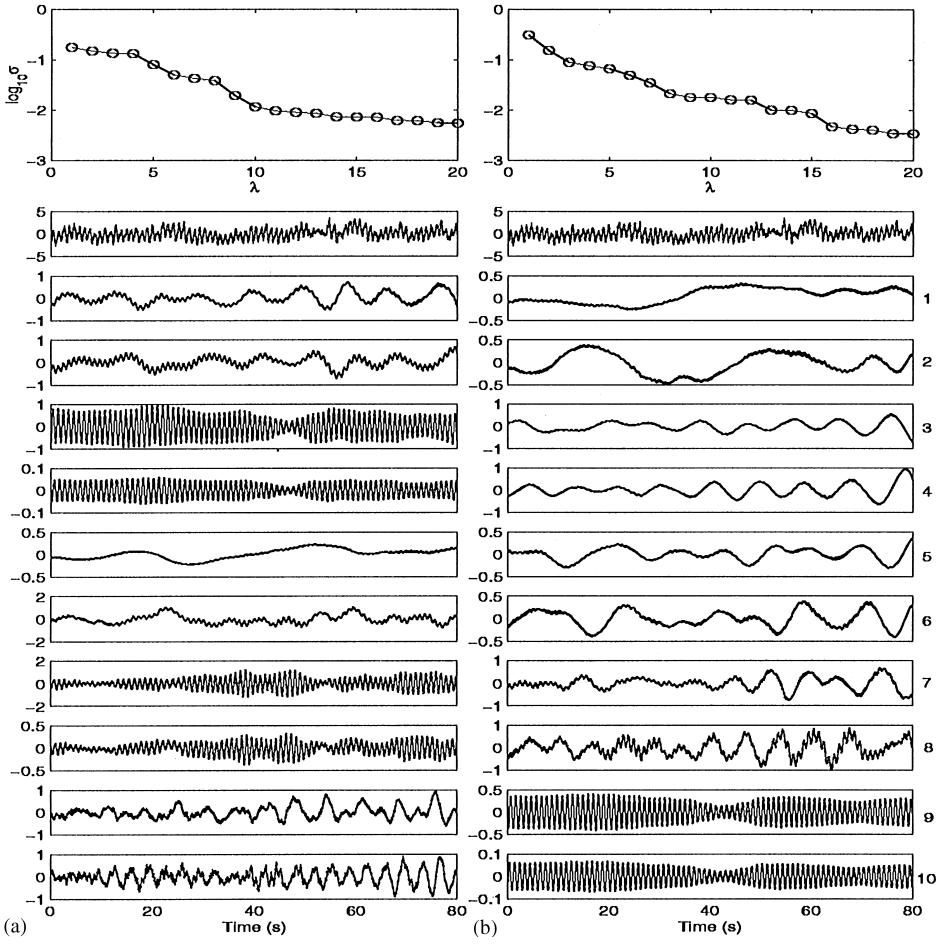

Fig. 9. The first 20 eigenvalues (top row), the segment of the blood flow signal (2nd row) and plots of the first ten KL modes at (a) $\tau = 0.24$ s, $t_w = 160$ s and $d = 50$ and (b) $\tau = 0.24$ s, $t_w = 320$ s and $d = 100$. The first ten modes represent (a) 84% and (b) 86% of the whole signal. At longer window and higher embedding dimension slower modes dominate.

repetition times greater than 1 min observed in the wavelet transform of the blood flow signal. This illustrates that the choice of embedding parameters, and the time scale of observation in particular, influences decomposition. On the other hand, with an optimal set of parameters, we may expect to obtain modes that correspond to a particular oscillatory process.

5. Summary

We have shown that the KL decomposition of a simple sine signal results in two modes, when the time lag τ is not a multiple of half of the period. For multiperiodic

signals this condition will not in general be met, and so we will obtain m up to $2m$ modes from an m-periodic signal.

Analytically, by the use of a simple example, Haken [26] has clearly shown that the reconstruction of an attractor depends sensitively on the choice of time delay. The decomposition itself also depends strongly on the choice of the embedding parameters: time lag τ, window length t_w and embedding dimension d. In analysing blood flow signal, for example, increasing the window length and using a greater embedding dimension causes the slower components to dominate.

Although some recommendations can be found in literature (see [27] and the references therein) the parameter choice for reconstruction of a phase space from scalar signals is in practice still empirical. The results presented illustrate the difficulty of achieving optimal embedding of a simple numerically generated scalar signal. In case of measured scalar signals the problem is even more pronounced. We have shown that the reconstruction of measured scalar signal in the phase space is ambiguous. Moreover, it requires a priori knowledge of the system producing the signal, which is often incomplete. Consequently, a measured scalar signal cannot be unambiguously decomposed into its principal components: further development of techniques for defining criteria for optimal embedding is needed.

The decomposition of blood flow signal for a large set of embedding parameters always resulted in pairs of oscillatory modes. The number of dominant modes depended on chosen value of parameters, however in all cases a finite number was obtained. Therefore, we can reliably conclude from KL decomposition that the blood flow signal contains oscillatory components, confirming results already obtained using different signal analysis techniques [8–12].

Acknowledgements

This work was supported by the Slovenian Ministry of Science and Technology and the Slovenian–German Scientific-Research Project Collaboration. Aneta Stefanovska was partially supported by the Alexander von Humboldt Foundation. We acknowledge valuable discussion or correspondence with Hermann Haken, Viktor Jirsa, Rudolph Friedrich and Peter McClintock.

References

[1] B.W. Hyndman, R.I. Kitney, B.McA. Sayers, Nature 233 (1971) 339–341.
[2] S. Akselrod, D. Gordon, F.A. Ubel, D.C. Shannon, A.C. Berger, R.J. Choen, Science 213 (1981) 220–222.
[3] P.Ch. Ivanov, M.G. Rosenblum, C.-K. Peng, J.E. Mietus, S. Havlin, H.E. Stanley, A.L. Goldberger, Physica A 249 (1998) 587–593.
[4] P. Ch. Ivanov, L.A.N. Amaral, A.L. Goldberger, S. Havlin, M.G. Rosenblum, Z. Struzik, H.E. Stanley, Nature 399 (1999) 461–465.
[5] S. Thurner, M.C. Feurstein, M.C. Teich, Phys. Rev. Lett. 80 (1998) 1544–1547.
[6] A. Marrone, A.D. Polosa, G. Scioscia, S. Sramaglia, A. Zenzola, Phys. Rev. E 60 (1999) 1088–1091.

[7] L.A.N. Amaral, A.L. Goldberger, P.Ch. Ivanov, H.E. Stanley, Phys. Rev. Lett. 81 (1998) 2388–2391.
[8] A. Stefanovska, M. Bračič, Contemporary Phys. 40 (1999) 31–55.
[9] A. Stefanovska, M. Bračič, K.D. Kvernmo, IEEE Trans. Biomed. Eng. 46 (1999) 1230.
[10] M. Bračič, A. Stefanovska, Bull. Math. Biol. 60 (1998) 919–935.
[11] A. Stefanovska, M. Bračič, Control Eng. Practice 7 (1999) 161–172.
[12] M. Bračič, A. Stefanovska, Bull. Math. Biol. 60 (1998) 417–433.
[13] G. Bergkooz, P. Holmes, J.L. Lumley, Ann. Rev. Fluid Mech. 25 (1993) 539.
[14] K. Karhunen, Ann. Acad. Sci. Fenn. A1, Math. Phys. 37, 1946.
[15] M. Loève, Fonctions aleatoires de second ordre, C.R. Acad. Sci., Paris, 1946.
[16] R. Friedrich, A. Fuchs, H. Haken, Spatio temporal EEG patterns, in: H. Haken, H. Koepchen (Eds.), Rhythms in Physiological Systems, Springer, Berlin, 1991.
[17] V.K. Jirsa, R. Friedrich, H. Haken, Physica D 89 (1995) 100–122.
[18] A. Hutt, C. Uhl, R. Friedrich, Phys. Rev. E 60 (1999) 1350–1358.
[19] G.E. Nilsson, T. Tenland, P.A. Öberg, IEEE Trans. Biomed. Eng. 27 (1980) 597–604.
[20] S. Gordeyev, F.O. Thomas, Bull. Am. Phys. Soc. 42 (1997) 2115–2126.
[21] N. Packard, J. Crutchfield, D. Farmer, R. Shaw, Phys. Rev. Lett. 45 (1980) 712–716.
[22] D.S. Broomhead, P. King, Physica D 20 (1985) 217–236.
[23] F. Takens, in: D.A. Rand, L.S. Young (Eds.), Detecting Strange Attractors in Turbulence, Lecture Notes in Mathematics 898, Springer, New York, 1981.
[24] R. Mañé, in: D.A. Rand, L.S. Young (Eds.), On the Dimension of the Compact Invariant Sets of Certain Non-linear Maps, Lecture Notes in Mathematics 898, Springer, New York, 1981.
[25] A.I. Mees, P.E. Rapp, L.S. Jennings, Phys. Rev. A 36 (1987) 340–346.
[26] H. Haken, Principles of Brain Functioning, Springer, Berlin, 1996, pp. 309–312.
[27] R. Hegger, H. Kantz, T. Schreiber, Chaos 9 (1999) 413–435.

ELSEVIER

Physica A 283 (2000) 451–461

PHYSICA A

www.elsevier.com/locate/physa

Synchronization and modulation in the human cardiorespiratory system

Maja Bračič Lotrič[a,*], Aneta Stefanovska[a]

[a] *Laboratory of Nonlinear Dynamics and Synergetics, Faculty of Electrical Engineering, University of Ljubljana, Trža ška 25, Ljubljana, Slovenia*

Received 15 February 2000

Abstract

We analyse phase and frequency synchronization in the human cardio-respiratory system. The method for analysis of noisy nonstationary bivariate data is applied to simultaneously measured cardiac and respiratory activity. Short epochs of phase and/or frequency locking between respiratory and cardiac rhythms are detected in healthy relaxed subjects (non-athletes). We reveal that the strength of phase synchronization is inversely related to the extent of respiratory modulation of the heart rate.

PACS: 87.22.As; 87.45.Hw; 05.40+j

Keywords: Coupling; Synchronization; Frequency modulation; Cardiorespiratory system

1. Introduction

The cardiac and respiratory systems are known to be coupled by several mechanisms [1]. Due to their interaction, the heart rate increases during inspiration and decreases during expiration. This respiratory modulation of heart rate, known as respiratory sinus arrhythmia (RSA), was observed as early as in 1733 [2]. In systems of coupled oscillators another phenomenon may arise – the adjustment of their rhythms or synchronization.

In the early studies of cardio-respiratory synchronization, Hildebrandt reported preferred time delays between the onset of inspiration and the preceding heartbeat, and the integer number of heartbeats per respiratory cycle [3]. The preference of integer ratios existed only in statistical terms. Raschke [4] investigated phase and

* Corresponding author. Fax: +386-1-4264-630.

E-mail addresses: maja@osc.fe.uni-lj.si (M. Bračič-Lotrič), aneta@osc.fe.uni-lj.si (A. Stefanovska).

0378-4371/00/$ - see front matter
PII: S0378-4371(00)00204-1

frequency coordination in different states of the system and reported strong phase coordination between cardiovascular and respiratory subsystems during sleep, and diminished under conditions of strain or disease. Both, Hildebrandt and Raschke proposed that synchronization, or frequency and phase coordination as they named it, establishes a system of economical co-action and thus favor the functional economy of the organism [3,4].

The notion of synchronization has long been restricted to periodic oscillators. Methods for detection of synchronization between such irregular and non-stationary oscillators as are the human heart and respiratory systems were proposed only recently (see Ref. [5]).

2. Synchronization

Synchronization lacks a unique definition. In a wide sense, synchronization can be treated as an appearance of some relation between the state vectors $\mathbf{u}(t)$ of two processes due to their interaction [6]. A general synchronization is thus defined as the presence of a relation between the states of interacting systems, $\mathbf{u}_2(t) = \mathscr{F}[\mathbf{u}_1(t)]$. If interacting systems are identical the states can coincide $\mathbf{u}_1(t) = \mathbf{u}_2(t)$ and the synchronization is complete. If the parameters of coupled systems slightly mismatch, the states are close $|\mathbf{u}_1(t) - \mathbf{u}_2(t)| \approx 0$, but remain different.

In classical sense of periodic, self-sustained oscillators, synchronization is usually defined as locking (entrainment) of the phases

$$\varphi_{n,m} = n\Phi_1 - m\Phi_2 = \text{const}\,, \tag{1}$$

where n and m are integers, Φ_1,Φ_2 are phases of the two oscillators and $\varphi_{n,m}$ is the generalized phase difference.

Condition 1 is valid for quasi-periodic oscillators only. For more general forms of nonlinear oscillators (e.g. relaxation oscillators), a weaker condition for phase locking

$$|n\Phi_1 - m\Phi_2 - \delta| < \text{const}\,, \tag{2}$$

was proposed [7]. In such cases, the $m : n$ phase locking manifests as a variation of $\varphi_{n,m}$ around a horizontal plateau. The amplitudes of phase synchronized oscillations can be quite different and need not be related.

For periodic oscillators, the condition of phase locking (1) is equivalent to the notion of frequency locking

$$nf_1 = mf_2\,, \tag{3}$$

where $f = \langle\dot{\Phi}\rangle/2\pi$ and brackets mean time averaging. If n periods of the first oscillator have exactly the same duration as m periods of the second oscillator, the rhythms are $n : m$ entrained.

Synchronization of periodic oscillators thus means the appearance of phase locking and adjustment of frequencies. If we consider synchronization in the presence of noise, synchronization of chaotic systems, or synchronization of oscillators with modulated

natural frequencies, phase and frequency locking may not be equivalent any more [6,8]. One can distinguish between several forms of synchronization: frequency and phase locking, phase locking without frequency locking and frequency locking without phase locking [9].

For weak noise $\varphi_{n,m}$ fluctuates in a random way around a constant value; the frequencies are then nearly locked, i.e., the condition of frequency locking 3 is fulfilled on average, $n\langle f_1\rangle = m\langle f_2\rangle$. Strong noise can also cause phase slips. In such cases, the question synchronous or not synchronous cannot be answered in a unique way, but only treated in a statistical sense. Phase synchronization can be understood as an appearance of a peak in the distribution of the cyclic relative phase

$$\Psi_{n,m} = \varphi_{n,m} \bmod 2\pi\,, \tag{4}$$

and interpreted as the existence of a preferred stable value of phase difference between the two oscillators.

In case of cardio-respiratory coupling, the noise originates not only from measurements and external disturbances, but also from the fact that there are other subsystems that take part in the cardiovascular control [10] and their influence is considered as noise in synchronization analysis.

2.1. Cardiorespiratory synchrogram

According to its definition (Eq. (1)), a $m:n$ phase synchronization can be found by plotting the generalized phase difference $\varphi_{m,n} = n\Phi_1 - m\Phi_2$ versus time and looking for horizontal plateaus. For noisy systems the cyclic relative phase $\Psi_{n,m}$ is used instead of $\varphi_{n,m}$ to avoid the impact of phase slips due to noise. There are two problems with this approach: (i) integers m and n can only be obtained by trial and error and (ii) if several synchronization regimes exist, the method cannot reveal them all nor the transitions between them.

To overcome these problems, the cardiorespiratory synchrogram was introduced [5,9]. It is constructed by plotting the normalized relative phase of a heartbeat within m respiratory cycles

$$\psi_m(t_k) = \frac{1}{2\pi}(\Phi_r(t_k) \bmod 2\pi m)\,, \tag{5}$$

where t_k is the time of the kth heart beat and Φ_r is the instantaneous phase of respiration. Φ_r is defined on the real line and it is observed stroboscopically at times t_k, as presented in Fig. 1. In a perfect $n:m$ phase locking, $\psi_m(t_k)$ attains exactly the same n different values within m adjacent respiratory cycles, and the synchrogram consists of n horizontal strips. In the presence of noise, strips become broadened. By this technique only one integer, m should be chosen by trial and several regimes can be identified within one plot.

The times of P peaks in the ECG signal, which correspond to the excitation of the atria, were taken as the markers of heart beats. They were detected from the signal by an automatic procedure and then also manually edited. To calculate the instantaneous

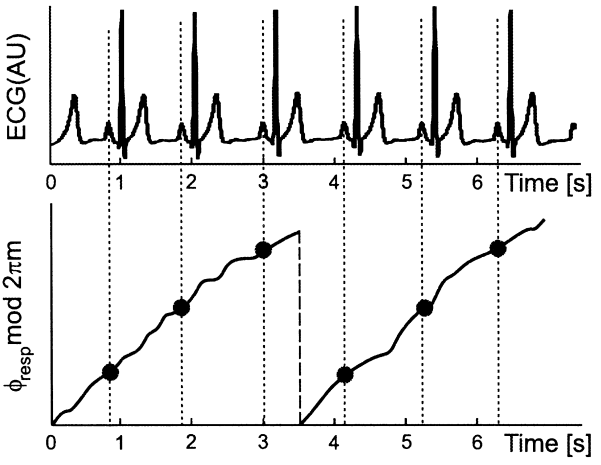

Fig. 1. The derivation of cardiorespiratory synchrogram from the phase of respiration and times of heart beats (P peaks in the ECG).

phase of respiration $\Phi_r(t)$, either the Hilbert transform [6,11] or the method based on marker events can be used [8]. By the second method, marker events that characterize the cycle of the oscillator are first determined. A 2π increase in the phase is then attributed to the interval between subsequent marker events. Within this interval, the instantaneous phase is

$$\Phi(t) = 2\pi\frac{t - t_k}{t_{k+1} - t_k} + 2\pi k\,, \quad t_k \leqslant t < t_{k+1}\,, \tag{6}$$

where t_k is the time of kth marker event. Defined in this way, the phase is a monotonically increasing piecewise-linear function of time defined on the real line. The maxima of inspiration were taken for the marker events of the respiration oscillator. They were detected automatically and again manually edited. Fig. 2 compares phases obtained by both methods. The results are similar and the main source of differences is the linear interpolation of phase in the case of the marker events method.

3. Cardiorespiratory synchronization in healthy subjects

The electric activity of the heart and respiration signals were measured on 32 healthy subjects of different age and sex. Subjects between 23 and 83 years of age were included. None of them was intensively physically active. The measurement time was 20 min and the sampling frequency 400 Hz for the ECG and 40 Hz for the respiratory signal.

Fig. 3 gives the instantaneous frequencies of heart and respiratory systems for an 800 s long segment of a signal measured from a young healthy male subject, we shall refer to him as subject A. The instantaneous frequencies were obtained from marker

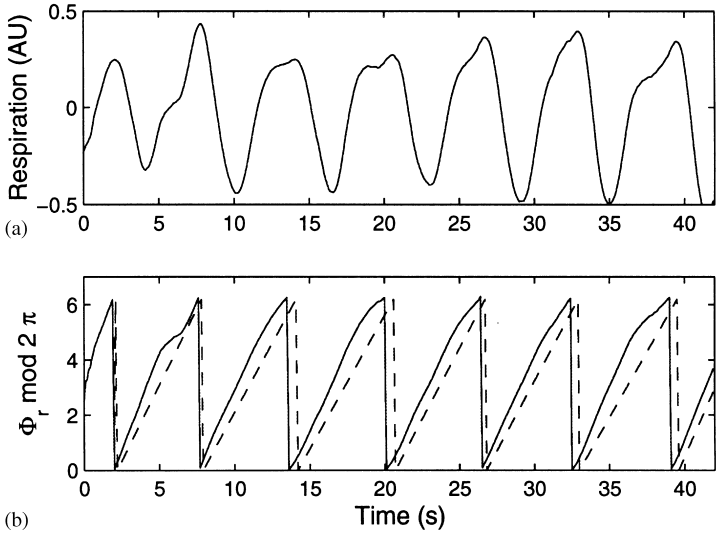

Fig. 2. The detrended respiratory signal (a) and its instantaneous phase (b) retrieved by analytic signal concept (solid line) and based on marker events (broken line). In the second case, the phase cannot be determined for times before the first marker event.

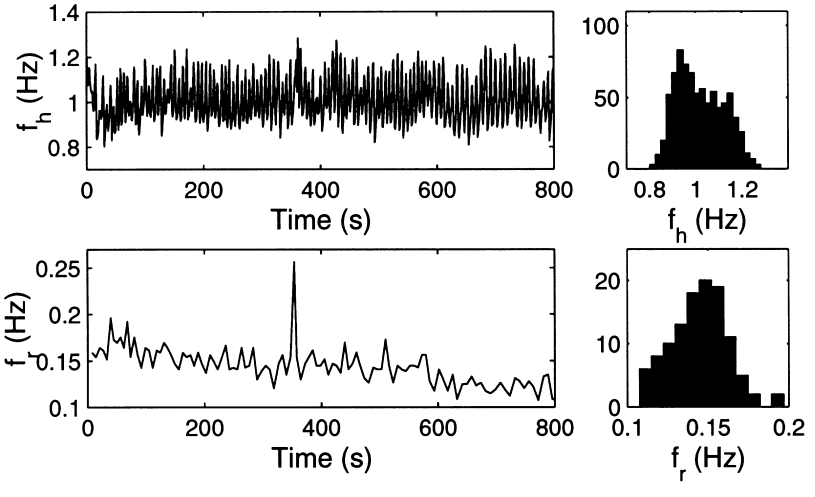

Fig. 3. Instantaneous frequencies of the heart (f_h) and respiratory (f_r) activity and the corresponding histograms of values for subject A.

events of both oscillators, i.e., the R peaks of the ECG signal (markers of the pumping action of the heart) and the local maxima in respiration signal. Both frequencies are time variable. The subject exhibited a relatively strong variability of heart rate which oscillated between 0.8 and 1.2 Hz. The respiratory frequency also oscillated in time.

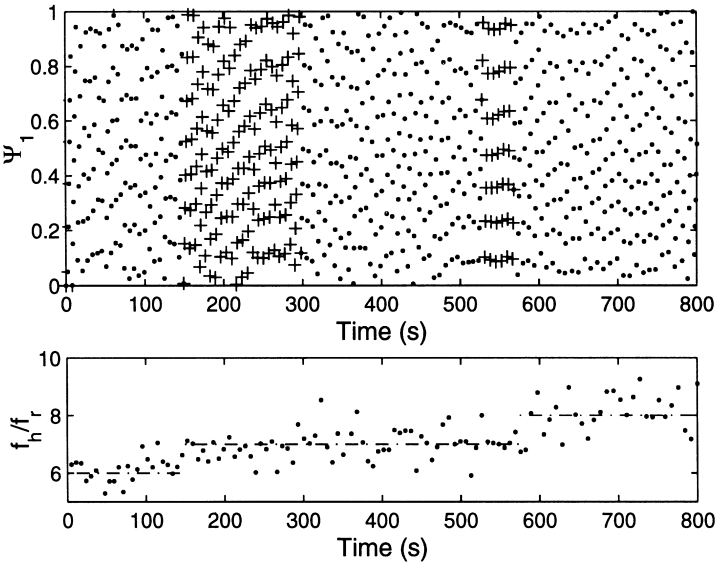

Fig. 4. The cardiorespiratory synchrogram ψ_1 and the instantaneous frequency ratio f_h/f_r for subject A. Between 150 and 300 s a frequency synchronization appears and both phase and frequency synchronization appear between 510 and 580 s.

A slight decline during the time of observation was noticeable. There is an irregular breath around 350 s.

From the ECG and respiratory signals, the cardiorespiratory synchrogram was calculated. The synchrogram for subject A obtained for $m = 1$ is given in Fig. 4. The instantaneous frequency ratio f_h/f_r is plotted in Fig. 4 below. It was obtained by counting the number of heart beats within each respiratory cycle and adding parts of those heart beats that were in this respiratory cycle only partially.

During the first 150 s there was no apparent pattern in the synchrogram and the frequency ratio varied around 6. Between 150 and 300 s we could see seven parallel inclined curves. During this time, the frequency ratio was approximately constant, being around 7. Parallel curves indicate frequency synchronization [9], however, the rhythms were not phase locked. Between 300 and 510 s there was no obvious pattern in the synchrogram, but we could see that the instantaneous frequency ratio became constant for a few respiration periods around 450 s.

Between 510 and 580 s, seven horizontal lines appeared in the synchrogram, indicating phase synchronization. During this time, the frequency ratio was also constant, $f_h/f_r = 7$, although both frequencies varied in time. This is thus an example of phase and frequency synchronization in the cardiorespiratory system. Within the whole 20 min of recordings, phase and frequency synchronization occurred simultaneously only during 1 min in subject A.

After 580 s neither phase nor frequency synchronization was detected and the average frequency ratio was increased.

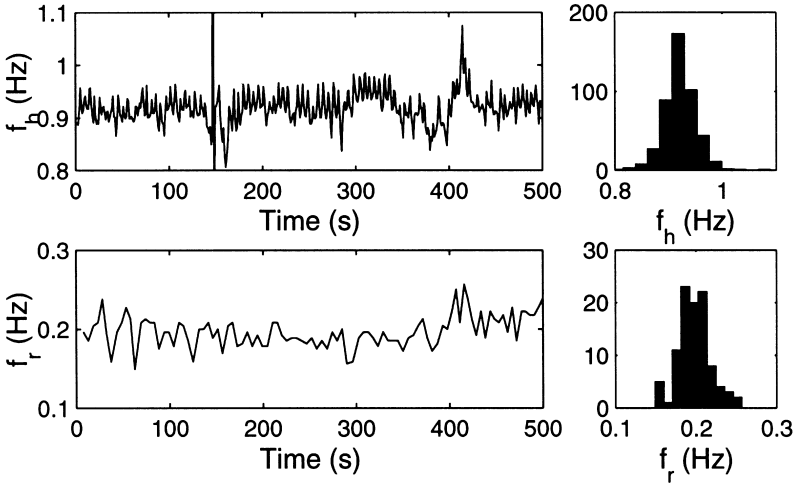

Fig. 5. Instantaneous frequencies of the heart (f_h) and respiratory (f_r) activity and the corresponding histograms of values for subject B.

An even clearer example of frequency synchronization without phase synchronization was observed for an elderly female subject (subject B). The instantaneous frequencies of heart and respiration for a 500 s long segment of the signals recorded from this subject are given in Fig. 5. The heart rate varied between 0.8 and 1 Hz which is less than for subject A. The variability of the respiration frequency is comparable to subject A, although the frequency itself is higher.

Fig. 6 presents the synchrogram ($m = 1$) and the instantaneous frequency ratio for subject B. Between 150 and 350 s five parallel curves appeared with sinelike variations in time. Apparently, the generalized phase difference exhibited an oscillatory behaviour during this time. It cannot be characterized as a phase locking as it is defined by Eq. (2), although it reflects some kind of coupling. Since the frequency ratio is almost constant during this time ($f_h/f_r = 5$), we can speak about frequency locking.

We can see from these two examples that a variety of phenomena may arise from the interaction between cardiac and respiratory systems. Some can be classified using the existing methods of uni- and bivariate data analysis, while others need to be further investigated.

3.1. Characterization of synchronization

It is difficult to find a measure that would characterize the strength of synchronization in the system. Since in noisy systems, phase synchronization is understood in a statistical sense as the existence of preferred values of generalized phase difference, measures based on quantifying the distribution of phases were proposed. To reliably detect synchronous epochs, Tass et al. [7] have proposed two indexes, one based on Shannon entropy and the other based on conditional probability.

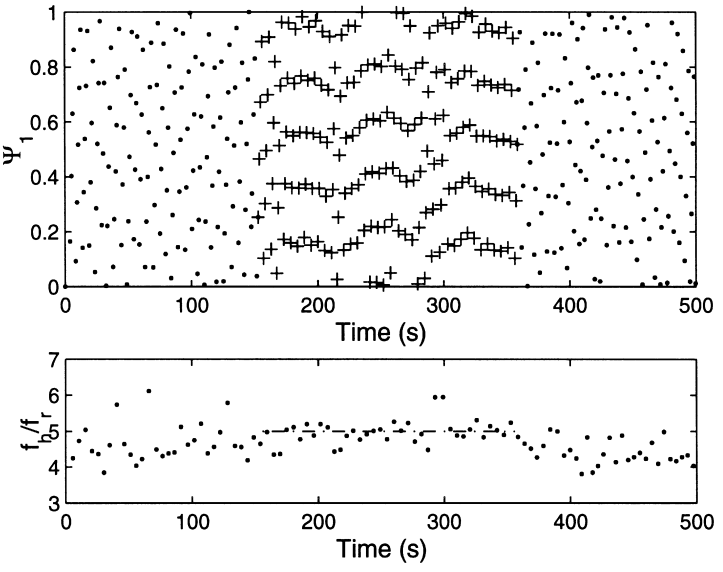

Fig. 6. The cardiorespiratory synchrogram ψ_1 and the instantaneous frequency ratio f_h/f_r for subject B. Frequency synchronization without phase synchronization appears between 150 and 350 s.

We shall use the latter one, which is defined in the following way: Suppose we have two phases, $\Phi_1(t_k)$ and $\Phi_2(t_k)$. We divide the interval of each phase into N bins and calculate

$$r_l(t_k) = \frac{1}{M_l} \sum e^{i\Phi_2(t_k)}, \quad l = 1, \ldots, N, \tag{7}$$

for all k such that $\Phi_1(t_k)$ belongs to bin l and M_l is the number of points in this bin. If there is a complete mutual interdependence between the two phases, $|r_l(t_k)| = 1$, whereas it is zero if there is no dependence at all. Finally, we calculate the average over all bins

$$\lambda = \frac{1}{N} \sum_{l=1}^{N} |r_l(t_k)| \tag{8}$$

which measures the conditional probability of Φ_2 to have a certain value provided Φ_1 is in a certain bin [7].

In application of the conditional probability index to the cardiorespiratory synchrogram, we can make use of the fact that by its definition the synchrogram gives us the phase of respiration Φ_r at times when the phase of heart rate is $\Phi_h \bmod 2\pi n = 0$. It is therefore sufficient to use only one bin for the phase of the heart.

As we have seen in the synchrogram plots, transitions between different synchronized and non-synchronized states may appear within the time of observation, or frequency synchronization may occur without phase synchronization. However, the index based on conditional probability increases only in the presence of phase synchronization and is not sensitive to frequency synchronization without phase synchronization.

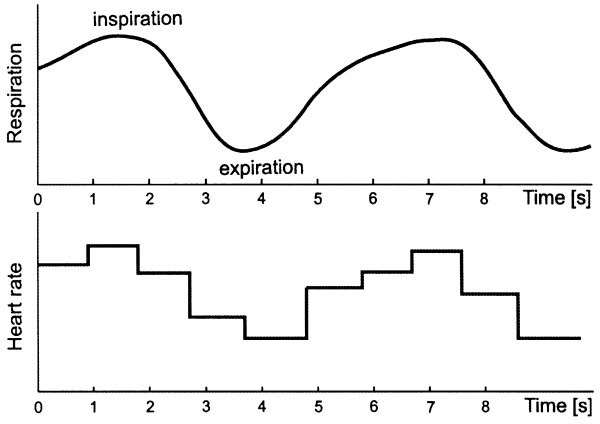

Fig. 7. The respiratory modulation of heart rate – the heart beats faster during inspiration and slower during expiration.

3.2. Synchronization and modulation

In the systems of coupled nonlinear oscillators both synchronization and modulation of rhythms may arise. The respiratory modulation of the heart rate is a well-known phenomenon. As illustrated in Fig. 7, the heart rate increases during inspiration and decreases during expiration. The degree of this variability of heart rate can be estimated in different ways [12]. The standard deviation of the RR intervals can be taken as a simple measure of the heart rate variability. This measure, however, also includes the heart rate variability caused by mechanisms other than respiration [10].

To investigate the relation between synchronization and modulation, we have compared the conditional probability index for the first phase in the synchrogram, i.e., $\lambda(\psi_{1,1})$ averaged over the whole signal with the standard deviation of the RR intervals for all 32 subjects. The results are presented in Fig. 8. We can see that subjects with low heart rate variability have high conditional probability index, while subjects with higher variability have lower conditional probability index. This negative correlation is also statistically significant ($R = -0.37,\ p = 0.035$).

4. Discussion

The modulation of heart rate by respiration is a well-known phenomenon, while there are only few indications of true entrainment between the two rhythms. Most studies have led to the conclusion that there is a comparatively weak coupling between respiration and cardiac rhythms, and the resulting rhythms are generally not phase locked [13]. Recently, evidences of temporary cardiorespiratory synchronization were reported [5,9,14–18].

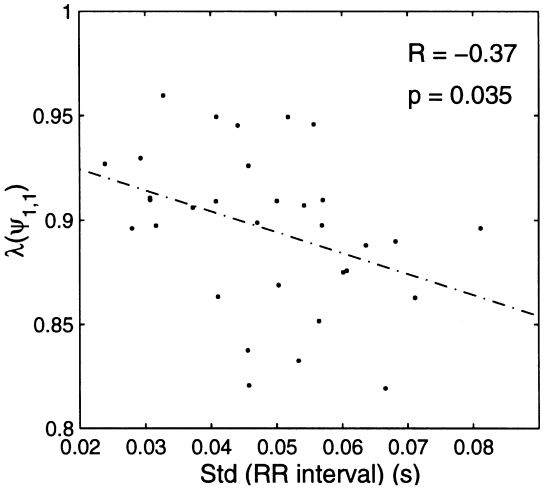

Fig. 8. The correlation between the index based on conditional probability $\lambda(\psi_{1,1})$ and the standard deviation of RR intervals for 32 subjects.

Schäfer et al. found well-expressed synchronization in a group of young athletes (high-performance swimmers) using the synchrogram technique [5,9,14,15]. They have also noticed that subjects with the strongest synchronization had no remarkable RSA, whereas subjects with the highest RSA exhibited no synchronization [5]. Therefore, they have concluded that phase locking of respiratory and cardiac rhythms and modulation are two competing aspects of cardiorespiratory interaction.

Our results confirm the presence of episodes of synchronization in healthy relaxed subjects. However, these episodes did not exceed 2 min within the 20 min of recording for any of the subjects. Longer synchronization, such as reported by Schäfer et al. in athletes were not found in a more general population of non-athletes (performing recreative physical activity only).

We have also studied the relation between the strength of phase synchronization and the variability of heart rate which is mainly, although not completely, due to respiratory modulation of heart rate. A statistically significant negative correlation was found which is in agreement with the observations of Schäfer et al. [5]. Nevertheless, we must be aware of the limitations of this analysis. First, we have taken only phase synchronization into account, although we have seen that other kinds of synchronization may appear. Secondly, an average over the whole signal was taken for each subject although phase synchronization appears only in parts of the signal. The phase synchronization is understood in a statistical sense as the existence of preferred values of the phase difference.

Based on the presented results, it is evident that couplings which exist between heart and respiratory systems enable both modulation and synchronisation to occur. The two interacting systems are however not isolated and they are subject to the influence of

other physiological systems contributing to cardiovascular control as well as to external perturbations. Their impact may change the stability or even the existence of phase locked solutions. Therefore, continual phase transitions between different synchronized and non-synchronized states are present in a normal healthy system.

Acknowledgements

We gratefully acknowledge J. Petrovčič and M. Čenčur for their help in setting the measurements and valuable discussions with P. Tass, C. Schäfer and M.G. Rosenblum. The study was supported by the Slovenian Ministry of Science and Technology.

References

[1] R.M. Berne, M.N. Levy (Eds.), Physiology, Mosby, St. Louis, MO, 1998.
[2] S. Hales, Statical Essays II, Haemastaticks, Innings Manby, London, 1733.
[3] G. Hildebrandt, The autonomous time structure and its reactive modifications in the human organism, in: L. Resing, U. an der Heiden, M.C. Mackey (Eds.), Temporal Disorder in Human Oscillatory Systems, Springer, Berlin, 1987, pp. 160–174.
[4] F. Raschke, Coordination in the circulatory and respiratory systems, in: L. Resing, U. an der Heiden, M.C. Mackey (Eds.), Temporal Disorder in Human Oscillatory Systems, Springer, Berlin, 1987, pp. 152–158.
[5] C. Schäfer, M.G. Rosenblum, J. Kurths, H.H. Abel, Nature 293 (1998) 239–240.
[6] M.G. Rosenblum, A.S. Pikovsky, J. Kurths, Phys. Rev. Lett. 76 (1996) 1804–1807.
[7] P. Tass, M.G. Rosenblum, J. Weule, J. Kurths, A.S. Pikovsky, J. Volkmann, A. Schnitzler, H.-J. Freund, Phys. Rev. Lett. 81 (1998) 3291–3294.
[8] A.S. Pikovsky, M.G. Rosenblum, G.V. Osipov, J. Kurths, Physica D 104 (1997) 219–238.
[9] C. Schäfer, Analysis of synchronization in complex systems: application to physiological data, Ph.D. Thesis, University of Potsdam, Potsdam, 1998.
[10] A. Stefanovska, M. Bračič, Contemp. Phys. 40 (1999) 31–55.
[11] D. Gabor, J. IEE 93 (1946) 429–457.
[12] Task Force of the ESC and NASPE, Circulation 93 (1996) 1043–1065.
[13] L. Glass, M.C. Mackey, From Clock to Chaos: The Rhythms of Life, Princeton University Press, Princeton, NJ, 1998.
[14] M.G. Rosenblum, J. Kurths, A.S. Pikovsky, C. Schäfer, P. Tass, H.-H. Abel, IEEE Eng. Med. Biol. Mag. 17 (1998) 46–53.
[15] C. Schäfer, M.G. Rosenblum, H.H. Abel, J. Kurths, Phys. Rev. E 60 (1999) 857–870.
[16] M.G. Rosenblum, A.S. Pikovsky, C. Schäfer, P. Tass, J. Kurths, Phase synchronization: from theory to data analysis, in: S. Gielen, F. Moss (Ed.), Handbook of Biological Physics, Vol. 4, Neuro-informatics, Elsevier, in press.
[17] H. Seidel, H. Herzel, IEEE Eng. Med. Biol. Mag. 17 (1998) 54–57.
[18] M. Paluš, D. Hoyer, IEEE Eng. Med. Biol. 17 (1998) 40–45.

Contemporary Physics, 1999, volume 40, number 1, pages 31 – 55

Physics of the human cardiovascular system

ANETA STEFANOVSKA and MAJA BRAČIČ

Contemporary measurement techniques permit the non-invasive observation of several cardiovascular functions, both from the central and peripheral points of view. We show that, within one cycle of blood through the cardiovascular system, the same dynamics characterizes heart function as well as blood flow in the capillary bed where cells exchange energy and matter. Analyses of several quite different signals derived from respiration, cardiac function and blood flow, all reveal the existence of five almost periodic frequency components. This result is interpreted as evidence that cardiovascular dynamics is governed by five coupled oscillators. The couplings provide co-ordination among the physiological processes involved, and are essential for efficient cardiovascular function. Understanding the dynamics of a system of five coupled oscillators not only represents a theoretical challenge, but also carries practical implications for diagnosis and for predicting the future behaviour of this life giving system.

1. Basic role and structure

In the course of evolution, individual cells organized into cellular systems of increasing complexity and, as animals evolved, they further differentiated into specialized tissues and organs. At this level of organization cells were no longer capable of individually sustaining autonomous life. A collective system that provides and distributes oxygen and nutrient materials to each cell and takes away the products of their metabolism became essential, and also evolved. It is the cardiovascular system, a closed circuit of vessels, that enables the life of each individual cell in the human organism, as well as in all mammals.

To enable it to take care of the nutritional and immunological needs of individual cells, the blood is kept in continuous motion from the left heart, via the aorta, arteries, arterioles, capillaries, venules, veins, vena cava, to the right heart, through the pulmonary artery to the lungs, and finally, through the pulmonary vein, back to the left heart (figure 1). The total volume of blood (4–6 l, or 7–8% of the body weight) circulates along this path in one minute, on average in a relaxed, healthy subject in repose [1,2]. With 60 beats per minute the heart of a man outputs 5.5 litres on average in a minute. The process of respiration, by which the blood exchanges gases with the atmosphere, is also involved in the regulation of pressure and flow, and it dominates in the venous flow. Along the vessels the flow is also regulated by myogenic and neurogenic processes [1,2]. Both are involved in vasomotion—continuous oscillatory movement of the vessels. The myogenic process results from the continuous contraction and relaxation of smooth muscle in the vessels' walls. This process affects the radial component of the vessel movement and is based on the concentration difference of ions inside and outside the muscle membrane. The neurogenic process is controlled by the autonomous nervous system. Having its origin in some centres in the brainstem that are connected to other parts of the central nervous system, and sensors throughout the whole network of vessels, it provides synchronization of the function of the entire system. It mainly affects the longitudinal component of the vessels' movements.

The place where the cells of the human body have direct access to the blood is named the capillary bed (figure 2). It serves both transport and exchange functions. The capillary bed is the network of capillaries, feeding arteriole and draining venule, that act collectively as a functional module. The average length of a capillary is about 200–250 μm, and its diameter ranges from 8 μm to 10 μm depending on the site, but for the most part is comparable with or even smaller than the diameter of the red blood cells. The flow of blood in vessels whose diameters are comparable with that of red blood cells is termed microcirculation [3]. While some of the blood passes directly to the venules, thus making circulation continuous, some stays in the capillaries closed by pre-capillary

Authors' address: Group of Nonlinear Dynamics and Synergetics, Faculty of Electrical Engineering, University of Ljubljana, Ljubljana, Slovenia. e-mail: maja@osc.fe.uni-lj.si and aneta@osc.fe.uni-lj.si

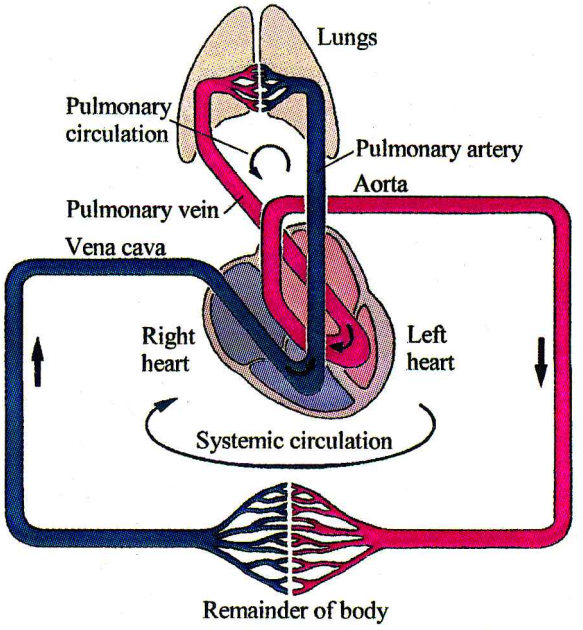

Figure 1. Blood circulates through the cardiovascular system, a closed system of vessels. In one minute on average the whole volume of blood passes through the heart and the lungs, and is then distributed to the different parts of the body according to their individual needs. Oxygenated blood is portrayed as red, deoxygenated as blue. Modified from [2], with permission.

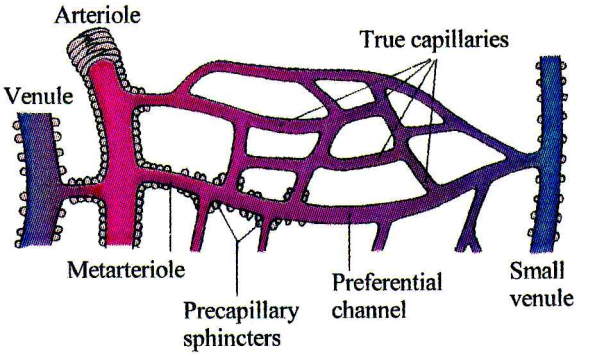

Figure 2. A typical capillary bed, where the cells of human body have direct access to the blood. An exchange of energy and matter occurs along the capillary walls so that the cardiovascular system is thermodynamically open. Modified from [2], with permission.

sphincters. The latter are rings of smooth muscles that rhythmically switch between the open and closed condition.

The exchange of matter and energy between the blood and the tissues occurs across the capillary wall, so that the system is thermodynamically open. The capillary bed can be conceived of as two concentric tubular barriers—an inner tube, a layer of endothelial cells, and an outer tube, the basement membrane. The latter is directly continuous with the tissue ground substance [4]. The endothelial cells are interdigitated to form the interior fibrillar layer, some 500—600 Å thick. The two layers, although continuous in their structure [5], are capable of selection among the substances that await to enter the intracellular space. From there, they become involved in all forms of tissue metabolism, both physical and chemical. These processes occur on time scales longer than one minute, however, and will not be considered in the analysis presented below.

In what follows, we shall summarize current understanding of the system responsible for the circulation of the blood and for controlling the concentrations of dissolved gases and nutrients within it—the cardiovascular system—restricting our attention to those processes that occur within one cycle of blood through the system. The rhythmic metabolic process that influences blood transport by facilitating exchange across the capillary wall is thus the slowest dynamic process that will be considered. We will find that physics has a major role to play in accounting for the operation of this wonderful self-regulating biological mechanism. We will also see that, contrary to popular perception, the heart of a healthy person at rest does not beat at a constant rate. Indeed, unevenness of the heart rhythm seems to be absolutely essential to physical well-being.

2. Background

From the earliest times, blood has been recognized as the life-giving fluid. Until the beginning of the seventeenth century, however, it had been believed that the blood was prepared in the liver and then moved through veins into organs, where it was consumed. From veins it came to the right heart where it divided into two streams, one supplying the lungs and the other, through 'interseptal pores', going to the left heart. This was seen as a place where the blood mixed with the air (pneuma), became heated and then passed to the aorta. The first criticism to this view, which was formulated by Galen of Pergamum in the second century, was proposed by Ibn el-Nafis not earlier than in thirteenth-century. He proposed that the blood from the right heart continued to the lungs, where spread in the pulmonary substance to mix with the air and then returned to the left heart. The role of valves in the heart was first described by Andrea Casalpino in 1571, who then introduced the term *circulatio* [6].

It is to William Harvey that we owe the conception and proof of the idea that blood does indeed circulate. He was able to show that the valves in the heart are so arranged as to allow the passage of blood in only one direction. Further, by watching the motion of the heart in living animals he concluded that in the phase of emptying the ventricles, known as systole, the blood is expelled to the

lungs via the pulmonary artery and to the rest of the body via the aorta. In the phase when the atria are filling, known as diastole, he observed that the blood enters the heart through the vena cava and the pulmonary vein (figure 1). He calculated that if only a drachma (3.55×10^{-6} m^3) of blood were expelled at each beat, in half an hour the heart would use up all the blood in the body, thus completely emptying the veins and distending the arteries. After more than two decades of systematic work, Harvey formulated his results in 1628, when he concluded that the circulation of the blood is 'the sole and only end of the motion and contraction of the heart' [6]. The fact that blood moves in a circle, entering the veins from arteries, was supported by Marcello Malpighi, who in 1661, using a microscope, discovered the capillaries [7].

Harvey's discovery of blood circulation opened the doors to modern physiology, but at least two centuries were to elapse before science had developed sufficiently to pass through them. Even today, the fact that the lungs and the heart are the only organs through which the entire amount of blood passes on average in each cycle is often overlooked. Their interplay in maintaining the flow and pressure levels still needs to be clarified. The blood flow through those organs is usually treated separately, mainly analysing flow in the heart and/or veins (see [8] and the references therein), and gas exchange in the lungs.

In the following subsections we will trace the development of our understanding of physics of blood circulation, grounded on Harvey's observations. First, we will consider the mechanical function of the heart and the flow of blood through vessels. Then, secondly, we will discuss the regulatory mechanisms that are involved in maintaining rhythmic flow of blood through the cardiovascular system.

2.1. *Mechanics of the blood flow*

The study of mechanics of the blood flow is marked by the work of Jean Poiseuille. After completing his doctoral research on *The force of the aortic heart* in 1828 [9], he turned his attention to circulation through small vessels. To be able to control all parameters involved, he built a model device where he studied the liquid flow in small diameter glass capillaries. Poiseuille set out to find a functional relationship among four variables: the volumetric efflux rate of distilled water from a tube Q, the driving pressure differential P, the tube length L, and the tube diameter D. The diameter of his glass tubes ranged from 15 μm to 600 μm, however larger than the size of human capillaries. He varied the other parameters, too, and by careful measurements established the relation among the above parameters as

$$Q = \frac{K'' P D^4}{L}\,, \tag{1}$$

where K'' is a function of temperature and the type of liquid flowing. Later, Eduard Hagenbach solved the problem of Poiseuille flow by application of the Navier–Stokes equations. He showed that $K'' = \pi/128\mu$, where μ is the viscosity of the fluid. Although viscosity was defined by Navier in 1823, Poiseuille himself did not use this term, so that the present-day form of the Poiseuille's relation was completed by Hagenbach who, in 1860, proposed calling it Poiseuille's law. The value of μ derived from K'', which Poiseuille obtained, agrees with currently accepted values to within 0.1%, which illustrates the remarkable precision of his experiments. His quest for the utmost possible precision was motivated in part by the fact that accepted opinion, including that of the authorities of his time, Thomas Young and Claude Navier, held that Q is approximately proportional to D^3.

At about the same time a German hydraulic engineer, Gotthilf Hagen, published in 1839 a paper on the flow of water in cylindrical tubes. Although it is general opinion that the careful and precise experiments of Poiseuille were fully convincing, the law governing fluid flow through a tube is also named the Hagen–Poiseuille law.

It was George Stokes himself who, in 1845, solved the problem of Poiseuille flow as an application of the Navier–Stokes equations, but he did not publish his results because he believed that they conflicted with experiment: he was evidently unaware of Poiseuille's work.

The Navier–Stokes equations are used universally today to describe fluid flow, including velocity profiles in large arteries. The equations are derived from the basic principles of conservation of mass and momentum. The conservation of mass is expressed by the continuity equation

$$\frac{\partial \rho}{\partial t} + \nabla \cdot [\rho \mathbf{v}] = 0\,, \tag{2}$$

where $\rho = \rho(\mathbf{x}, t)$ is the density of the fluid, t is the time, $\mathbf{v} = \mathbf{v}(\mathbf{x}, t)$ the velocity vector, and ∇ is the gradient vector operator. For a scalar function ρ, $\nabla \cdot \rho =$ grad ρ, and for the vector $\mathbf{v}$, $\nabla \cdot \mathbf{v} =$ div $\mathbf{v}$.

Conservation of momentum leads to the equation of motion

$$\rho \left[\frac{\partial \mathbf{v}}{\partial t} + [\mathbf{v} \cdot \nabla] \mathbf{v} \right] = \nabla \cdot \sigma + \rho \mathbf{f}\,, \tag{3}$$

where σ is a stress tensor and $\mathbf{f} = \mathbf{f}(\mathbf{x}, t)$ denotes the body force per unit mass. For a fluid, the stress tensor is

$$\sigma = -p\mathbf{I} + \mathbf{d} \text{ with } \mathbf{I} = \text{unit tensor.} \tag{4}$$

Here, $-p\mathbf{I}$ represents an isotropic part, having the same form as the stress tensor for a fluid at rest with a hydrostatic pressure p, and tensor $\mathbf{d}$ represents the non-isotropic part, caused by the fluid motion. However, to deduce the dependence of $\mathbf{d}$ on the local velocity gradients, it is assumed that d_{ij} is a linear function of the various

components of the velocity gradients and that the fluid is isotropic, called a Newtonian fluid. Under the above assumptions $\mathbf{d}$ is expressed as

$$\mathbf{d} = 2\mu\left[\mathbf{e} - \frac{1}{3}[\nabla\cdot\mathbf{v}]\mathbf{I}\right] \text{ with } e_{ij} = \frac{1}{2}\left[\frac{\partial v_i}{\partial x_j} + \frac{\partial v_j}{\partial x_i}\right], \quad (5)$$

where $\mathbf{e}$ is the symmetrical part of the velocity gradient tensor, known as the rate of strain tensor, and μ is the fluid viscosity depending on the temperature. By substituting (5) into (3), the expression for the velocity is obtained

$$\rho\left[\frac{\partial\mathbf{v}}{\partial t} + [\mathbf{v}\cdot\nabla]\mathbf{v}\right] = \rho\mathbf{f} - \nabla p + \nabla\cdot\left[2\mu\left[\mathbf{e} - \frac{1}{3}[\nabla\cdot\mathbf{v}]\mathbf{I}\right]\right]. \quad (6)$$

Equations (2) and (6) are known as the Navier–Stokes equations for fluid motion. For the case where temperature differences are small enough for the temperature to be taken as uniform over the fluid, and for a fluid that is incompressible, they reduce to

$$\nabla\cdot\mathbf{v} = 0, \quad (7)$$

$$\rho\left[\frac{\partial\mathbf{v}}{\partial t} + [\mathbf{v}\cdot\nabla]\mathbf{v}\right] = \rho\mathbf{f} - \nabla p + \mu\nabla^2\mathbf{v}. \quad (8)$$

A complete analytic solution of the Navier–Stokes equations is in general extremely difficult. Although for most regimes of interest numerical solutions may be obtained, finding them is still a matter of intensive research for many types of fluid. Readers interested in a complete derivation and numerical solution for velocity profiles in large arteries are referred to [10] and the references therein. Based on the Navier–Stokes equations, both laminar and turbulent types of flow are studied. Laminar arises in linear regimes, and turbulent flow results from nonlinear characteristics of the system. Linear flow usually has a Poiseuille velocity profile, while a variety of velocity profiles can be obtained in the case of turbulence. Turbulent flow is observed mainly in large arteries, where pressure gradients and velocities are high, whereas laminar flow is characteristic for most of the small vessels [10,11].

The boundary conditions for the Navier–Stokes equations are complicated, and the initial conditions are difficult to define. A simplified description of the cardiovascular system as a whole might serve to obtain the values of initial conditions. The equations (7) and (8) are obtained on the assumptions that the fluid is incompressible, Newtonian and isothermal—which might seem reasonable approximations, but the vessels themselves undergo dynamic changes in geometry which are not taken into account.

The mechanical approach is based on the assumption that the system is conservative and that it can be characterized by the equations of mass, momentum and energy conservation. The physics of the system is studied locally, with separate parts of the system being considered in isolation. The whole approach needs a very detailed prior understanding of the system in order to be able to provide a good description of the observed behaviour. But the more precisely we try to understand the mechanics of the system, the more detail we need, and the less we are able to consider its global characteristics and to understand the mechanisms involved in one cycle of the blood through the system.

2.2. *Regulation of the heart function*

2.2.1. *Autorhythmicity of the heart.* As already indicated, the heart function consists of two phases: systole, the period of the cycle when the heart is emptying; and diastole, the period when it is filling. In order to function efficiently, the cardiac pumping action must proceed in a coordinated fashion. The coordination is maintained by excitatory signals generated within the heart itself. It was noticed as early as 1777 that arteries contracted and dilated in phase with heart action, but it was not until 1831 that Ernst Weber showed that these were controlled by the same type of nerves [6]. In 1845 Alfred and Ernst Weber obtained evidence that the vagus nerve can inhibit heart action, which had already been suggested by Alfred Volkmann in 1837. Shortly afterwards, the other type of nerves that innervate the heart—the sympathetic nerves—were described by Claud Bernard. When they are severed, the muscles of the heart and vessels become less stiff, causing the vessels to dilate. External stimuli of sympathetic nerves provoke muscle stiffening, or contraction. Those two states are known in physiology as vasodilatation and vasoconstriction, while the continuous constriction and dilation, by which the blood is pushed forward, is known as vasomotion.

Today it is known that the cardiac centres in the pons and in the medulla oblongata, which are both part of the brainstem†, exert a direct influence on the activity of the heart, by way of sympathetic and parasympathetic nerves. The action of the heart is therefore primarily controlled by the autonomous nervous system.

The rhythmic pulsation of the heart is however maintained by excitatory signals‡ generated within the heart

†The brainstem consists of the medulla oblongata, pons and midbrain. The medulla oblongata is an enlarged continuation of the spinal cord extending up into the pons. All nerve fibres linking the brain to the spinal cord, ascending and descending, as well as nerve fibres linking cerebrum to cerebellum pass through the brainstem, thus making it a crossroads of the nerve pathways. Centres of the autonomic nervous system that provide basic control mechanisms for blood pressure, heart and respiratory function are also located in the brainstem.

‡Nerve excitation is the state of automatic, progressive breakdown of its membrane charge, producing a propagating potential, the action potential, along the nerve. Cells in which an action potential can be elicited are called excitable. Excitability is a typical property of nerve and muscle cells.

itself. Under suitable conditions a heart removed from the body will continue to beat at a constant frequency [2]. This occurs through the action of specialized cells of the pacemaker and conducting system (figure 3). The sinoatrial node is the primary pacemaker of the heart, having the highest discharge rate, i.e. the frequency of generating an action potential, based on ion concentration differences across the membrane. The mechanism by which the action potential is generated and propagated through the tissue is however beyond the scope of this article. Readers interested in it are referred to [2,7].

The parasympathetic nerves branch off from the vagus nerves on both sides of the cervical region in the spinal cord. The right branch of the vagus nerve goes to the right atrium, where it is concentrated at the sinoatrial node (SA), while the left branch goes to the atrioventricular node (figure 3). Accordingly, stimulation of the right vagus predominantly effects the heart rate. Externally applied electrical stimuli to the cardiac vagi does slow the heart. It may reduce the cardiac output, or even stop the heart, but these effects are due to vagi slowing or stopping the generation of the stimuli by the SA node. When the body is at rest, the SA node drives the heart at a rate of about 60 impulses/min. The left vagus effects the velocity of transmission of electrical impulses from atria to ventricles and thus the time between the atrial and ventricular contraction. In this way the left vagus also influences the heart rate. There is only sparse parasympathetic innervation of ventricles. Its role there is indirect and serves to inhibit the sympathetic action.

The sympathetic nerves come from the upper thoracic segments of the spinal cord. They are uniformly distributed

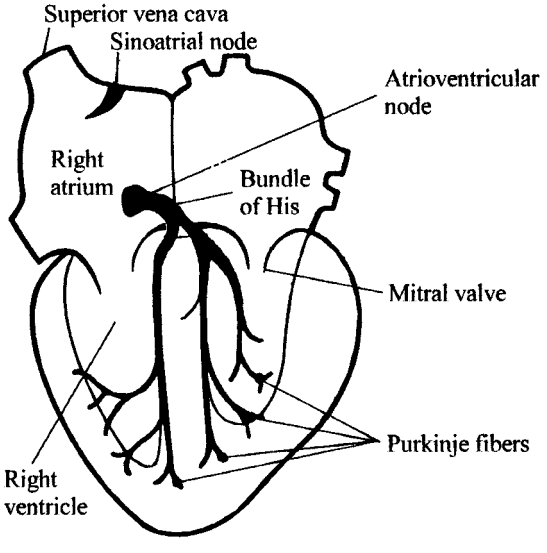

Figure 3. The pacemaker and conducting system of the heart as seen in the frontal section. Modified from [2], with permission.

to all parts of the heart. Their activity increases the heart rate by increasing the rhythmicity of the SA node and, more importantly, they increase the strength and speed of contraction of muscles in both atria and ventricles. In biological emergencies, such as flight, fright or fight, an increase in sympathetic activity is of vital importance to the organism in securing maximal mobilization of the pumping mechanisms of the heart [1].

2.2.2. *Electrical and mechanical action of the heart.* After the electrical nature of the excitation of smooth muscles in the heart and the vessels was appreciated, attempts were initiated to record the corresponding electrical signals. Using a galvanometer, Carlo Matteucci showed in 1838 that the heart muscle generated a measurable electric charge. In 1903 William Einthoven modified the string galvanometer to record continuously the electrical activity of the heart, creating what was effectively an early electrocardiograph (ECG). Both the characteristics of the electrical activity in the heart, and their mechanisms, have been intensively studied since then and standards have been established to make the ECG universally useful [2].

The electrical potentials can be detected by electrodes placed at various points of the body. The basic bipolar limb leads, named I, II and III, as proposed by Einthoven, are based on the triangle formed by the shoulders and the crotch. The electrical signal is obtained as a difference of potentials sensed by plus and minus electrode with respect to the third electrode, giving a ground potential. A typical signal obtained by electrodes on both shoulders and one below the heart, from one of the so-called precardial leads [2], is presented in figure 4. Each portion of the ECG represents electrical activity in a particular part of the heart, and the specific peaks were denoted as P-Q-R-S-T, the R-peak being the maximal value in most of the electrode configurations.

The standard analysis considers the time interval between the characteristic peaks, obtained after averaging over some number of beats. By convention, P and T are named waves, and the distance between two waves is called a segment, while an interval comprises both waves and segments. From the ECG curve an atrial and a ventricular part can be distinguished, as well as the states when valves are open or closed. During the P wave the excitation spreads over both atria, and within the PQ segment the atria as a whole continue to be excited. The QRS complex corresponds to the excitation of both ventricles, and the T wave reflects recovery from the excitation of the ventricles.

The states of mitral valve, the valve between left atrium and ventricle, and the aortic valve, the valve between left ventricle and aorta, are presented in figure 4. The mitral valve closes at the R-peak and at the end of QRS complex the aortic valve opens. The blood is then ejected into the aorta. This phase is named systole.

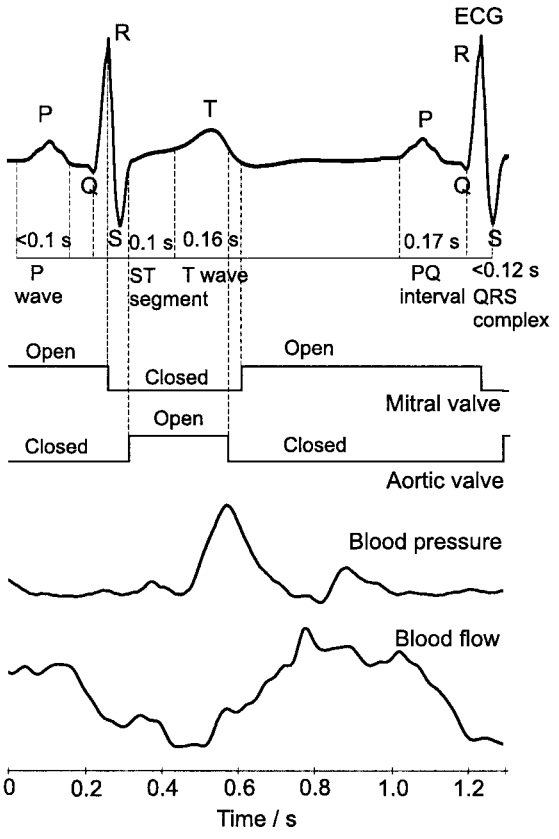

Figure 4. A typical signal from the electric activity of the heart together with the corresponding states of mitral and aortic valves (top), the blood pressure (middle) and the peripheral blood flow (bottom) during one pumping cycle of the heart.

At the end of the T wave the aortic valve closes and shortly after the mitral valve opens to allow the passage of blood from ventricles to atria. This is the phase of filling or diastole. Similar phases occur also in the right heart with the ejection period being initiated slightly earlier and the systole slightly later. These time differences are relatively small (of the order of 10–30 ms) and have no particularly effect on the dynamics of blood flow. The corresponding valves in the right heart are named tricuspid and pulmonary valves. The tricuspid and mitral valves are also named atrioventricular (AV) valves, while the aortic and pulmonary valves are named arterial valves.

The excitatory events described above govern the mechanical activity of the heart by causing the contraction of muscle cells in the heart, known as myocardial cells. Opening and closing of the valves is brought about by pressure changes in the adjacent heart cavities or vessels. The motion of the valves in turn affects the mode of contraction of the myocardium. When the intraventricular pressure exceeds the arterial diastolic pressure of $\sim$10 kPa in the aorta and $\sim$1.2 kPa in the pulmonary artery, both arterial valves open and blood begins to be expelled. The intraventricular pressure continues to rise, until it reaches its maximum of 16 kPa in the left and 2.7 kPa in the right ventricle. Towards the end of systole it falls again. The flow of blood through the system is driven by the pressure difference. Its value depends on the side of the system, being higher in the arterial side, and varies with respect to the size of the vessels. On the capillary side it is modulated by both the central and the peripheral mechanisms. In figure 4 one cycle of the electrical activity of the heart together with the arterial pressure and the blood flow through a capillary bed in the skin of a human hand is presented. The electrical activity results in a pressure wave that drives the flow of blood through the system.

2.2.3. *Heart rate variability.* Thus far, we have discussed the mechanism of a single heart cycle. The time between two successive R-peaks, i.e. the period of a complete heart cycle, is however not constant, but rather varies in time. In their pioneering work Hyndman *et al.* [12], Sayers [13] and Chess *et al.* [14], in the 1970s, focused attention on the existence of physiological rhythms imbedded in the beat-to-beat heart rate signal.

By plotting the inverse value of the time between two successive R-peaks, the instantaneous heart rate (IHR), as a function of time, a new time series is generated (figure 5).

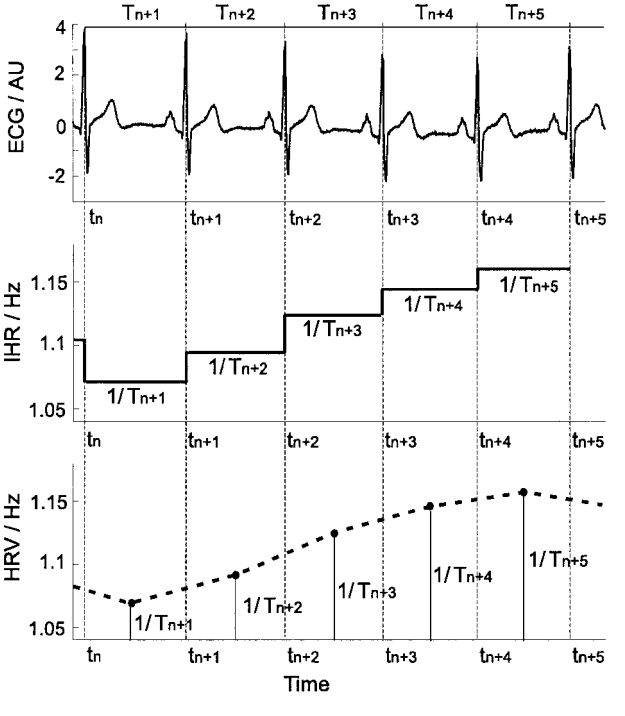

Figure 5. Steps in derivation of the heart rate variability (HRV) signal.

However, the signal that we derive is discrete and not continuous and has a variable sampling time (figure 5). After interpolation the signal named heart rate variability (HRV) is obtained. Numerous methods of interpolation have been proposed, but they all influence spectral components in various ways. The analyses that we present below are obtained by linear interpolation between two IHR values (figure 5). The signal is than re-sampled with a constant sampling time of 0.1 s.

Among all physiological signals, HRV is the one least influenced by movement artefacts, or by instrumental noise. It has also an additional advantage. While the measurements of most physiological signals are inevitably influenced by interference from other physiological processes, the value of the R-peak corresponds to the pumping cycle of the heart and determines precisely a distinct moment of the heart beat.

Akselrod *et al.* [15] were the first to introduce spectral analysis of the HRV signal to evaluate quantitatively the beat-to-beat cardiovascular control. Since then, HRV has been analysed extensively using the Fourier transform of the signal itself, or its autoregressive model, i.e. non-parametric and parametric methods (see [16] and the references therein). The linear frequency analysis is based on the assumption that it is possible to decompose a time series into the finite number of periodic sinusoidal functions with different frequencies and phases. The Fourier spectrum of the ECG, recorded for 20 min on a healthy, resting subject is presented in figure 6a.

When the shape of the original time-series is non-sinusoidal, higher harmonic components of the fundamental frequency are necessary to reconstruct the function. Thus the spectrum of an ECG consists of a fundamental frequency of $\sim$1 Hz (60 beats per minute), and components at higher integer multiples of this basic frequency, i.e. at 2 Hz, 3 Hz, etc, as can be seen in figure 6a. As already mentioned, the heart rate in a healthy subject varies, which is why its basic frequency is not sharp. The nature of its variability can be studied by analysing the HRV signal. Its Fourier spectrum is presented in figure 6*b*. Because of the discrete nature of the events the basic sampling rate of the HRV is inherently the heart rate itself, and consequently this provides maximum frequency in the HRV spectrum. The highest frequency in the spectrum, $f_{\max}$ is determined by the sampling frequency, $f_s = 1/t_s$, and the relation $f_{\max} = f_s/2$. For example, if the heart rate is $\sim$1 Hz, then $f_{\max}$ in the HRV spectrum is $\sim$0.5 Hz.

The peaks in the HRV signal correspond to the periodic processes that modify the basic heart frequency. It has already been recognized that the information contained in the HRV signal is of great clinical and physiological importance. Different diseases were shown to manifest themselves in a specific way in the HRV spectrum. Recently, standards of measurement, physiological interpretation and clinical use of the HRV were proposed [17]. It has been suggested that a sampling rate between 250 and 500 Hz is optimal to record the shape of the ECG curve and define the R-peak. The importance of the time of observation is also pointed out. The recording is recommended to last at least 10 times the period of the lower-frequency bound of the investigated component, but should not be substantially extended beyond this in order to ensure the stationarity of the signal. Two different types of measurements were suggested: short-term (5 min) and long-term (24 h) recordings. Three main frequency domains are distinguished in the short-time recordings: (i) high frequency (HF) range, 0.15–0.4 Hz, (ii) low frequency (LF) range, 0.04–0.15 Hz, and (iii) very low frequency (VLF) range, $\leq$0.04 Hz. From the long-term recordings the VLF range is defined from 0.003 to 0.04 Hz, and for the

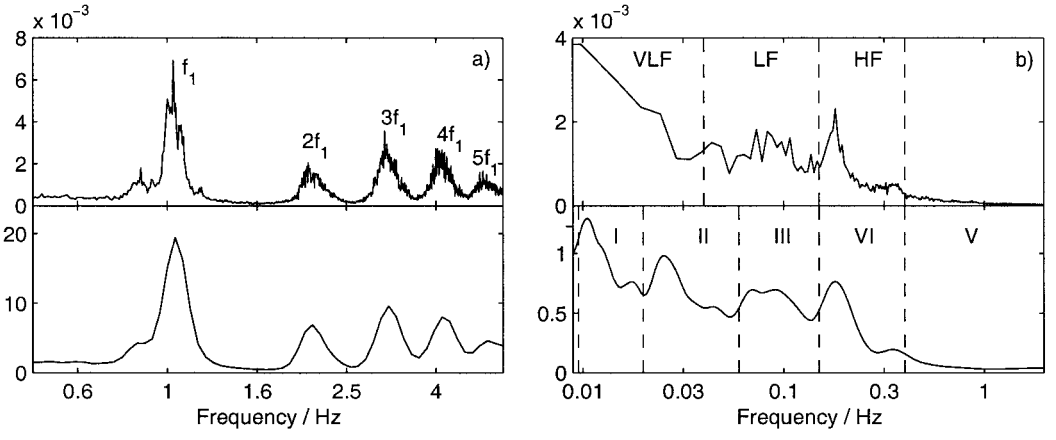

Figure 6. Fourier (top) and wavelet (bottom) transforms of (*a*) the ECG and (*b*) HRV signals. The Fourier spectra are obtained as an average of spectra calculated for 200 s time segments, shifted along the signal for 100 s. The wavelet transform is also averaged in time, obtained with (*a*) $f_0 = 3$ and (*b*) $f_0 = 1$.

frequencies $\leq$0.003 Hz an ultra low range (ULF) was defined. These frequency domains in the HRV spectrum, calculated using Fourier transform, are presented in the top section of figure 6b.

The physiological origin of the periodic processes involved in the modulation of the heart rate is not well understood. It has been proposed that vagal activity is the major contributor to the HF component, while disagreement exists in respect to the LF component. It is considered either as a marker of sympathetic modulation or, alternatively, that it includes both sympathetic and vagal influence. The physiological interpretation of the lower-frequency components warrants further elucidation (see [17] and the references therein). This interpretation is however based on considering only the electrical activity of the heart muscles and is focused on understanding the nerve function that is involved in the observed fluctuations of the heart rate.

As early as 1733, Hales observed that changes in blood pressure and heart rate were related in a regular manner to the respiratory pattern in the horse [18]. Ludwig's invention of the kymograph allowed his observation in 1847 that the dog heart rate increased on inspiration and decreased on expiration [19]. This phenomenon is known as 'respiratory sinus arrhythmia' and is interpreted as a dynamic response of the heart achieved by central nervous modulation of the input to the sino-atrial node. Here, we would like to stress the importance of distinguishing the quantities that are regulated, which are blood pressure and flow, as well as a vessel's resistance and conductance, and the way that information about their values is transmitted. It is the nervous system that conveys the information about these quantities, derived from mechanical and chemical sensors at various points within the cardiovascular system. In general, the function of all nerve cells in the body is to receive information, to carry it to other parts of the system, to compare it to other information, and finally to control the function of other cells. That is why they operate on smaller time scales, than for example the scale on which the blood is distributed through the body [20].

In attempting to understand the function of physiological systems, one of the greatest difficulties is to recognize the distinction between cause and effect. The functioning of the cardiovascular system results from an interplay of a variety of mechanisms that serve to keep the values of pressure and flow within certain limits. Therefore, in the pages that follow we will present our understanding of the physics of the cardiovascular system on the assumption that the quantities characterizing its function are mechanical, while the electrical activity of the nerves serves for communication within the system. Because an understanding of the physiological origin of the periodic events that contribute to heart rate variability is of central importance for a physical as well as a mathematical representation of the system, we will turn once again to this question.

3. Frequency analysis of cardiovascular signals

The heart rate variability signal allows us to observe the function of the heart in time. By extracting the information that it contains, the basic principles of heart function may be studied under normal conditions as well as in perturbed states. However, we cannot apply classical perturbation theory directly, but rather must observe its function after reversible perturbations, such as physical exercises and application of vasodilator substances, or after irreversible perturbations resulting from diseases.

The HRV signal allows for observations of the function of the cardiovascular system from a central viewpoint (at the heart itself). Later in this section we shall introduce another signal derived from flow through the vascular bed, namely the peripheral blood flow. This signal provides a peripheral view—from one of the places where blood exchanges substances with the cells—of the dynamics of the cardiovascular system.

The time of observation is of crucial importance in determining the type and amount of information that can be extracted from a signal. As we have already stated, our goal is to understand the dynamics of one cycle of the blood through the cardiovascular system. As it takes approximately one minute, and its dynamics is not strictly periodic, we have chosen the observation time to be 20 min.

3.1. *Methods of analysis*

The existence of rhythmic activity in the HRV signal has already been pointed out, so we shall start with an analysis of the cardiovascular system in the frequency domain. Let us first discuss the Fourier transform in more detail.

3.1.1. *Fourier transform.* A physical signal (with finite energy) may be presented in either time or frequency domains. The Fourier transform

$$G(f) = \int_{-\infty}^{\infty} g(t)\, \exp(-\mathrm{i}2\pi f t)\, \mathrm{d}t \tag{9}$$

and its inverse

$$g(t) = \frac{1}{2\pi}\int_{-\infty}^{\infty} G(f)\, \exp(\mathrm{i}2\pi f t)\, \mathrm{d}f\ , \tag{10}$$

are the mathematical tools which connect the two domains [21]. The representation in the frequency domain $G(f)$ consists of an amplitude and corresponding phase for each frequency f. The power spectrum of the function $P(f) = |G(f)|^2 + |G(-f)|^2$ gives the power (energy density in the frequency domain) in a given frequency interval between f and $f + \mathrm{d}f$.

When a time series of finite length $T = Nt_s$ sampled at discrete points nt_s is considered, the calculation of the Fourier transform reduces to a finite sum over all measured values. The resultant discrete Fourier transform (DFT)

$$G(f_k) = \sum_{j=0}^{N-1} g(jt_s) \exp(-i2\pi jk/N) \qquad (11)$$

is O ... defined only for discrete frequencies $f_k = k/T$, $k = N-1$. The finite length of the signal bounds the frequency resolution ($\Delta f = 1/T$) and the lowest detected frequency whilst finite sampling time determines the upper frequency limit ($f_{max} = 2/t_s$). Since the sum is taken over finite time, the signal is assumed to be periodic with period T. A frequency between any f_k and f_{k+1} will contribute to all $G(f_k)$, known as leakage [22]. To reduce leakage, the original signal is windowed. The choice of the transform window is a compromise between making the central peaks as narrow as possible versus making the tails fall rapidly. Thus it is the window length and shape that then determines the frequency resolution.

Spectral properties of measured signals are commonly estimated by the periodogram

$$P(f_k) = \frac{1}{N^2}|G(f_k)|^2, \quad k = 0, k = N/2,$$

$$P(f_k) = \frac{1}{N^2}(|G(f_k)|^2 + |G(f_{N-k})|^2), \quad k = 1, \ldots, N/2 - 1. \qquad (12)$$

The normalizing factor in the periodogram estimate is chosen in such a manner that the sum of all $P(f_k)$ equals the average square value of the original time series.

Fourier transforms of the ECG and HRV signals presented in figure 6, are obtained as average periodograms, calculated from 160 s time segments, taken at a regular intervals of 80 s.

3.1.2. *Wavelet transform.* The representation of time series in the frequency domain bears no information about the time. Namely, the Fourier transform (9) and its inverse (10) reproduce the time series as a superposition of periodic functions. These have sharp peaks in the frequency domain, but are spread over all time. If a characteristic frequency varies with time, the corresponding peak will be broader than its instrumental width as determined by the data window.

The time-varying nature of characteristic frequencies in the cardiovascular signals demands an analysis in the time-frequency domain. Yet, the relatively broad frequency band within which characteristic peaks are expected raises a problem in relation to time and frequency resolution. In the time-frequency analysis, a window of fixed length is shifted along the signal to achieve time localization and the frequency content of each window is evaluated. The window length introduces a scale into the analysis and determines the time and frequency resolution. By the uncertainty principle, sharp localization in time and frequency are mutually exclusive. Therefore, the choice of window length is in practice a trade-off between time and frequency resolution. If both low and high frequencies with different time spans are to be detected simultaneously in a signal, a suitable choice is very difficult. This is the problem Morlet was facing while analysing seismic data, which comprised different features in time and frequency. To overcome the shortcomings of the Fourier method he came up with the basic idea of wavelet analysis in 1983 [23]. Later, Grossman and Morlet laid the mathematical foundations of the wavelet transform technique [24].

Wavelet analysis is a scale-independent method. As in the windowed Fourier transform, one begins with a window function, called a mother wavelet $\psi(u)$. This function introduces a scale (its width) into the analysis. Commitment to any particular scale is avoided by using not only $\psi(u)$, but all possible scaling of $\psi(u)$. The mother wavelet is also translated along the signal to achieve time localization. Thus, a family of generally non-orthogonal basis functions

$$\Psi_{s,t} = |s|^{-p}\psi\left(\frac{u-t}{s}\right). \qquad (13)$$

is obtained. The parameter p is an arbitrary non-negative number. The prevailing choice in the literature is $p = 1/2$ [25]. In this case, the norm of the wavelet $||\psi||$ and thus its energy is unaffected by the scaling operator.

The continuous wavelet transform of a signal $g(u)$ is defined as

$$\tilde{g}(s,t) = \int_{-\infty}^{\infty} \bar{\Psi}_{s,t}(u) g(u)\, du. \qquad (14)$$

The wavelet transform $\tilde{g}(s,t)$ is a mapping of the function $g(u)$ onto the time scale plane. The interpretation of $\tilde{g}(s,t)$ depends on the mother wavelet being used.

Not every function can be used as the mother wavelet. Only those that enable us to reconstruct the original function $g(u)$ from its wavelet transform $\tilde{g}(s,t)$ are admissible. The sufficient condition for the reconstruction [25] is

$$\int_{-\infty}^{\infty} \psi(u)\, du = 0. \qquad (15)$$

The total energy of the signal $g(u)$ can be calculated as

$$||g||^2 = C^{-1} \int \int_{\Re^2} |s|^{2p-3} |\tilde{g}(s,t)|^2\, ds\, dt, \qquad (16)$$

where the constant C is determined by the shape of the mother wavelet. The function

$$\rho = C^{-1}|s|^{2p-3}|\tilde{g}(s,t)|^2 \qquad (17)$$

can therefore be interpreted as the energy density of the signal in the time scale plane [26]. It is often called a scalogram.

In numerical applications, the scale s and time t are restricted to discrete values only. The natural discretization of the scaling parameter is $s_m = \sigma^m$, where $m \in \mathbb{Z}$ and the step $\sigma \neq 1$. Within the scale σ^m the signal is sampled only at times $t_n = n\sigma^m\tau$, $\tau > 0$, which means that the sampling rate is automatically adjusted to the scale.

For certain mother wavelets, orthogonal basis can be obtained by using $\sigma = 2$, resulting in a special application of the wavelet transform, known as multi-resolution analysis (MRA). The original signal, sampled at t_s, is split into a 'blurred' version on a coarser time scale $2t_s$ and a detail on scale t_s. This process is then repeated, giving a sequence of more and more blurred versions together with details removed at every scale. Several applications of MRA to cardiovascular signals were reported [27,28], mainly to capture the main features of the signal.

In this paper, we follow instead the original idea of Morlet. By choosing $\sigma = 1.05$, and a mother wavelet well concentrated in both time and frequency, we can detect precisely the frequency content in a given time interval. Morlet proposed the use of a Gaussian function, modulated by a sine wave. In the time domain, it is written as

$$\psi(u) = \pi^{-1/4}\left[\exp(-\mathrm{i}2\pi f_0 u) - \exp(-2\pi f_0^2/2)\right]\exp(-u^2/2)\,. \tag{18}$$

The choice of f_0 is a compromise between localization in time and in frequency. For smaller f_0, the shape of the wavelet favours localization of singular time events, whilst for larger f_0 more periods of the sine wave in the window make the frequency localization better. For $f_0 > 0.8$, the value of the second term in (18) is so small that it can be ignored in practice and a simplified expression for the Morlet wavelet in the time domain is

$$\psi(u) = \pi^{-1/4}\exp(-\mathrm{i}2\pi f_0 u)\exp(-u^2/2)\,. \tag{19}$$

The corresponding wavelet family consists of Gaussians, centred at time t with standard deviations s. In the frequency domain we have Gaussians with a central frequency $f = f_0/s$ and a standard deviation of $1/2\pi s$. Therefore, the wavelet transform at a given scale s can also be interpreted as band-pass filtering giving an estimation of the contribution of the frequencies in this band. The relation between the scale and the central frequency for the Morlet wavelet is

$$f = \frac{f_0}{s}\,. \tag{20}$$

The frequency resolution changes with frequency: at low frequencies (large scales) the resolution is better than at high frequencies (small scales). Accordingly, the time resolution is better for high than it is for low frequency components. In order for peaks to be detected at f_1 and f_2 ($f_1 > f_2$), they must be separated by at least one half of the standard deviation of the peak at the higher frequency, namely $f_1 - f_2 \geq f_1/4\pi f_0$. The choice of f_0 thus determines the current frequency resolution. We have taken $f_0 = 1$.

The wavelet transform contains information on amplitude, frequency and time. In figure 7 the absolute value of the wavelet transform of the HRV signal in the time-frequency plane is presented. However, it is difficult to capture all this information at once, especially since several almost periodic phenomena are present. Their amplitudes and frequencies also vary in time. Therefore, various two-dimensional projections are used. We will use scalograms averaged over time to compare wavelet transforms obtained from different signals, in different subjects and under different conditions. An averaged scalogram of the HRV signal is presented in the lower part of figure 6*b*. Compared to the spectrum calculated by Fourier transform, the low frequency resolution is improved, allowing us to define the frequency intervals for the characteristic processes more precisely. By providing an improved estimation of the frequency content of the HRV signal, a better understanding of the physiological mechanisms of the oscillatory processes involved becomes possible. To gain new insight into those processes, we now present analyses of the peripheral blood flow, measured simultaneously with other cardiovascular signals.

3.2. *Cardiovascular signals*

Today several measurement techniques enable non-invasive, continuous, observation of a number of other cardiovascular functions in addition to the electrical activity of the heart. A sensor based on piezoelectric properties of some crystals can be used for pressure recordings in larger vessels. The same principle is used to follow the movements of the thorax in the inspiration and expiration phases of lung function. The Doppler principle

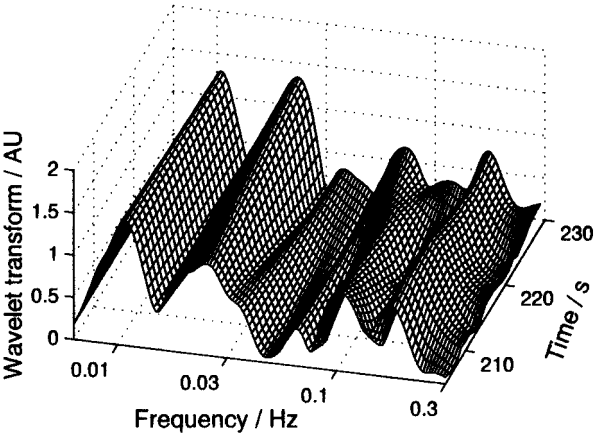

Figure 7. The wavelet transform of the HRV signal in the time-frequency plane.

allows for measurements of blood flow velocity. The tissue under observation is bathed in either ultrasound or coherent light. Ultrasound penetrates deeply, however, so that it can not be directed selectively. That is why, when ultrasound based instruments are used clinically to measure blood flow velocity, they are restricted to large vessels.

For peripheral blood flow measurements optical sensors with wide dynamic range are used. The laser light can be directed into a very small area. Its depth of penetration is smaller than that of the ultrasound and it can be controlled by selecting the wavelength and emitted power. Thus, it can detect blood flow in the capillary bed. As already mentioned, this is where matter and energy are exchanged between the blood and tissue cells, so that we may expect all processes involved in blood flow regulation to be reflected in the corresponding signal.

3.2.1. *Peripheral blood flow.* Only four years after the first working laser was demonstrated by Maiman in 1960 [29], Cummins *et al.* [30] proposed a method of measuring the velocity of particles in solution by interpretation of the Doppler-frequency-shifted light. Some years later, Riva *et al.* [31] applied this technique to the measurement of red blood cell velocities in the glass tube flow model. However, it was Stern [32] who first used the laser Doppler technique for blood perfusion measurement in the undisturbed microcirculation in 1975. Nilsson *et al.* [33,34] subsequently provided detailed technical and experimental evaluations of the technique.

The near-infrared laser is frequently used to measure the velocity and concentration of red blood cells within a hemisphere of volume $\sim 2\,\mathrm{mm}^3$. A fibre-optic probe carries a beam of laser light which is then widely scattered and partly absorbed by the tissue. Light scattered from moving blood cells undergoes a Doppler shift in the wavelength while the wavelength of light scattered from static objects remains unchanged (figure 8). The magnitude and frequency distribution of the wavelength changes are related to the number and velocity of blood cells. The back-scattered light is collected by a fibre and converted into an electrical signal. This signal is proportional to the flow but unrelated to the direction of blood cell movement.

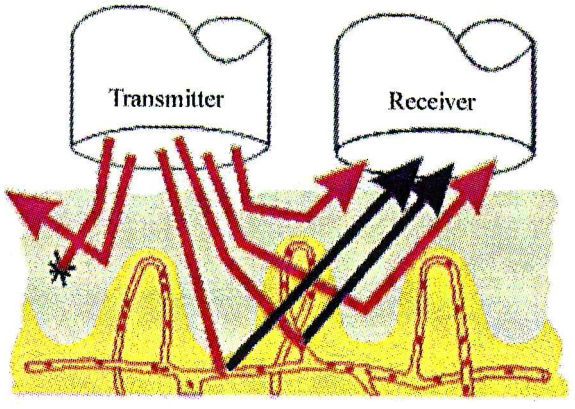

Figure 8. Sketch showing how a beam of laser light is scattered and absorbed in the tissue. From [35], with permission.

This technique of blood flow measurement is limited by the fact that in the case of occlusion, i.e. stopping of the flow through the measured area, there is a residual value called the 'biological zero', as illustrated in figure 9. Even during occlusion some blood remains in the area under observation. It is the random Brownian movement of the remaining red blood cells that results in this residual value. As a result, the flow cannot be expressed straightforwardly in absolute units (e.g ml/s/mm^3), but only in arbitrary units (AU). To obtain an absolute measure, the value of the biological zero has to be determined for every measurement.

We show in figure 9 that during occlusion the oscillations vanish completely. Moreover, the detection of oscillatory changes in the flow is not influenced by the lack of absolute units, as long as we provide a calibration with a reference value. The problem of biological zero is therefore irrelevant to our quest for information about the oscillatory nature of the peripheral blood flow. From figure 9 we can also see that the amplitude of oscillations is comparable in magnitude to that of the steady flow on which they are superimposed, immediately demonstrating the importance of the oscillations in characterizing the dynamics of blood flow.

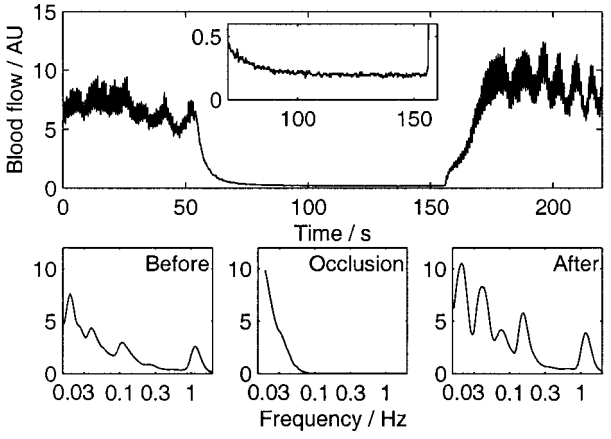

Figure 9. The peripheral blood flow (top) and its wavelet transforms (below), before, during and after occlusion of the vessels proximal to the measurement site. An apparent residual flow, named the 'biological zero' remains during occlusion, whereas the oscillations vanish. The amplitude of oscillations, before and after occlusion, is comparable in magnitude to that of the steady flow on which they are superimposed, demonstrating the importance of the oscillations in characterizing the dynamics of blood flow.

Even in the early analyses of laser Doppler blood flow recordings [34,36], the oscillatory nature of the flow was noted. Hoffman *et al.*, using a frequency histogram, reported oscillations, synchronized with the heart rate and also oscillations in the HF and LF range [37]. Both windowed Fourier and wavelet analyses of signals recorded for 20 min revealed five characteristic frequencies in the interval from 0.0095 Hz to 2 Hz [38,39]. The characteristic peaks typically appear around 1 Hz, 0.3 Hz, 0.1 Hz, 0.04 Hz and 0.01 Hz, almost at the same frequencies as those discussed above: the first one in the ECG spectrum and the latter four in the spectrum of the HRV signal.

The energy of each particular oscillation varies with the vessel's diameter and network density, i.e. the local flow resistance. There are two possibilities for making the signals comparable in terms of energy. One is a quantitative assessment of the resistance in the adjacent network, where the flow is measured. At present, a reliable, non-invasive technique is unfortunately not available. The other possibility is to choose measurement sites where, based on anatomical evidences, similar vessel resistance is expected. When the blood flow is measured on the sites with similar resistance, the contribution of each oscillatory process does not depend on the measurement site, or time of the measurements [39]. In figure 10 the energy within

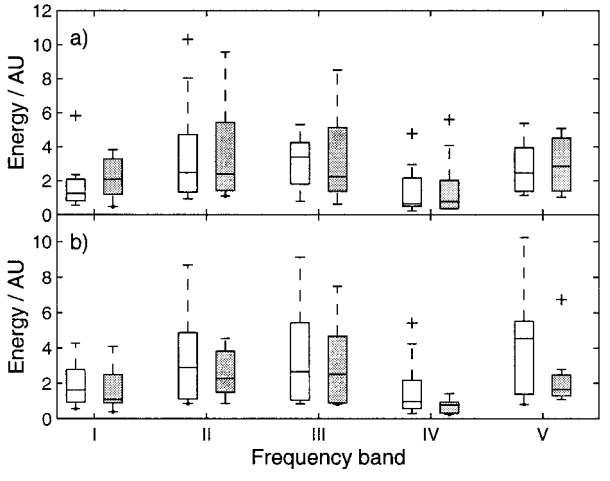

	Frequency band	Origin
I	0.0095 – 0.02 Hz	metabolic
II	0.02 – 0.06 Hz	neurogenic
III	0.06 – 0.15 Hz	myogenic
IV	0.15 – 0.4 Hz	respiratory
V	0.4 – 2 Hz	heart

Figure 10. (*a*) Time and (*b*) space invariance of the oscillatory components of the peripheral blood flow, measured in the areas where the vessels have similar density and resistance. For details, see text.

intervals around each of the five peaks (labelled I–V) is presented for two sets of measurements: (a) simultaneous measurements on two different sites and (b) two consecutive measurements on the same site. We have shown that no statistically significant difference exists and therefore that the energy of each interval can be taken as time and space invariant. We will address the question of interval bounds and statistical presentation later in section 3.2.4.

3.2.2. *Simultaneous measurements.* In searching for the physiological origin of the oscillations observed in the ECG, HRV and peripheral blood flow we made *simultaneous* recordings of several cardiovascular functions [38,40,41]. Signals of cardiovascular origin were measured on healthy young male subjects. During the measurement the subjects were lying still on a bed and they were asked to relax. The ECG and blood pressure were sampled at 400 Hz, while a sampling rate of 40 Hz was used for respiration and blood flow signals. The recordings lasted 20 min. Before evaluating the frequency content the trend was removed from all signals and all but ECG were resampled to 10 Hz. The left part of figure 11 presents a 25 s segment of the respiration, ECG, HRV, blood pressure and peripheral blood flow on the right arm and the right leg after pre-processing. The blood pressure was recorded on the index finger of the left hand, while the sensors for blood flow measurements were placed over the bony prominences, of the wrist and ankle joint.

The peaks of the average wavelet transforms appear at similar, in some cases even at exactly the same, frequencies in all measured signals (figure 11, right). Differences exist, however, in the amplitudes of the oscillations. For the ECG and blood pressure signals the amplitude of the heart beat frequency dominates the spectrum. The spectrum of a respiratory signal has one dominant peak, at $\sim$0.2 Hz. In the HRV signal this peak is of comparable amplitude to those of slower oscillation between 0.0095 Hz and 0.15 Hz. In the signal of peripheral blood flow the amplitudes of all oscillations are of the same range. Hence, we can see that the peripheral blood flow reflects the activities of both the local and the central mechanisms of cardiovascular regulation.

3.2.3. *Physiological nature of oscillations.* Not all of the observed oscillations are yet understood in physiological terms. Those that can be selectively observed—the heartbeat and respiration—are of course relatively well understood. In other cases only indirect evidence is available, and we will see that the position is less clear.

The basic frequency in the ECG signal, around 1 Hz corresponds of course to the heart rate. At rest, its value ranges from 0.6 Hz in sportsmen to 1.6 Hz in subjects with impaired cardiovascular systems. The heart's pumping activity is manifested in every single vessel and is also

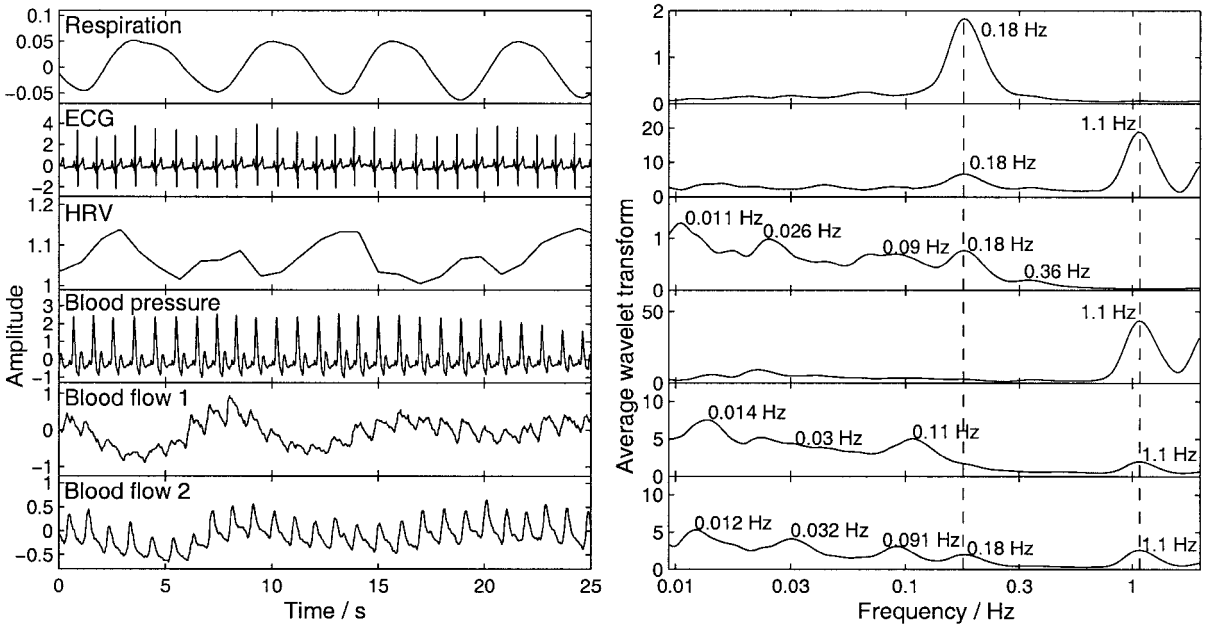

Figure 11. Simultaneously measured cardiovascular signals (left) and their wavelet transforms (right). HRV is in Hz, other values are in arbitrary units.

present in the microcirculation through the capillary bed. It is highly dominant at the outlet of the heart, as well as in the larger vessels. Its contribbution gradually diminishes with decreasing vessel diameter. The elasticity of the vessels, and their structural properties, also affect the magnitude of this flow component.

The spectral peak at around 0.2–0.3 Hz, corresponding to 12–18 events per minute, well known in physiology as the breathing frequency [2]. The existence of respiratory modulation of the heart rate has long been recognized [18]. This frequency, observed earlier in the HRV and blood pressure signals, was designated [12,15,42] as the HF interval, and attributed to the parasympathetic autonomous control. In the peripheral blood flow signal the respiratory origin of this peak was discussed by Hoffman *et al.* [37]. By simultaneous recordings of both respiratory and blood flow signals, direct evidence was also obtained [38,43].

In early analyses of the blood pressure and HRV signals, oscillations with periods of $\sim$10 s were associated with blood pressure regulatory mechanisms [12,42]. Since then several pieces of indirect evidence as to their local origin have been reported. These oscillations are a manifestation of the myogenic activity of the smooth muscle cells displaced in the walls of resistive vessels. The smooth muscle cells respond continually to changes in the intravascular pressure [44]. This response is mediated by oscillations in the ion concentrations, mainly Ca^{++}, across the membrane of vascular smooth muscles. For isolated vessels, the myogenic origin of these oscillations was demonstrated either by measuring dynamically the diameter changes of vessels [45], or ion concentrations [46], though not in humans. In figure 11 the peak around 0.1 Hz is clearly visible in both blood flow signals, the frequency of the peak typically being higher on the hands than on the legs.

The peak of $\sim$0.04 Hz was observed in both the HRV and blood pressure signals [41,42] and in the peripheral blood flow signal [38]. It is attributed either to metabolic [42], or to neurogenic processes. Although these oscillations cannot be selectively measured, indirect evidence for their origin was reported by Kastup *et al.* [47]. After disconnecting nerves from the vessels, known as denervation, which suppresses the neurogenic regulation of the vessel radius, they observed that the $\sim$0.04 Hz oscillations disappeared. This peak can be detected in the averaged scalograms of all simultaneously measured signals presented in figure 11. It usually appears smeared due to the variation of its period with time.

Long recordings and good frequency resolution also enabled us to isolate a peak at $\sim$0.01 Hz. We have found it in all cardiovascular signals, although its exact position differs from one to another, suggesting that it is of local origin. There is indirect evidence [48] that this oscillation is related to the endothelial function. Moreover, some experiments suggest that nitric oxide, a metabolic substance

that is released from endothelial cells, has an influence on the state of contraction of the vessel musculature. Recent studies demonstrate that nitric oxide plays an essential immunological and citotoxic role in the human organism. The reader seeking physiological insight into the involvement of this substance in the dynamics of blood flow are referred to [49] and the references therein.

3.2.4. *Frequency bands and quantitative measures.* The positions of the spectral peaks change with time and also differ from one subject to another. For every peak, however, a frequency interval exists within which it is found in all subjects. The local minima of the average wavelet transform, were used to divide the frequency band between 0.0095 Hz and 2 Hz into five intervals.

The intervals defined in figure 6*b* differ from the recommended standards for heart rate variability [17]. The frequency resolution of the wavelet transform enabled us to detect several peaks in the VLF interval ranging from 0.003 to 0.04 Hz, of which two were above 0.0095 Hz. Therefore, we have split this part of VLF interval into (I) from 0.0095 Hz to 0.002 Hz where, according to our studies [48,49], the metabolic process is manifested and (II) from 0.02 Hz to 0.06 Hz, where the neurogenic process is manifested [47]. The interval (III) from 0.06 Hz to 0.15 Hz, where the myogenic process is most probably manifested, corresponds to the LF interval; however, its lower bound was set to 0.06 Hz since a peak around 0.04 Hz was detected. Interval (IV) from 0.15 Hz to 0.4 Hz on which the respiratory activity, measured simultaneously, has its dominant peak is the same as the HF interval, while the last interval, (V) from 0.4 Hz to 2 Hz is the interval of heart frequency.

These intervals were chosen based on over 500 scalograms of around 100 subjects, either healthy subjects, athletes, or subjects with some cardiovascular impairment. Nevertheless, a revision of the boundary values using, for example, higher order spectral analysis is needed. The identification of high harmonics and linear combinations of basic peaks could provide better distinction between the peaks.

The intervals were chosen in such a way that the peak corresponding to any given physiological prosess is always in the same interval. Thus, we can roughly ascribe the energy within one interval to the activity of that process, and we can thus obtain a quantitative measure of process oscillations [39], which can be used to compare different signals.

According to equation (17), the physical quantity behind the scalogram is the energy density. The average energy in a given frequency band $\mathcal{E}_i(f_{i1},f_{i2})$ is

$$\mathcal{E}_i(f_{i1},f_{i2}) = \frac{1}{t}\int_0^t \int_{1/f_{i2}}^{1/f_{i1}} \frac{1}{s^2}|\widetilde{g}(s,t)|^2 \,\mathrm{d}s\,\mathrm{d}t\,. \qquad (21)$$

The energy is averaged over time and p= ½ is taken. However, the absolute value of the energy defined by equation (21) may sometimes be misleading. If the total energy of the signal increases, it is very probable that the energy in each band will increase. In such cases, it is in our interest to find out if and how the distribution of the energy among the processes has changed. Therefore, we shall introduce the normalized energy in a given frequency band $e_i(f_{i1},f_{i2})$

$$e_i(f_{i1},f_{i2}) = \frac{\mathcal{E}_i(f_{i1},f_{i2})}{\mathcal{E}_{\mathrm{total}}}\,, \qquad (22)$$

where $\mathcal{E}_{\mathrm{total}}$ is the energy of the signal contained in the frequency band of our interest, i.e. between 0.0095 Hz and 2 Hz.

To avoid anomalies in the average scalograms introduced by particular subjects, we will base our analyses on homogeneous groups of subjects. Statistical plots will be used to present the median values, 10%, 25%, 75% and 90% of the range. The value that drops out of these limits is represented as a cross. To compare the values between the groups, the Mann–Whitney test for statistical significance will be used [50]. If the probabilities of the median being equivalent is below p= 0.05 the differences between the groups are set as significant.

3.2.5. *Reversible changes.* Because the cardiovascular system operates continuously, we can reveal many of its functional characteristics even from a normal resting state. Additional insight can be obtained by observing how it reacts to perturbations. In living organisms, the choice of ways of introducing perturbations is limited. One possibility is to induce changes by delivering pharmacological substances, for example vasodilator substances [49]. Another possibility is to impose changes by increased physical activity. In the following, we will present the exercise-induced changes, evaluated by the wavelet transform of the peripheral blood flow signals.

Signals were measured for nine young healthy male subjects. In each case, three signals were recorded before, and two after, 40 min of exercise on a treadmill at a 3° uphill gradient [51]. Each of the signals was recorded for 20 min. The maximal oxygen uptake (VO_{2max}) had been evaluated a day prior to the measurements for individual subjects, and the exercise intensity was standardized to a level of 80% VO_{2max}. During the measurement of peripheral blood flow, the subjects were in a supine position in a room in which the temperature was maintained constant.

Sixty second segments of typical blood-flow signals recorded before and after exercise, and the group median values of normalized energies, obtained from the wavelet transforms calculated from the entire signals, are presented in figure 12. It is obvious that both the steady level, and the amplitude of oscillations, are markedly higher after

exercise. Although the characteristic frequencies and amplitudes of oscillations have changed, five characteristic peaks were found in the averaged scalograms of all signals, both before and after the excercise.

The energy within each frequency interval was calculated from the wavelet transform of the measured signals. The exercise induced a substantial increase in total energy, comparing to that in the blood flow while resting (figure 13). The energy in the last measurement, which on average was made between the 35 and 55 min after exercise, had decreased almost to the initial value. Changes in the frequencies of the peaks, and normalized energies within the corresponding intervals, are illustrated in the lower plot of figure 12, while the statistical plots are given in figure 13. It is evident that exercise induced significant changes in heart rate, and in the respiration and myogenic frequencies. It is well known that the heart rate and respiration frequency increase during exercise and remain higher for some time afterwards. The myogenic process not only has a higher characteristic frequency immediately after exercise, but its normalized energy has also increased significantly.

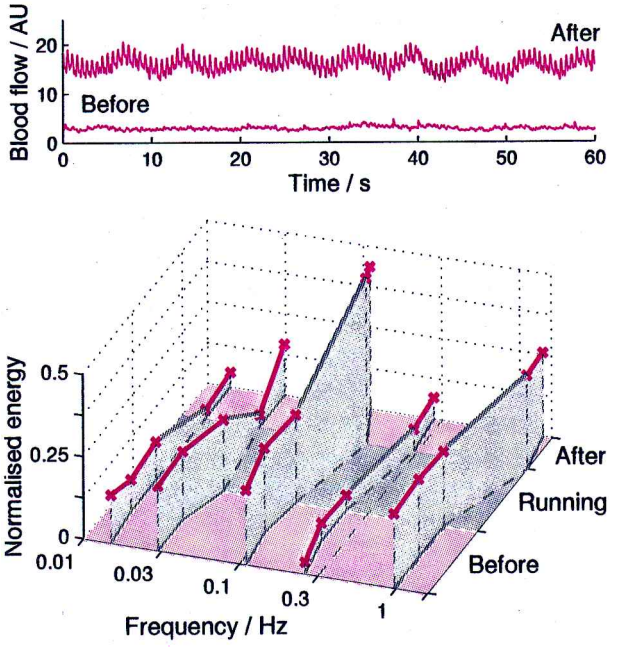

Figure 12. A 60 s segment of the blood flow signal before and after exercise (upper plot) and the group median values of normalized energies and frequencies of all peaks (lower plot).

Indeed, we may conclude that increased myogenic activity, with the characteristic frequency between 0.06 Hz and 0.15 Hz, is the main change induced by a single episode of exercise. It is interesting that the normalized energies of the neurogenic process, with its characteristic peak around 0.04 Hz, and metabolic process, with its characteristic peak around 0.01 Hz, are reduced after exercise. All changes decay shortly after exercise. However, imposed demands of the cells lead to enhanced metabolic process as well as increased energy of the heart peak when exercise is regularly repeated. Such changes were observed in a group of sportsmen, as compared to the controls [39].

3.2.6. *Irreversible changes.* A single episode of exercise induces short-time changes and, after their decay, the original dynamics is re-established. Impairment of the cardiovascular system, on the other hand, can result in irreversible changes. In this section we present the results of a clinical study which included subjects with cardiovascular diseases. In addition to a control group, consisting of 17

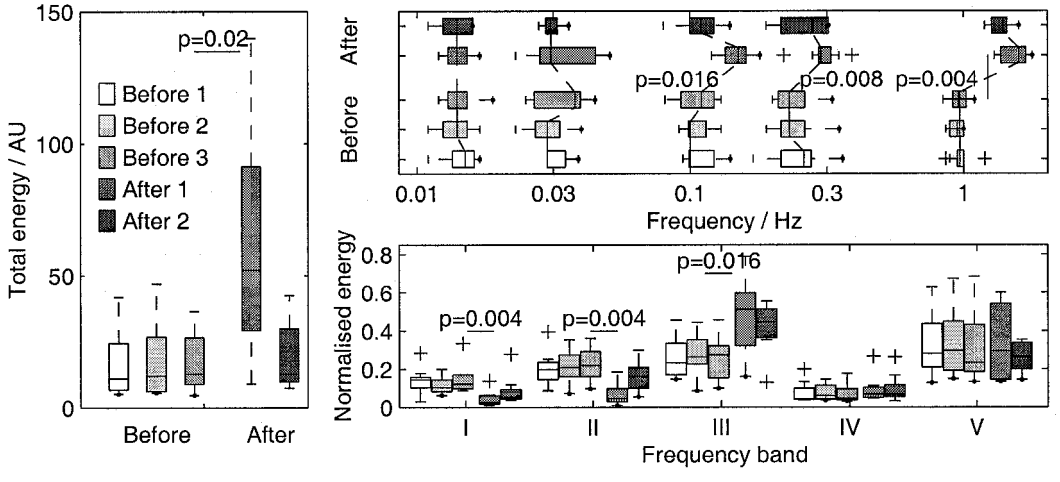

Figure 13. The total energy of the blood flow signals, the frequencies of the peaks and the normalized energy of intervals around each peak, for all five measurements, before and after exercise.

young male subjects, a group of 15 subjects at least 4 days after myocardial infarction, and a group of 13 subjects with diabetes were included in the study. The set of signals described in section 3.2.2. was measured for all subjects, while at rest. We report only the main findings here. The complete set of results will be presented and discussed elsewhere.

While infarction affects mainly the pumping function of the heart, diabetes changes the metabolic efficiency of the cells and by this resistance of the vessels. Consequently, the heart is permanently imposed to an increased work load. These changes are clearly manifested in the HRV signal. The total energy of the signal is significantly lower in the two groups of patients than it is in the control group (figure 14). For comparison, the total energy of the HRV signal measured for a subject in coma is presented in the same figure. The energy of this signal is practically zero, representing a state in which there are almost no variations in the heart rate.

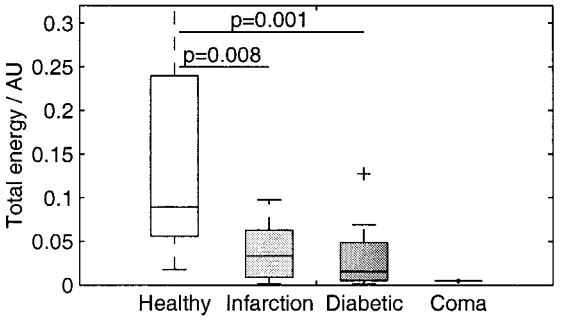

Figure 14. Total energy of the HRV signal measured in healthy subjects, patients after myocardial infarction, diabetic patients and a patient in coma.

The decreased variability of the heart rate is manifested as a sharpening of the characteristic peaks in all other cardiovascular signals, as presented in figure 15. In this case the arteriolar and venous pressure were measured invasively, via an inserted fluid-filled catheter and transducer system, as a part of the routine procedure in intensive care units. Since the peaks hardly varied at all in time, the Fourier method gave distinct spectral peaks. Moreover, peaks appearing at linear combinations of the characteristic frequencies are also observable. It is also obvious that the ratio between characteristic frequencies tends to become rational.

We can interpret these results as illustrating that cardiovascular impairment results in significantly reduced interactions among the processes involved in control of the the blood flow. This, among other changes, results in decreased variability of the heart rate and therefore smaller energy of the HRV signal. This may mean that the other processes are less efficient in signalling their needs to the heart, and/or that the heart is unable to cope with their demands.

The reduction in heart variability is often interpreted as decreased complexity and chaos in the activity of the heart [27,52]. However, it is the study of changes in the spectral components that gives us insight into the pathology of diseases [53,54]. Evaluation of the contribution of each spectral component might provide a diagnostic and predictive tool for a whole range of diseases related to the cardiovascular system.

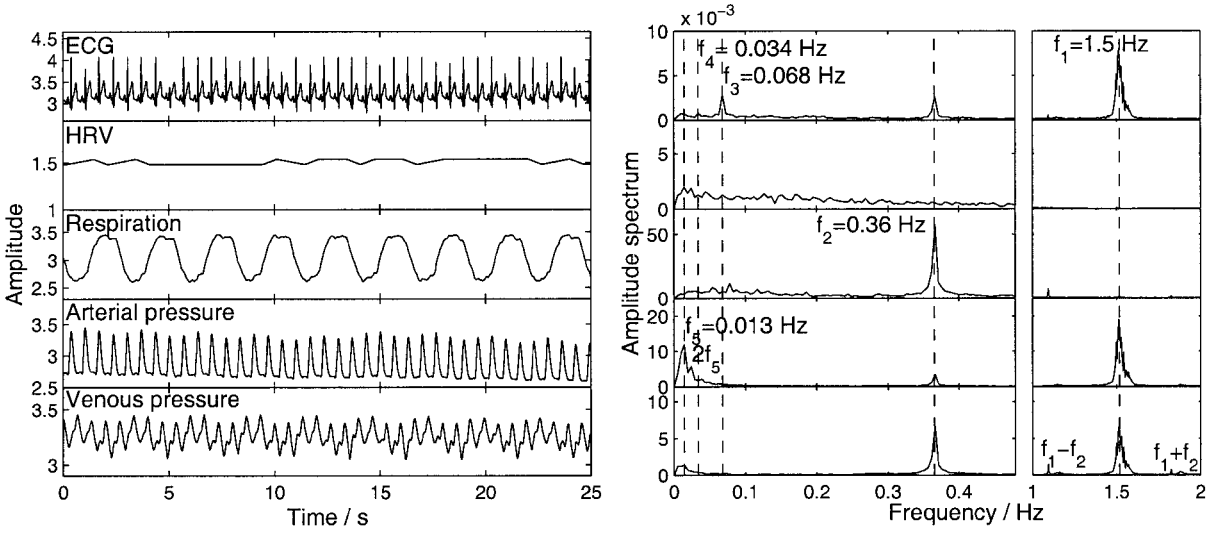

Figure 15. Signals recorded from the cardiovascular system of an intensive care patient (left) and corresponding amplitude spectra (right). HRV is in Hz, other values are in arbitrary units.

4. Nonlinear analysis

The ultimate goal of a physical description of a system is a mathematical formulation as a set of differential equations. Before we proceed to such a description, we must learn as much as possible about the system in question. So far, we have analysed the cardiovascular signals in the frequency domain. The analyses imply that, on a time scale of $\sim$1 minute, five almost periodic processes contribute to the dynamics of the blood flow. Developments in the theory of nonlinear dynamics, and its numerical applications to chaotic time series over the last three decades, have provided several methods for estimating the invariants of the dynamics from scalar signals, as we shall now describe.

4.1. *System characterization*

Based on frequency analysis, the following conclusions can be drawn regarding the physical nature of the system: (i) well-defined spectral peaks at characteristic frequencies are present in the signals; (ii) peaks at the same frequencies were found in all signals, regardless of the measured quantity or the measurement site; (iii) although the peaks are not sharp, and vary in time for each one of them a finite frequency interval exists within which its variations are confined; (iv) the existence of the peaks is not influenced by irreversible or reversible changes, implying their robust nature and the corresponding structural stability of their sources; (v) from their response to perturbations we may conclude that a mutual dependence exists among the sources. These results lead to the inference that the source of each observed peak is an oscillator, and that the oscillators are mutually coupled. Robustness and structural stability are characteristic of certain nonlinear oscillators.

The time evolution of an oscillator may be obtained as one of the solutions of a general differential equation

$$\dot{\mathbf{x}}(t) = \mathbf{g}(\mu, \mathbf{x}(t)) \quad \mathbf{x}(0) = \mathbf{x}_0, \mathbf{x} \in \mathfrak{R}^d, \tag{23}$$

where $\mathbf{x}(t)$ is a state vector, $\dot{\mathbf{x}}(t) = \mathrm{d}\mathbf{x}/\mathrm{d}t$ and the flow $\mathbf{g}$ is some general nonlinear function. The vector of control parameters μ is kept constant during the observations. By changing the control parameter, transitions between different types of behaviour can be induced. Graphically, the solutions can be presented as time series $x_1(t), x_2(t) \ldots x_d(t)$, or alternatively as a trajectory in a geometric phase space $\mathfrak{R}^d$. The phase space, filled with trajectories, is called the phase portrait of the dynamical system. After transients are over, the motion of $\mathbf{x}(t)$ settles typically near a subset of the phase space, called an attractor. The phase space volume occupied by a real physical system can either be preserved or contracted by time evolution. In the first case, the system is conservative, in the other dissipative. For dissipative systems, the volume occupied by the attractor can be relatively small compared to the initial volume of the phase space.

The simplest attractor of a dynamical system is a stable fixed point. A periodic motion, on the other hand, results in a limit cycle. A superposition of periodic motions, quasi-periodic motion, has an attractor in the shape of a torus. Figure 16 presents the phase portrait of the respiratory signal. The almost periodic nature of the signal, already discussed in the time and frequency domain, results in a limit cycle in phase space. Since the other systems influence the respiratory function only slightly, we may observe the limit cycle in two dimensions, although it is broadened. In blood flow, the contributions of all processes are comparable and a higher dimensional phase space is needed to portray the attractor. For this almost quasi-periodic flow with five characteristic frequencies the attractor is expected to be a 5-torus.

However, when nonlinearities are involved, even a finite dimensional system need not be quasi-periodic. The motion within an attractor may be unstable in some directions. These instabilities are manifested as an exponential separation of trajectories. Such systems exhibit a sensitive dependence on initial conditions—which is the hallmark of chaotic behaviour.

The characterization of nonlinear dynamical systems is based on geometrical and statistical properties of the attractor, such as its entropy, various dimensions (information, Hausdorff, correlation ...) and Lyapunov exponents [55,56]. Its statistical properties become relevant as soon as the dynamics is sufficiently complicated that geometrical information about the shape of the attractor is no longer available. From here on, it is the statistical theory which can distinguish different degrees of complexity. The basic tool which enables us to measure statistical properties of the system is the ergodic theory. Ergodic theory states that a time average equals a space average. Or, in other words, that a trajectory of the system explores the entire phase space that is energetically available to it [57].

The numerical algorithms for calculation of the correlation dimension [58] and Lyapunov exponents [55] have frequently been applied to characterize nonlinearities in biological signals (see [59–61] and references therein).

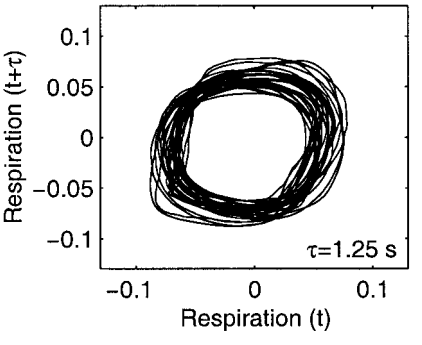

Figure 16. The respiratory signal embedded in two-dimensional phase space.

Since the very long observation time introduces non-stationarities, the number of points necessary for a successful estimation of correlation dimension for high-dimensional systems [62] can only be obtained by over-sampling. Oversampling, however, emphasizes the noise in the signal. Therefore the correlation dimension cannot be reliably estimated for the case of biological signals resulting from high-dimensional systems [63]. It was proposed, however, that the correlation dimension can still be used for qualitative characterization [64]. By comparing correlation integrals obtained from original time series and their surrogates, i.e. randomized sequences with similar spectral and statistical properties as the original signal, one may distinguish between deterministic and stochastic or noise-dominated signals. We have shown that all measured signals are largely deterministic [40].

The number of points is crucial for all algorithms used for the characterization of nonlinear system from measured signals, including the estimation of Lyapunov exponents. As we shall see below, an algorithm is available for the estimation of Lyapunov exponents, based on an approximation of the local flow in phase space. In this case, the quality of approximation is more important than the number of points itself.

4.2. *The Lyapunov exponents*

The Lyapunov or characteristic exponents measure the rate of convergence or divergence of nearby trajectories in the phase space. Thus, they determine both the stability of the trajectories and the system's sensitivity to initial conditions. This makes them one of the most meaningful characterizations of a nonlinear dynamical system. Using Lyapunov exponents, one can distinguish between fixed points and periodic, quasi-periodic or chaotic motions.

The Lyapunov exponents characterize the response to small perturbations of the trajectories of the system (24). The time evolution of a small perturbation is governed by linearized equation in the tangent space

$$\delta\dot{\mathbf{x}}(t) = D\mathbf{g}(\mu, \mathbf{x}(t))\delta\mathbf{x}(t) \quad \delta\mathbf{x}(0) = \delta\mathbf{x}_0, \qquad (24)$$

where $D\mathbf{g}$ is the Jacobi matrix of the flow $\mathbf{g}$. At the end of the last century, A. M. Lyapunov introduced a measure of average contraction of the perturbation to a given trajectory as

$$\lambda(\delta\mathbf{x}_0) = \lim_{t\to\infty} \frac{1}{t} \log\left(\frac{||\delta\mathbf{x}(t)|_{\delta\mathbf{x}_0}||}{||\delta\mathbf{x}_0||}\right), \qquad (25)$$

today known as the Lyapunov exponents. Using d linearly independent initial conditions $\delta\mathbf{x}_{01} \ldots \delta\mathbf{x}_{0d}$, one obtains a fundamental system of solutions $\lambda_1 \geq \lambda_2 \ldots \geq \lambda_d$. For ergodic systems the set of λ_i does not depend on the initial condition $\delta\mathbf{x}_{0i}$ and so the λ_i are global properties of the attractor [65]. As such, they bear no information about the local behaviour on the attractor. Therefore, local Lyapunov exponents were introduced [66]. In this case, the limit $t \to \infty$ is not taken in equation (25). These values may vary significantly over the attractor, but their means converge towards the global exponents.

If any λ_i is positive, small perturbations will grow exponentially. If all λ_i are negative, any perturbation will decrease and the attractor is a stable fixed point. In the case of a zero exponent, the size of the perturbation does not change in time. A stable periodic state, for example, has one zero exponent corresponding to a perturbation tangent to the limit cycle, and all the other exponents are negative. A quasi-periodic system with k incommensurate frequencies has k zero exponents, and all others are negative. Every attractor of a smooth dynamic system, given by equation (23), has at least one zero Lyapunov exponent corresponding to a perturbation tangent to the trajectory. Such a perturbation simply moves one along the same orbit. The exponents of a Hamiltonian system come in conjugate pairs, consisting of a positive and a negative exponent of the same magnitude, and two of them vanish [55]. One zero exponent is associated with the conservation of energy and the other with the fact that the evolution equations are differential.

For systems whose equations of motion are known explicitly there is a straightforward method of computing all Lyapunov exponents [67]. This method cannot, however, be applied directly to experimental data. There are two approaches to estimating the exponents from measured signals. In the first, introduced by Wolf *et al.* [68] and Rosenstein *et al.* [69], two nearby points in the phase space are followed and only the largest exponent is evaluated. The second approach, introduced by Eckmann and Ruelle [55], as well as by Sano and Sawada [70], is based on estimating the Jacobians of the map.

For scalar time series $s(t)$ the attractor can be reconstructed by the method of delay coordinates, introduced by Packard *et al.* [71]

$$\mathbf{x}(t) = [s(t), s(t+\tau), \ldots, s(t+(d-1)\tau)], \qquad (26)$$

where $t = t_s, 2t_s, \ldots nt_s - (d-1)\tau$, d is the dimension of the embedding space and the time lag τ is an integer multiply of the sampling time t_s.

In the points along a chosen trajectory on the embedded attractor, a set of neighbouring points is evolved for a chosen time (evolution time). Based on these two sets, the local flow is approximated by a set of basis functions. From subsequent Jacobi matrices, d Lyapunov exponents are calculated (for details see [56]). The great advantage of this method compared to the trajectory tracing method is that one can deal with arbitrary vectors in tangent space while the observed data points are used only to approximate local flow. Thus, we can calculate all exponents (including negative ones) as long as the approximation of the flow is adequate.

The number of calculated exponents is equal to the dimension of the reconstructed phase space d. If d is too small, the attractor is not able to unfold and the calculated exponents are erroneous. On the other hand, if d is too large, the reconstructed attractor is contained in a submanifold of dimension $m < d$, and $d - m$ spurious exponents that are unrelated to the dynamics of the system are obtained. Under time reversal, true exponents change sign, while the spurious ones do not [56]. In this way, they can be identified.

In low embedding dimensions, the global Lyapunov exponents of the blood-flow signal vary from one dimension to the other, but as the dimension reaches 10, two patterns are observed: either four paired and one zero or five paired exponents are calculated. In the latter case, one pair equals zero within the calculation error [72,73]. Among the exponents of the reversed signal, four or five pairs were observed again. The other exponents were found to be negative and of the same magnitude as some of the exponents obtained from the original signal, also with negative sign. Therefore, they can be identified as spurious.

To reveal local properties of the attractor, local Lyapunov exponents were calculated. Figure 17 presents the distribution of the values of the first nine exponents, calculated in an 11-dimensional embedding space. Paired values are obtained again—four paired and one zero exponent.

The appearance of an exponent equal to zero within the calculation error shows that the blood flow dynamics is governed by a deterministic system. Paired values are an indication of the almost Hamiltonian nature of the system that regulates the flow of blood on a time scale of minutes. Moreover, the number of pairs, namely five, support the hypothesis that five oscillatory subsystems are involved in the regulation.

5. System description

We have obtained some convincing evidence that the system is largely deterministic: the existence of characteristic frequency peaks in all measured signals; their non-vanishing autocorrelation function [40]; a zero Lyapunov exponent of peripheral blood flow signal; and differences between the correlation integrals of original signals and their surrogates.

It is therefore possible to describe the dynamics within the cardiovascular system as a solution of a set of differential equations. The oscillatory nature of the processes involved in blood flow regulation, and their finite number, provided the starting point for the formulation of these equations. It must be borne in mind that the processes are mutually interdependent. Their joint action is directed towards a single goal: to provide matter and energy continuously to each cell. To achieve this goal, they must act collectively so that, at any given moment, the reaction of each depends on the state of all the others. In the mathematical formulation, these mutual dependences appear as couplings between the oscillators.

5.1. *Couplings*

The effect of coupling between two oscillators on their behaviour depends on its strength. Weak couplings result in a variation of the characteristic frequencies of the oscillators, while strong couplings may lead to qualitative changes in the system behaviour, i.e. phase transitions.

If couplings did not exist in the cardiovascular system, we would have sharp peaks and the characteristic frequencies, which in healthy subjects at rest are only tending towards a rational ratio, may further become commensurate. The resonance phenomenon, for example, is one of the possible scenarios of how the system collapses. The other possible scenario is that in this case the characteristic frequencies might become completely incommensurate. The couplings enable the exchange of information among the processes and are therefore fundamental to the appropriate functioning of the cardiovascular system.

Understanding the physical and physiological nature of these couplings is obviously essential to understanding how the whole system works. The frequency and amplitude of each observed oscillation reflect both the activity of the oscillator itself and the effect of all couplings. Although the

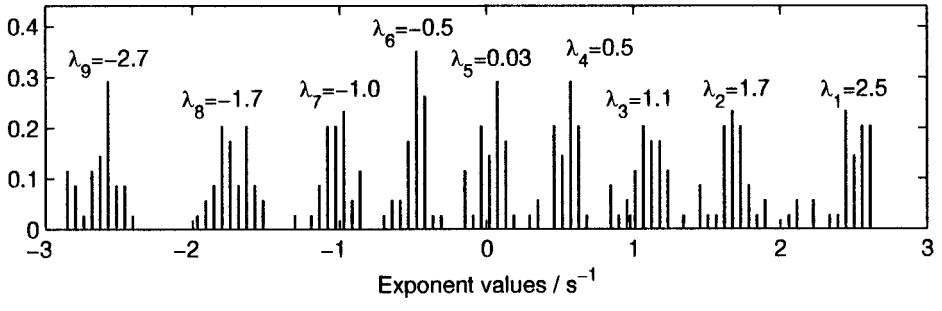

Figure 17. The distribution of local exponents of the blood flow signal of a healthy person, calculated from 40 different starting points.

effect of couplings cannot be measured separately, we may however extract it from the data using a variety of techniques for the analysis of phase, frequency and amplitude couplings.

One of earliest couplings to be identified, and the most frequently investigated, is that between the heart and respiratory activity, known as the respiratory arrhythmia. Although it is usually studied from the HRV signal, it is also visible in the peripheral blood flow signal. We present in figure 18 the corresponding wavelet transform. Frequency and amplitude variations of the flow component, driven by the heart are also shown. They are presented as projections of the peak value of the wavelet transform onto the time-frequency and time-amplitude planes. It is notable that the heart frequency is modulated by the frequency of respiration, while the amplitude of the flow, synchronized with the heart beat, is modulated by slower oscillatory processes, dominated by the myogenic frequency of around 0.1 Hz.

We can see from the scalograms that the peaks at lower frequencies vary in time as well. It may be assumed that couplings, similar to the one presented in figure 18, also exist among the other oscillators. Based on the analysis of the system in different states, normal and perturbed, we may presume that all couplings are weak.

5.2. *Coupled oscillators*

In the following, we present differential equations which govern the regulation of the peripheral blood flow in a single point of the vessels network. While the Navier–Stokes equations, presented in section 2 give the Euler description of the flow, we use the Lagrangian description to follow the contribution of individual processes to the flow.

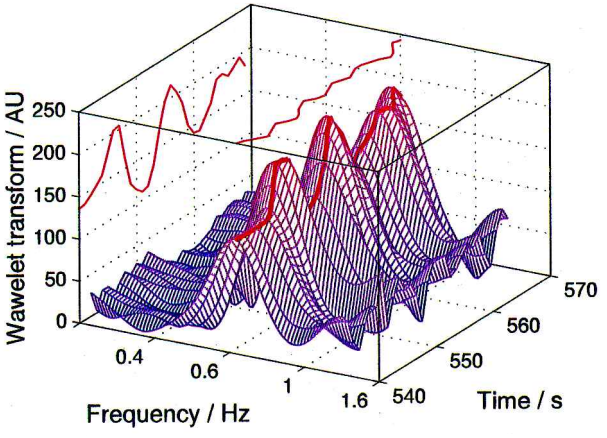

Figure 18. The wavelet transform of the peripheral blood flow signal within the frequency interval corresponding to heart activity. Variations of frequency and amplitude are plotted as projections of the peak value onto the time–frequency and time–amplitude planes.

First, we shall introduce the flow (x_i) and its velocity (y_i), contributed by each oscillator separately and then consider their collective activity. The same type of oscillator will be used for all five processes. In view of the experimental evidence showing that the oscillators are both robust and nonlinear in nature, a form

$$\dot{x}_i = -x_i q_i - y_i 2\pi f_i \,,$$

$$\dot{y}_i = -y_i q_i + x_i 2\pi f_i \,, \quad q_i = \alpha_i((x_i^2 + y_i^2)^{1/2} - a_i) \,, \qquad (27)$$

was chosen [38]. The index i denotes the ith oscillator, i= 1 the heart, i= 2 the respiratory, i= 3 the myogenic, i= 4 the neurogenic and i= 5 the metabolic oscillator. a_i is the amplitude, and f_i the characteristic frequency of the oscillator. The constant α_i determines the stability of the limit cycle. It is interesting to compare (27) with the van der Pol oscillator [74], which has often been used to describe heart activity. The latter is a relaxation oscillator, and most of the energy is exchanged in a particular part of a cycle. In the cardiovascular system, this is true only at the output of the heart, whereas in the periphery energy is uniformly exchanged during the whole cycle. The shape of the flow in one heart beat cycle, presented in figure 4, also differs from the solution of the van der Pol equations.

Equation (27) describes an autonomous oscillator. The couplings lead to additional terms in the equation. The present understanding of couplings allows us to specify only the sign of coupling terms. Therefore, linear couplings will be used. For the heart oscillator, we obtain

$$\dot{x}_1 = x_1 q_1 - y_1 2\pi f_1 + \eta_2 x_2 - \eta_3 x_3 - \eta_4 x_4 + \eta_5 x_5 - \eta_6(\Phi_1 - \Phi_2) \,,$$

$$\dot{y}_1 = y_1 q_1 + x_1 2\pi f_1 + \eta_2 y_2 - \eta_3 y_3 - \eta_4 y_4 + \eta_5 y_5 \,. \qquad (28)$$

Φ_1 and Φ_2 represent the inflow and outflow of blood at the point observed. The coefficient η_2 represents the influence of respiration to the heart rate. During inspiration the heart beats faster, while in the expiration phase its rate decreases. Both the myogenic and neurogenic activities contribute to the stiffness of the vessels and by this increase the resistance to the flow. Therefore, their influences are introduced by $-\eta_3$ and $-\eta_4$. The metabolic activity reduces stiffness and decreases resistance to the flow. This coupling is introduced via η_5.

As it is evident from the HRV signal, all processes have an impact on the pumping action of the heart and through this on the flow and velocity of the blood. The respiratory activity, on the other hand, is influenced least by the rest of the system.

The equations for the respiratory flow and velocity components can then be written as

$$\dot{x}_2 = x_2 q_2 - y_2 \omega_2 + \theta_4 x_4 + \theta_5 x_5 + \theta_6(\Phi_1 - \Phi_2) \,,$$

$$\dot{y}_2 = y_2 q_2 + x_2 \omega_2 + \theta_4 y_4 + \theta_5 y_5 \,. \qquad (29)$$

Only the neurogenic (θ_4) and metabolic (θ_5) activities modulate the flow component, driven by the pressure difference generated by the respiratory activity. The neurogenic influence is considered because breathing is under a continuous autonomous control. Moreover, the bilateral transection of the vagus nerve has been shown to result in slower breathing and deeper inspiration [2]. The lungs also adapt their activity to the metabolic needs of the cells. The higher the metabolic activity the deeper and faster the respiration is.

In the proposed model, the other three systems—myogenic, neurogenic and metabolic—were also described in an analogous way. The experimentally observed characteristic frequencies were used to characterize each of them, and their interrelations were approximated by linear couplings, based on physiological evidence. However, additional studies are necessary to elucidate further the origin and nature of these slower oscillators and their mutual couplings.

Note that, in formulating our mathematical description, we have consciously chosen an oscillator as the basic unit for construction of our model. Although this choice is based on the experimental and clinical evidence discussed above, and although many biological systems have been shown to be governed by oscillators [75–77], it is not the only possible choice. In addition to van der Pol, Clynes [78] also described the heart activity with an oscillator. He used a harmonic oscillator with a variable frequency and two separate equations to describe the variability during inspiration and expiration. The majority of the proposed models, however, interpret the observed oscillations in the HRV and blood pressure signals in terms of nonlinearities and time delays [79–85]. They concentrate mainly on short-term blood pressure control mechanisms, including respiratory oscillations and oscillations with a period of $\sim$10 s.

The reason why we favour coupled oscillators as a model of the processes governing blood flow through the cardiovascular system, rather than a set of delay-differential equations, is twofold. First, the delay is introduced somewhat artificially to create an oscillatory behaviour that is already inherent for our basic units. In reality, there is physiological evidence that the underlying processes can also function autonomously, supporting the idea of an oscillator-based model. Secondly, whereas delays are certainly important in reactions to isolated transients, the cardiovascular system is constantly reacting to small perturbations. Its existence is determined by its ability to cope on a continuing basis with changes resulting from the mutual interaction of the processes involved. In the coupled oscillator model, the time needed for mutual interactions is manifested as phase shifts between the oscillators.

The full version of the proposed model consists of ten coupled first order differential equations. An analytic solution of such a system would be, to say the least, hard to obtain. The alternative possibility is a numerical calculation, which is however sensitive to the choices of integration method and of parameter values. A recently discussed method based on analogue circuits [86] seems potentially a promising way of studying the solutions of high order differential equations of this kind.

For the present, however, instead of solving the equations directly, we have obtained a solution starting from the known physical and physiological properties of the cardiovascular system [87]. The effects of all experimentally observed processes on one pumping cycle of the heart were considered and a mathematical description of oscillations in the blood flow was acquired. Physical characteristics of vessels were described by the windkessel† model [88]. This consists of a capacitor representing the compliant aorta, and a resistor representing the stiffer peripheral vessels, connected in parallel. Earlier variants of this model attempted to describe either the wave motion of the blood [89] or the regulatory processes [8,90], but dealt separately with individual sections of the cardiovascular system. Given the couplings that are known to exists between the processes, however, a proper understanding of the flow dynamics clearly requires consideration of the physics of the system as a whole, treated as an entity.

5.3. *Relations among the oscillators*

The relationship between the blood flow Φ, the pressure P and the vessel's resistance R is defined by Ohm's law

$$\Phi = \frac{P}{R}\,.$$

Each of these variables oscillates around its steady-level

$$\Phi = \Phi_0 + \Delta\Phi_0\,,\quad P = P_0 + \Delta P_0\,,\quad R = R_0 + \Delta R_0\,.$$

The fluctuations are determined by the state variables of the oscillators x_i. From the existing physiological evidence discussed above, we may assume that the heart's activity (x_1) directly increases the blood flow value

$$\Delta\Phi = \varepsilon_1 x_1,$$

and the respiratory activity (x_2) increases the pressure difference

†The windkessel model is based on mechanical properties of vessels and describes the pulse-wave propagation of the blood. Vessels that consist of a relatively large proportion of elastic fibres, such as the aorta, the pulmonary arteries and the adjacent parts of the great arteries, are called windkessel vessels. With each pulse any given segment of such a vessel distends to store a volume of blood. As it subsequently contracts back to its original dimensions, it pushes blood on to the next segment. The name windkessel (German for air chamber) has been given to these vessels and their function because of the resemblance to the air-filled chambers that similarly affect the velocity and pressure of fluids driven by pistons through systems of pipes.

$$\Delta P = \varepsilon_2 x_2 .$$

Furthermore, the myogenic (x_3) and the neurogenic (x_4) activity constrict the vessels and resist the flow, while the metabolic activity (x_5) dilates the vessels and decreases its resistance

$$\Delta R = \varepsilon_3 x_3 + \varepsilon_4 x_4 - \varepsilon_5 x_5 .$$

From the point of view of the capillary bed, where the cells of the human body have direct access to the blood, the peripheral flow consists of an inflow Φ_1, which is driven by the heart through the arteries, and an outflow Φ_2 through the veins, which is pumped by the pressure difference generated by the lungs

$$\dot{\Phi}_1 = \xi(\Delta\Phi + \frac{\Phi_0}{R_0}\Delta R - \Phi_1) ,$$

$$\dot{\Phi}_2 = \chi(\frac{1}{R_0}\Delta P - \Phi_2) . \qquad (30)$$

The constants ξ and χ determine the flow dynamics.

5.4. *The flow along a vessel*

Above, we have considered the oscillations of the blood flow at a single point in the cardiovascular system. The contribution of each process differs at different points of the system. However, all five characteristic frequencies were found in different physiological signals and on different sites along the vessel's network. Therefore, we may assume that blood flows in the form of travelling waves. The heart's contribution to the flow at each point results not only from the influences of local regulatory mechanisms, but also from the values of pressure and flow along the entire system. Therefore, equations (28) and (29) were rearranged [91]

$$\dot{x}_1 = x_1 q_1 - y_1\omega_1 + \eta_2 x_2 - \eta_3 x_3 - \eta_4 x_4 + \eta_5 x_5 + \eta_6 \int_0^l P(z,t)\,\mathrm{d}z + \eta_7 \int_0^l \Phi(z,t)\,\mathrm{d}z ,$$
$$\dot{y}_1 = y_1 q_1 + x_1\omega_1 + \eta_2 y_2 - \eta_3 y_3 - \eta_4 y_4 + \eta_5 y_5 , \qquad (31)$$

$$\dot{x}_2 = x_2 q_2 - y_2\omega_2 + \theta_4 x_4 + \theta_5 x_5 + \theta_6 \int_0^l P(z,t)\,\mathrm{d}z + \theta_7 \int_0^l \Phi(z,t)\,\mathrm{d}z ,$$
$$\dot{y}_2 = y_2 q_2 + x_2\omega_2 + \theta_4 y_4 + \theta_5 y_5 . \qquad (32)$$

Here, $\Phi(z,t)$ is the flow at any point of the circulatory system. It is generated by the heart, therefore $\Phi(0,t) = \varepsilon_1 x_1(t)$. The pressure P is generated by the lungs and $P(0,t) = \varepsilon_2 x_2(t)$. We have assumed the flow in the z direction, and l is a length in this direction. The blood returns to the right atrium of the heart at a pressure of 0 Pa , and at almost 0 Pa from the pulmonary vein to the left atrium [92]. There, the value of $P(l,t)$ becomes 0. By analogy, we may assume the value of flow at this boundary condition to be $\Phi(l,t) = 0$.

The wave motion of the blood along the cardiovascular system can be written as

$$\frac{\partial\Phi}{\partial t} = -\kappa_1\frac{\partial P}{\partial z} - \kappa_2 x_5 , \quad \kappa_i > 0$$

$$\frac{\partial P}{\partial t} = -\mu_1\frac{\partial\Phi}{\partial z} + \mu_2 x_3 + \mu_3 x_4 , \quad \mu_i > 0, \qquad (33)$$

where κ_i, μ_i are control parameters.

The values of these control parameters in equations (31)–(33) may differ with respect to the part of the system under consideration: arterial, capillary or venous. The blood pressure values are higher at the origin of the aorta and lower at the entrance of the vena cava into the heart. The arterial flow near the heart is dominated by the heart pump oscillations, while on the way to the capillaries the myogenic activity takes charge over the regulation of the flow. At the capillary bed the amplitude of oscillations of the metabolic activity dominates.

The model was built to summarize the experimental findings and known physiological facts. It still needs to be evaluated, analytically and numerically, and further experiments are also needed. With appropriate choice of parameter values, we expect it to serve in obtaining the initial conditions for locally oriented models, such as described by Navier–Stokes equations. Moreover, equations for wave motion of the blood may reduce locally to Navier–Stokes equations.

6. Outlook

On the way towards reaching an understanding of the cardiovascular system, physics, mathematics, physiology and clinical medicine meet under the wings of nonlinear dynamics. Therefore, the current comprehension of the physical and physiological properties of the processes involved in the control of blood circulation has been combined with experimental findings in order to arrive at a characterization of the system dynamics.

Processes on many different time scales and of widely different structural complexity are reflected in a single cycle of blood through the system. On one hand, this fact makes the understanding of the system difficult. However, we have shown that the system exhibits clear signatures of deterministic dynamics. The same dynamic properties characterize all signals generated by the system, regardless of the measurement site, and are also preserved in time. Therefore, the system can be treated as a single entity. This, on the other hand, provides a simplification that offers the possibility of evaluating the microscopic and macroscopic mechanisms together.

Several methods of linear and nonlinear analysis have been applied to extract the dynamics characterizing the measured signals. Although an enormous development of nonlinear dynamics has occurred during the last three decades, much work remains to be done on the theory and numerical methods for dealing with finite high-dimensional systems. We believe that studying the physics of the cardiovascular system may provide a motivation for further progress in the field. Its understanding is not only a theoretical challenge, but may also provide useful diagnostic and predictive tools for this life-giving system.

Acknowledgements

We wish to thank Peter V. E. McClintock for continuous encouragement and support during the writing of the manuscript and his most useful comments. A.S. is grateful to Hermann Haken and colleagues at the Institute of Theoretical Physics I, University of Stuttgart for numerous discussions. She is indebted to the Alexander von Humboldt Foundation.

The work was supported by the Slovenian Ministry of Science and Technology and partially by the Slovenian–German Science and Technology co-operation. We acknowledge E. Weber-Jensen for providing measurements on the subject in coma, D. Štajer and V. Urbančič-Rovan for patient selection and clinical support during recordings on patients after myocardial infarction and diabetic patients, and M. Čenčur for technical support. Some of the measurements were made possible by Moor Instruments, who kindly lend us the laser Doppler flowmeter.

References

[1] Keele, C. A., Neil, E., and Joels, N. (editors), 1982, *Samson Wright's Applied Physiology* (Oxford: Oxford University Press).
[2] Schmidt, R. F., and Thews, G. (editors), 1989, *Human Physiology* (Berlin: Springer-Verlag).
[3] Fung, Y. C., and Zweifach, B. W., 1971, *Ann. Rev. Fluid Mech.*, **3,** 189–210.
[4] Zweifach, B. W., 1966, *ASME, Biomechanics*, **1,** 121–131.
[5] Karnowsky, M. J., 1968, *J. Gen. Physiol.*, **52,** 64–95.
[6] McGrew, R. E., 1985, *Encyclopedia of Medical History* (London: Macmillan).
[7] Lippold, O. C. J., and Winton, R. F. (editors), 1979, *Human Physiology* (Edinburgh: Churchill Livingstone).
[8] Strackee, J., and Westerhof, N., (editors), 1993, *The Physics of Heart and Circulation* (Bristol: Institute of Physics Publishing).
[9] Sutera, S. P., and Skalak, R., 1993, *Ann. Rev. Fluid Mech.*, **25,** 1–19.
[10] van Steenhoven, A. A., 1993, Velocity profiles in large arteries. *The Physics of Heart and Circulation*, edited by J. Strackee and N. Westerhof (Bristol: Institute of Physics Publishing), pp. 295–320.
[11] Fung, Y. C., 1996, *Biomechanics: Circulation* (New York: Springer).
[12] Hyndman, B. W., Kitney, R. I., and Sayers, B. McA., 1971, *Nature*, **233,** 339–341.
[13] Sayers, B. McA., 1973, *Ergonomics*, **16,** 16–17.
[14] Chess, G. F., Tam, R. M. K., and Calaresu, F. R., 1975, *Amer. J. Physiol.*, **228,** 775-780.
[15] Akselrod, S., Gordon, D., Ubel, F. A., Shannon, D. C., Berger, A. C., and Choen, R. J., 1981, *Science*, **213,** 220–222.
[16] Di Renzo, M., Parati, G., Pedotti, A., and Zanchetti, A. (editors), 1997, *Frontiers of Blood Pressure and Heart Rate Analysis*, (Amsterdam: IOS Press).
[17] Task Force of the ESC and the NASPE, 1996, *Circulation*, **93,** 1043–1065.
[18] Hales, S., 1773, *Statical Essays II, Haemastaticks* (London: Innings Manby).
[19] Ludwig, C., 1847, *Arch. Anat. Physiol.*, **13,** 242–302.
[20] Hildebrandt, G., 1987, The autonomous time structure and its reactive modifications in the human organism. *Temporal Disorder in Human Oscillatory Systems*, edited by L. Resing, U. van der Heiden and M. C. Mackey (Berlin: Springer), pp. 160–174.
[21] Fourier, J. B. J., 1888, Théorie analytique de la chaleur. *Oeuvres de Fourier*, Tome premier, edited by G. Darboux (Paris: Gauthiers-Villars).
[22] Press, W. H., Teukolsky, S. A., Vetterling, W. T., and Flannsry, B. P., 1992, *Numerical Recipes in C* (Cambridge: Cambridge University Press).
[23] Morlet, J., 1983, Sampling theory and wave propagation, *Issues in Acoustic Signal/Image Processing and Recognition*, NATO ASI Series, Vol. I, edited by C. H. Chen (Berlin: Springer-Verlag).
[24] Grossmann, A., and Morlet, J., 1984, *SIAM J. Math. Anal.*, **15,** 723–736.
[25] Daubechies, I., 1992, *Ten Lectures on Wavelets* (Philadelphia: SIAM).
[26] Kaiser, G., 1994, *A Friendly Guide to Wavelets* (Boston: Birkhäuser).
[27] Thurner, S., Feurstein, M. C., and Teich, M. C., 1998, *Phys. Rev. Lett.*, **80,** 1544–1547.
[28] Stefanovska, A., Leger, P., Bračič, M., Bračič, T., Bendayan, P., and Boccalon, H., 1998, *Technol. Health Care* (in the press).
[29] Maiman, T. H., 1960, *Nature*, **187,** 493–494.
[30] Cummins, H. Z., Knable, N., and Yeh, Y., 1964, *Phys. Rev. Lett.*, **12,** 150–153.
[31] Riva, C., Ross, B., and Benedek, G. B., 1972, *Invest. Opthalmol.*, **11,** 936–944.
[32] Stern, M. D., 1975, *Nature*, **254,** 56–58.
[33] Nilsson, G. E., Tenland, T., and Öberg, P. Å., 1980, *IEEE Trans. Biomed. Eng.*, **27,** 597–604.
[34] Salerud, E. G., Tenland, T., Nilsson, G. E., and Oberg, P. Å., 1983, *Int. J. Microcirc.: Clin. Exp.*, **2,** 91–102.
[35] Perimed, A. B., Järfälla, Sweden, http://www.perimed.se.
[36] Wilkin, J. K., 1986, *Am. J. Physiol.*, **250,** H765–H768.
[37] Hoffman, U., Yanar, A., Franzeck, U. K., Edvards J. M., and Bollinger, A., 1990, *Microvascular Res.*, **40,** 293–301.
[38] Stefanovska, A., 1992, Dissertation, University of Ljubljana, Ljubljana.
[39] Bračič, M., and Stefanovska, A., 1998, *Bull. Math. Biol.* **60,** 919 – 935.
[40] Stefanovska, A., and Krošelj, P., 1997, *Open Sys. & Information Dyn.,* **4,** 457–478.
[41] Bračič, M., and Stefanovska, A., 1998, *Open Sys. & Information Dyn.* (in press)
[42] Kitney, R. I., Fulton, T., McDonald, A. H., and Linkens, D. A., 1985, *J. Biomed. Eng.*, **7,** 217–224.
[43] Mück-Weymann, M. E., Albrecht, H.-P., Hager, D., Hiller, D., Hornstein, O. P., and Bauer, R. D., 1996, *Microvasuclar Res.*, **52,** 69-78.
[44] Johnson, P. C., 1991, *NIPS*, **6,** 41–42.
[45] Bertuglia, S., Colantuoni, A., and Intaglietta, M., 1994, *Microcirc. Res.*, **48,** 68–84.
[46] Griffith, T. M., and Edwards, T. H., 1994, *Am. J. Physiol.*, **266,** H1801–H1811.
[47] Kastrup, J., Bühlow, J., and Lassen, N. A., 1989, *Int. J. Microcirc.: Clin. Exp.*, **8,** 205–15.

[48] Stefanovska, A., Bračič, M., and Kvernmo, H. D., 1998, *IEEE Trans. Biomed. Eng.* (submitted).
[49] Kvernmo, H. D., Stefanovska, A., Kirkebøen, K. A., and Kvernebo, K., 1998, *Microvascular Res.* (submitted).
[50] Iversen, G. R., and Gergen, M., 1997, *Statistics—The Conceptual Approach* (New York: Springer).
[51] Kvernmo, H. D., Stefanovska, A., Bračič, M., Kirkebøen, K. A., and Kvernebo, K., 1998, *Microvascular Res.* (in the press).
[52] Ivanov, P. Ch., Rosenblum, M. G., Peng, C.-K., Mietus, J., Havlin, S., Stanley, H. E., and Goldberger, A. L., 1996, *Nature*, **383,** 323–327.
[53] Lombardi, F., Sandrone, G., Torzillo, D., and Malliani, A., 1995, Spectral analysis of blood pressure and heart rate in patients with myocardial infarction. *Computer Analysis of Cardiovascular Signals*, edited by M. Di Renzo, G. Mancia, G. Parati, A. Pedotti and A. Zanchetti (Amsterdam: IOS Press), pp. 267–274.
[54] Weise, F., and Heydenreich, F., 1995, Power spectrum analysis of heart rate in diabetic patients: A marker of autonomic dysfunction. *Computer Analysis of Cardiovascular Signals*, edited by M. Di Renzo, G. Mancia, G. Parati, A. Pedotti and A. Zanchetti (Amsterdam: IOS Press), pp. 283–292.
[55] Eckmann, J.-P., and Ruelle, D., 1985, *Rev. Mod. Phys.*, **57,** 617–656.
[56] Abarbanel, H. D. I., Brown, R., Sidorowich, J. J., and Tsimiring, L. Sh., 1993, *Rev. Mod. Phys.*, **65,** 1331–1392.
[57] Lichtenberg, A. J., and Lieberman, M. A., 1983, *Regular and Chaotic Dynamics* (New York: Springer-Verlag).
[58] Grassberger, P., and Procaccia, I., 1983, *Phys. Rev. Lett.*, **50,** 346–349.
[59] Glass, L., and Kaplan, D., 1993, *Medic. Progr. Technol.*, **19,** 115– 128.
[60] Griffith, T. M., 1996, *Cardiovascular Res.*, **31,** 342–358.
[61] Peng, C. K., Halvin, S., Hausdorff, J. M., Mietus, J. E., Stanley, H. E., and Goldberger, A. L., 1997, Fractal mechanisms and heart rate control: Long-range correlations and their breakdown with disease. *Frontiers of Blood Pressure and Heart Rate Analysis*, edited by M. Di Renzo, G. Parati, A. Pedotti and A. Zanchetti (Amsterdam: IOS Press), pp. 3–14.
[62] Eckmann, J.-P., and Ruelle, D., 1992, *Physica* D, **56,** 185–187.
[63] Stefanovska, A., Strle, S., and Kroöselj, P., 1997, *Phys. Lett.* A, **235,** 24–30.
[64] Theiler, J., Eubank, S., Longtin, A., Galdrikian, B., and Farmer, J. D., 1992, *Physica* D, **58,** 77–94.
[65] Oseledec, V. I., 1968, *Trans. Moscow Math. Soc.*, **19,** 197–231.
[66] Abarbanel, H. D. I., Brown, R., and Kennel, M. B., 1991, *J. Nonlinear Sci.*, **1,** 175–199.
[67] Bennetin, G., Galgani, L., Giorgilli, A., and Strelcyn, J. M., 1980, *Meccanica*, **15,** 9–30.
[68] Wolf, A., Swift, J. B., Swinney, H., and Vastano, J. A., 1985, *Physica* D, **16,** 285–317.
[69] Rosenstein, M. T., Collins, J. J., and De Luca, C. J., 1993, *Physica* D, **65,** 117–134.
[70] Sano, M., and Sawada, Y., 1985, *Phys. Rev. Lett.*, **55,** 1082–1085.
[71] Packard, N., Crutchfield, J., Farmer, D., and Shaw, R., 1980, *Phys. Rev. Lett.*, **45,** 712–716.
[72] Bračič, M., and Stefanovska, A., 1998, *Bull. Math. Biol.*, **60,** 417–433.
[73] Bračič, M., and Stefanovska, A., 1998, Lyapunov exponents of simulated and measured quasi-periodic flows. *Signal Analysis and Prediction*, edited by A. Prochazka, J. Uhlir, J. P. Rayner and N. G. Kingsbury (Boston: Birkhäuser), pp. 479–488.
[74] van der Pol, B., and van der Mark, J., 1928, *Phil. Mag. [Suppl.]*, **6,** 763–775.
[75] Haken, H., 1987, *Advanced Synergetics* (Berlin: Springer).
[76] Murray, J. D., 1989, *Mathematical Biology* (Berlin: Springer).
[77] Winfree, A. T., 1990, *The Geometry of Biological Time* (Berlin: Springer).
[78] Clynes, M., 1960, *J. Appl. Physiol.*, **15,** 863–874.
[79] Kitney, R. I., Selman, A., McDonald, A., and Linkens, D., 1982, *Automedica*, **4,** 141–153.
[80] deBoer, R. W., Karemaker, J. M., and Strackee, J., 1987, *Am. J. Physiol.*, **253,** H680–H689.
[81] Baselli, G., Cerutti, S., Civardi, S., Malliani, A., and Pagani, M., 1988, *IEEE Trans. Biopmed. Eng.*, **35,** 1033–1046.
[82] Saul, J. P., Berger, R. D., Hui Chen, M., and Choen, R. J., 1989, *Am. J. Physiol.*, **256,** H153–H161.
[83] tenVoorde, B. J., Faes, Th. J. C., Janssen, T. W. J., Scheffer G. J., and Rompelman, O., 1995, Respiratory modulation of blood pressure and heart rate studied with computer model of baroreflex control. *Computer Analysis of Cardiovascular Signals*, edited by M. Di Renzo, G. Mancia, G. Parati, A. Pedotti and A. Zanchetti (Amsterdam: IOS Press), pp. 119–134.
[84] Seidel, H., and Herzel, H., 1995, Modelling heart rate variability due to respiration and baroreflex. *Dynamical Phenomena in Living Systems*, edited by E. Mosekilde and O.G. Mouritsen (Berlin: Springer), pp. 202–228.
[85] Cavalcanti, A., and Belardinelli, E., 1996, *IEEE Trans. Biomed. Eng.*, **43,** 982–989.
[86] Luchinsky, D. G., and McClintock, P. V. E., 1997, *Nature*, **389,** 463–466.
[87] Novkovski, N., and Stefanovska, A., Oscillations in the blood circulation, preprint.
[88] Frank, O., 1899, *Z. Biol.*, **37,** 483–526.
[89] Li, J. K.-J., 1996, *Comparative Cardiovascular Dynamics of Mammals* (Boca Raton: CRC Press).
[90] Kitney, R. I., and Seydenjad, S. R., 1997, Investigation of HRV by model analysis. *Frontiers of Blood Pressure and Heart Rate Analysis*, edited by M. Di Renzo, G. Parati, A. Pedotti and A. Zanchetti (Amsterdam: IOS Press), pp. 67–88.
[91] Stefanovska, A., Strle, S., and Bračič, M., Haken, H., 1998, *Open Sys. & Information Dyn.* (in the press).
[92] Folkow, B., and Neil, E., 1971, *Circulation* (New York: Oxford University Press).

Aneta Stefanovska is head of the Group of Nonlinear Dynamics and Synergetics, in the Faculty of Electrical Engineering, University of Ljubljana, Slovenia, where she received her PhD degree. Part of the research for her PhD she carried out at the Institute of Theoretical Physics and Synergetics at the University of Stuttgart, Germany, to which she returns regularly, currently as a Fellow of the Alexander von Humboldt Foundation. She initiated her PhD studies by investigating the effects of electric currents on blood flow in soft tissues, but then became fascinated by the nonlinear and complex dynamics of the blood circulation. The resultant experiments and analyses led to her proposal in 1992 of a model of coupled autonomous oscillators regulating blood flow in the cardiovascular system. Her research is devoted to extending and deepening understanding of the beauty and function of this life giving system.

Maja Bračič received her Diploma Degree in electrical engineering in 1993 from the University of Ljubljana, Slovenia, for work on the Lyapunov exponents characterizing blood flow. As a young researcher at the Faculty of Electrical

Engineering at the University of Ljubljana, she continued her work in developing and applying the techniques of linear and nonlinear dynamics to studies of real systems. Among them, the human cardiovascular system proved to be one of the most challenging. She performed extensive analyses of its behaviour by analysing signals related to its function which all illustrate that in spite of being complex and nonlinear, it is not complicated beyond understanding. Her main interest lies in the analysis of the couplings within the system, and she is currently preparing her PhD thesis on this topic.

Eur J Appl Physiol (1998) 79: 30–36

ORIGINAL ARTICLE

Hebe Désirée Kvernmo · Aneta Stefanovska
Knut Arvid Kirkebøen · Bjarne Østerud
Knut Kvernebo

Enhanced endothelium-dependent vasodilatation in human skin vasculature induced by physical conditioning

Accepted: 10 July 1998

Abstract Functional alterations to the endothelial cells of the vascular system may contribute to the improved circulatory performance induced by physical conditioning. We evaluated microvascular reactivity to iontophoretic application of acetylcholine (ACh) and sodium nitroprusside (SNP) through the skin and blood perfusion measurements in the same area using laser Doppler flowmetry. Whereas ACh acts on smooth muscle cells of the vascular system via the production of vasodilator substances from the endothelium, SNP is an endothelium-independent vasodilator acting on vascular smooth muscle cells directly. The study was performed using two groups of subjects with different levels of aerobic endurance, long distance runners competing at national level ($n = 9$) and controls ($n = 9$). The subjects were tested for 40 min on a treadmill before and after an exercise test at 80% of their maximal oxygen uptake. During stimulation by ACh cutaneous perfusion increased to a higher level in the athletes than in the controls (overall $P < 0.05$), whereas an acute period of exercise abolished this difference (overall $P > 0.6$). There was no significant difference between the athletes and the controls with respect to the SNP-induced increase in cutaneous perfusion either before ($P > 0.9$) or after ($P > 0.9$) exercise. The higher cutaneous perfusion responses to stimulation with ACh in the athletes than in the controls may support the hypothesis that regular exercise modifies the responsiveness of the cutaneous endothelium. The difference in ACh-induced perfusion and in unstimulated forearm perfusion between the two groups was present only at rest. This finding indicated that mechanisms were introduced during exercise, which compensated for the lower endothelial sensitivity to stimulation in the controls at rest.

Key words Acetylcholine · Cutaneous blood flow · Endothelium-dependent vasodilatation · Physical exercise · Laser Doppler flowmetry

H.D. Kvernmo
Institute of Medical Biology, University of Tromsø,
N-9037, Tromsø, Norway

H.D. Kvernmo (✉)
Department of Orthopaedic Surgery, Ullevål Hospital,
N-0407 Oslo, Norway

A. Stefanovska
Institute for Theoretical Physics I, University of Stuttgart,
D-70550, Stuttgart, Germany

A. Stefanovska
Faculty of Electrical Engineering,
University of Ljubljiana, SI-1000 Ljubljiana, Slovenia

K.A. Kirkebøen
Institute for Experimental Medical Research, Ullevål Hospital,
N-0407, Oslo, Norway

K.A. Kirkebøen
Department of Anaesthesia, Ulleråal Hospital,
N-0407 Oslo, Norway

B. Østerud
Institute of Medical Biology, University of Tromsø,
N-9037 Tromsø, Norway

K. Kvernebo
Department of Cardiothoracic Surgery, Ullevål Hospital,
N-0407, Oslo, Norway

Introduction

Research on the mechanisms behind the improved circulatory performance induced by physical conditioning in humans has mainly focused on cardiac function, pulmonary capacity and structural alterations of the microvasculature (Blomquist and Saltin 1983; Johnson 1989). However, it is also possible that control of the vascular system can be modified by physical exercise. One potential mechanism would be that repetitive vasodilatations induced by exercise sessions may produce adaptive changes in the intrinsic responsiveness of the vascular endothelium.

The properties of the vasodilatation of the endothelial system can be assessed by stimulation with acetylcholine (ACh). This method is based upon the novel discovery of

Furchgott and Zawadzki (1980) that the rabbit aorta dilates in response to the application of ACh only in the presence of an intact endothelium. Their experiments have suggested the existence of a mediator diffusing from endothelial cells to vascular smooth muscle cells and causing vasodilatation. Several years later it was discovered that this "endothelial-derived relaxing factor" was identical to nitric oxide (NO; Ignarro et al. 1987; Palmer et al. 1987). This ACh stimulation has been used to demonstrate impaired endothelium-mediated vasodilatation in diabetes mellitus, essential hypertension, hypercholesterolaemia, heart failure, and atherosclerosis (Drexler 1997; Andreassen et al. 1998).

Recent studies have demonstrated enhanced vascular responsiveness to endothelium-dependent vasodilators in skeletal muscle in exercise-trained subjects (Delp 1995; Kingwell et al. 1996), whereas the cutaneous responsiveness to endothelium-dependent vasodilators in response to exercise has not been tested. Increased flow and the correspondingly increased shear stress to the vessel wall have been found to be stimuli which elicit vasodilatation in the resistance vessels of skeletal muscle (Miller and Vanhoutte 1988; Koller and Kaley 1991). From this discovery and with the knowledge that increased core temperature during exercise results in an increased thermoregulatory contribution to the perfusion, we anticipated that adaptive changes induced by physical conditioning could also be detected in the cutaneous vasculature.

The aim of the present study was to test the hypothesis that physical conditioning enhances endothelial responsiveness to vasodilators in human cutaneous vasculature. The responsiveness to the endothelium-dependent substance ACh delivered iontophoretically through the forearm skin was compared with the endothelium-independent vasodilator, sodium nitroprusside (SNP), in two groups of healthy, male subjects of different levels of aerobic conditioning. Blood perfusion was recorded in the same area using the *non invasive* technique of laser Doppler flowmetry (LDF).

Methods

Subjects

The subjects used in the experiment were nine male long-distance runners (athletes) who had competed in national events for more than 5 years. They were tested in June while undergoing intense training [median 11.0 (range 8.5–17.0) hours a week; median 8.5 (range 5.0–11.0) times a week] and competing in at least one event each week. Their training program during this period included intense interval training. The subjects acting as controls comprised nine healthy, less well-trained soldiers (controls) who performed some physical activity [median 1.5 (range 0.5–7) hours a week; median 1.5 (range 0.5–3.5) times a week]. The subjects had not taken any medication during the week prior to the study. None of the subjects were smokers. Exclusion criteria were a history of cardiovascular disease or other illness. After being informed of the design of the study they gave their written consent. The study was approved by the local Ethics Committee.

Aerobic endurance level

The maximal oxygen uptake ($\dot{V}O_{2\,max}$) was measured during running on a motor driven treadmill at 3° uphill gradient (Hermansen 1973) using the Sensor Medics oxygen analyser (MMC Horizon System, USA). The oxygen uptake ($\dot{V}O_2$) was measured at 4–5 different submaximal levels, each level being measured for 4 min. Heart rate was recorded continuously using an electro-cardiograph (Sirekust 341, Siemens, Germany).

Laboratory procedure

All the subjects were asked to refrain from strenuous exercise for 24 h before the study to avoid the short-term effects of exercise. The $\dot{V}O_{2max}$ test procedure was therefore performed at least 24 h prior to the exercise test. Food intake before the exercise test was restricted to a light meal 2 h prior to the exercise test. The LDF measurements were carried out in a room with the temperature maintained constant at 22 (21–23)°C with the subjects in a supine position. At least 20 min were allowed for the subjects to become accustomed to the room temperature and the situation before the LDF measurements were made on the skin of the left forearm. Skin perfusion was measured immediately before and from 15 min after the exercise test. Skin temperature was measured using a digital skin thermometer (Fluke 2190, John Fluke, USA). The exercise test was performed on a treadmill at 3° uphill gradient for 40 min at 80% of the subjects' individual $\dot{V}O_{2max}$ after warming up for 10 min at 50% of their $\dot{V}O_{2max}$. The entire procedure is given in Table 1.

Plasma lactate

Before starting the exercise test and immediately after its finish blood from antecubital veins was drawn with minimal stasis by repetitive venipuncture using a 20-G needle and placed in pre-cooled plastic tubes containing 3.8% sodium citrate in a 9:1 blood:anticoagulant ratio. The blood was stored on ice (maximum 20 min) before centrifugation (20 min at 22°C and 1500 *g*) and the plasma samples were stored in aliquots at –70°C until further analysis.

Determination of packed cell volume, haemoglobin concentration and mean cell volume (MCV in ethylenediaminetetra-acetic acid EDTA) anticoagulated blood were made on an automatic analysing device (Coulter counter model S plus STKR, Coulter Electronics, Inc., Fl., USA) in EDTA blood. The plasma volume changes were determined according to an equation by which short-term changes in plasma volume can be calculated from changes in the PCV provided that no changes are observed in MCV (Van Beaumont 1972). Plasma lactate concentrations after the exercise test were adjusted for the changes in plasma volume observed after exercise.

Table 1 The laboratory procedure. $\dot{V}O_{2\,max}$ Maximal oxygen uptake, *LDF* laser Doppler flowmetry, *ACh-b* iontophoresis with acetylcholine (ACh) before running, *SNP-b* iontophoresis with sodium nitroprussid (SNP) before running, *ACh-a* iontophoresis with ACh after running, *SNP-a* iontophoresis with SNP after running, $\dot{V}O_{2,50\%}$, $\dot{V}O_{2,80\%}$ 50% and 80% of $\dot{V}O_{2\,max}$

Day 1:
$\dot{V}O_{2\,max}$-test
Day 3 or later:
22-min resting LDF
22-min ACh-b
22-min SNP-b
3-min blood sampling
10-min warming up at $\dot{V}O_{2,50\%}$
40-min exercise test at $\dot{V}O_{2,80\%}$
3-min blood sampling
22-min ACh-a
22-min SNP-a

Laser Doppler flowmetry

The principles of LDF have been thoroughly described elsewhere (Nilsson et al. 1980): LDF gives a semiquantitative assessment of microvascular blood perfusion, which is expressed in arbitrary units (a.u.). The LDF measurements from the skin reflect blood flow in capillaries, arterioles, venules and dermal vascular plexa; they have also been shown to reflect a minor nutritive and a major thermoregulatory part of the perfusion (Bollinger et al. 1991). A commercially available monitor was used for LDF (MBF 3D, Moor Instruments, Axminster, Devon, UK). A sampling frequency of 40 Hz and a time constant of 0.1 s were selected. The LDF measurements were obtained with two fibers, using an optic probe (P10A, Moor Instruments, England), and the data were stored on a personal computer.

Iontophoresis

The technique of iontophoresis allows polar drugs to cross the skin using a small, direct current. It has been shown to be possible to assess reactivity of the microvascular system when blood perfusion is being measured simultaneously in the same area (Müller et al. 1987; Westermann et al. 1988; Andreassen et al. 1998).

A combined probeholder, for iontophoresis and perfusion measurement, was fixed with double-sided adhesive tape on the volar side of the right forearm (Fig. 1) after the skin had been cleaned with isopropyl alcohol and left to dry in the air. The perspex probeholder had a small chamber for deposition of the test solutions which was then in direct proximity to the laser Doppler probe. A battery powered constant current stimulator (MIC 1, Moor Instruments Ltd, England) was used to provide a direct current for the drug iontophoresis. The active electrode was made of platinum, and charged according to the active ions of the drug. Quantities of 1% solutions of ACh (E. Merck, Germany) and SNP (E. Merck, Germany) were used. For ACh anodal current was used to transfer the cation (ACh^+) during iontophoresis, and for SNP cathodal current was applied to transfer the anion as has been described by Müller et al. (1987) and Westermann et al. (1988). A reference electrode was attached to the wrist of the right arm of the subjects.

The doses of drugs delivered were directly proportional to the total charge in millicoulombs which migrates through the skin surface, determined from the product of the constant current measured in milliampers and the duration of current flow in seconds. By applying small currents of brief duration, a transfer of vasoactive drugs into the epidermis beneath the chamber was accomplished. Drug doses were altered by varying the amount or the time of the current. To avoid current-induced stimulation of local sensory nerves, currents higher than 200 mA or total charges greater than 8 mC were avoided (Westermann et al. 1988). Based on pilot studies and earlier recommendations (Westermann et al. 1988) we made dose-response curves for both ACh and SNP, using charges of 0.75 mC (75 mA for 10 s), 1.5 mC (150 mA for 10 s), 3.0 mC (150 mA for 20 s) and 6.0 mC (200 mA for 30 s) with the response being measured for 300 s after each charge of the iontophoresis (Fig. 2a, b). These charges produced a stepwise increase in laser Doppler perfusion, reaching a saturation level at 6.0 mC (Fig. 2a, b). We subtracted the value of the perfusion during the unstimulated state from the response values obtained during iontophoresis of different doses.

For each subject five curves were recorded. One curve was obtained during 22 min of rest, and four curves were obtained during iontophoresis. Calibration of the laser Doppler equipment was checked before measurements on each of the test subjects. The different doses of the same substance (ACh or SNP) were applied at the same location. The test positions for ACh and SNP were separated by at least 5 cm. The chamber used in all the experiments allowed a skin area of 0.64 cm^2 to be treated.

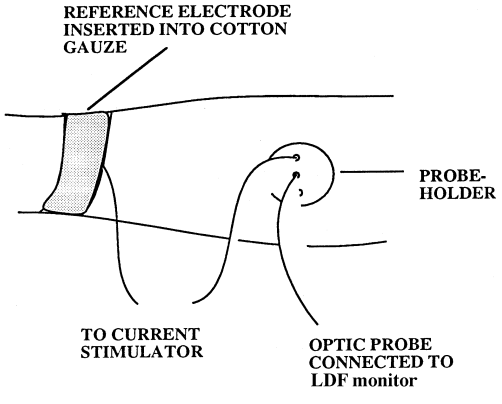

Fig. 1 Iontophoresis procedure on human forearm: arrangement of laser Doppler flowmeter probe holder and electrode for evoking iontophoretic vasodilatation responses

Statistical analysis

Data are illustrated either as group median with range, or as box plots. The five horizontal lines at the boxes are the 10, 25, 50, 75, and the 90th percentiles. Values above or below the 10th and 90th percentile are represented as data points. A two-way analysis of variance (ANOVA; repeated measure design) was used to compare the skin perfusion data between the athletes and the controls. The repeated measures were performed on the data after transformation to obtain normal distribution and equal variance in the two groups. When differences were obtained, post-hoc analyses were performed using the Mann-Whitney test for non-parametric comparisons between the two groups at the different doses. The Mann-Whitney test for comparison of independent samples was also used to evaluate differences between the athletes and the controls in

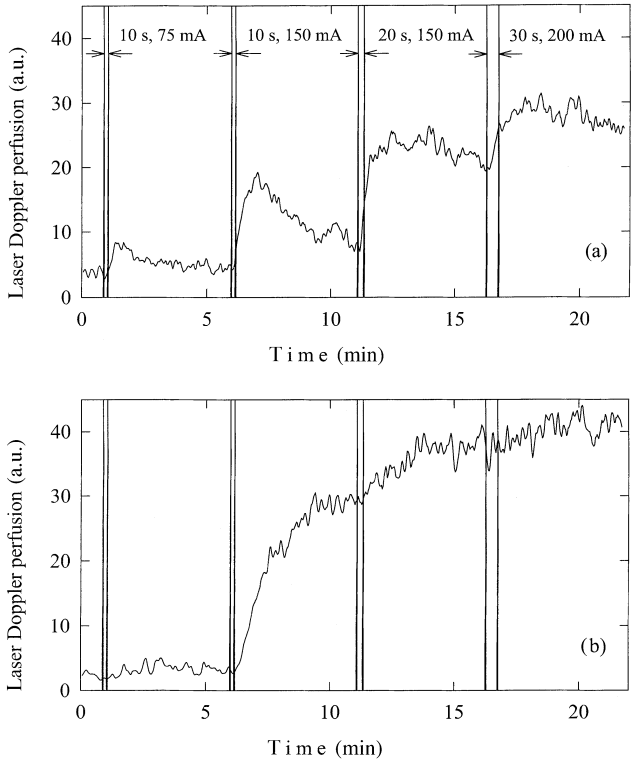

Fig. 2 Laser Doppler perfusion of the response to increasing concentrations of acetylcholine (**a**) and sodium nitroprussid (**b**). The dose-response curves were made by using the charges of 0.75 mC, 1.5 mC, 3.0 mC, and 6.0 mC. The response measuring period for each dose was 300 s

anthropometric and performance data. Statistically significant differences were defined as $P < 0.05$.

Results

Anthropometric and performance data

Anthropometric and performance data of both groups are summarized in Table 2. We found a lower resting heart rate and mean anterial pressure in the athletes compared to the controls, whereas no difference in skin temperature was seen. The lactate concentration was higher in the controls than in the athletes after exercise.

Basal perfusion in the unstimulated state at rest and after exercise

Before exercise perfusion of the forearm skin was significantly higher in the athletes than in the controls [median 5.3 (range 3.6–6.9) vs median 3.1 (range 2.3–4.5), $P < 0.005$]. Both groups had a higher skin perfusion after exercise, compared to the values before exercise ($P < 0.05$). After exercise there were no significant differences between the groups either before the iontophoresis with ACh [median 14.5 (range 6.6–44.0) vs median 10.0 (range 4.3–15.4) $P > 0.3$] or before the iontophoresis with SNP [median 6.9 (range 4.0–15.5) vs median 5.2 (range 4.8–7.0), $P > 0.3$].

Effects of ACh

Iontophoresis with ACh before standardized exercise induced a significant dose-dependent increase in skin perfusion in both the athletes and the controls ($P < 0.05$ for both groups; Fig. 3a). This ACh-induced increase in skin perfusion was higher in the athletes than in the controls (overall $P < 0.05$), giving a significant difference for a dose of 0.75 mC ($P < 0.05$). At a dose of 1.5 mC P equalled 0.08. Iontophoresis with ACh after standardized exercise produced a significant dose-dependent increase in skin perfusion in both athletes and controls ($P < 0.03$ for both groups), but there was no significant difference between the two groups (overall $P > 0.6$) (Fig. 3b).

Effects of SNP

A significant dose-dependent increase in skin perfusion during iontophoresis with SNP was demonstrated in both the athletes and the controls ($P < 0.03$ for both groups), but there was no significant difference between the two groups (overall $P > 0.9$; Fig. 4a). Also after exercise, a dose-dependent increase in skin perfusion was demonstrated in both the athletes and the controls ($P < 0.03$ for both groups). There was no significant difference between the two groups (overall $P > 0.9$; Fig. 4b).

Table 2 Anthropometric and performance data of athletes and controls. $\dot{V}O_{2\,max}$ Maximal oxygen uptake, $\dot{V}O_{2,80\%}$, 80% of $\dot{V}O_{2\,max}$, MAP mean arterial blood pressure, ΔPV plasma volume changes in response to running

	Athletes ($n = 9$)		Controls ($n = 9$)	
	Median	Range	Median	Range
Age (years)	26	18–32	20	19–21[a]
Body mass (kg)	76	70–79	75	70–90
Height (cm)	187	171–192	180	176–197
Heart rate (beats · min^{-1})				
Pre-exercise	51	44–60	57	51–72[a]
15-min post-exercise	63	52–78	95	78–105[b]
At $\dot{V}O_{2\,max}$	189	181–194	199	193–212[b]
MAP (mmHg)				
Pre-exercise	106	87–113	91	79–100[a]
15-min post-exercise	92	82–109	90	80–95
Skin temperature (°C)				
Pre-exercise	33.1	32.3–34.9	33.4	32.1–34.4
Post-exercise	33.9	32.3–35.3	33.7	33.2–34.1
$\dot{V}O_{2\,max}$ (ml · kg^{-1} · min^{1})	68.9	62.0–73.0	51.5	44.4–61.4[c]
Running velocity at $\dot{V}O_{2,80\%}$ (m · min^{-1})	227	217–243	177	143–198[c]
ΔPV (%)	−14.3	−14.6 to −14.3	−13.4	−15.7 to −1.9
Lactate (mmol · l^{-1})				
Pre-exercise	0.7	0.3–1.0	0.5	0.3–0.7
Post-exercise	1.9	0.7–5.6	3.2	1.0–6.2

[a] $P < 0.05$, [b] $P < 0.005$, [c] $P < 0.0001$

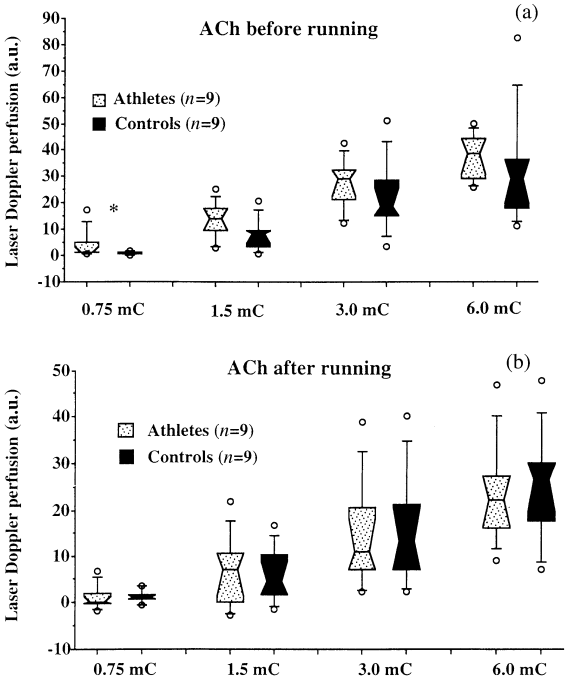

Fig. 3 Laser Doppler perfusion in response to iontophoretic applications of acetylcholine (*ACh*) before (**a**) and after (**b**) running in athletes and controls. The *five horizontal lines on the box* show the 10, 25, 50, 75, and the 90th percentiles. The values above or below the 10th and 90th percentile are represented as data points. * $P < 0.05$ (ANOVA, repeated measure design)

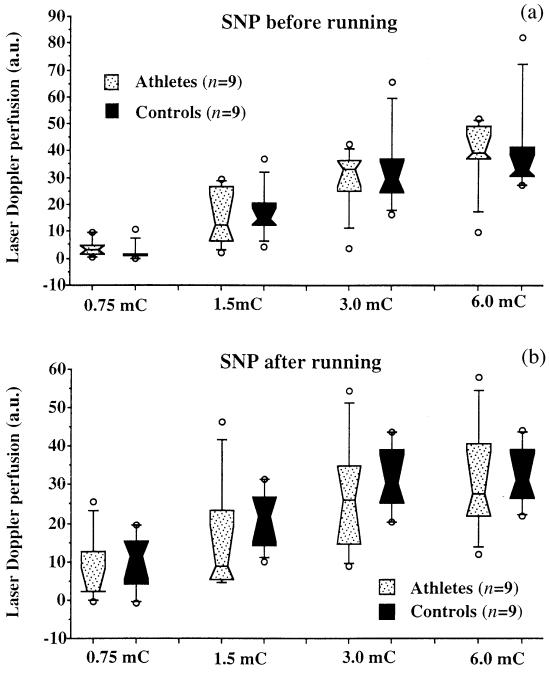

Fig. 4 Laser Doppler perfusion in response to iontophoretic applications of sodium nitroprussid (*SNP*) before (**a**) and after (**b**) running in athletes and controls. The *five horizontal lines on the box* show the 10, 25, 50, 75, and the 90th percentiles. The values above or below the 10th and 90th percentile are represented as data points

Discussion

Assessing endothelium-dependent vasodilatation in forearm skin following iontophoresis with ACh, the present data indicated increased responsiveness of the vascular endothelium in the athletes at rest, compared to the less well-trained controls. Endothelium-independent responses following iontophoresis with SNP, however, were similar to those of the control subjects.

From comparable levels of perfusion in unstimulated skin graded iontophoretic administration of ACh and SNP resulted in successive increases in perfusion in both groups. The observation that ACh-induced skin perfusion responses at rest were significantly higher in the athletes than in the controls was consistent with our hypothesis that the endothelium of the microvascular system becomes more susceptible to stimulation as aerobic capacity increases. These results are in agreement with a recent study using venous occlusion pletysmography in humans (Kingwell et al. 1996), in which intra-arterial infusion of ACh produced higher perfusion responses in athletes than in controls. Enhanced ACh-induced vasodilatation after endurance training has also been demonstrated in the thoracic aorta and pulmonary artery of the rabbit (Chen and Li 1993), as well as in the abdominal aorta of the rat (Delp et al. 1993). Recently ACh-induced vasodilatation in human skin has been shown to correlate closely to peak $\dot{V}O_2$ in heart transplant recipients (Andreassen et al. 1998).

The exact mechanisms underlying the ACh-induced vasodilatation in human cutaneous vasculature may differ from that observed in other vessels. Whereas ACh facilitates vasodilatation indirectly via the conversion of L-arginine to NO in the vascular endothelium of the aorta and arterioles (Moncada et al. 1991), ACh in the cutaneous circulation may in addition induce endothelium-dependent vasodilatation via other pathways. An in vitro study of human subcutaneous resistance vessels has demonstrated that both NO and prostaglandins may be involved in ACh-induced relaxation (Richards et al. 1990). In addition, Morris and Shore (1996) have concluded in their study of the mechanisms underlying ACh-induced responses of cutaneous blood flow that mediators other than prostaglandins and sensory nerve activation may be involved in skin perfusion following iontophoresis with ACh. Kreidstein et al. (1992) in their study of skin flaps have demonstrated the presence of endothelium-dependent and endothelium-independent vasodilatation. They have convincingly shown that the vascular relaxation effect of ACh was significantly reduced by inhibitors of NO synthesis; however, the ACh-induced vasodilatation was not completely blocked. To what extent adenosine, prostaglandins, endothelium-dependent hyperpolarization factor and other substances contribute to the ACh-induced vasodilatation in the cutaneous vasculature remains to be investigated.

To evaluate whether physical conditioning makes smooth muscle cells of the vascular system more sensi-

tive to vasodilators, we have compared vasodilatation induced by SNP in athletes and controls. The SNP has been shown to evoke vascular relaxation by directly increasing guanosine 3′,5′-cyclic monophosphate in vascular smooth muscle cells (Rapoport et al. 1983). Our data showed almost identical SNP-induced increases in skin perfusion in the two groups both at rest and after exercise. This would indicate that the enhanced ACh-induced skin perfusion before exercise was not due to enhanced sensitivity of vascular smooth muscle cells to vasodilators, but rather to increased levels of endothelial factors (most probably NO) reaching vascular smooth muscle cells. This is in agreement with previous studies on animals (Delp et al. 1993) and humans (Kingwell et al. 1996), in which a similar sensitivity to SNP was found at rest for both trained and untrained subjects.

Our results demonstrated enhanced ACh-induced perfusion in athletes compared to controls at rest. No such differences were, however, observed for the responses to SNP. Increased flow and correspondingly increased shear stress to the vessel wall have been shown to be stimuli which elicit vasodilatation in the resistance vessels of skeletal muscles (Miller and Vanhoutte 1988; Koller and Kaley 1991). We hypothesized that the increased muscle blood flow during exercise could be detected indirectly in the perfusion of forearm skin, since increased core temperature provides an increased thermoregulatory contribution to the perfusion. The skin temperature did not differ between the two groups. The observed difference in ACh-induced perfusion at rest therefore would indicate a true difference in the sensitivity of the endothelial cells to inducing vasodilatation, probably as a result of repetitive increases in blood flow during training sessions.

We could find no data after exercise which were comparable to the ACh-responses obtained before exercise. However, a previous study has demonstrated a minor contribution of NO to exercise-induced vasodilatation (Gilligan et al. 1994). In muscles, an increased concentration of metabolic products, altered mechanical forces and changes in the neurohumural milieu, have all been postulated to be important in the development of adaptations in the endothelium which occur with exercise training (Delp 1995). In the present study we demonstrated higher plasma lactate concentrations in the controls than in the athletes after exercise. We therefore speculate that the smaller cutaneous responses to the endothelium-dependent vasodilator ACh in the controls may have indicated an inadequate capacity of the endothelium to induce relaxation of vascular smooth muscle in the small arterioles of exercising muscle, which led to hypoperfusion and increased lactate concentrations.

To what extent lactate or other substances in the plasma contribute to the exercise-induced vasodilatation in the cutaneous vasculature remains unknown. However, there may be factors which make the vessels more sensitive to vasodilator stimuli after repetitive periods of physical exercise. The finding that ACh-induced skin perfusion at rest is significantly higher in athletes than in controls may therefore have relevance not only to the understanding of exercise physiology, but it may also have therapeutic implications for diseases with impaired endothelium-dependent vasodilatation, such as diabetes mellitus, hypertension, hypercholesterolaemia, atherosclerosis and heart failure. Regular exercise may be recommended for sufferers of these diseases as a non-pharmacological approach to restore endothelium-dependent dilatation.

Study limitations

It has been suggested that vasodilatation obtained by iontophoresis with ACh vehicle and SNP vehicle may also stimulate local sensory nerves (Morris et al. 1996; Andreassen et al. in press). However, a study using the same dose-response curve as in the present study has demonstrated that the drug vehicle had significant influence on increases in skin perfusion from the third iontophoresis of ACh and from the second iontophoresis of SNP (Andreassen et al. 1998). Thus, the observed difference between the athletes and the controls in the present study represented a true difference since the difference was observed at the lowest dose of ACh.

We chose to test the subjects at 80% of their individual $\dot{V}O_{2\,max}$, assuming that the exercise intensity would then be equal in the two groups. This standardization resulted in a lower running speed in the controls compared to the athletes. Even though we made this standardization, we found a higher plasma lactate concentration after exercise in the controls than in the athletes. However, the differences demonstrated between the two groups after exercise would probably have been even more pronounced if they had been tested at the same speed. In cross-sectional study designs one also has to bear in mind potential differences in genetic, dietary and other life-style factors between athletes and controls, which may alter endothelial function.

In conclusion, physical conditioning resulted in enhanced endothelium-dependent vasodilatation in the cutaneous vasculature, as demonstrated by the higher ACh-induced perfusion among the athletes compared to the controls. The unaltered response to SNP showed that differences in vascular smooth muscle responsiveness for vasodilatation did not account for this difference. The difference in ACh-induced perfusion and in forearm perfusion in the unstimulated state between the two groups was present only at rest. This finding would indicate that mechanisms are introduced during exercise, which compensate for the lower endothelial sensitivity to stimulation as seen in the controls at rest. The observed difference between the groups illustrates the applicability of cutaneous LDF measurements to investigations such as these.

Acknowledgements The authors are indebted to Prof. Harald Refsum, head of the Department of Clinical Physiology at Ullevål

Hospital where all the measurements were made, for his stimulating interest. The excellent technical assistance of Anne Edvardsen and Karin Lia, and the support with the statistical analysis by Tom Wilsgård, are gratefully acknowledged. We would also like to thank Moor Instruments, England, for providing the devices used in this study, with special thanks to Rodney Gush. Aneta Stefanovska was supported by the Slovenian Ministry of Science and Technology and by the Alexander von Humboldt Foundation, and Hebe Désiréc Kvernmo was supported by the Norwegian Research Council for Science and Humanities.

References

Andreassen AK, Kvernebo K, Jørgensen B, Simonsen S, Kjekshus J, Gullestad L (1998) Exercise capacity in heart transplant recipients: relation to impaired endothelium-dependent vasodilatation of the peripheral microcirculation. Am Heart J 136:320–328

Blomquist CG, Saltin B (1983) Cardiovascular adaptations to physical training. Annu Rev Physiol 45:169–189

Bollinger A, Hoffmann U, Franzeck UK (1991) Evaluation of flux motion in man by the laser Doppler technique. Blood Vessels 28:21–26

Chen HI, Li HT (1993) Physical conditioning can modulate endothelium-dependent vasorelaxation in rabbits. Arterioscler Thromb 13:852–856

Delp MD (1995) Effects of exercise training on endothelium-dependent peripheral vascular responsiveness. Med Sci Sports Exerc 27:1152–1157

Delp MD, McAllister RM, Laughlin MH (1993) Exercise training alters endothelium-dependent vasoreactivity of rat abdominal aorta. J Appl Physiol 73:1354–1363

Drexler H (1997) Endothelial dysfunction: clinical implications. Prog Cardiovasc Dis 30:287–324

Furchgott RF, Zawadzki JW (1980) The obligatory role of endothelial cells in the relaxation of arterial smooth muscle by acetylcholine. Nature 288:373–376

Gilligan DM, Panza JA, Kilcoyne CM, Waclawiw MA, Casino PR, Quyyumi AA (1994) Contribution of endothelium-derived nitric oxide to exercise-induced vasodilatation. Circulation 90:2853–2858

Hermansen L (1973) Oxygen transport during exercise in human subjects. Acta Physiol Scand [Suppl] 339:1–104

Ignarro, LJ, Byrns RE, Buga GM, Wood KS (1987) Endothelium-derived relaxing factor from pulmonary artery and vein possesses pharmacological and chemical properties identical to those of nitric oxide radical. Circ Res 61:866–879

Johnson JM (1989) Circulation to skeletal muscle. In: Patton HD, Fuchs AF, Hille B, Scheer AM (eds) Textbook of physiology. Saunders, New York. pp 887–897

Kingwell BA, Tran B, Cameron JD, Jennings GL, Dart AM (1996) Enhanced vasodilation to acetylcholine in athletes is associated with lower plasma cholesterol. Am J Physiol 270:H2008–H2013

Koller A, Kaley A (1991) Endothelial regulation of wall shear stress and blood flow in skeletal muscle microcirculation. Am J Physiol 260:H862–H868

Kreidstein ML, Pang CY, Carlsen LN, Xu N (1992) Evidence for endothelium-dependent and endothelium-independent vasodilation in human skin flaps. Can J Physiol Pharmacol 70:1208–1216

Miller VM, Vanhoutte PM (1988) Enhanced release of endothelium-derived factor(s) by chronic increases in blood flow. Am J Physiol 255:H446–H451

Moncada SR, Palmer MJ, Higgs EA (1991) Nitric oxide: physiology, pathophysiology, and pharmacology. Pharmacol Rev 43:109–142

Morris SJ, Shore AC (1996) Skin blood flow responses to the iontophoresis of acetylcholine and sodium nitroprusside in man: possible mechanisms. J Physiol 496:531–542

Müller PH, Keller R, Imhof P (1987) Laser Doppler flowmetry, a reliable technique for measuring pharmacologically induced changes in cutaneous blood flow? Methods Find Exp Clin Pharmacol 9:409–420

Nilsson GE, Tenland T, Öberg PÅ (1980) Evaluation of a laser Doppler flowmeter for measurement of tissue blood flow. IEEE Trans Biomed Eng 27:597–604

Palmer RMJ, Ferrige AG, Moncada S (1987) Nitric oxide release accounts for the biological activity of endothelium-derived relaxing factor. Nature 327:524–526

Rapoport RM, Draznin MB, Murad F (1983) Endothelium-dependent relaxation in rat aorta may be mediated through cyclic GMP-dependent protein phosphorylation. Nature 306:174–176

Richards NT, Poston L, Hilton L (1990) Cyclosporin A inhibits endothelium-dependent, prostanoid-induced relaxation in human subcutaneous resistance vessels. J Hypertens 3:159–163

Van Beaumont W (1972) Evaluation of hemoconcentration from hematocrit measurements. J Appl Physiol 31:712–713

Westerman RA, Widdop RE, Hannaford J, Low A, Roberts RGD, Kent P, Sideris K, Yip T, Hales JRS, Stephens FRN (1988) Laser Doppler velocimetry in the measurement of neurovascular function. Austr Phys Eng Sci 11:53–65

Embedded Secure Document

The file *http://www.lancs.ac.uk/depts/physics/research/nbmphysics/ljubljana/people/aneta/Valcki_Maja.pdf* is a secure document that has been embedded in this document. Double click the pushpin to view.

Embedded Secure Document

The file *http://www.lancs.ac.uk/depts/physics/research/nbmphysics/ljubljana/people/aneta/Lyapuni_Maja.pdf* is a secure document that has been embedded in this document. Double click the pushpin to view.

ELSEVIER

20 October 1997

PHYSICS LETTERS A

Physics Letters A 235 (1997) 24–30

On the overestimation of the correlation dimension

Aneta Stefanovska [a], Sašo Strle [b], Peter Krošelj [a]

[a] *Faculty of Electrical Engineering, University of Ljubljana, Ljubljana, Slovenia*

[b] *Faculty of Mathematics and Physics, University of Ljubljana, Ljubljana, Slovenia*

Received 7 March 1997; revised manuscript received 28 May 1997; accepted for publication 30 June 1997

Communicated by A.P. Fordy

Abstract

The effect of non-linear mapping from the time domain to the phase space may result in an overestimation of the correlation dimension. We analyse the origin of the overestimation and suggest a criterion for the number of points necessary to approach the true scaling region in the correlation integral. © 1997 Elsevier Science B.V.

PACS: 05.45.+b

1. Introduction

In this Letter we consider the practical application of the method of calculation of the correlation dimension [1–5]. Analyses of a model of coupled oscillators, up to a 5-torus, are presented. Such a simple model was chosen for two reasons: (i) it resembles the frequency spectra of time series recorded from the cardiovascular system, whose complex dynamics we intend to ascertain [6–8], and (ii) the true value of its dimension is known. The reconstruction of the phase space using the method of delayed coordinates [9–11] is thus straightforward, since both crucial parameters – the embedding time and the embedding dimension – can be determined. Moreover, the effect of the number of points used to reconstruct the attractor can be studied. The importance of the number of points has already been reported and several criteria have been proposed [12–15]. We show that in the case of an insufficient number of points a false plateau may be found due to non-linear mapping from the time domain to the phase space. As a result, an overestimation of the attractor dimension would be obtained. We approach this problem analytically and suggest a revision of the criterion proposed by Eckmann and Ruelle [15].

2. The algorithm and time series

The reconstruction of a system dynamics usually begins with no knowledge of the number of state variables involved. There are therefore no time series available for each state variable. Indeed, quite often we start with one measured time series consisting of a finite number of points (n) sampled at equal time intervals, the sampling time (t_s). The trajectories are then reconstructed using the method of delay coordinates

$$x(t) = [x(t), x(t+\tau), \ldots, x(t+(d-1)\tau)], \quad (1)$$

where $t = t_s, 2t_s, \ldots, nt_s - (d-1)\tau$ and d is the dimension of the embedding space. The embedding time $\tau = It_s$ (I integer) is used for the reconstruction of

PII S0375-9601(97)00552-5

the phase space. For a sufficiently large value of the embedding dimension d – and if some additional conditions are satisfied – the reconstructed trajectory has the same topological and geometrical properties as the system's phase space trajectory [9–11]. The choice of both parameters – d and τ – is crucial for the appropriate reconstruction of an attractor. Different methods were proposed to estimate optimal values of these parameters, based on the autocorrelation function or higher order correlation functions of the time series, on mutual information, on calculation of the false nearest neighbours, or on power spectra [16–21].

The algorithm proposed by Grassberger and Procaccia (GP) [1,3] involves the computation of a correlation integral whose power-law behaviour is used to estimate the dimension of the attractor. The correlation integral is defined as

$$C(\varepsilon, n) = \frac{1}{n(n-1)} \sum_{i=1}^{n_v} \sum_{\substack{j=1 \\ j \neq 1}}^{n_v} H(\varepsilon - \| \boldsymbol{x}_i - \boldsymbol{x}_j \|) , \tag{2}$$

where H is the Heaviside function, $\boldsymbol{x}_i$ and $\boldsymbol{x}_j$ are vectors which locate points on the trajectory that has been embedded in a d-dimensional space, $\| \ \|$ represents the distance norm which can be either the standard Euclidean norm or the maximum norm, and n_v is the number of vectors, $n_v = n - d - 1$. The correlation dimension D_2 is defined by the limit

$$D_2(\varepsilon, n) = \lim_{\varepsilon \to 0} \lim_{n \to \infty} \frac{\ln C(\varepsilon, n)}{\ln \varepsilon} , \tag{3}$$

or, when it exists,

$$D_2 = \lim_{\varepsilon \to 0} \lim_{n \to \infty} \frac{\mathrm{d} \ln C(\varepsilon, n)/\mathrm{d}\varepsilon}{\mathrm{d} \ln \varepsilon / \mathrm{d}\varepsilon} . \tag{4}$$

Thus, the power law is reflected as the saturation of the curves plotted in $\mathrm{d} \ln C(\varepsilon, n)/\mathrm{d}\varepsilon$ versus $\mathrm{d} \ln \varepsilon / \mathrm{d}\varepsilon$ (let us introduce the expression "dimensionality diagram" for this plot), and should be considered for $\varepsilon \to 0$ and $n \to \infty$. Generalisations of (2) to order-q correlation integrals, where q in principle ranges from $-\infty$ to $+\infty$, have been used to estimate order-q dimensions [2,4].

In practice, the sum (2) is taken only for those i's and j's that are separated by more than z sampling times to avoid artificial correlation among consecutively sampled points on the attractor [32]. The algorithm is in fact based on the calculation of the number of vectors displaced by a distance of less than ε from the reference vectors. In our computations, i reference vectors are randomly chosen ($i = 1, \ldots, r; r \leqslant n$) and the distance between them and j vectors ($j = 1, \ldots, m; m \leqslant n$), separated by more than z points, in the set is then calculated.

2.1. The time series

The test time series, reconstructed by a sampling frequency of $f_s = 1000$ Hz, are obtained from the system of uncoupled oscillators

$$x_t(t) = A_1 \sin(\omega_1 t + \alpha_1) + \ldots + A_5 \sin(\omega_5 t + \alpha_5) . \tag{5}$$

The basic frequencies f_l ($f_l = \omega_l / 2\pi$) are chosen independent over rationals, with values of $f_1 = 6.625$, $f_2 = 14.823$, $f_3 = 37.875$, $f_4 = 49.987$ and $f_5 = 133.123$ Hz, while the phases are $\alpha_l = 0$, and the amplitudes either (i) $A_l = 1$ or (ii) $A_l = 1/f_l$.

3. Varying the parameters

The model based on quasi-periodic time series enables an unambiguous choice of all the parameters involved: the sampling time, the number of points, the embedding time, the embedding dimension, as well as the system complexity. In addition, it mimics to a certain extent the time series measured from the cardiovascular functions [6–8], and hence contributes to the a priori knowledge necessary to approach their analysis. To learn the role of each of the parameters we have undertaken a series of numerical experiments [22]. Here we report only the values of D_2 obtained for a range of parameters, and for a model complexity ranging from a limit cycle, up to a 5-torus.

The quantitative value of the correlation dimension should be obtained, by definition, at $\varepsilon \to 0$. In practice, it is determined as a slope of the correlation integral for small ε. One searches for linear regions where the slope is constant. Only then can we consider that the slope equals the limit value, and that the limits exists. This procedure is repeated for each embedding dimension. The values obtained are then plotted in

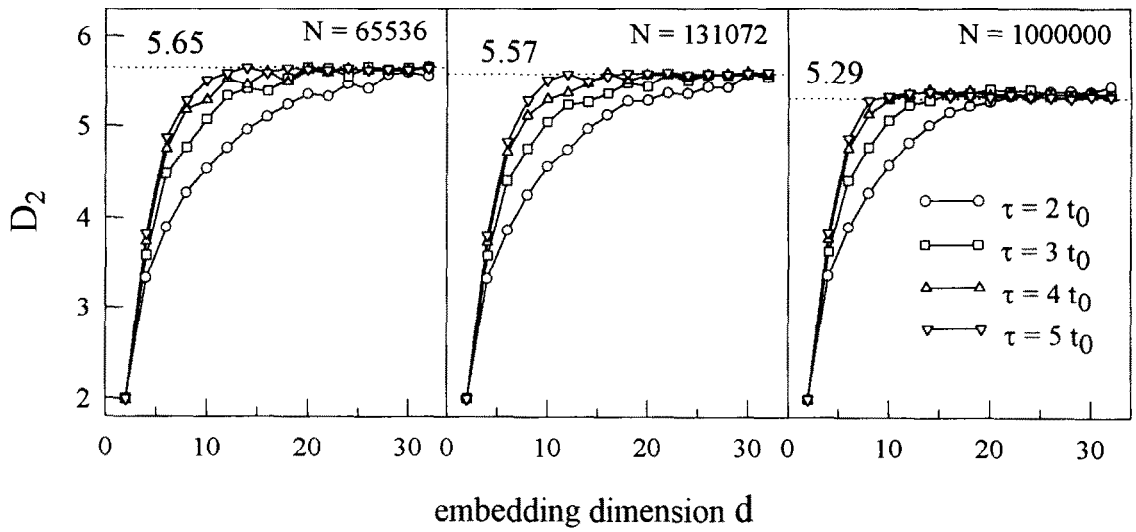

Fig. 1. The values of D_2 for a 5-torus with $A_1 = \ldots = A_5 = 1$ calculated for a different number of points.

Table 1
Correlation dimension for a limit cycle and a 2-, 3-, 4- and 5-torus ($A_1 = \ldots = A_5 = 1$) calculated at a different number of points

Number of basic frequencies l	n	Correlation dimension D_2			
		$\tau = 2t_s$	$\tau = 3t_s$	$\tau = 4t_s$	$\tau = 5t_s$
1	65536	1.002	1.005	1.005	1.003
	131072	1.003	1.003	1.004	1.002
2	65536	2.05	2.05	2.06	2.06
	131072	2.05	2.04	2.04	2.04
3	65536	3.14	3.17	3.17	3.17
	131072	3.09	3.11	3.11	3.09
4	65536	4.39	4.56	4.56	4.54
	131072	4.32	4.50	4.56	4.56
5	65536	5.45	5.65	5.66	5.65
	131072	5.40	5.55	5.57	5.60
	1000000	5.26	5.27	5.29	5.29

the saturation diagram. Values obtained for 5-tori with $A_l = 1$, for embedding dimensions ranging from $d = 2$ to $d = 32$, are presented in Fig. 1. The quantitative value for D_2 is usually calculated for some interval of d at which the obtained values settle. The values summarized in Table 1 are the averages of values obtained at embedding dimensions at which saturation is obtained. For example, D_2 for 5-tori is an average over values obtained for $16 \leqslant d \leqslant 32$.

Here, we can seek a confidence interval at each d. Ramsey and Yuan [23] have already analysed and discussed the problem of bias and error bars in dimension calculations. We found that it is more important to check the linearity of segments in the dimensionality diagram and the convergence of the values in the saturation diagram. This is in fact a check on the existence of the limit defined in Eq. (3).

In spite of the large number of points considered, the calculated numbers presented in Fig. 1 and Table 1 are not integers, as would be expected. Indeed, all are higher than the true values. The overestimation increases as the system complexity increases. Using the same five-dimensional system Jedynak et al. [24] obtained values around 5.5 and argued that they cannot even serve as approximations of the correct values. Let us, therefore, examine the scales at which the plateau in the dimensionality diagram occurs, and the impact of the number of points used for the reconstruction of an attractor.

3.1. Why does overestimation occur?

Inspecting Table 1 and Fig. 1 we see that the extent of overestimation depends on the number of points considered. However, let us first discuss the scaling region as it occurs in the dimensionality diagram presented in Fig. 2. The scaling regions occurs at $\ln \varepsilon \sim 1 \pm 0.2$. But, for $d > 6$, the values of D_2 are greater than expected. In fact, all curves tend toward the true value

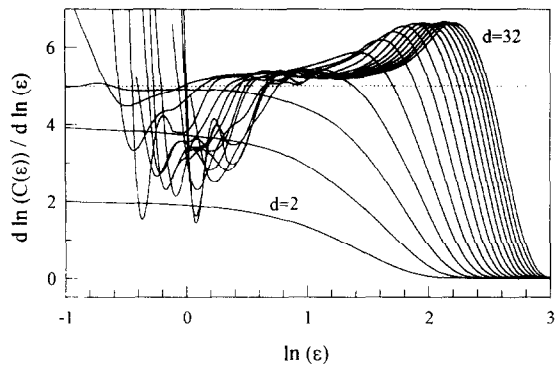

Fig. 2. Dimensionality diagram for a 5-torus ($A_1 = \ldots = A_5 = 1$, $t_s = 1$ ms, $n = 1\,000\,000$, $r = 20\,000$, $m = 40\,000$, $z = 10$ and $\tau = 2t_s$). The true plateau is at $\ln\varepsilon \sim 0$, where the error due to an insufficient number of points dominates. Therefore we estimate D_2 for $\ln\varepsilon \sim 1$ and obtain values greater than the true value.

5, although they become dispersed when approaching $\ln\varepsilon < 0.0$, where the limit and the true scaling region are to be found.

To analytically consider the problem of overestimation on the limit cycle let us make the following assumptions:

(i) the attractor is a circle in the phase space (Fig. 3a);

(ii) the number of points n from which the attractor is reconstructed is big enough to be considered infinite, and

(iii) the points are equidistantly sampled in time, hence their distribution density on the attractor is uniform and is equal to $n/2\pi$.

Within an angle 2φ there are

$$n(\varepsilon) = \frac{n\varphi}{\pi} \tag{6}$$

points. If we cover the attractor by balls of radius ε, the corresponding angle is given by the relation

$$\sin\frac{\varphi}{2} = \frac{\varepsilon}{2A}, \tag{7}$$

as is evident from Fig. 3a. The above relations yield

$$\varphi = 2\arcsin\frac{\varepsilon}{2A} \tag{8}$$

and

$$n(\varepsilon) = \frac{2n}{\pi}\arcsin\frac{\varepsilon}{2A} \tag{9}$$

for the number of points within such a ball.

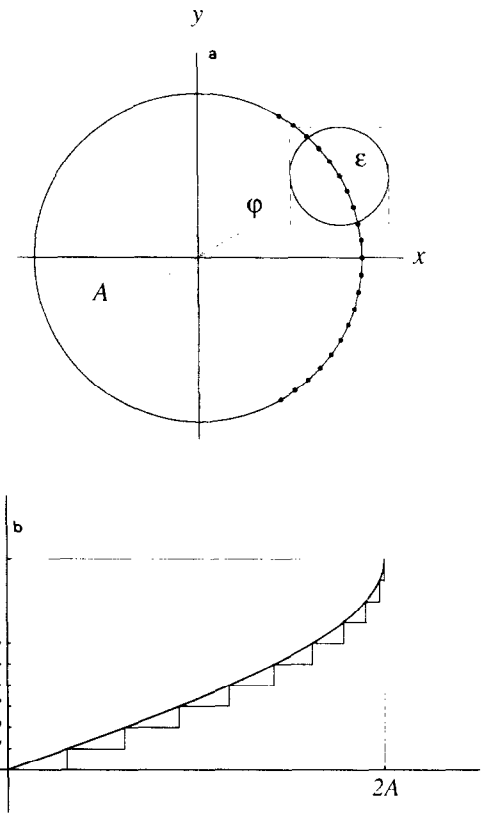

Fig. 3. For the calculation of the correlation integral we vary ε and count the number of points inside the ball. An equivalent result can be obtained by replacing balls with squares (a). The step function represents the actual number of points inside the ball of radius ε and at a large number of points is well approximated by the continuous function (b).

Since we consider the number of points on the attractor to be infinite, the number $n(\varepsilon)$ of points inside the ball is a continuous function. Under the assumptions made, the values of $C(\varepsilon, n)$ and $n(\varepsilon)$ are either equal or differ by a multiplicative constant only. Then, according to the GP algorithm, we can search for the derivative of the function $\ln n(\varepsilon)$,

$$\frac{\mathrm{d}\ln n(\varepsilon)}{\mathrm{d}\ln\varepsilon} = \frac{\mathrm{d}\ln n(\varepsilon)}{\mathrm{d}\varepsilon}\frac{\mathrm{d}\varepsilon}{\mathrm{d}\ln\varepsilon}. \tag{10}$$

We obtain

$$\frac{\mathrm{d}\ln n(\varepsilon)}{\mathrm{d}\varepsilon} = \frac{\mathrm{d}\ln[(2n/\pi)\arcsin(\varepsilon/2A)]}{\mathrm{d}\varepsilon}$$

$$= \frac{1}{\arcsin(\varepsilon/2A)}\frac{1}{\sqrt{1-(\varepsilon/2A)^2}}\frac{1}{2A},$$

$$\frac{d\varepsilon}{d\ln\varepsilon} = \varepsilon . \tag{11}$$

Let us introduce $\varphi/2 = t$, so $\varepsilon/2A = \sin t$. Then for $t \neq 0$

$$\frac{d\ln n(\varepsilon)}{d\ln\varepsilon} = \frac{\sin t}{t\sqrt{1-\sin^2 t}} = \frac{\tan t}{t} > 1 . \tag{12}$$

The value of the above expression is strictly greater than 1, for all $\varphi > 0$ and hence for all $\varepsilon > 0$. Moreover, the value of ε cannot be arbitrarily small; indeed, we are restricted by the number of points with which the attractor is reconstructed. By decreasing the radius of balls with which we cover the attractor, we come to a value at which there are not enough points inside the ball. Hence, because $\varphi \neq 0$ and the mapping from the time domain to the phase space is non-linear, the result is an overestimation of the dimension. Only in the limit do we obtain correct results, since the segment on the circle becomes linear.

We have considered an ideal geometry of the attractor of the sinusoidal function – a circle. It is more probable that it will be reconstructed as an ellipse. In one dimension we have long linear segments and short strongly non-linear segments. In high-dimensional space – in the case of a quasi-periodic signal – the body of the attractor, an n-torus, is a geometrically more complicated object with extensive foldings, and the overestimation is even more pronounced. Moreover, when we have a system of oscillators – each one of them having a different frequency – there are always some for which the phenomenon caused by the effect of non-linear mapping from the time domain to the phase space becomes pronounced.

The observed dispersion of the results occurs due to the fact that $n(\varepsilon)$ is a discrete valued function and not a continuous one, as presented in Fig. 3b. As we continuously decrease the value of ε the remaining number of points inside the balls also decreases. At a certain value of ε, the fact that we are dealing with a discrete and small number of points results in a large relative error due to quantization. This error also occurs at big ε, but is negligible due to the large number of points inside the balls. Hence, the only way to avoid this problem is to choose relatively large values of ε. However, this is in contradiction with the fact that, by definition of the correlation dimension, ε should tend toward 0. Since we usually stop at a certain positive value of ε, a systematic error occurs, as we saw in the calculations presented above.

It could be argued that the phenomenon presented above might reflect a behaviour unique to quasi-periodic systems. However, this phenomenon occurs as a result of finite separability, since ε always has a positive value. Hence, an overestimation can be expected to occur for any attractor. For example, the Cantor set embedded in the circle can easily be shown to be characterised by the same effect as shown by Eq. (12).

Let us note that an underestimation can also occur. This phenomenon has been presented by Möller et al. [25]. They analysed the digitizing error by varying digitizing resolutions, at a constant number of points, and have shown an underestimation of various chaotic as well as quasi-periodic attractors when small precision is used.

3.1.1. The number of points

At this stage one may ask: how many points would it be sufficient to take? The importance of the number of points used to reconstruct the attractor and to calculate the correlation integral has already been addressed [12–15]. Smith's analysis [12] indicates that the number of points required to estimate the dimension of an attractor to within 5% of its true value increases at least as fast as $n_{\min} \geqslant 42^M$, where M is the greatest integer smaller than the dimension of the set. However, Grassberger et al. [26] have argued that this pessimistic estimate is based on assumptions that are not applicable to the correlation dimension. Nerenberg and Essex [13] have also reviewed the criterion proposed by Smith and have proposed an order of magnitude smaller. A less severe criterion was proposed by Procaccia [14]. He suggested a relation $D_{2_{\max}} = \ln n$, which means that for a 5-torus we need 10^5 points – fewer than were taken in our calculations. This relation does not take into account the scaling region. Eckmann and Ruelle [15] proposed the following relation for the largest correctly estimated dimension,

$$D_{2_{\max}} = \frac{2\ln n}{\ln(1/\rho)} , \tag{13}$$

where $\rho = \varepsilon/E \ll 1$ and E is the diameter of the reconstructed attractor. Accordingly, for $\rho = 0.1$ we need $n = 1000$ in order to estimate $D_2 \leqslant 6$. The results we have presented thus far are obtained from

considerable larger data sets and are still greater than the true values.

To reliably estimate the D_2 we need a sufficiently long interval $(\varepsilon_{\min}, \varepsilon_{\max})$. Only then can we determine the slope $\mathrm{d}\ln C(\varepsilon, n)/\mathrm{d}\ln\varepsilon$, which is the estimate of the dimension: $(\varepsilon_{\max}/\varepsilon_{\min})^{D_2} \gg 1$. For the $\varepsilon_{\min}$ chosen, the value of $n_{\min}$ is determined by the diameter E of the reconstructed attractor (the upper limit of which is bounded above by the peak-to-peak value of the time series A_{pp} and the dimension of the embedding space d). Finally, it is necessary (but not sufficient) to have at least one point in each hypercube (cube or square) with a side ε, and for dimension D_2 one needs $n \geqslant (E/\varepsilon_{\min})^{D_2}$. From this it follows that

$$D_{2_{\max}} = \frac{\ln n}{\ln(1/\rho)}. \tag{14}$$

In this case the value of $D_{2_{\max}} \leqslant 6$ is reliably estimated for $\rho = 0.1$ and $n = 1\,000\,000$. One can use expression (14) to estimate an order of magnitude only. To approach the optimal $\varepsilon_{\min}$ in practice we should first calculate the dimension D_2 for some value of $\varepsilon_{\min}$. We then decrease $\varepsilon_{\min}$ by a factor k ($\varepsilon_{\min} \to \varepsilon_{\min}/k$), increase the number of points by a factor k^{D_2}, and repeat the calculations. When the two values differ, the influence of folding still remains significant, hence the calculated value cannot be considered to be correct.

4. Summary and discussion

The effect of overestimation, due to non-linear mapping from the time domain to the phase space, can substantially influence the correlation integral. The quantitative characterisation of an attractor reconstructed from measured time series may, in particular, be unreliable. The presented results lead to the following conclusions.

(i) The number of points necessary to approach the true scaling region may be considered as sufficient when a clear scaling region, well beyond the scales influenced by non-linear mapping from the time domain to the phase space, is obtained.

(ii) It was already shown that the method of calculation of the correlation integral is extremely sensitive to the presence of noise, or drift [22,27–29,7]. Even a small percentage of noise corrupts small scales, where the true plateau is to be found. In this case an increase in the number of points could not substantially improve the accuracy of estimation.

It may be argued that quasi-periodic time series are not an appropriate benchmark for the correlation integral algorithm. They may have a coherence time that is longer than the length of the time series, and this can result in long-term correlations. However, for measured time series we do not know a priori what type of dynamics they contain. They may well also contain quasi-periodic dynamics. The choice of quasi-periodic test time series was motivated by the fact they resemble the frequency spectra of measured time-series [7]. Indeed, a number of reports dealing with time series of cardiovascular functions (ECG, IHR, blood pressure), which are all nearly quasi-periodic, have been published. In the main, the chaotic time series, such as Hénon, Lorenz, McKey–Glass, are used as test signals (see Refs. [30,31] and references therein). Further, the reconstruction of the phase space using the method of delayed coordinates is straightforward for quasi-period time series, since both crucial parameters, τ and d, can be precisely determined.

The difficulty of using dimensions and similar measures to distinguish between deterministic and stochastic or noise-dominated signals has led a number of investigators to propose the use of surrogate time series [33–35]. It was proposed that the correlation integral can be used for qualitative characterisation – by comparing values obtained from the original time series and their surrogates one may distinguish between deterministic and stochastic or noise-dominated time series. In addition, a great deal of research has been focused on the problem of reducing noise from experimentally obtained time series [36–41]. However, in time series of biological origin the noise usually originates from the interference of a number of physiological functions, since it is not possible to selectively measure only one function. Moreover, it is difficult to distinguish the noise contribution. Based on our experiences with measured time series of various cardiovascular functions, which result from at least a five-dimensional system [6,8], one may infer on a finite-dimensionality by comparing correlation integrals of original time series and their surrogates [7]. However, a sufficient scaling region to estimate a valid correlation dimension cannot be obtained.

Acknowledgement

This study is supported by the Slovenian Ministry of Science and Technology.

References

[1] P. Grassberger, I. Procaccia, Phys. Rev. Lett. 50 (1983) 346.
[2] H.G.E. Hentschel, I. Procaccia, Physica D 8 (1983) 435.
[3] P. Grassberger, I. Procaccia, Physica D 9 (1983) 189.
[4] K. Pawelzik, H.G. Schuster, Phys. Rev. A 35 (1987) 481.
[5] J.-P. Eckmann, D. Ruelle, Rev. Mod. Phys. 57 (1985) 617.
[6] A. Stefanovska, Dissertation (University of Ljubljana, Ljubljana, 1992).
[7] A. Stefanovska, P. Krošelj, S. Strle, Open Sys. & Inf. Dyn., in print.
[8] M. Bračič, A. Stefanovska, Open Sys. & Inf. Dyn., in print.
[9] N.H. Packard, J.P. Crutchfield, J.D. Farmer and R.S. Shaw, Phys. Rev. Lett. 45 (1980) 712.
[10] F. Takens, Detecting strange attractors in turbulence, in: D.A. Rand, L.S. Young, eds., Lecture Notes in Mathematics 898 (Springer, New York, 1981).
[11] R. Mañé, On the dimension of the compact invariant sets of certain non-linear maps, in: D.A. Rand and L.S. Young, eds., Lecture Notes in Mathematics 898 (Springer, New York, 1981).
[12] L.A. Smith, Phys. Lett. A 133 (1988) 283.
[13] M.A.H. Nernberg, C. Essex, Phys. Rev. A 42 (1990) 7065.
[14] I. Procaccia, Nature 333 (1988) 498.
[15] J.-P. Eckmann, D. Ruelle, Physica D 56 (1992) 185.
[16] A.M. Fraser, H.L. Swinney, Phys. Rev. A 33 (1986) 1134.
[17] W. Liebert, H.G. Schuster, Phys. Rev. A 142 (1989) 107.
[18] A.M. Albano, A. Passamante, M.E. Farrell, Physica D 54 (1991) 85.
[19] M.B. Kennel, R. Brown, H.D.I. Abarbanel, Phys. Rev. A 45 (1992) 3403.
[20] M.T. Rosenstein, J.J. Collins, C.J. DeLuca, Physica D 73 (1994) 82.
[21] J.M. Lipton, K.P. Dubke, Phys. Lett. A 210 (1996) 290.
[22] A. Stefanovska, P. Krošelj, S. Strle, Open Sys. & Inf. Dyn. 3 (1985) 149.
[23] J.B. Ramsey, H.-J. Yuan, Phys. Lett. A 134 (1989) 287.
[24] A. Jedynak, M. Bach, J. Timmer, Phys. Rev. E 50 (1994) 1770.
[25] M. Möller, W. Lange, F. Mitschke, N.B. Abraham, U. Hübner, Phys. Lett. A 138 (1989) 176.
[26] P. Grassberger, T. Schriber, C. Schaffruth, Int. J. Bif. Chaos 1 (1991) 521.
[27] A.M. Albano, P.E. Rapp, A. Passamante, Phys. Rev. E 52 (1995) 196.
[28] T. Schreiber, H. Kantz, Observing and predicting chaotic signals: in Predictability of Complex Dynamical Systems (Springer, New York, 1996).
[29] D. Kugiumtzis, Physica D (1997), in print.
[30] T.M. Griffith, Cardiovascular Research 31 (1996) 342.
[31] L. Glass, Physics Today, August 1996, p. 40.
[32] J. Theiler, Phys. Rev. A 34 (1986) 2427.
[33] P.E. Rapp, A.M. Albano, T.I. Schmah and L.A. Farwell, Phys. Rev. A 47 (1993) 2289.
[34] J. Theiler, S. Eubank, A. Longtin, B. Galdrikian, J.D. Farmer, Physica D 58 (1992) 77.
[35] P.E. Rapp, A.M. Albano, I.D. Zimmerman and M.A. Jiménez-Montaño, Phys. Rev. A 192 (1994) 27.
[36] E.J. Kostelich, J.A. Yorke, Phys. Rev. A 38 (1988) 1649.
[37] A.R. Osborne, A. Provenzale, Physica D 35 (1989) 357.
[38] E.J. Kostelich, J.A. Yorke, Physica D 41 (1990) 183.
[39] S.M. Hammel. Phys. Lett. A 148 (1990) 421.
[40] J.D. Farmer, J.J. Sidorovich, Physica D 47 (1991) 373.
[41] M. Davies, Physica D 79 (1994) 174.